MECHANISM AND IMPLICATIONS OF DESTABILIZING TIP60, A TUMOUR SUPPRESSOR

ZHANG YANZHOU

NATIONAL UNIVERSITY OF SINGAPORE

2016

MECHANISM AND IMPLICATIONS OF DESTABILIZING

TIP60, A TUMOUR SUPPRESSOR

ZHANG YANZHOU

(B.Sc. ZJU)

A THESIS SUBMITTED

FOR THE DEGREE OF DOCTOR OF PHILOSOPHY

CANCER SCIENCE INSTITUTE

NATIONAL UNIVERSITY OF SINGAPORE

2016

Supervisor:

Dr. Sudhakar Jha

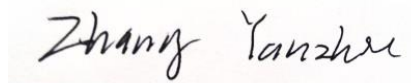Examiners:

Associate Professor Lih Wen DENG

Dr. Ruby Yun-Ju HUANG

Professor Bing ZHU, Institute of Biophysics, Chinese Academy of Science

DECLARATION

I hereby declare that the thesis is my original work and it has been written by

me in its entirety. I have duly acknowledged all the sources of information

which have been used in the thesis.

This thesis has also not been submitted for any degree in any university

previously.

_____

ZHANG YANZHOU

13 February 2017

Acknowledgements

Table of Contents

Summary

HIV-Tat-interacting protein of 60 KDa (TIP60) is a lysine acetyltransferase implicated in transcription, DNA damage response and apoptosis. It is known to be downregulated in multiple cancers. TIP60 is shown to act as a haploinsufficient tumour suppressor in MYC-induced lymphomagenesis. Additionally, downregulation of TIP60 is shown to be a potential marker for cancer malignancy and poor Overall Survival (OS).

In cervical cancers, Human Papillomavirus (HPV) E6 oncogene targets cellular p53, BAK and some of the PDZ domain containing proteins for proteasome mediated degradation through E6AP ligase. Other than this, E6 oncoprotein from both high-risk and low-risk HPVs were shown to target TIP60. However, the destabilization of TIP60 mediated by E6 was E6AP independent suggesting a novel mechanism yet to be identified. Additionally, whether destabilization of TIP60 contributes to HPV E6 mediated tumour transformation remains unclear. A proteomic analyses revealed that EDD1/UBR5, an E3 ubiquitin ligase overexpressed in cancers, is a binding partner of TIP60. Cycloheximide treatment and ubiquitination assay reveal that EDD1 negatively regulates TIP60's protein stability through ubiquitination dependent proteasome degradation. More importantly, HPV E6 utilizes EDD1 to mediate TIP60 destabilization. Colony formation assays show that gain-of-function either by overexpressing TIP60 or by depleting EDD1 in HPV positive cervical cancer cells significantly inhibits colony formation *in vitro*. This is strongly supported by the *in vivo* studies where re-activation of TIP60 in cervical cancer cells dramatically reduces tumour formation. In summary, a novel ligase through which E6 destabilizes TIP60

was identified. More interestingly, this study implying a distinct tumour suppressor role for TIP60 in cervical cancers shows that reactivation of TIP60 through inhibiting EDD1 could be of therapeutic value.

Other than tumour growth, metastasis is an important feature of cancer. Among various signalling pathways, TIP60 is implicated in regulating epithelial-mesenchymal transition (EMT), an essential process of cancer metastasis. In my attempt to identify the role of TIP60 in inhibiting cancer metastasis, I have used *in vitro* and *in vivo* models to show that TIP60 expression abrogates cell migration and metastatic potential of breast cancer cells. Mechanistically, this was through TIP60's ability to destabilize DNMT1 and inhibit SNAIL2's function (SNAIL2 mediated EMT/cell migration). Depletion of TIP60 stabilizes DNMT1 and increase SNAIL2 levels, resulting in EMT. Recruitment of DNMT1 to SNAIL2 targets in the absence of TIP60 increases DNA methylation on their promoter region and further represses expression of epithelial markers. In pathophysiological scenario, TIP60 is significantly down-regulated in breast cancer patients with poor Overall Survival (OS) and Disease-Free Survival (DFS) prognoses. These data suggest that levels of TIP60 can be a prognostic marker of breast cancer progression and stabilization of TIP60 could be a promising strategy to treat cancers.

Taken together, my study reveals the mechanism of TIP60's tumour suppressor function including inhibition of both tumour growth and metastasis. I have summarised my work into five categories (introduction, objective, materials and methods, results and discussion), which are divided into nine chapters.

List of Tables

List of Figures

List of abbreviation

5-aza-2'-DC; 5-azac-2'-deoxycytidine

ATM; Ataxia Telangiectasia Mutated kinase

BRCA1; Breast cancer 1, early onset

CDH1; E-CADHERIN

CDH2; N-CADHERIN

ChIP; chromatin immunoprecipitation

CHX; cycloheximide

CK2; casein kinase 2

Co-IP; co-immunoprecipitation

DFS; disease free survival

DSB; DNA double strand break

EMT; epithelial to mesenchymal transition

E6AP; E6-associated protein

FN1; fibronectin

GEO; Gene Expression Omnibus

ssGSEA; single sample Gene Set Enrichment Analysis

HDAC; histone deacetylase

HR; homologous recombination

HP1; heterochromatin protein 1

HPV; human papilloma virus

KD; catalytically inactive

NHEJ; non-homologous end joining

NSG; NOD.Cg-Prkdcscid Il2rgtm1Wjl/SzJ mice

OS; overall survival

qPCR; quantitative polymerase chain reaction

RMA; Robust Multichip Average

SNAI2; SNAIL2

TSA; Trichostatin A

TIP60; Tat interacting protein 60 kilo Dalton

UPS; ubiquitin-proteasome system

VIM; VIMENTIN

WT; wild-type

ZEB1; Zinc finger E-box-binding protein 1

Chapter 1: Introduction

In 1996, by using Yeast Two Hybrid assay, G. Chinnadurai et al identified a protein specifically interacting with HIV Tat transactivator through the N-terminal 31 amino acids which contains the essential cysteine rich portion of Tat activation domain (Kamine et al., 1996). They named this protein **TIP60** – Tat interactive protein 60 kDa. In their study, they also found that overexpression of TIP60 results in an increase of Tat transactivation of HIV-1 promoter without changing the basal activity of HIV-1 promoter or the heterologous RSV promoter, suggesting that TIP60 is a cofactor of HIV Tat protein in activating HIV expression.

Since then multiple groups including ours have identified role of TIP60 and have demonstrated its importance in regulating cellular pathways (Chen et al., 2015; Du et al., 2010b; Jha et al., 2010; Tang et al., 2013) (**Figure 1**). TIP60 has been implicated in multiple cellular pathways such as DNA damage response, apoptosis, chromatin remodelling and transcriptional regulation (Jha and Dutta, 2009; Sapountzi et al., 2006; Squatrito et al., 2006). This is through its ability to acetylate both histone and non-histone proteins, and by doing so it acts as a regulator of these proteins, for example p53 and Ataxia Telangiectasia Mutated (ATM) kinase (Sun et al., 2005; Sun et al., 2007; Sykes et al., 2006; Tang et al., 2006). These studies suggest that TIP60 modulate function of a wide range of cellular proteins that are essential in multiple cellular pathways.

As an important regulator in cell, dysregulation of TIP60 correlates with multiple diseases including cancers. In 2007, Gorrini *et al.* identified TIP60 as

a haplo-insufficient tumour suppressor using E(mu)-MYC transgenic mice that are heterozygous for TIP60 gene (Gorrini et al., 2007). Further research also found that down-regulation of TIP60 highly correlates with cancer progression and could be a prognostic marker for cancer progression (Sakuraba et al., 2009).
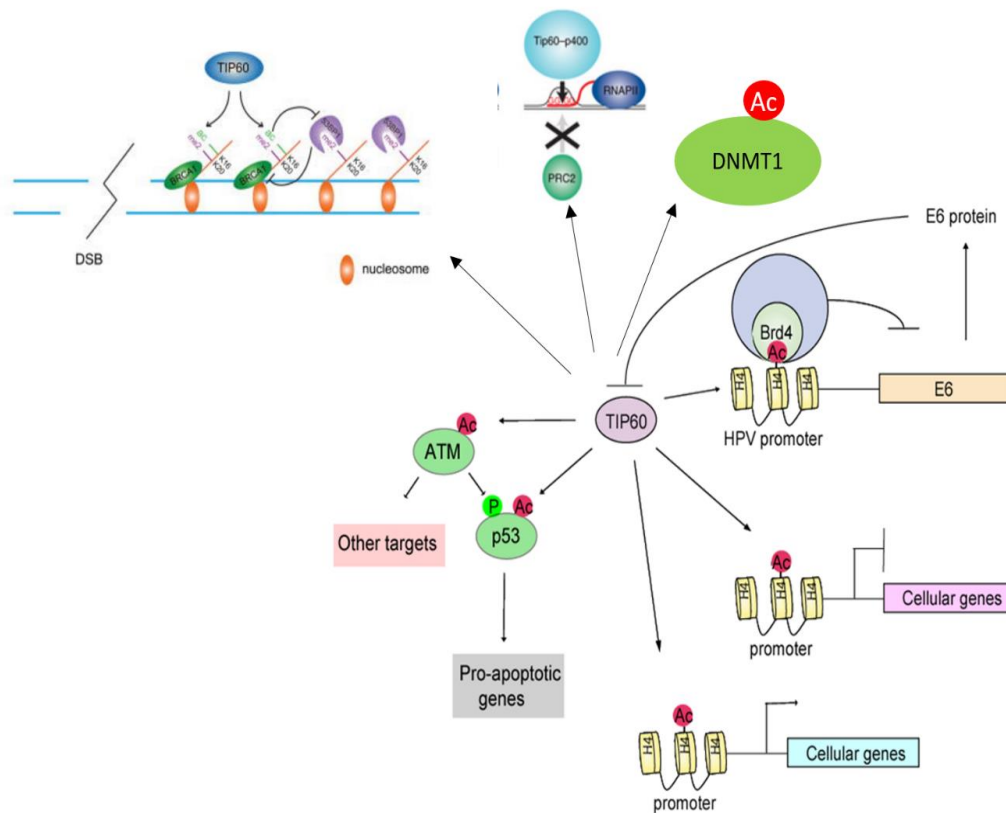
Figure 1 TIP60 is involved in multiple cellular pathways.

Adapted from (Chen et al., 2015; Du et al., 2010b; Jha et al., 2010; Tang et al., 2013).

1.1 TIP60 is a lysine acetyltransferase

1.1.1 Structural characteristics of TIP60

TIP60 is encoded by *HTATIP* gene located at 11q13.1 and consists of 14 exons (Sapountzi et al., 2006). There are at four different splice variants of TIP60 due to alternative splicing (**Figure 2**). Isoform 2 is most studies form of TIP60. Isoform 1 results from an additional translation of intron 1 which might have regulatory function (Legube and Trouche, 2003). Isoform 3 results from an exclusive translation of exon 5 that encodes a proline rich region and appears to function similar to isoform 1 (Ran and Pereira-Smith, 2000). Isoform 4 results from an additional translation of intron 1 and an exclusive translation of exon 5.

TIP60 was first identified as a histone lysine acetyltransferase in 1997 by Yamamoto and Horikoshi (Yamamoto and Horikoshi, 1997). In their study, TIP60 was identified as a nuclear protein with a conserved region named MYST domain (**Figure 3**) which is also found in other acetyltransferase such as MOZ (Borrow et al., 1996), MOF (Hilfiker et al., 1997), YBF2/SAS3 (Reifsnyder et al., 1996) and SAS2 (Ehrenhofer-Murray et al., 1997; Reifsnyder et al., 1996), indicating a acetyltransferase function of TIP60. The group of acetyltransferases that contain MYST domain are categorized under MYST family of acetyltransferase. The common feature of this family is transfers acetyl group from Acetyl-CoA to lysine residues of target protein.

The structure of human TIP60 and yeast Esa1 are similar (**Figure 3**). The catalytic domain of TIP60 includes a region that mediates Acetyl-CoA binding and a C2H2-type zinc finger, which might be involved in substrate recognition. Within the MYST family, TIP60 is closely related to MOF as

both contain a chromodomain N-terminal of MYST domain and they are known to acetylate common substrates such as histone H4 and p53 (Sykes et al., 2006; Taipale et al., 2005).
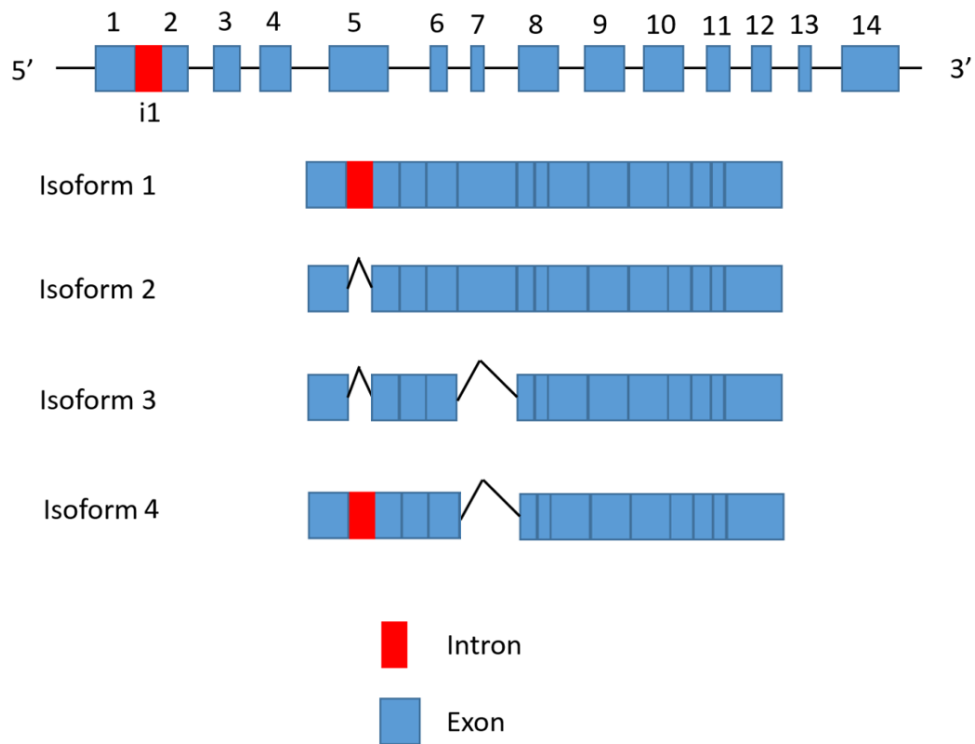
Figure 2 Schematic of TIP60 isoforms.
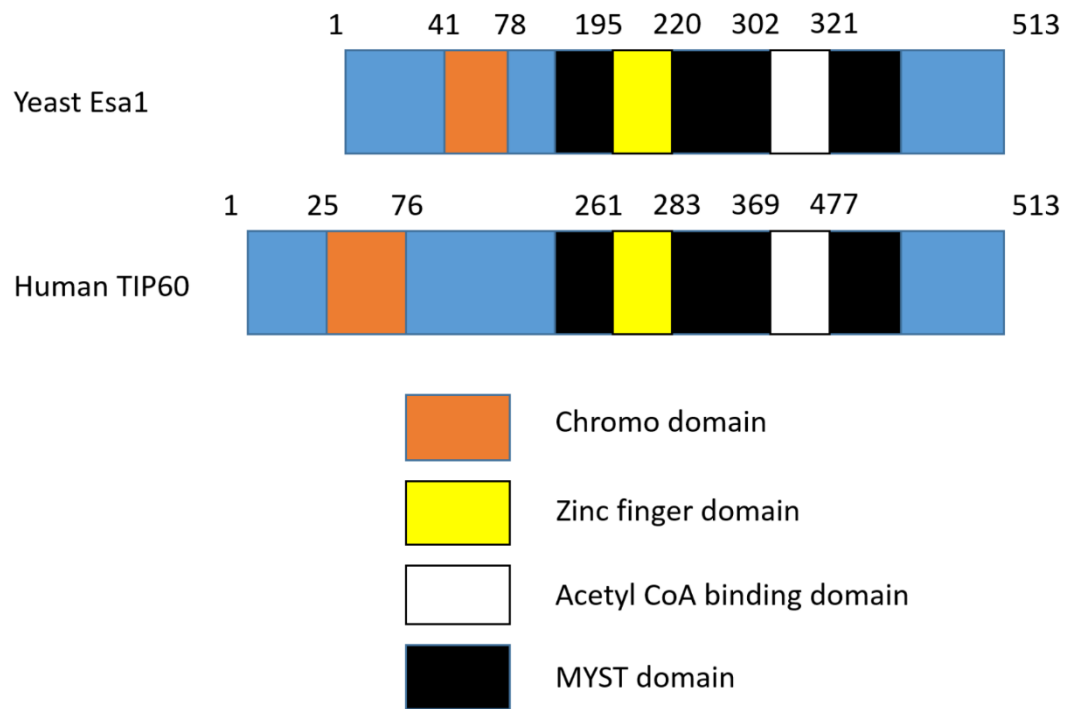
Figure 3 Diagram highlighting functional domains of human TIP60 and yeast Esa1. Numbers indicate the amino acids of TIP60 proteins.

1.1.2 Histone targets of TIP60

In 1998, Kimura and Horikoshi identified six lysines in core histones that are acetylated by TIP60; lys-5 of histone H2A, lys-14 of histone H3 and lys-5, lys-8, lys-12, lys-16 of histone H4. Further, it is reported that TIP60 is usually a part of a histone remodeller complex – NuA4 – where it functions as a histone acetyltransferase. NuA4 complex, also known as TIP60 complex in human, is a multiprotein complex consist of at least 16 subunits (**Figure 4**) (Doyon and Cote, 2004). TIP60 is the catalytic subunit of human NuA4 complex and plays a central role in the function of the complex. This complex is capable of at least three interrelated enzymatic activities: histone H2A/H4 acetylation, ATP-dependent histone H2AZ/H2B dimer exchange and DNA helicase (Auger et al., 2008). Studies have implicated that it involved in multiple cellular pathways that correlates with TIP60 regulated pathways.

TIP60 is recruited to the chromatin and mediates histone acetylation as a complex. For example, TIP60 is recruited to the chromatin by c-MYC with four other components of the NuA4 complex: TRRAP, p400, TIP48 and TIP49 (Frank et al., 2003). This is essential for c-MYC induced histone H4 acetylation, as overexpression of catalytic inactive of TIP60 decrease the level of c-MYC induced histone acetylation (Frank et al., 2003).

1.1.3 Non-histone targets of TIP60

TIP60 not only acetylates histones but also non-histone proteins. TIP60 usually acetylates non-histone proteins independently instead of forming TIP60 complex. Till now, several non-histone proteins, including post-translational modifier and transcription factors, are identified as TIP60's targets. TIP60 mediated acetylation on these non-histone targets usually

regulate their activity which might lead to tumour suppression, for example, ATM (Sun et al., 2005; Sun et al., 2007), p53 (Sykes et al., 2006; Tang et al., 2006) and p21 (Lee et al., 2013). However, further research also identified that TIP60 acetylates c-MYC (Patel et al., 2004) and cancer metastasis inducer TWIST1 (Shi et al., 2014), and this is important for their oncogenic function, indicating a bivalent role of TIP60 in carcinogenesis.
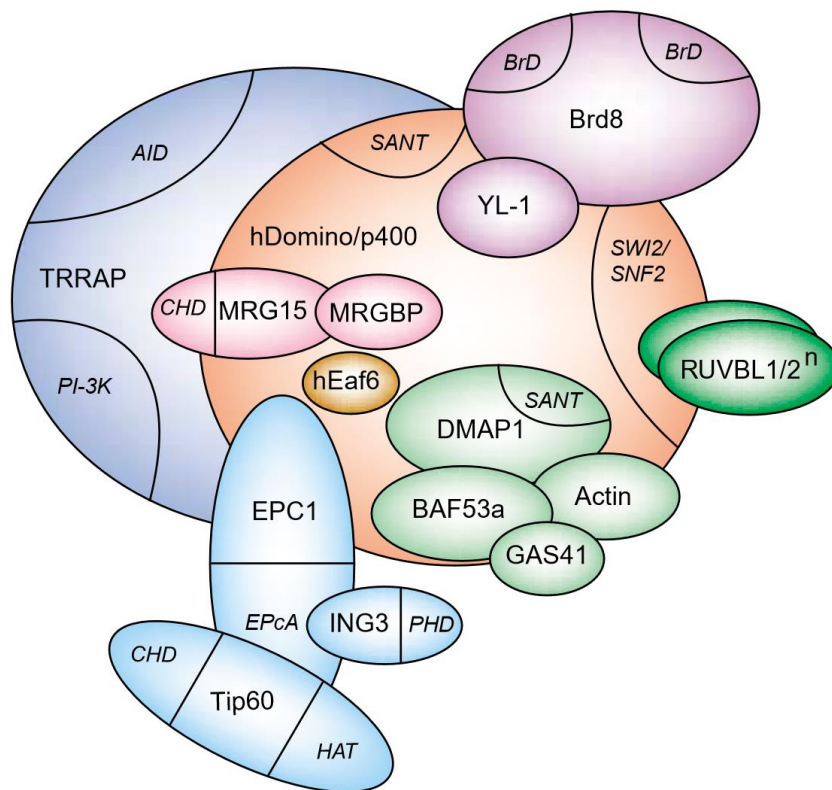
Human NuA4 HAT complex

Current Opinion in Genetics & Development

Figure 4 Schematic representation of human NuA4 complex.
Adapted from (Doyon and Cote, 2004).

1.2　TIP60 in regulating DNA damage response

DNA damage arises from the error of replication and/or exposure of exogenous reagent. There are different kinds of DNA damage and DNA double stand break (DSB) is one kind, which is difficult for cell to repair. TIP60 is essential for DSB repairing. DSB is repaired in two ways: homologous recombination (HR) and non-homologous end joining (NHEJ). NHEJ is generally considered to be error-prone, whereas HR is generally considered to be error-free (Sun et al., 2010). TIP60 has been implicated in response to homologous recombination repair pathway. This is through two roles of TIP60 in DSB: chromatin remodelling by human NuA4 complex at DSB sites and activation of ATM signalling pathway. By activating the DNA damage response (DDR), TIP60 protects cells from genome instability caused by DSB and supresses the transforming events that might lead to cancer.

1.2.1 TIP60 activation during DNA damage response

TIP60 is activated during DSB by interacting with H3K9Me3 through its chromodomain (Sun et al., 2009). H3K9Me3 is known to predominantly locate in heterochromatin (Barski et al., 2007; Regha et al., 2007). For DSB localized around heterochromatin, the original H3K9Me3 could play a role in recruiting TIP60. However, majority of cellular H3K9Me3 is bound by heterochromatin protein 1 (HP1) (Jacobs and Khorasanizadeh, 2002; Nielsen et al., 2002), which questions how H3K9Me3 could be available to TIP60? Recent studies found the involvement of casein kinase 2 (CK2) (Ayoub et al., 2008; Sun et al., 2009) in regulating binding of HP1 to H3K9Me3. Phosphorylation of HP1 by CK2 results in release of HP1 bounded to H3K9Me3, which creates unoccupied domains of H3K9Me3 for interacting

with TIP60 chromodomain (Ayoub et al., 2008; Sun et al., 2009). However, released HP1 remains chromatin bound via its chromoshadow domain instead of re-localizing to nucleoplasm (Luijsterburg et al., 2009). Further release of HP1 from chromatin requires phosphorylation on KAP-1 by active ATM. This would further release HP1/KAP-1 complex from chromatin and generate a relaxation region to facilitate DNA repairing (Ziv et al., 2006).

However, this does not explain how TIP60 is activated on open chromatin region that lacks H3K9Me3. Recent studies found that a complex containing HP1, KAP-1 and a H3K9 methyltransferase SUV39H1 are rapidly enriched on the chromatin at DSB sites (Ayrapetov et al., 2014). SUV39H1 catalyses H3K9Me3 and facilitates additional HP1/KAP-1/SUV39H1 enrichment around DSB sites through interaction between HP1 and nascent H3K9Me3. This would result in spreading of H3K9Me3 and recruiting TIP60 to DSB sites, providing a mechanism of TIP60 activation around euchromatin region that lack H3K9Me3.

1.2.2 Histone acetylation by TIP60 at DNA damage sites

Acetylation, among all the other modifications, has a role to change the surface charge distribution of the targeted proteins and further change the accessibility of the genome or other proteins. Acetylation of histones by TIP60 (NuA4) complex is also very important for DNA damage response pathway. When there are DNA double strand breaks, TIP60 mediated acetylation on histone H4 lysine 16 (H4K16Ac) acts as a switch of homologous recombination (HR) repair pathway and non-homologous end joining (NHEJ) repair pathway (Tang et al., 2013). Mechanistically, H4K16Ac promotes homologous recombination by promoting BRCA1 recruitment to DSB sites

and inhibits non-homologous end joining by inhibiting H4K20Me2 mediated 53BP1 recruitment (Tang et al., 2013). In addition to this, Jacquet et al recently demonstrated that TIP60 is involved in promoting HR pathway by competing with RNF168 (Jacquet et al., 2016). 53BP1 recruitment to DSB sites not only involves H4K20Me2 but also H2AK15Ub. TIP60 acetylation on H2AK15 inhibits RNF168 ubiquitination on the same sites, thereby inhibiting 53BP1 recruitment at DNA damage sites.

Taken together, TIP60 promotes HR and ablate NHEJ by inhibiting both H4K20Me2 and H2AK15Ub mediated recruitment of 53BP1.

1.2.3 TIP60 and ATM activation

ATM activation initiates the signalling pathways that would recruit DNA damage repair molecules and activate cell cycle checkpoints. ATM phosphorylation on H2AX provides a platform for the recruitment of DNA repair complex including 53BP1, BRCA2 and NBS1 (Stucki et al., 2005). ATM phosphorylation on p53 and CHK2 plays a crucial role in cell cycle arrest. Thus activation of ATM is a crucial step in DNA damage response.

Recent studies reveal TIP60's catalytic activity is crucial for ATM activation. TIP60 interacts with the FATC domain of ATM, and acetylates K3016 of ATM (Sun et al., 2007). Mutation of lysine 3016 of ATM results in defective ATM dependent activation of DDR, suggesting an important role of TIP60 acetylation in ATM activation. Inactivation of MRN complex (also reported be involved in ATM activation (Sun et al., 2009)), ablates acetylation and activation of ATM by TIP60. Interestingly, loss of functional MRN complex delays both recruitment of TIP60 to DSB sites and activation of

TIP60, suggesting that MRN complex might be involved in recruitment of TIP60-ATM to DSB sites, which would lead to the activation of TIP60 by H3K9Me3 and acetylation of ATM by TIP60.

1.3 TIP60 as a regulator of transcription factors

1.3.1 TIP60 acetylates transcription factors which function as tumour suppressor

TIP60 is reported to mediate acetylation on several transcription factors and this would lead to tumour suppression. The most well-known transcription factor acetylated by TIP60 is p53. Acetylation of p53 on lysine 120 by TIP60 modulates the decision between cell cycle arrest and apoptosis, which is crucial for p53 dependent apoptosis but not p53 induced cell cycle arrest (Sykes et al., 2006; Tang et al., 2006). The K120R mutation results in mis-regulation of p53 pro-apoptotic targets such as BAX and PUMA, however the non-apoptotic targets such as p21 and hMDM2 remain unaffected.

Another transcription factor known to be acetylated by TIP60 is p21. Acetylation of p21 on lysine 161 and 163 by TIP60 is required for stabilization of p21 and this is necessary for p21 induced cell cycle arrest during DNA damage response (Lee et al., 2013). Acetylation mimetic mutations K161Q and K163Q decrease the polyubiquitination of p21 in H1299 cells and further enhance p21 mediated cell cycle arrest. Lee et al. also found these mutations to delay growth of p21 null MEFs.

1.3.2 TIP60 acetylates oncogenic transcription factor

It is also reported that TIP60 could mediate acetylation of oncogenic transcription factors that is essential for their oncogenic activity. Among them,

the most well-known is c-MYC. TIP60 mediated acetylation on oncoprotein c-MYC (Patel et al., 2004) increase its stability. However, the acetylation site on c-MYC by TIP60 is yet to be identified. Additionally, not only TIP60 but also GCN5 acetylates c-MYC, and GCN5 seems occupy the predominant role in acetylating c-MYC. Therefore, role of TIP60 in c-MYC acetylation and functional regulation need further investigation.

Another oncogenic transcription factor acetylated by TIP60 reported recently is TWIST1 (Shi et al., 2014). TIP60 mediates TWIST1 di-acetylation on K73 and K76, which is required for TWIST1 and BRD4 interaction. Furthermore, the interaction between TWIST1 and BRD4 is essential for WNT5A expression and important for breast cancer progression. However, this study only identified TIP60-TWIST1-BRD4 axis in WNT5A expression cancer cells, whether TIP60-TWIST1-BRD4 axis is essential to WNT5A non-expression cancer cells need to be further investigated. Additionally, TIP60 has been implicated as a tumour suppressor in many cellular pathways, however this study found that TIP60 could facilitate the progression of WNT5A driven breast cancer. This bivalent role of TIP60 needs further investigation.

1.4 TIP60 in transcriptional regulation

1.4.1 TIP60 as a co-activator of transcription

It is believable that TIP60 could also interact with several transcription factors and further assist the regulation of the downstream of these transcription factors (**Figure 5A**). For example, TIP60 complex is recruited to MYC target gene through interacting with c-MYC. This would result in an increased acetylation of histone H4 and further activation of target genes (Frank et al., 2003). Overexpression of catalytic inactive TIP60 delays the acetylation on histone H4 induced by c-MYC, and also reduced recruitment of c-MYC to chromatin.

TIP60 is also known to be a co-activator of NF-κB (nuclear factor kappa light chain gene enhancer in B cells) in the regulation of its target genes, for example, *KAI1*, a metastasis suppresser gene. TIP60 is recruited to *KAI1* promoter by NF-κB p50. This would activate the transcription of *KAI1* gene and inhibit cancer metastasis (Kim et al., 2005). However, β-catenin could replace TIP60 on *KAI1* promoter when it is overexpressed or TIP60 is depleted. This would further repress *KAI1* expression that results in promoting cancer metastasis. Therefore, the balance between TIP60 and β-catenin determine the expression level of *KAI1* and further determine the metastatic status of cancer.

Other than these, TIP60 is important in E2F1 target gene transcription as well. It is reported that E2F1 recruits TIP60 complex to target promoter in late G1 phase and results in histone H4 hyper-acetylation on target promoter which would activate target gene (Taubert et al., 2004). Additionally, TIP60 complex interacts with myeloid transcription factor C/EBPα (CCAAT/enhancer binding

proteins), resulting in an enhancement of acetylation on histone H3 and H4 and activates downstream targets including C/EBPα itself (Bararia et al., 2008).

1.4.2 TIP60 as co-repressor of transcription

In most cases, TIP60 is reported to co-activate expression of genes. However, TIP60 can also act as a co-repressor of certain gene expression. TIP60 acts as a co-repressor through either recruits repressor complex (**Figure 5B**) or interacts with transcription factor with repressive function (**Figure 5C**). For example, TIP60 is reported to interact with both HDAC7 (histone deacetylase 7) and STAT3 (Xiao et al., 2003), This allows TIP60 to recruit HDAC7 to STAT3 target sites (**Figure 5B**) and represses STAT3 target gene expression (Xiao et al., 2003). Additionally, it is reported that TIP60 represses transcription by associating with transcription repressor ZEB1 (zinc finger E box binding protein) in certain cell types (Hlubek et al., 2001).
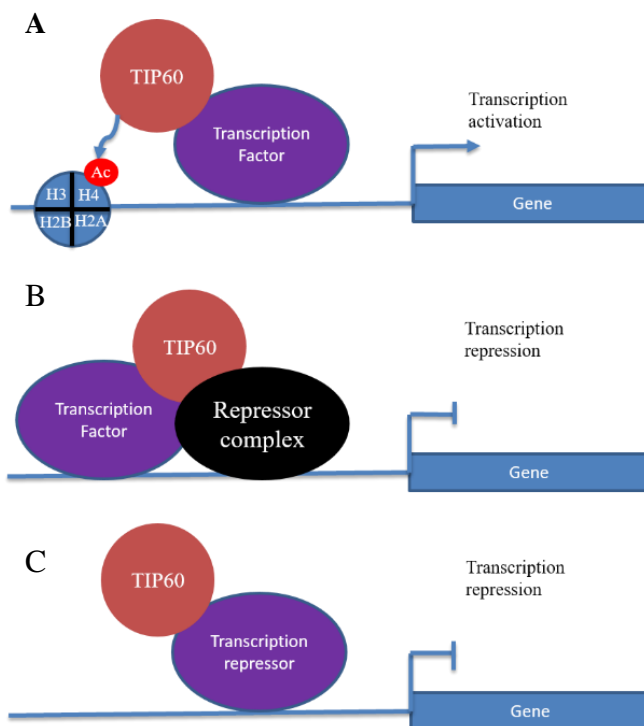
Figure 5 Models of TIP60 involvement in transcription.

(**A**) TIP60 is recruited by transcription factor, resulting in hyperacetylaiton on H4 and further activation of transcription. (**B**) TIP60 recruits repress complex and inhibit transcription activity. (**C**) TIP60 associates with transcription repressor to repress transcription.

1.5　TIP60 is regulated by post-translational modification

TIP60 is tightly regulated in cell via various processes. Regulation of TIP60 by protein-protein interaction and post-translational modification is well documented. However, regulation of TIP60 at transcription level is not well studied. Interestingly, TIP60 is known to be positively regulated by circadian transcription factor, CLOCK and this is through binding of CLOCK to the E-box motif on TIP60 promoter (Miyamoto et al., 2008).

Regulation of TIP60 by protein binding has been discussed in detail section 1.1.2, 1.2.2 and 1.4. Hence, in this section, regulation of TIP60 by post-translational modification will be discussed in detail.

1.5.1 Acetylation on TIP60

TIP60 can be acetylated by p300/CBP acetyltransferase on lysine 268 and lysine 282 of TIP60 that is located within the zinc finger domain of TIP60, however, the effects of these acetylation on TIP60 are yet to be explored (Col et al., 2005).

TIP60 is known to be auto-acetylated in response to DNA damage. The auto-acetylation of TIP60 occurs on lysine 327 of TIP60 that is located within the active site of the MYST domain (Wang and Chen, 2010; Xiao et al., 2014; Yang et al., 2012a). Interestingly, acetylation upregulates TIP60's catalytic activity, as mutations on K327 (K327R and K327Q) abolishes both TIP60 auto-acetylation on wild-type TIP60 and its targets such as histone H4 (Yang et al., 2012a). Mechanistically, this auto-acetylation of TIP60 results in dissociation of TIP60 oligomer and enhances its association with substrates (Wang and Chen, 2010). Among deacetylases, SIRT1 has been identified to

deacetylate K327 of TIP60 and negatively regulates its activity (Wang and Chen, 2010). Moreover, p300 has been shown to interact with TIP60 and facilitates TIP60 auto-acetylation on K327 and shown to be involved in the activation of FOXP3 (Xiao et al., 2014).

1.5.2 Phosphorylation on TIP60

TIP60 was identified to be phosphorylated at Serine 86 (Ser86) and Serine 90 (Ser90) when human TIP60 was overexpressed in insect cells. Interestingly, TIP60's acetyltransferase activity is modulated by these phosphorylation (Lemercier et al., 2003). Further, Ser90 was identified to be phosphorylated by Cyclin B/Cdc2 (cell division cycle 2) *in vitro* and *in vivo*. Consistent with this, Ser90 phosphorylated TIP60 accumulates in G2/M phase of the cell cycle and this is abolished after treat the cell with cyclin kinase inhibitor, Roscovitine (Seliciclib or CYC202) (Lemercier et al., 2003). This suggests that TIP60 is activated in G2/M phase and important for the regulation of G2/M cell cycle arrest.

Ser86 was identified to be phosphorylated by GSK3β (glycogen synthase kinase 3) (Charvet et al., 2011; Lin et al., 2012) and this phosphorylation of TIP60 is involved in p53 dependent cell apoptosis (Charvet et al., 2011). As discussed in section 1.3.1, TIP60 mediated acetylation on p53 K120 determines p53 to induce cell apoptosis rather than cell cycle arrest. Charvet et al demonstrated that TIP60 phosphorylation resistant mutant S86A, was unable to acetylate p53 K120 and activate PUMA expression (Charvet et al., 2011). In addition to this, it was also reported that Ser86 phosphorylation of TIP60 is involved in regulation of autophagy (Lin et al., 2012). GSK3-TIP60-ULK1 forms a signalling pathway. GSK3 mediated Ser86 phosphorylation on

TIP60 stimulates TIP60 dependent acetylation on ULK1 kinase and results in activation of ULK1 dependent autophagy under serum deprived condition.

Recently, a new site, tyrosine 44 (Tyr44) of TIP60 was identified to be phosphorylated by a tyrosine kinase named c-Abl (Kaidi and Jackson, 2013). This phosphorylation of TIP60 promotes its interaction with H3K9Me3 which is required for TIP60 mediated acetylation on ATM and activation of ATM dependent signalling in response to DNA damage.

1.5.3 Ubiquitination on TIP60

TIP60 is an unstable protein with short half-life, which ranges from 30 minutes to 2 hour. In cell, low level of TIP60 is maintained via Proteasome. Degradation by Proteasome is triggered by mono- or poly-ubiquitination on target proteins catalysed by ubiquitin ligase. However, little is known about the regulation of TIP60 thorugh ubiquitin-proteasome system (UPS) and ubiquitin ligase involved in ubiquitination on TIP60 is under explored. TIP60 is known to be targeted for proteasome degradation by MDM2 (mouse double minute 2) (Legube et al., 2002). MDM2 was demonstrated to be involved in targeting TIP60 to proteasome degradation. MDM2 mediates TIP60 proteasome degradation through physically interacting with TIP60 and through its E3 ligases activity it poly-ubiquitinates TIP60. This helps maintain low level of TIP60 in normal physiological scenario. However, when cells are exposed to DNA damage, for example, exposure to UV irradiation this inhibits MDM2 mediated TIP60 proteasome degradation resulting in accumulation of TIP60 in response to DNA damage. However, the mechanism of the inhibition of MDM2 mediated TIP60 degradation is still unclear.

TIP60 was also known to be targeted by p300/CBP-associated E4-type ubiquitin ligase (Col et al., 2005). This is utilized by HIV Tat to destabilized TIP60 resulting in impairment of TIP60 dependent apoptotic cell response to DNA damage. Interestingly, p300/CBP acetyltransferase activity is not involved in this process.

Since TIP60 has a high turnover, involvement of ligase(s) other than MDM2 and p300/CBP cannot be overruled.

1.6 TIP60 represses viral genome transcription and is destabilized by viral oncoproteins through ubiquitin proteasome system

TIP60 is destabilized by viral oncoproteins via ubiquitin-proteasome system (UPS), for example HIV Tat protein utilize p300/CBP-associated E4-type ubiquitin ligase to destabilize TIP60 (Col et al., 2005). In addition to HIV TAT, human papillomaviruses (HPVs) also targets TIP60 to UPS.

HPV are non-enveloped DNA viruses that infect mucosal or cutaneous squamous epithelium and cause hyper-proliferation (Howley and Livingston, 2009; zur Hausen, 2002). HPV infection causes cancer mainly due to the destabilization of p53 and pRB by viral E6 and E7 protein respectively (Munger and Howley, 2002; zur Hausen, 2002). HPV E6 interacts by its N-terminal residues with p53 and with a cellular ubiquitin ligase E6AP (E6-associated protein), forming a complex that results in ubiquitin-mediated degradation of p53 by the proteasome (Cooper et al., 2003; Huibregtse et al., 1991, 1993; Scheffner et al., 1993).

Recently our group discovered that TIP60 was also destabilized by HPV E6 in cervical cancer (Jha et al., 2010). This destabilization was proteasome

dependent since MG132 treatment restored TIP60 level. Interestingly, deletion and mutational analysis of E6 reveals that this is through the N-terminal region of E6 and does not require interaction with E6AP suggesting a novel ligase might be utilized by E6 to destabilize TIP60.

As far as biological significance is concerned, it was demonstrated that TIP60 could repress viral gene transcription and this was through TIP60-dependent acetylation of H4 on HPV promoter, and recruitment of BRD4-repressor complex (Jha et al., 2010). These data suggests that E6 destabilizes TIP60 to release the expression of early viral proteins, and ablation of p53 dependent cellular pathways. These data also highlight an important role of TIP60 in regulating virus transcription and the reason why viral proteins such as HPV E6 would target TIP60 for degradation. Whether regulation is common to other oncoviruses or restricted to HIV and HPV needs further investigation.

1.7 Down-regulation of TIP60 might be a potential marker for the malignancy of cancer

TIP60 is downregulated in multiple cancers. As mentioned above, TIP60 is downregulated in various virus-induced cancers including HPV induced cervical cancer. Apart from that, the TIP60 gene expression is downregulated in colon carcinomas and lung cancers (ME et al., 2006). Moreover, loss of nuclear TIP60 staining is found in mammary carcinomas (Gorrini et al., 2007). These studies indicate that reduced TIP60 expression correlates with tumour development. This is consistent with the studies identifying association between TIP60 expression, cancer metastasis and survival of patients. Along these lines, Chen et al. used tissue microarray containing a large number of

melanoma biopsies and evaluated the expression of TIP60 in pathophysiological scenario and clinical outcome (Chen et al., 2012). Their data demonstrated that reduced TIP60 expression is significantly associated with melanoma metastasis and predicts a poorer survival in melanoma patients. They also showed that forced TIP60 expression inhibits melanoma cell migration.

Downregulation of TIP60 was also observed in colorectal cancer. TIP60 downregulation showed significant correlation with larger tumour size, poorly differentiated type, peritoneal dissemination, distant metastasis, and higher stage of TNM classification (Sakuraba et al., 2009). These suggested that TIP60 was more frequently downregulated in advanced colorectal carcinoma and downregulation of TIP60 could be a potential marker for the malignancy of colorectal cancer.

1.8 Epithelial mesenchymal transition and cancer metastasis

Epithelial-mesenchymal transition (EMT) is a highly conserved cellular program that allows polarized, immotile epithelial cells to convert to motile mesenchymal cells (Yang and Weinberg, 2008). EMT process can be categorised into three major changes in cellular phenotype (Boyer and Thiery, 1993; Hay, 1995): (1) morphological changes from a cobblestone-like monolayer of epithelial cells with an apical-basal polarity to dispersed, spindle-shaped mesenchymal cells with migratory protrusions; (2) changes of differentiation markers from cell-cell junction proteins and cytokeratin intermediate filaments to vimentin filaments and fibronectin and (3) the functional changes associated with the conversion of stationary cells to motile cells that can invade through extra cellular matrix (ECM). Although all three

changes are not observed during EMT; acquisition of the ability to migrate and invade ECM as single cells is considered a functional hallmark of the EMT program (Yang and Weinberg, 2008).

EMT program has been implicated in the dissemination of single carcinoma cells from primary epithelial tumours (Thiery, 2002). Systemic spread of tumour cells has already been detected from early lesions in HER-2 transgenic mice and in human ductal carcinoma, which suggest that metastasis is not necessarily a late event in tumour progression (Husemann et al., 2008). Additionally, morphological evidence has shown that EMT occurs at invasive fronts of human tumours (Prall, 2007). Similarly, in colon carcinoma, EMT occurs at the invasive front and produces single migratory cells that shows reduced E-CADHERIN expression (Thiery et al., 2009).

Many EMT-inducing transcription factors, including SNAIL1, SNAIL2, dEF1, SIP1, TWIST1, FOXC2, and GOOSECOID, have been associated with tumour invasion and metastasis (Yang and Weinberg, 2008). The involvement of several EMT-inducing transcription factors has been reported in human carcinomas. For example, overexpression of TWIST1 was associated with distant metastasis and poor survival in N-MYC-amplified neuroblastomas (Valsesia-Wittmann et al., 2004) and in melanomas (Hoek et al., 2004).

The main functions of these transcription factors are to bind to the promoter of cell adhesion molecules to inhibit their expression or binding to the promoter of cell migration related proteins to activate their expression. During the EMT process, changes in cell morphology associate with downregulation of cell adhesion proteins such as E-CADHERIN and EpCAM,

and upregulation of cell migration related proteins such as FIBRONECTIN or VIMENTIN.

1.9   TIP60 antagonizes DNMT1

There are three classes of DNA methyltransferase (DNMTs): DNMT1, DNMT2 and DNMT3 (DNMT3A and DNMT3B) (Bestor, 2000). *De novo* DNA methylation is catalysed by DNMT3A and DNMT3B, whereas maintenance of DNA methylation during cell proliferation is done by DNMT1 (Jones and Baylin, 2007). Among all the DNMTs, DNMT1 is the most abundantly expressed (Espada et al., 2011). DNMTs are progressively upregulated in cancers including colorectal adenoma-carcinoma (Schmidt et al., 2007), suggesting an oncogenic function of DNMTs.

TIP60 is known to form a complex with DNMT1 through UHRF1, resulting in TIP60 mediated acetylation on DNMT1 and promoting DNMT1 ubiquitination-dependent degradation (Du et al., 2010b). This regulation of DNMT1 maintains the proper DNMT1 level at different stages of cell cycle *i.e* promote DNMT1 degradation at the end of S phase or the beginning of G2 phase (Du et al., 2010b). Previous studies also reported that TIP60 mediated DNMT1 degradation can be facilitated by RGS6 (Regulator of G-protein signalling 6) to suppress Ras-induced cellular transformation (Huang et al., 2014), suggesting a tumour suppressor function of TIP60 by targeting DNMT1 for degradation.

Chapter 2: Objectives and Significance

2.1. The mechanism and the biological implications of E6 mediated TIP60 degradation

As discussed earlier, HPV E6 mediated destabilization of TIP60 was independent of E6AP. When I embarked onto this project, E6AP was the only E6 associated ligase identified. Thus, suggesting an interesting challenge of identifying the molecular mechanism that is utilized by HPV E6 to destabilize TIP60.

But why would these viruses destabilize TIP60, in particular high-risk HPVs. TIP60 has been implicated in apoptosis and cell cycle arrest through acetylation of p53. However, these viruses target p53 for degradation, suggesting a novel function of TIP60 in virus-induced cancers. Thus, I decided to investigate the biological implications of restoring TIP60 in virus-induced cancers.

2.2. The mechanism of TIP60 mediated inhibition of cancer metastasis

As discussed earlier, downregulation of TIP60 was correlated with cancer metastasis suggesting TIP60's role in inhibiting cancer metastasis. Thus I focused on investigating role of TIP60 in inhibiting cancer metastasis using both *in vitro* and *in vivo* models. Following which, I identify the molecular mechanism of TIP60 mediated inhibition of cancer metastasis.

Chapter 3: Materials and Methods

Cell lines: HeLa, MDA-MB-468 and HEK293T cells were cultured in Dulbecco's modified Eagle's medium high glucose (Sigma-Aldrich, Cat. NO. D5796) supplemented with 10% fetal bovine serum (Sigma-Aldrich, Cat. NO. F7524). Ca-SKI cells were grown in RPMI medium (HyClone, Cat. NO. SH30027.01) supplemented with 10% fetal bovine serum (Sigma-Aldrich, Cat. NO. F7524). MCF10A cells (ATCC CRL-10317^{TM}) were cultured in Dulbecco's modified eagle's media (DMEM)/F12 (1:1) media (Gibco, Cat. No. 11330-032) supplemented with 5% horse serum (Gibco, Cat.No. 16050-122), 20 ng/ml epithelial growth factor (Peprotech, Cat. No.AF-100-15), 0.5 mg/ml hydrocortisone (Sigma-Aldrich, Cat. No. H-0888), 100 ng/ml cholera toxin (Sigma-Aldrich, Cat. No. C-8052) and 10 μg/ml insulin (Sigma-Aldrich, Cat. No. I-1882). MDA-MB-231-luc-D3H2LN (PerkinElmer, Cat. No. 119369) cells were cultured in DMEM with high glucose (Sigma-Aldrich, Cat. No. D-5796), supplemented with 10% foetal bovine serum (Sigma-Aldrich, Cat. No. F-7524), 1 mM sodium pyruvate (Gibco, Cat.No. 11360-070) and 1% of 100× MEM non-essential amino acid solution (Sigma, Cat. No. M-7145). HCC1937 cells were cultured in DMEM with high glucose, supplemented with 10% fetal bovine serum and 1 mM sodium pyruvate. Cell cultures were incubated at 37ºC with 5% CO_2.

siRNA transfection: siRNAs target different genes were transfected using Lipofectamine RNAiMax reagent from Invitrogen/Life Technologies (Cat. No. 56532). The siRNA mixture used contained 15 μl Lipofectamine RNAiMax, 2 ml optimum media (Gibco, Cat. No. 31985-070) and 20 nM siRNA. The transfection mixture was incubated for 20 min at room

temperature and then 1×10^6 cells were seeded in a 10-cm plate together with the siRNA mixture. After 6 h, the transfection mixture was replaced by growth media. Cells were harvested 72 h after siRNA transfection.

Plasmids transfection: HeLa cells were transfected using calcium phosphate precipitation method. Briefly, 7×10^5 cells were seeded into 10-cm dish 16 hours before transfection. On the day of transfection, 10 μg total DNA were mixed with 190 μl TE buffer (10 mM Tris-HCL pH 8.0, 1 mM EDTA), 22 μl 2 mM $CaCl_2$ and 200 μl 2X HBS buffer (274 mM NaCl, 10 mM KCl, 1.4 mM Na_2HPO_4, 42 mM HEPES pH 7.05). After incubating in room temperature for 20 minutes, the DNA mixtures were added into cells drop by drop. Cells were harvested 24 hours after transfection. HEK293T cells were transfected using Lipofectamine 2000 reagent from Invitrogen/Life Technologies (Invitrogen/Life Technologies, Cat. No. 52887) following the manufactory protocol.

siRNA sequences: *siControl*: Forward: 5'-CGUACGCGGAAUACUUCGAdTdT-3'; Reverse: 5'-UCGAAGUAUUCCGCGUACGdTdT-3'. *siTIP60*: Forward: 5'-UGAUCGAGUUCAGCUAUGAdTdT-3'; Reserve: 5'-UCAUAGCUGAACUCGAUCAdTdT-3'. *siEDD1*: Forward: 5'-CAACUUAGAUCUCCUGAAAdTdT-3'; Reverse: 5'-UUUCAGGAGAUCUAAGUUGdTdT-3'. *siSNAI2* (Cat. No. sc-38393), *siDNMT1* (Cat.No.sc-35204) and *siDNMT3B* (Cat. No. sc-37759) were purchased from Santa Cruz Biotechnology.

Plasmids: pCDNA-β-Gal, pCDNA-16E6, shRNA constructs against control and EDD1 were kindly provided by Prof. Lawrence Banks (ICGEB, Trieste). MSCV-Flag-TIP60WT, MSCV-Flag-TIP60*WT, MSCV-Flag-TIP60*KD were generated in lab. *, siRNA resistant; KD, catalytic inactive form. pcDNA SNAIL2-MYC was purchased from Addgene. FUW-FLAG-DNMT1-E2A-mCherry-T2A was kindly provided by Prof. Daniel G Tenen (CSI, Singapore).

Mutagenesis: To generate siRNA-resistant wild-type or catalytically inactive TIP60, the siRNA binding sites were mutated by using QuikChange II XL Site-Directed Mutagenesis Kit (Agilent, Cat. No. 200522). The PCR primers used for mutagenesis: TIP60*: forward:

reverse: 5'-CCACTTTGGAGAGTTCgTAtgaaAAtTCaATtAGCAGCTTGCCGTAGCC-3'. TIP60KD: forward: 5'-CTGCCTCCCTACgAGCGCCGGGagTACGGCAAGCTG-3'; reverse: 5'-CAGCTTGCCGTActCCCGGCGCTcGTAGGGAGGCAG-3'.

Western analysis: Proteins were separated on SDS-PAGE gels, transferred onto nitrocellulose membranes (BioRad, Cat. No. 9004-70-0), and detected using a primary antibody against β-GAL (Promega, Cat. NO. Z37880, 1:10000), EDD1 (SantaCruz Biotechnology, Cat. NO. sc-9562, 1:500), ACTININ (SantaCruz Biotechnology, Cat. NO. 166524, 1:1000). β-ACTIN (SantaCruz Biotechnology, Cat.No. sc-81178, 1:1000), FIBRONECTIN

(SantaCruz Biotechnology, Cat. No. sc-8422, 1:500), EpCAM (Cell Signaling, Cat. No. 2626S, 1:1000), SNAIL2 (Cell Signaling, Cat. No. 9585S, 1:1000), FLAG (SantaCruz Biotechnology, Cat.No. sc-807, 1:1000), E-CADHERIN (BD Biosciences, Cat.No. 610182), DNMT1 (Abcam, Cat. No. 92314) and TIP60 rabbit polyclone antibody was generated in the lab.

Protein half-life examination: The half-life of TIP60 and DNMT1 are examined by cycloheximide (Sigma Aldrich, Cat. No. C7698) treatment. Briefly, 3.5×10^5 cells were seeded into 6-cm dishes 16 hours before treatment. On the day of treatment, 100 µg/ml cycloheximide were added into the media and cells were harvested after 0, 1 or 2 hours treatment for TIP60 and 0, 6, 12 hours treatment for DNMT1. Protein half-life was then examined by western blot.

Purification of mRNA: Total RNA was isolated using TRIZOL reagent (Invitrogen/Life Technologies, Cat No. 15596-026) following the manufacturer's protocol. RNA was dissolved in nuclease-free water for reverse transcription-PCR.

Reverse transcription and quantitative PCR: Complementary DNA (cDNA) was synthesised using iScript cDNA Synthesis Kit (Bio-Rad, Cat. No. 170-8891) according to manufacturer's protocols. Quantitative PCR (qPCR) was performed with primer sets corresponding to primer list table (**Table 1**) and using iTaq Universal SYBR Green Supermix (Bio-Rad, Cat. No. 172-5125) on an Applied Biosystems 7500 Fast Real Time PCR system. Results were analysed and are represented as fold change.

Table 1 Sequences of primers used for RT-qPCR

	Forward (5'-3')	Reverse (5'-3')
TIP60 endogenous	GGCTCAGACCAACTCCAAGG	TCCGGATCCCTTCTCACTGT
TIP60	AATGTGGCCTGCATCCTAAC	TGTTTTCCCTTCCACTTTGG
CDH1	TTACTGCCCCCAGAGGATGA	TGCAACGTCGTTACGAGTCA
EpCAM	GCTGGCCGTAAACTGCTTTG	ACATTTGGCAGCCAGCTTTG
VIM	CTGCCAACCGGAACAATGAC	CATTTCACGCATCTGGCGTT
SNAI1	TCTTTCCTCGTCAGGAAGCC	GATCTCCGGAGGTGGGATGG
SNAI2	CTCCTCATCTTTGGGGCGAG	CTTCAATGGCATGGGGGTCT
TWIST1	TCGGACAAGCTGAGCAAGATT	GCAGCTTGCCATCTTGGAGT
CDH2	CCGGTTTCATTTGAGGGCAC	TCCCTCAGGAACTGTCCCAT
FN1	AACCCTTCCACACCCCAATC	ACTGGGTTGCTGACCAGAAG
ZEB1	AGGATGACCTGCCAACAGAC	CTTCAGGCCCCAGGATTTCTT
ZEB2-1	CCCTGGCACAACAACGAGAT	AATTGCGGTCTGGATCGTGG
ZEB2-2	CCTCTGTAGATGGTCCAGTGA	GCGCTGAAGGTACTCCTCG
ACTIN	CCAGATCATGTTTGAGACCTTCAAC	CCAGAGGCGTACAGGGATAGC
GAPDH	CAGCCTCAAGATCATCAGCA	TGTGGTCATGAGTCCTTCCA
DNMT1	TACCTGGACGACCCTGACCTC	CGTTGCATCAAAGATGGACA
DNMT3B	GGCAAGTTCTCCGAGGTCTCTG	TGGTACATGGCTTTTCGATAGGA

Stable cell lines: Virus was generated by transfecting 5×10^6 293T cells with the plasmids [MSCV construct: i.e., MSCV vector control, TIP60 wild type (TIP60WT), siRNA-resistant TIP60 wild type (TIP60*WT), and siRNA-resistant catalytically inactive TIP60 (TIP60*KD); LPCX construct: i.e., LPCX vector control, TIP60 wild type (TIP60WT)] using Lipofectamine 2000 (Invitrogen/Life Technologies, Cat. No. 52887), as per manufacturer's protocol. Viruses were harvested after 72 h of transfection and were used to infect 1×10^6 MCF10A or HCC1937 or MDA-MB-468 or 2×10^6 MDA-MB-231-luc-D3H2LN cells or HeLa cells together with polybrene (Sigma-Aldrich, Cat. No. 107689) reagent (4 µg/ml). After 6 h, media containing the virus was replaced by growth media. After 24 h, puromycin was added into the growth media for selection. Media with antibiotics was changed every 48 h until the mock-transfected cells died. The cells were continuously selected for 2 weeks and for the creation of stable cell lines. EDD1 stably depleted [shRNA constructs: i.e. shTR2 (luciferase control) and shEDD1] HeLa cells and 293T cells were kindly provided by Prof. Lawrence Banks (ICGEB, Trieste). The list for stable cell lines is indicated in **Table 2**.

Table 2 List of stable cell lines generated.

MDA-MB-231-Luc-D3H2LN-MSCV	MM-Luc-MSCV
MDA-MB-231-Luc-D3H2LN-MSCV-FLAGTIP60WT	MM-Luc-FT60WT
MDA-MB-231-Luc-D3H2LN-MSCV-FLAGTIP60KD	MM-Luc-FT60KD
MCF10A-MSCV	M10MSCV
MCF10A-MSCV-FLAGTIP60WT	M10FT60WT

MCF10A-MSCV-FLAGTIP60*WT	M10FT60*WT
MCF10A-MSCV-FLAGTIP60*KD	M10FT60*KD
HCC1937-MSCV	HCC1937-MSCV
HCC1937-MSCV-FLAGTIP60WT	HCC1937-TIP60WT
HCC1937-MSCV-FLAGTIP60KD	HCC1937-TIP60KD
MDA-MB-468-MSCV	MM468-MSCV
MDA-MB-468-MSCV-FLAGTIP60WT	MM468-TIP60WT
MDA-MB-468-MSCV-FLAGTIP60KD	MM468-TIP60KD
HeLa-LPCX	HeLa-LPCX
HeLa-LPCX-TIP60	HeLa-TIP60
HeLa-shControl	HeLa-shControl
HeLa-shEDD1	HeLa-shEDD1
293T-shControl	293T-shControl
293T-shEDD1	293T-shEDD1
WT, wild type; KD, catalytic inactive; *, siRNA resistant	

Colony formation assay (CFA): 2×10^3 cells per well were seed in 6 well plates with media containing 5% FBS. After 2 weeks, the colonies were stained with Cristal Violet (Simga Aldrich, Cat. No. C3886) and quantified using Image J software (http://imagej.nih.gov/ij/).

Soft agar assays: 12 well plates were coated with bottom agar [2X DMEM supplemented with 20% FBS and 1% agar (BioRad, Cat. No. 161-3111) 1:1 mixture]. Then 1×10^3 cells were mix with upper agar (2X DMEM supplemented with 20% FBS and 0.8% agar 1:1 mixture) and seeded onto the bottom agar. Plates were incubated at 37 ℃ with 5% CO2 for 2 weeks. The colonies were stained with Giemsa stain and quantified using Image J software.

***In vivo* mice experiment**: NOD.Cg-Prkdcscid Il2rgtm1Wjl/SzJ (NSG) mice were obtained courtesy of Chan Shing Leng (National University of Singapore). HeLa-LPCX or HeLa-TIP60 cells were suspended in 100 µl of serum-free DMEM medium at a concentration of 1×10^5 cells/ml, or 1×10^6 cells/ml supplemented with BD Matrigel matrix (BD Biosciences, Cat. No. 354234), and were injected subcutaneously into the right or left flank of NSG mice. Tumours were excised and total tumour weight recorded. All animal studies were done according to approved protocols by the NUS Institutional Animal Care and Use Committee (IACUC), Singapore.

***In vitro* invasion assay**: *In vitro* invasion assay was performed as described previously (Korah et al., 2000) using the BD Matrigel[TM] Invasion chamber and 24-well plate 8.0 Micron insert (BD Biocoat[TM], Cat. No. 354480). Briefly, 50,000 MM-Luc-MSCV, or MM-Luc-FT60WT cells were seeded onto the top layer of the chamber and mixed with serum-free media. The bottom layer was filled with 750 µl growth media comprising 2% foetal bovine serum. After 8 h, cells that had invaded into the bottom layer were stained and quantitated using ImageJsoftware (http://imagej.nih.gov/ij/).

Wound-healing assay: Wound-healing assays were performed as described previously (Chen et al., 2012; Oxmann et al., 2008). Briefly, siRNA-transfected (*siControl, siTIP60, siDNMT1,siTIP60/siDNMT1, siSNAI2* and *siTIP60/siSNAI2*) MCF10A cells or the stable metastatic breast cancer cell line was seeded into the wells of 24-well plates at 100% confluence. Cells were then maintained in complete media for another 12 h for adhesion. Cells were then subjected to serum-starved conditions for next 24 h. A wound was created using a fine pipette tip and the detached cells were removed by gently washing the wells with phosphate-buffered saline. The closure of wound was monitored every 24 h. For MCF10A, HCC1937 and MDA-MB-468 cells, the area of the wound was measured at 0 h and the percentage of movement was calculated by using the following formula: (area of wound at 0 hours – area of wound at n hours) / area of wound at 0 hour $\times$ 100, where n is a specific time. For MDA-MB-231-luc-D3H2LN, the number of cells migrated during gap healing were counted. Each experimental group was repeated three times.

Immunofluorescence: MCF10A cells were transfected with *siControl* and *siTIP60* as described above and were grown on a cover slide, fixed with 3.7% paraformaldehyde (Sigma-Aldrich, Cat. No. P-6148), and incubated with E-CADHERIN (BD Biosciences, Cat. No. 610182, 1:500), β-CATENIN (BD Biosciences, Cat. No. 610153, 1:500) or FLAG (Santa Cruz Biotechnology, Cat.No. sc-807, 1:500) primary antibodies. Secondary antibodies used were Alexa Fluor 488 donkey anti-rabbit IgG (H+L) (Invitrogen/Life Technologies, Cat. No. A21206, 1:500) and Alexa Fluor 594 donkey anti-mouse IgG (H+L) (Invitrogen/Life Technologies, Cat. No. A21203, 1:500).

Chromatin immunoprecipitation quantitative PCR (ChIP-qPCR): ChIP was performed as described earlier (Jha et al., 2010; Karnani et al., 2007). Briefly, 5×10^6 cells were transfected with *siControl* or *siTIP60* in a 15-cm plate. After 72 h of siRNA treatment, cells were cross-linked with 1% formaldehyde (SantaCruz Biotechnology, Cat. No. sc-203049A) for 10 min at room temperature, and then washed twice with ice-cold phosphate-buffered saline. Cells were harvested by scraping and centrifuged at 1750 *g* for 15 min to collect the cell pellet. Cells were then resuspended in SDS lysis buffer (1% SDS, 0.01 M EDTA and 0.05 M Tris-HCl, pH 8.0) and sonicated (ON: 15 sec and OFF: 45 sec at 30% amplitude for 15 cycles) to obtain DNA fragments ranging from 100 to 500 bp. Chromatin was isolated by centrifuging at 15300 *g* for 15 min at 4ºC and the supernatant was collected for immunoprecipitation.

Immunoprecipitation was performed with anti-SNAIL2 antibody (Cell Signaling, Cat. No. 9585) or anti-DNMT1 antibody (Abcam, Cat. No. ab87656) overnight at 4°C, followed by incubation with protein A/G PLUS agarose beads (SantaCruz Biotechnology, Cat. No. sc-2003) for 3 h. Beads were then washed with (i) low-salt immune complex buffer (0.1% SDS, 1% TritonX-100, 0.002 M EDTA, 0.02 M Tris-HCl, pH 8.0, and 0.15 M NaCl), (ii) high-salt immune complex buffer (0.1% SDS, 1% Triton-X-100, 0.002 M EDTA, 0.02 M Tris-HCl, pH 8.0, and 0.5 M NaCl), (iii) LiCl buffer (0.25 M lithium chloride, 1% NP40, 0.001 M EDTA, 0.01 M Tris-HCl, pH 8.0, and 1% deoxycholate) and (iv) TE buffer (0.001 M EDTA and 0.01 M Tris-HCl, pH 8.0). Beads were eluted in 100 µl elution buffer (1% SDS and 0.0084% NaHCO$_3$) three times with agitation for 15 min each. Chromatin was reversed

cross-linked by adding 0.2 M NaCl and was heated at 65ºC for 4 h. The proteins bound to DNA were digested by adding 20 µg proteinase K (AppliChem, Cat. No. 39450-01-6) and incubated at 45ºC for 1 h. DNA was purified using a PCR purification kit (QIAGEN, Cat. No. 28106) and used as template for qPCR. The results were analysed and are represented as percent input. **Table 3** shows the sequence information for the primers used for qPCR (Stanisavljevic et al., 2011).

Table 3. Sequences of primers used for ChIP-qPCR. Red are the primer sets used in Figure 31, Figure 32 and Figure 39.

	Forward (5'-3')	Reverse (5'-3')
FN11	TATTTTATGGGTTTTCTTCCT	AGCGGCTGGGAGGAAAGGGAG
FN12	GGAGCCCGGGCCAATCGGCG	TGTGCAGCACAGCCGGCGCGG
FN13	TCCTTCCCCCAGAATCAATGAA	GGGAAGCCGAGTGTTTCTTCC
FN14	GTTGAGACGGTGGGGGAGAGA	CCGTCCCCTTCCCCA
EpCAM1	TTTAGTAGAGACAGGTTTTCA	TTTTATGTTTTAATTGTGAAT
EpCAM2	CGGGTGTGGTGGTGGGCGCCT	CCACCACACCCGGCTGATCCA
EpCAM3	AAGCCACAATAACCAGTTAGT	GGCAACAAGAGCGAAACTCCG
EpCAM4	TTTTATTTTTTGAGATGGAGT	TGGTGAAACCCATCTCAACTA
EpCAM5	TATGAAGTATTTATAATTATT	TAGAGCCAAATACTGAGAACC
EpCAM6	CTAATTTTGTATCTTTTAGTA	TTTTCGTTTTCATAAGCATTT
EpCAM7	GTTCTGGAAGGTTCTCTGCCT	CCATGGCGGCGTTAGGGATCT
EpCAM8	CACCAGCGGCCAGAGGTGAGC	GCGCGAGGCCTGGGGCACGCG
EpCAM promoter	TGGAAGGTTCTCTGCCTGTG	TCCTTTTAACCGGAGGAGCG
EpCAM 1st intron	AAACGGGCATAATAGGGAGGG	CGAGCAAAGCTGCGAAGTGA

DNA methylation analysis using bisulphite pyrosequencing: DNA methylation analyses were performed as described previously (Mikeska et al., 2011). Briefly, DNA was bisulphite converted using EpiTect Fast DNA bisulfite kit (Qiagen) according to the manufacturer's protocol. Prior to pyrosequencing, PCR reactions were carried out using PyroMark PCR kit (Qiagen) in a 50 µl reaction volume (PCR primers used: promoter region: forward: GAAGGTTTTTTGTTTGTGTTTGTAT; reverse: [Btn]ACCCTCTCCACAAATATAAACC. 1st intron region: forward: GGGTATAATAGGGAGGGGATTAAG; reverse: [Btn] CCAAAACCATTTCCCTACCAA; Btn, biotin). An initial polymerase activation step of 15 min at 95°C was followed by 40 cycles of 30 s at 94°C, 30 s at 56°C and 30 s at 72°C, and a final step of 5 min at 72°C. The biotinylated PCR products were extracted with streptavidin sepharose beads (GE Healthcare) according to the manufacturer's instructions and released into a PSQ 96 Low Plate (Biotage) containing 40 µl pyrosequencing primer (promoter region: GAGACGAAGTATTTGGGG; 1st intron region: GGGAGGGGATTAAGA) which has been diluted with annealing buffer to a final concentration of 0.4 µM. The plate was incubated at 80°C for 2 min, cooled to room temperature and run on a PyroMark ID machine (Biotage) using PyroMark Gold reagents (Qiagen) as specified by the manufacture. Results were analyzed with PyroMark software for DNA methylation quantification.

Co-immunoprecipitation (**co-IP**): 5 µg of pcDNA-SNAIL2-MYC and 5 µg of FUW-FLAG-DNMT1-E2A-mCherry-T2A were co-expressed in 293T cells. FLAG-DNMT1 was immunoprecipitated using FLAG-M2 agrose beads

(Sigma Aldrich, Cat. No. A2220) and associated SNAIL2-MYC was probed using SNAIL2 antibody indicated above. Untransfected 293T cells serves as transfection control and 293T cells overexpressed SNAIL2-MYC alone serves as IP control.

Bioluminescence assay in mice: Tail-vein injection was performed as described previously (Liang et al., 2005; Yang et al., 2012b). Briefly, 6-week-old NOD/SCID mice (Invivos, Singapore) were divided into three groups with four mice per group. Each mouse received a tail-vein injection of 5×10^5 MM-Luc-MSCV or MM-Luc-FT60WT or MM-Luc-FT60KD cells, and images were taken every 7 days after injection using IVIS 200 Pre-clinical *in vivo* Imaging System. All protocols for animal studies were reviewed and approved by the Institutional Animal Care and Use Committee at the National University of Singapore. Analyses of the images were performed as described previously (Craft et al., 2005; Wu et al., 2001) using Living Image software (IVIS imaging system).

Data preprocessing of Affymetrix microarray gene expression: Data processing of microarray gene expression of breast cancer samples is described elsewhere (Kumar et al., 2013). Briefly, 26 breast cancer cohorts on Affymetrix U133A or U133Plus2 were downloaded from Gene Expression Omnibus (GEO) and Array Express. Robust Multichip Average (RMA) normalisation was performed on each cohort and, the normalised data was standardised using ComBat (Johnson et al., 2007) to remove batch effects. The standardised data yielded a dataset of 3,992 breast cancer tumours, and 22 normal breast tissue samples.

Identification of breast cancer subtypes: Breast cancer subtype signature was obtained from the study by Prat et al. (2010) (Prat et al., 2010). Subsequently, single sample Gene Set Enrichment Analysis (ssGSEA) (Verhaak et al., 2010) was performed to estimate enrichment scores for the six breast cancer subtype signatures (Basal, Claudin-Low, Luminal-A, Luminal-B, ERBB2+, and Normal-like) expressed in each sample. Each sample was then assigned a subtype depending on the ssGSEA enrichment score.

Statistical analysis: Statistical significance evaluations were computed by Mann–Whitney test, Spearman Correlation Coefficient, log-rank test of Graphpad Prism® ver 5.04 and two sample two tailed student t-test. Error bars represent the standard deviation from at least three times experiments.

Chapter 4

TIP60 functions as a tumour suppressor in HPV-induced cervical cancer and is degraded by HPV E6 through ubiquitin proteasome system

4.1 Overexpressing TIP60 inhibits tumour growth

TIP60 is a tumour suppressor and is a transcriptional repressor of E6 expression. Therefore, I reasoned that gain-of-function of TIP60 might antagonize E6 mediated cellular growth and thereby inhibit tumour cell growth in HPV-induced cervical cancer cells. To address this, I used retroviral system to generate HeLa cells (**Figure 6A**) stably overexpressing FLAG-TIP60. I then characterized the growth ability of HeLa-TIP60 cells *in vitro* by colony formation assay. HeLa-LPCX vector control or HeLa-TIP60 expressing cells were seeded at very low density (2×10^3/per well in 6 well plate) for colony formation assays and maintained in antibiotic selection. After two weeks the colonies were fixed, stained and quantified. Representative images in **Figure 6B** and the quantifications in **Figure 6C** show that overexpression of TIP60 inhibited the ability of HeLa cells to form colonies by over 70%. Further, I questioned whether this phenomenon is due to the inhibition of E6 function. To address this, I overexpressed either pcDNA vector alone or pcDNA HPV18 E6 in HeLa-LPCX and HeLa-TIP60 cells (**Figure 6D**). Interestingly, I found that in vector control cells, overexpressing TIP60 decreases E6 endogenous level, which suggests that TIP60 might decrease HeLa cells colony formation ability through downregulating expression of E6. Then I performed colony formation assay, in **Figure 6B** and **Figure 6C**, I observed that by overexpression of E6 in HeLa-TIP60 cells

significantly rescued the colony formation when compared with vector control and there was no change in colony formation of HeLa-LPCX cells overexpressing E6 compared with vector control. These data suggested that TIP60 inhibits colony formation *in vitro* through antagonizing E6.
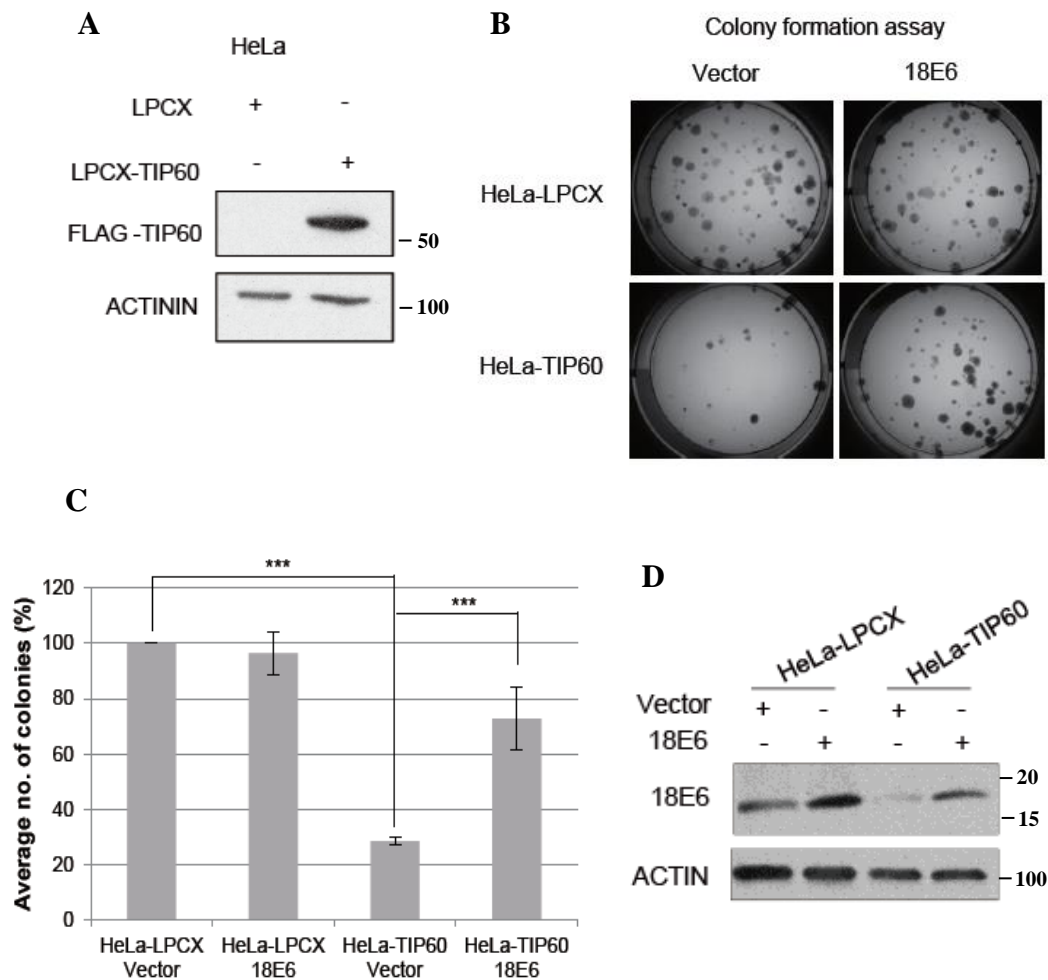
Figure 6. Overexpressing TIP60 inhibits colony formation of HeLa cells *in vitro* and HPV 18 E6 rescues the growth defect in HeLa-TIP60 cells.

(**A**) Western blot analysis confirming retroviral-induced TIP60 expression in HeLa-TIP60 cells. (**B**) Representative images from the CFA performed in HeLa stable cells indicated in **D**. (**C**) Bar graph represent the results obtained from quantifications of at least three independent experiments. Quantifications were performed using Image J software; error bars represent the standard deviation. Significance is represented as ***$p<0.001$. (**D**) HeLa-LPCX or HeLa-TIP60 cells were transiently transfected with indicated plasmids and western blotted for indicated antibodies.

Based on the *in vitro* results, I wanted to investigate this strong phenotype of TIP60 on cellular growth *in vivo.* NOD.Cg-Prkdcscid Il2rgtm1Wjl/SzJ (NSG) mice were subcutaneously injected with 1×10^6 HeLa-LPCX cells on the left and 1×10^6 HeLa-TIP60 cells on the right. Tumour sizes were measured every week. After seven weeks, the mice were sacrificed and the tumours were excised. The representative images from **Figure 7A**, **B** and quantifications from **Figure 7C** shows that the tumours induced by HeLa-LPCX cells were significantly reduced by 80% with TIP60 overexpression. I was then highly interested in verifying the TIP60 expression in these tumours. The total protein from the tumour tissue was extracted and western blotted with anti-FLAG antibody to detect overexpressed TIP60. As shown in **Figure 7D** anti-FLAG band corresponding to TIP60 was detected only from tumours induced by HeLa-TIP60 cells and not in the control. Mice from all the repeats are shown in **Figure 8**.
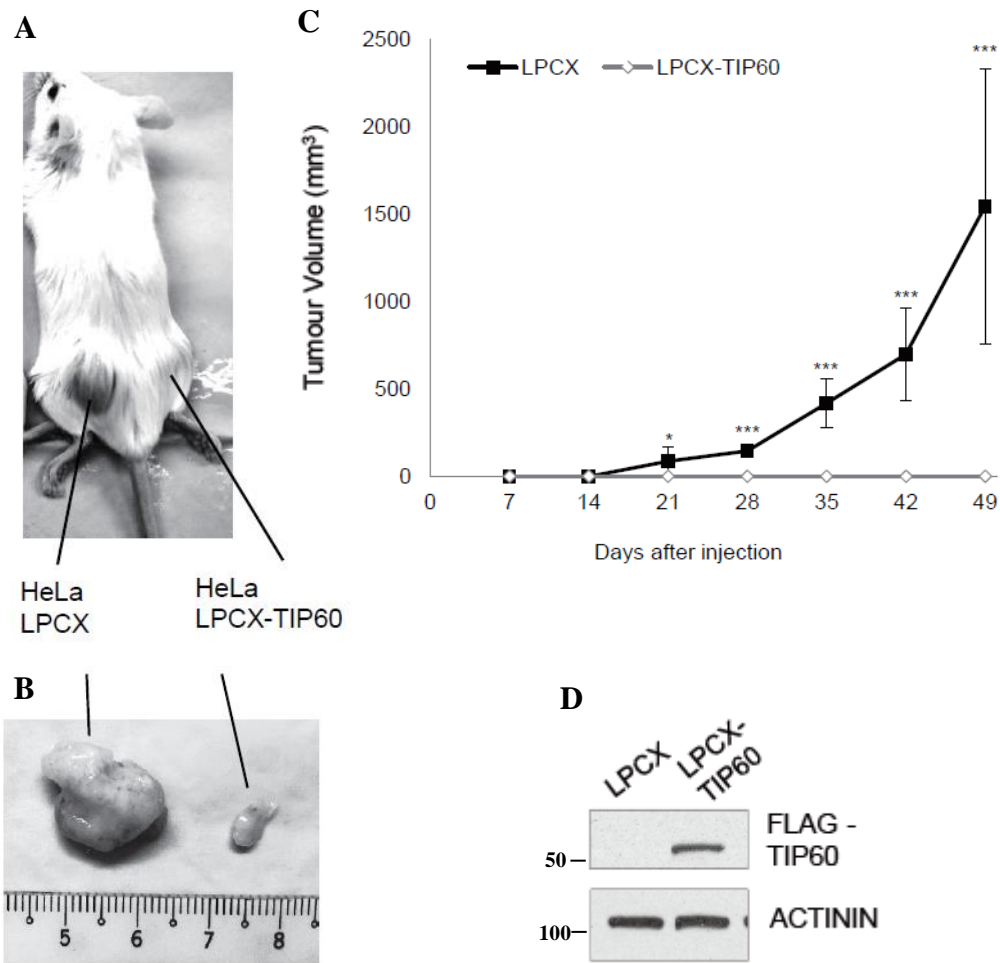
Figure 7. Overexpressing TIP60 inhibits tumour growth *in vivo*.

(**A**) Representative images of the mice subcutaneously injected with HeLa LPCX and HeLa LPCX-TIP60 cells on the left and the right side, respectively. (**B**) Images showing the difference in sizes of tumour obtained from HeLa LPCX and HeLa-TIP60 cells. (**C**) Graph showing tumour growth monitored in six mice at indicated times. The graph is represented in volume (mm^3) calculated using the formula: Volume (V)=Width (W)(2) × Length (L)/2. Error bar represented the standard deviation from six mice. Statistical significance was performed using student t-test and is represented as *, $p<0.05$; ***, $p<0.001$. (**D**) Protein isolated from tumours was analyzed by western blot using anti-FLAG antibody.
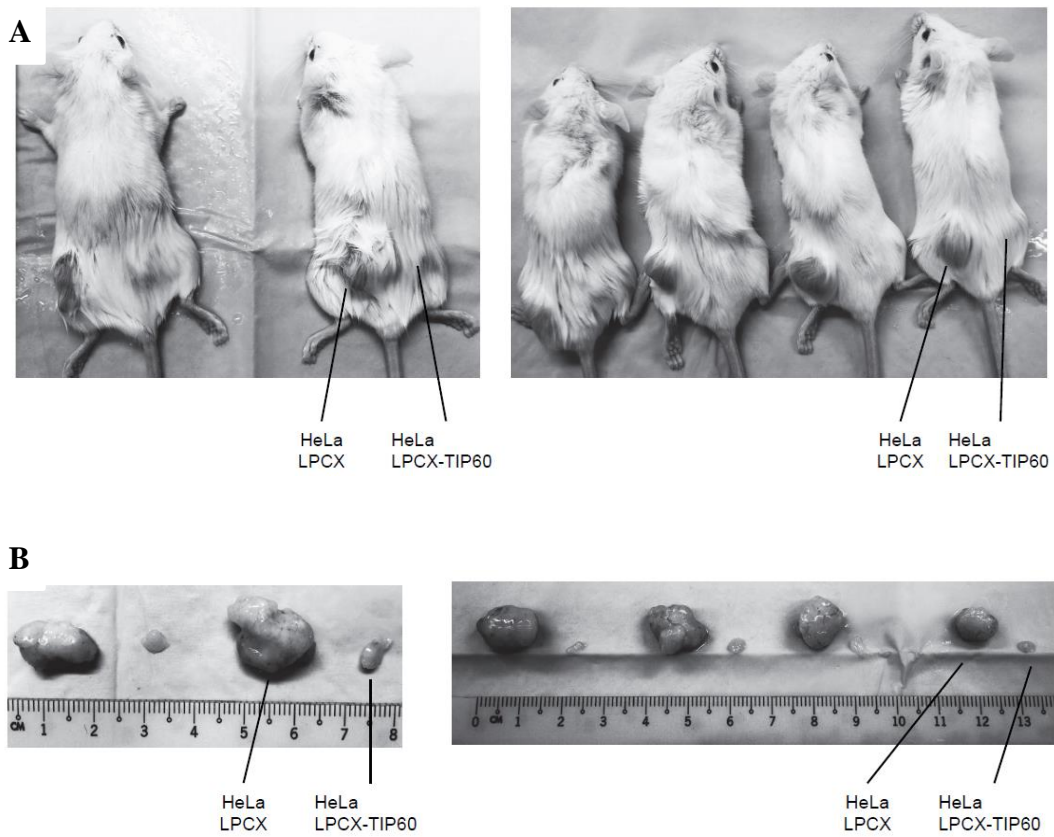
Figure 8. Mice (n=6) used in the *in vivo* experiment shown in **Figure 7**.

Overexpressing TIP60 inhibit tumour growth *in vivo*. (**A**) Representative images of the mice subcutaneously injected with HeLa LPCX and HeLa LPCX-TIP60 cells on the left and the right side, respectively. (**B**) Images showing the difference in sizes of tumour obtained from HeLa LPCX and HeLa LPCX-TIP60 cells.

4.2 HPV E6 utilizes E3 ubiquitin ligase EDD1/UBR5 to regulate TIP60 protein turn over

From mass spectrometry analyses of TIP60 interacting proteins, Dr. Vanitha Krishna Subbaiah identified E3 ubiquitin ligase EDD1/UBR5 as an interacting partner of TIP60 (data not shown). Therefore, I hypothesized that EDD1 might regulate the protein stability of TIP60. To investigate this, two stable cell lines were generated: HeLa shcontrol which served as control and HeLa shEDD1 which stably depleted EDD1 (**Figure 9**). Interestingly, depletion of EDD1 increased TIP60 protein level (**Figure 9A**) but not TIP60 mRNA level (**Figure 9B**), suggesting that EDD1 might regulate TIP60 level through regulating its protein stability. Then HeLa shcontrol or shEDD1 cells were treated with cyclohexamide (CHX) for indicated time point to block protein synthesis. The residual levels of endogenous TIP60 were then determined using anti-TIP60 antibody (**Figure 10A**). The quantification was shown in **Figure 10B**. Within 2 hours of CHX treatment, TIP60 protein stability increased by 60% upon depleting endogenous EDD1.

Based on these results, I decided to ascertain the effects of HPV E6 on TIP60 levels in the absence of endogenous EDD1. For this, we generated 293T cells stably expressing shEDD1, and depletion of EDD1 was confirmed by western blot (**Figure 11A**). In these stable cells, FLAG-TIP60 was transfected either in combination with pcDNA vector or pcDNA-HPV18 E6 and the total cellular lysates were analyzed by western blot (**Figure 11B**). Cyclohexamide treatments for indicated time points were performed in these transfected cells. Western blot was shown in **Figure 10C** and quantification in **Figure 11D**, **E**. From this experiment, I observed that depleting EDD1

stabilizes TIP60 also in 293T cell (**Figure 11C, D**). Additionally,

overexpressing HPV18 E6 destabilized TIP60 (**Figure 11C**). Furthermore, the

decreased protein stability of TIP60 caused by overexpressing E6 was rescued

by depleting EDD1 (**Figure 11C, E**). These results suggest that EDD1 co-

operates with E6 in destabilizing TIP60.
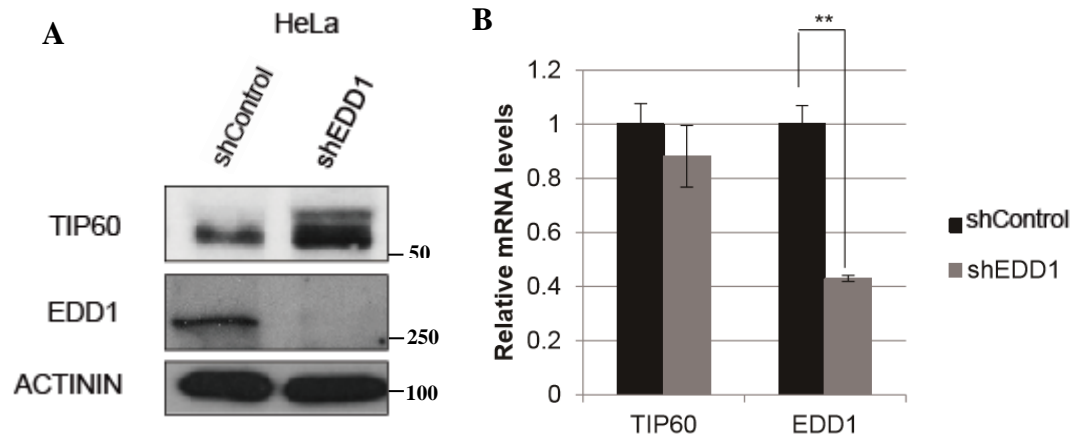
Figure 9. EDD1 regulates TIP60 at protein level but not at mRNA level.

(**A**) HeLa cells stably overexpressing either shcontrol or shEDD1 shRNA. Western blot using indicated antibodies shows a depletion of EDD1 and increase of TIP60 protein level. (**B**) Verification of the expression of EDD1 and TIP60 in HeLa shcontrol and HeLa shEDD1 cells at mRNA level using qPCR. EDD1 expression decreases significantly whereas expression of TIP60 does not change. Error bars represent standard deviation from at least three independent experiments. Statistical significance is represented as **, $p<0.01$.

A

B
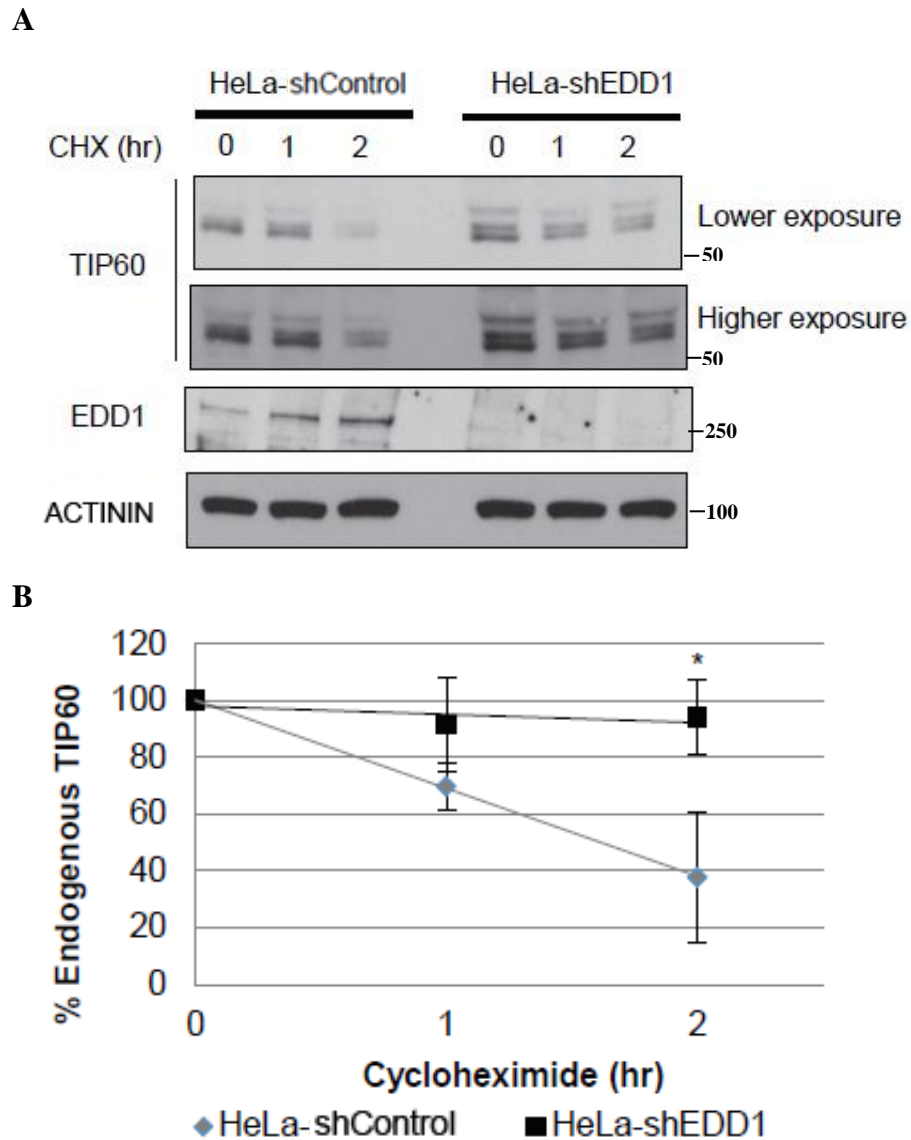
Figure 10. EDD1 regulates the stability of endogenous TIP60 in HPV-positive cells.

(**A**) HeLa-shcontrol and HeLa-shEDD1 cells were treated with 100 μg/ml of cycloheximide for indicated times, to inhibit RNA translation. The cellular lysates were probed with indicated antibodies. (**B**) Graph represents results from at least three independent cycloheximide treatment experiments performed in HeLa-shcontrol and HeLa-shEDD1 cells. The band intensities were quantified using Image J software. TIP60 levels were normalized to 100% at time zero. Error bar indicates the standard deviation from at least three independent experiments. Statistical significance was performed using student t-test and represented as *, $p<0.01$.

A

293T

shControl shEDD1

250 — | EDD1

100 — | ACTININ

B

293T

shControl shEDD1

Vector 18E6 Vector 18E6

20 —
15 — | 18E6

150 — | β GAL

C

293T

shControl | shEDD1

FLAGTIP60 | FLAGTIP60 | FLAGTIP60 | FLAGTIP60
+Vector | +18E6 | +Vector | +18E6

CHX (hr) 0 1 2   0 1 2   0 1 2   0 1 2

FLAG-TIP60 ——————————————————— — 50

β GAL ——————————————————— — 150

D

293T FLAG -TIP60 + Vector

♦ shControl ▲ shEDD1

% Exogenous TIP60

*

Cycloheximide (hr)

E

293T FLAG -TIP60 + 18E6

● shControl ■ shEDD1

% Exogenous TIP60

**

Cycloheximide (hr)
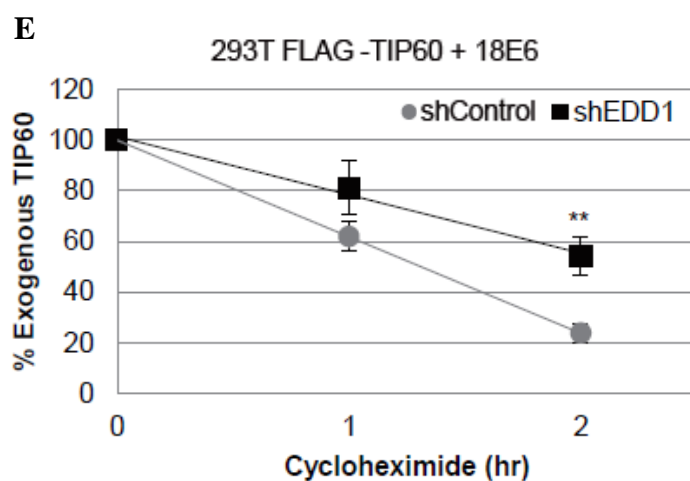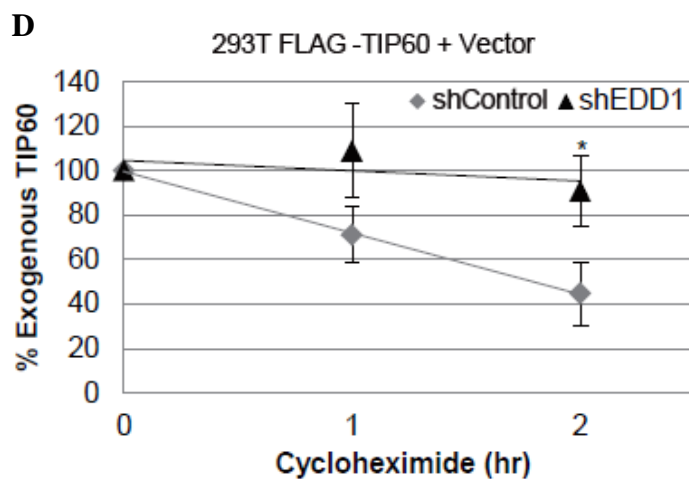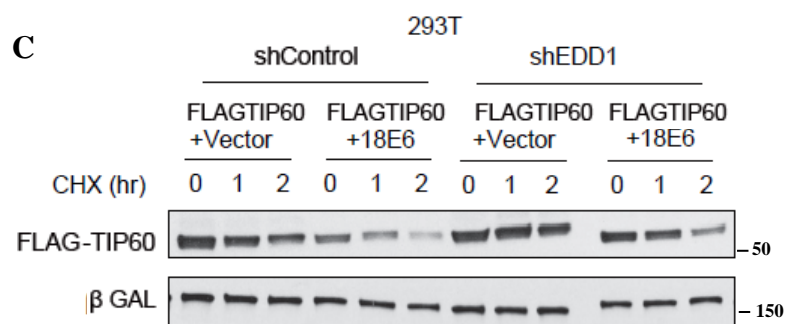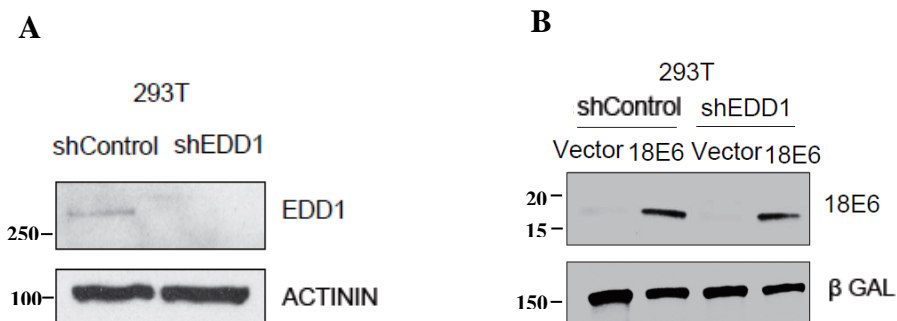
Figure 11. HPV 18 E6 utilized EDD1 to destabilize TIP60.

(**A**) Validation of 293T shEDD1 stable cell lines. (**B**) Overexpression of either vector or HPV18 E6 in 293T shControl and shEDD1 cells. Total cell lysates were probed with HPV18 E6 antibody to validate the expression. (**C**) Transfected cells from **B** were transfected along with FLAG-TIP60. After 24 h, cells treated with 100 μg/ml of cycloheximide for indicates times and the cellular lysates were probed with FLAG antibody to examine the stability of FLAG-TIP60. (**D** and **E**) Graph represented results from at least three independent cycloheximide treatment experiments. The band intensities were quantified using Image J software. FLAG-TIP60 levels were normalized to 100% at time zero. Error bar represented the standard deviation. Significance is represented as *, $p<0.05$; **, $p<0.01$.

4.3   Depleting EDD1 stabilizes TIP60 and inhibit tumour growth

As EDD1 destabilizes TIP60, I wanted to investigate whether stable depletion of endogenous EDD1 could result in a similar phenotype as observed with HeLa LPCX-TIP60 stable cells. To study this, I performed the *in vitro* and *in vivo* experiments as perform earlier with HeLa LPCX and HeLa LPCX-TIP60 cells.

In *in vitro* assay, I tested the ability of HeLa shControl and shEDD1 cells to form colonies using colony formation assay. The representative images in **Figures 12A** and quantification in **Figure 12B** show that loss of EDD1 (HeLa shEDD1) significantly inhibits the colony formation ability of HeLa cells similar to HeLa-TIP60 cells and this was TIP60 dependent, as depletion of TIP60 by shRNA rescued the inhibition on colony formation.

In the *in vivo* assay, I tested the tumour growth ability of HeLa shControl and shEDD1 cells in mice. To do so, 1×10^5 cells of both HeLa shcontrol (on the left side) and HeLa shEDD1 (on the right side) cells were injected subcutaneously into the mice. The tumour size was measured at 7-day intervals over a period of 5 weeks. The representative images (**Figure 13A** and **B**) and quantifications (**Figure 13C**) show that the tumours induced by HeLa shcontrol cells were significantly reduced when stably ablating endogenous EDD1 expression, suggesting the biological importance of TIP60's regulation by EDD1. The knockdown of EDD1 and stabilization of TIP60 in the tumours were verified by western blot analysis (**Figure 13D**). Mice from all repeats are shown in **Figure 14**.

A

B
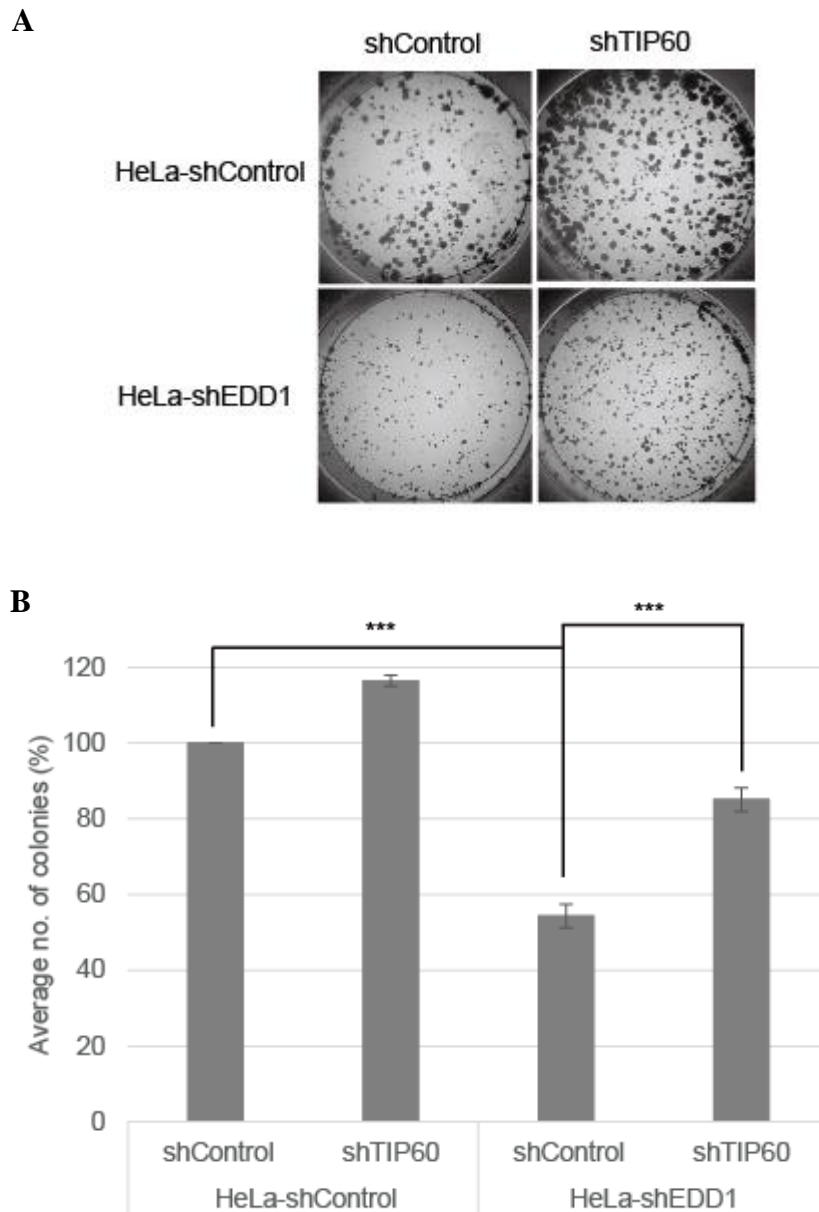
Figure 12. Inhibition of colony formation *in vitro* by depleting EDD1 is dependent on TIP60.

(**A**) Representative images from CFA on HeLa shControl and shEDD1 cells transfected with either shControl or shTIP60 construct. (**B**) Quantifications of at least three independent experiments. Quantifications were performed using Image J software; error bar representative the standard deviation. Significance is represented as ***$p<0.001$.
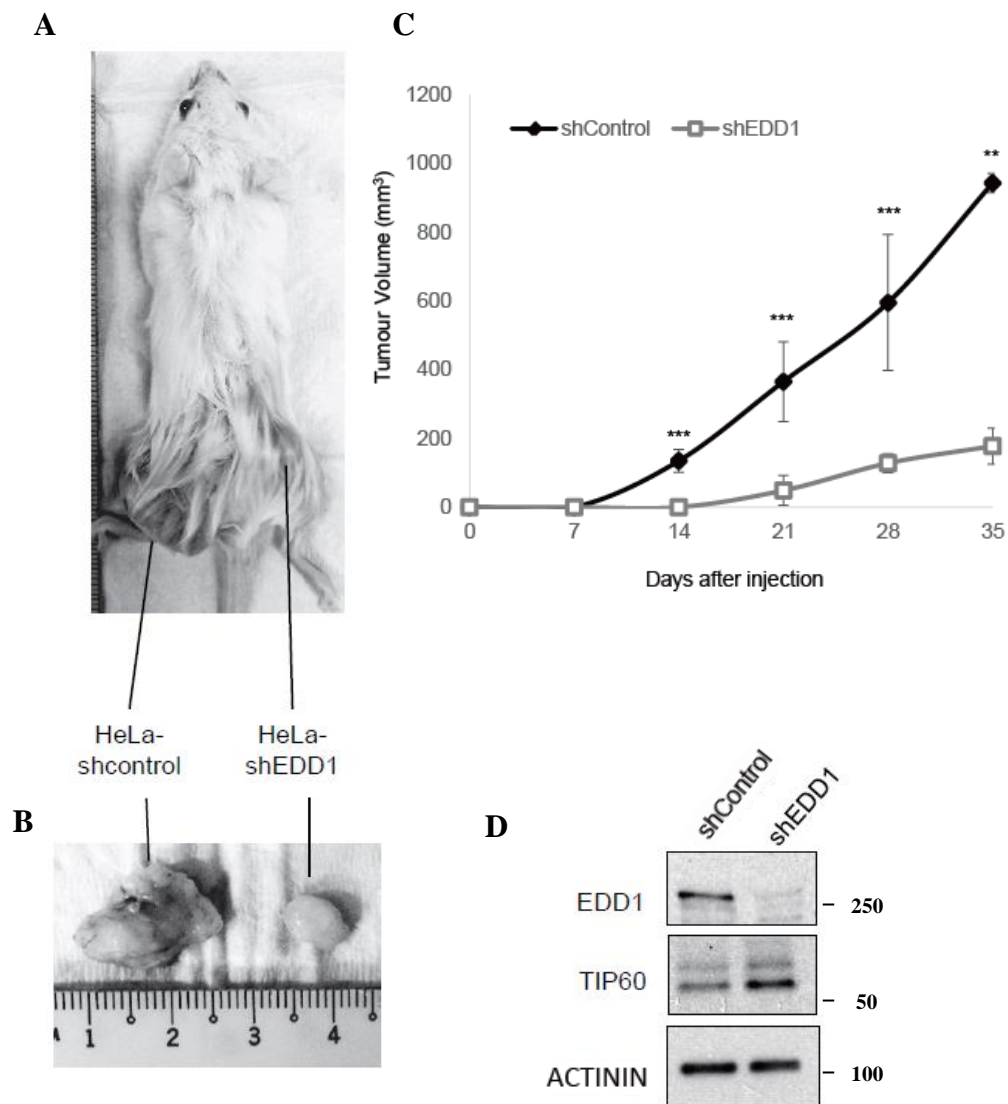
Figure 13. Depletion of EDD1 stabilizes TIP60 and inhibits tumour growth *in vivo*.

(**A**) Representative images of the mice subcutaneously injected with HeLa shControl and HeLa shEDD1 cells on the left and the right side, respectively. (**B**) Images showing the difference in sizes of tumour obtained from HeLa shControl and HeLa shEDD1 cells. (**C**) Graph showing tumour growth monitored in six mice at indicated times. The graph is represented in volume (mm^3) calculated using the formula: Volume (V)=Width (W)(2) × Length (L)/2. Error bars represent the standard deviation from six mice. Statistical significance was performed using student t-test and represented as **, $p<0.01$; ***, $p<0.001$. (**D**) Protein isolated from tumours injected with HeLa shControl and HeLa shEDD1 cells was analyzed by western blot using indicated antibodies.
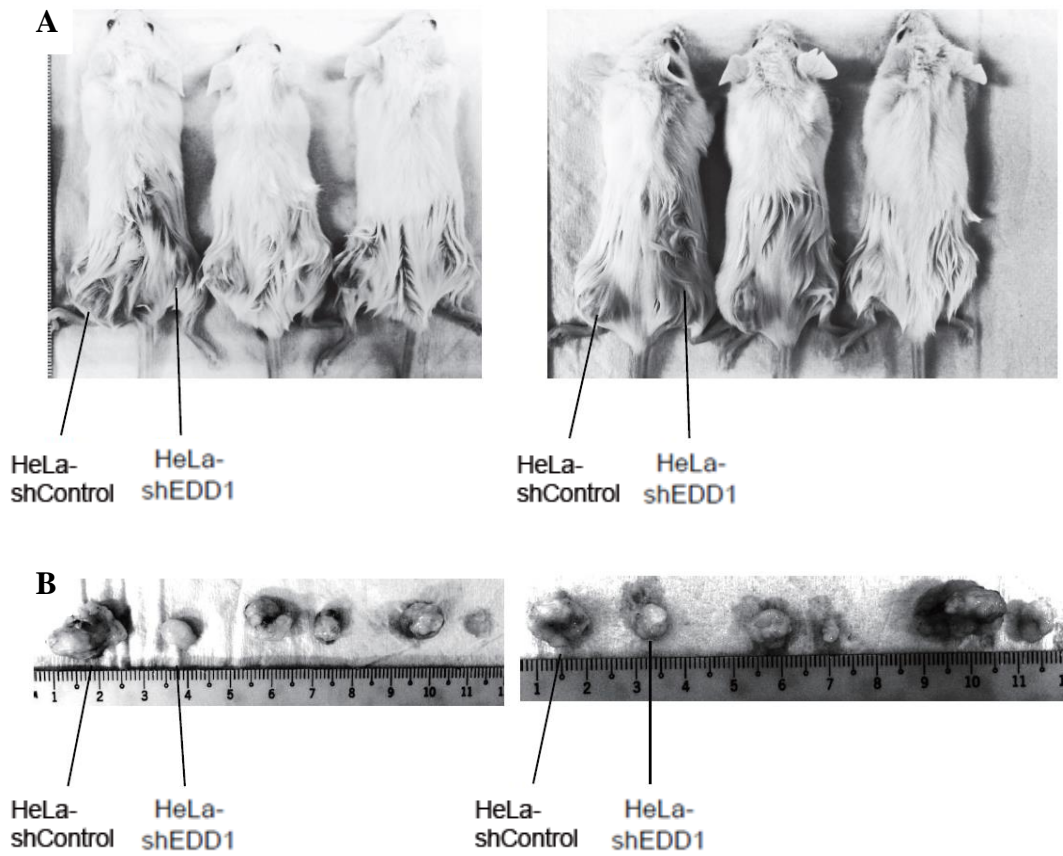
Figure 14. Mice (n=6) used in the *in vivo* experiment shown in **Figure 13**.

Depletion of EDD1 inhibits tumour growth *in vivo*. (**A**) Representative images of the mice subcutaneously injected with HeLa shControl and HeLa shEDD1 cells on the left and the right side, respectively. (**B**) Images showing the difference in sizes of tumour obtained from HeLa shControl and HeLa shEDD1 cells.

4.4 TIP60 acts as an inhibitor of cell migration in cervical cancer

I have demonstrated that restoring TIP60 levels either by overexpressing or by depleting EDD1 results in decreased growth. In addition to suppression of growth, I was interested in to investigating whether TIP60 is capable of inhibiting cancer metastasis as ability of cells to migrate and invade distant organ is huge problem in treatment of cancer. In order to characterize this, a preliminary wound-healing assay was performed using HeLa-LPCX and HeLa-TIP60 cells. A 40% decrease in cell migration was observed; suggesting that overexpression of TIP60 inhibits cell migration in HeLa cells (**Figure 15**).
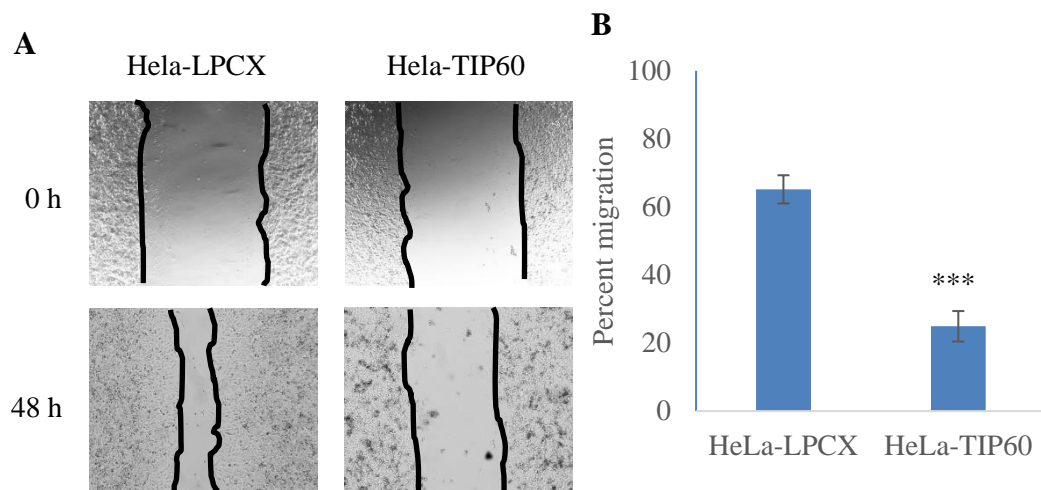
Figure 15. TIP60 inhibits cervical cancer cell migration *in vitro*.

Wound-healing assays were performed using HeLa-LPCX and HeLa-TIP60 cells. Representative images are shown in (**A**) and the quantitation in (**B**). ***, $p < 0.001$.

In order to further investigate the molecular mechanism of TIP60 mediated inhibition of cell migration, I decided to use breast cancer models which both metastatic and non-metastatic models.

Chapter 5

TIP60 inhibits cancer metastasis of breast cancer

As mentioned in Chapter 1, TIP60 expression level negatively correlated with cancer malignancy. A more comprehensive study screening expression of TIP60 in several breast cancer cell lines revealed that TIP60 level decreased in highly metastatic breast cancer cells compared to mild metastatic cells (**Figure 16**) (Pandey et al., 2015). This suggested that TIP60 might inhibit cancer metastasis of breast cancer.
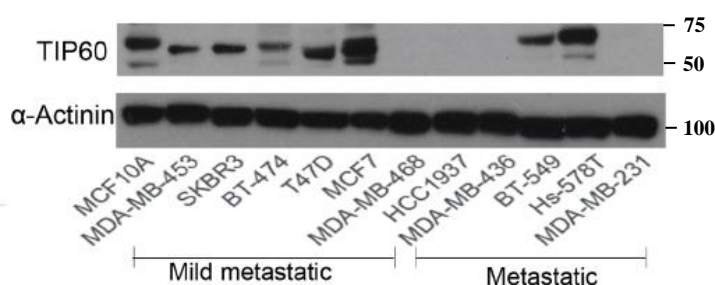
Figure 16. TIP60 protein levels in different breast cancer cell lines (Pandey et al., 2015).

5.1   Overexpressing TIP60 inhibits cell migration and invasion

To identify the role of TIP60 as an inhibitor of EMT, I overexpressed TIP60 in a highly metastatic triple negative breast cancer cell line (MDA-MB-231), and depleted TIP60 in non-tumourigenic breast epithelial cells (MCF10A). Wound-healing and Boyden chamber assays were used to score for migration and invasion potential in each of these two scenarios. For all the experiments related to the metastatic breast cancer cell line, I used a derivative of MDA-MB-231 cells that stably express the luciferase gene (MDA-MB-231-Luc-D3H2LN); this enabled us to not only monitor cell migration, early tumour growth and metastases *in vivo*, but also to quantify tumour burden in an animal model. To test TIP60's ability to inhibit metastasis, I modified this

cell line to either stably overexpressing wild-type TIP60 (MM-Luc-FT60WT) or its catalytically inactive form (MM-Luc-FT60KD) (**Table 2**). Cells stably expressing the vector (MM-Luc-MSCV) were used as the negative control. Overexpression of wild-type TIP60 inhibited cell migration *in vitro* by 50% (**Figure 17A, B**) and cell invasion by 20 % (**Figure 17C, D**). Interestingly, this inhibition was dependent on TIP60's catalytic activity, as overexpression of its catalytically inactive form failed to inhibit cell migration (**Figure 17A, B**).

Validation of the expression of TIP60WT and TIP60KD was performed by quantitative PCR and western blot (**Figure 18A, B**). Validation of the catalytic activity of TIP60WT and TIP60KD was performed by western based *in vitro* HAT assay using core histone as substrate (**Figure 18C**). Wild-type TIP60 and catalytic inactive form of TIP60 were purified from MM-Luc-FT60WT or MM-Luc-FT60KD cells. Wild-type TIP60 increased the level of pan acetyl H4 but catalytically inactive TIP60 could, indicating that TIP60KD is unable to transfer acetyl group to its substrate.
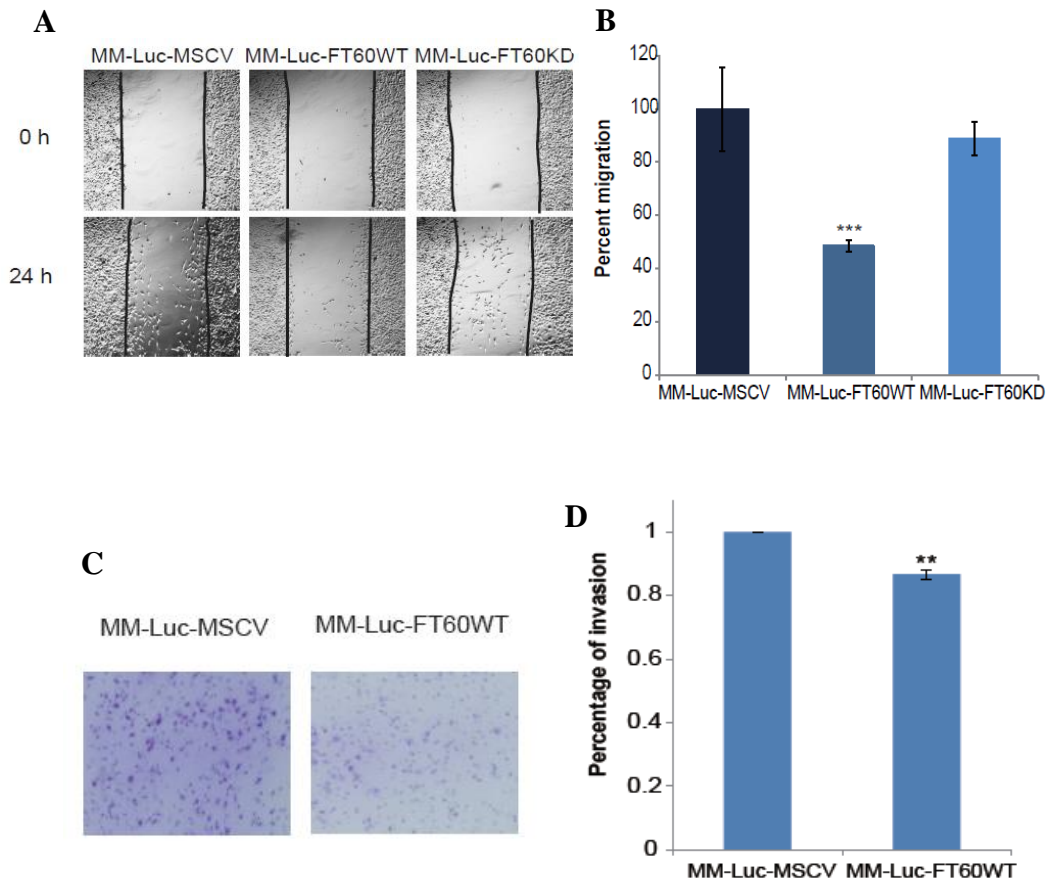
Figure 17. TIP60 inhibits cell migration and invasion *in vitro*.

(**A-B**) TIP60 inhibits cell migration. Wound-healing assays were performed using MDA-MB-231-Luc-D3H2LN cells expressing vector (MM-Luc-MSCV), wild-type TIP60 (MM-Luc-FT60WT), or the catalytically inactive form of TIP60 (MM-Luc-FT60KD) (see chapter 3). Representative images are shown in (**A**) and the quantitation in (**B**). ***, $p < 0.001$. (**C-D**) TIP60 inhibits cell invasion. Boyden chamber assays with matrigel were performed, as detailed in chapter 3. Representative images are shown in **C** and quantification in **D**. **, $p < 0.01$
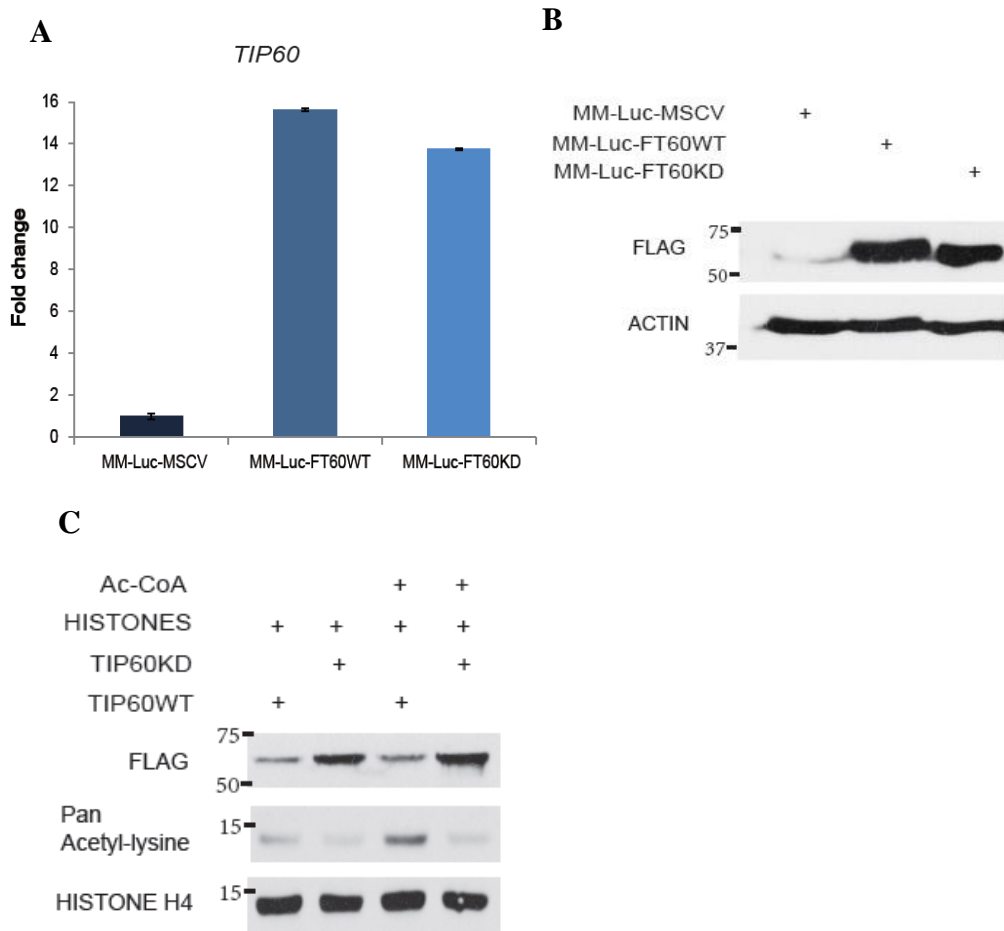
Figure 18. Validating the stable cell lines that overexpress either wild-type TIP60 or catalytically inactive form of TIP60.

(**A**) mRNA level of TIP60. (**B**) Protein level of TIP60. Error bars represent standard deviation. (**C**) Validation of the catalytic activity of wild-type TIP60 and catalytic inactive form of TIP60. Wild-type TIP60 and catalytic inactive form of TIP60 were purified from MM-Luc-FT60WT or MM-Luc-FT60KD cells. *In vitro* HAT assay using core histone as substrate was performed.

To confirm if the same phenotype could be observed in other metastatic breast cancer cell lines, wild-type TIP60 and catalytic inactive form of TIP60 were overexpressed in another two cell lines: HCC1937 (HCC1937-MSCV, HCC1937-TIP60WT, HCC1937-TIP60KD) and MDA-MB-468 (MM468-MSCV, MM468-TIP60WT, MM468-TIP60KD) (**Table 2**). Similar to the observation in MDA-MB-231 cells, overexpression of wild-type TIP60 inhibited the migration of both HCC1937 and MDA-MB-468 cells, however catalytic inactive form of TIP60 could not (**Figure 19**).
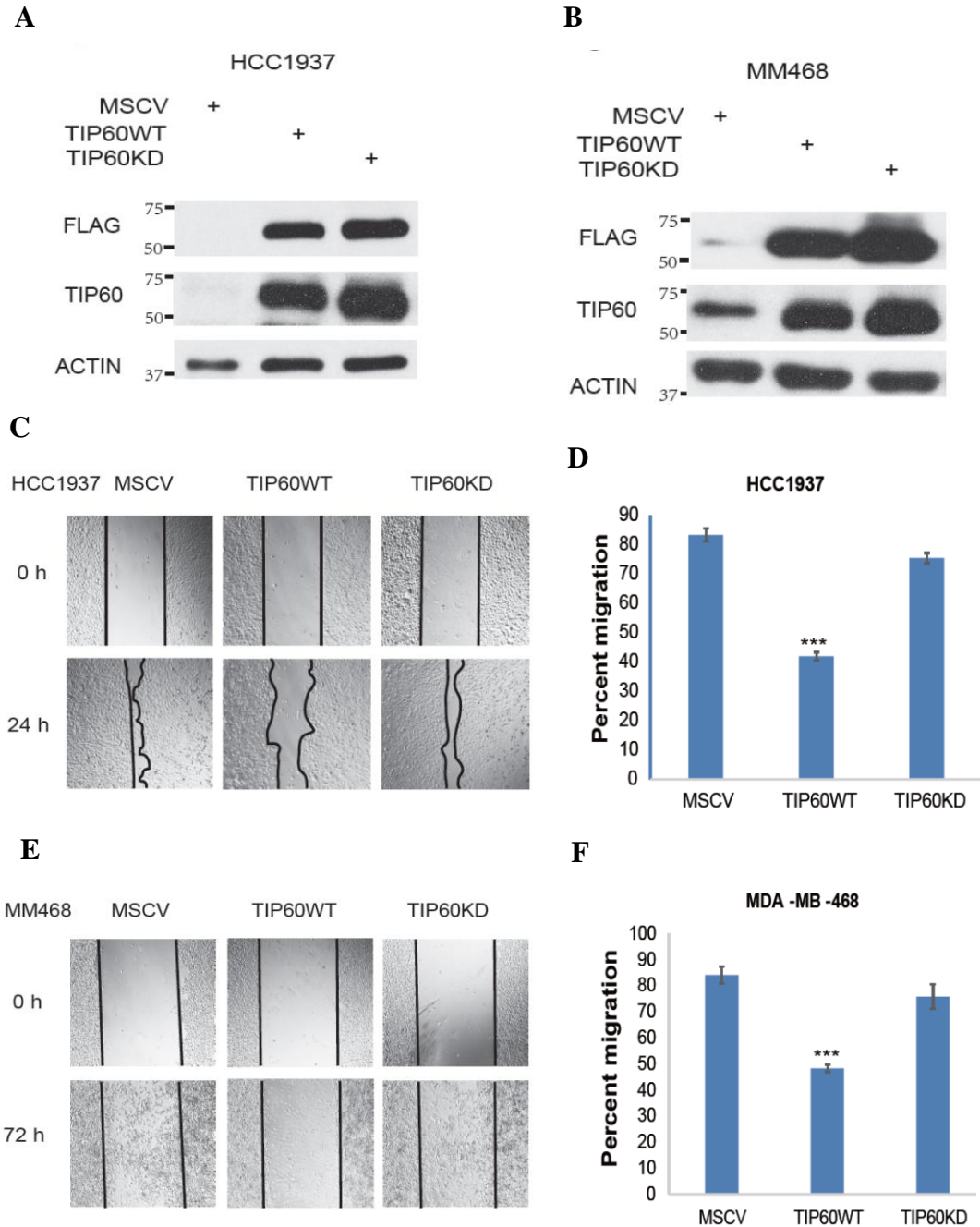
Figure 19. Overexpression of TIP60 inhibits cell migration in HCC1937 and MDA-MB-468 cells.

Wound-healing assays were performed using HCC1937 or MDA-MB-468 cells expressing vector (MSCV), wild-type TIP60 (TIP60WT), or the catalytically inactive form of TIP60 (TIP60KD) (see chapter 3 for details). (**A, B**) Validation of the expression of TIP60WT and TIP60KD. (**C, D**) TIP60 inhibits cell migration in HCC1937 cells. Cell migration images are shown in (**C**) and the quantitation in (**D**). *** P< 0.001. (**E, F**). TIP60 inhibits cell migration in MDA-MB-468 cells. Cell migration images are shown in (**E**) and the quantitation in (**F**). *** P< 0.001.

To extend these studies into an animal model system, I studied the metastasis of MDA-MB-231 cells in 6-week-old NOD/SCID mice, comparing the metastatic potential of TIP60WT and TIP60KD with control cells. In this *in vivo* study, MDA-MB-231 cells expressing the luciferase reporter gene (i.e., MM-Luc-MSCV, MM-Luc-FT60WT and MM-Luc-FT60KD) were injected into mice through the tail vein, and luminescence-based non-invasive imaging was used to monitor the metastasis of cells (**Figure 20A**). The quantifications from four repeats show that TIP60 overexpression led to a dramatic reduction in the metastatic potential of these cells scored by reduced lung metastasis as compared with the control cells and this is dependent on TIP60's catalytic activity (**Figure 20B**). The expression of TIP60WT and TIP60KD in both cell lines and tumour tissues were verified by western blot (**Figure 20C**). These data suggest an inhibitory role of TIP60 in breast cancer metastasis both *in vitro* and *in vivo*.
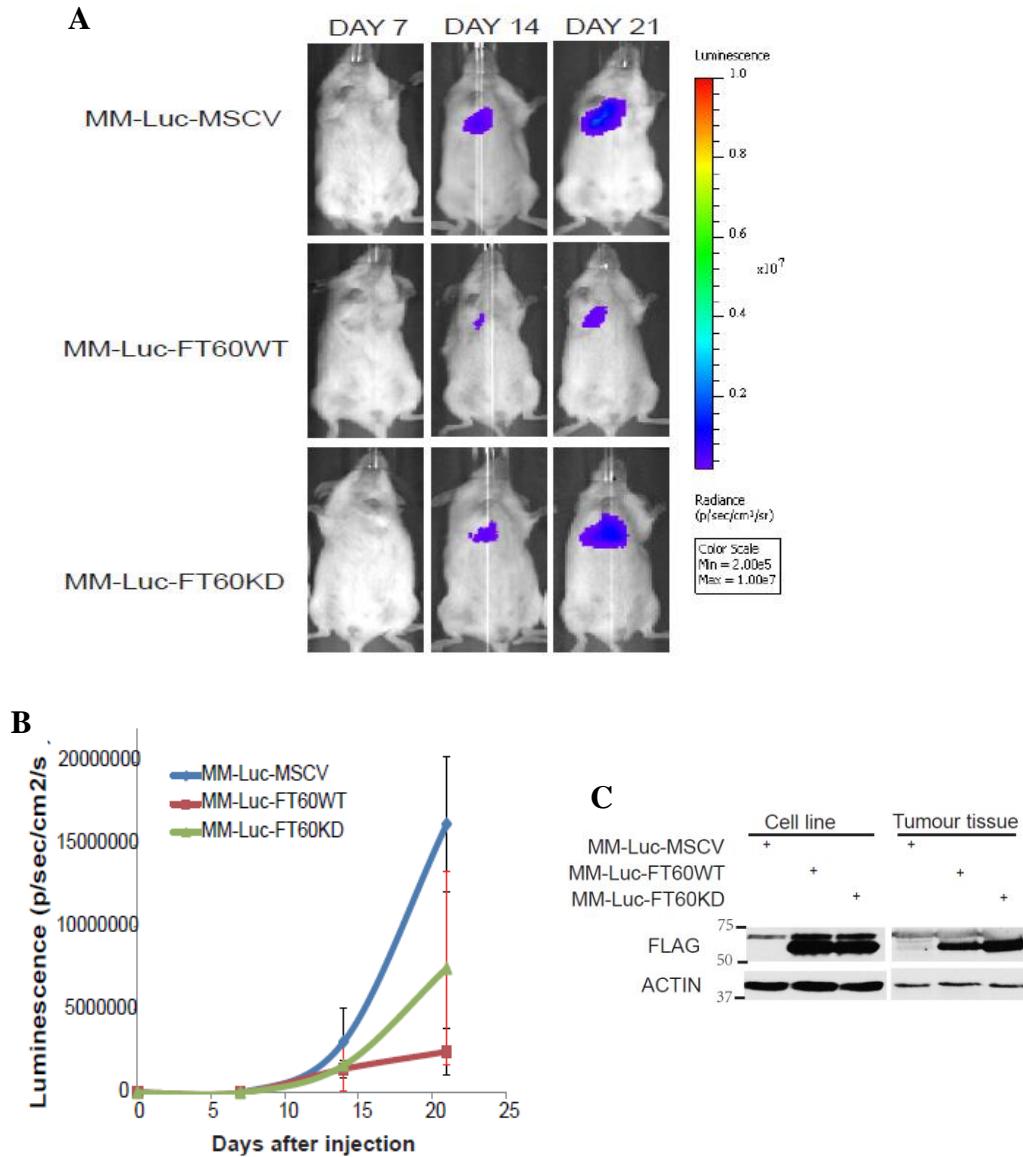
Figure 20. TIP60 inhibits metastasis in an *in vivo* animal model.

(**A**) Representative images. 5×10^5 MDA-MB-231-Luc-D3H2LN cells expressing vector (MM-Luc-MSCV), wild-type TIP60 (MM-Luc-FT60WT), or the catalytically inactive form of TIP60 (MM-Luc-FT60KD) were injected through the tail vein and tumour growth and metastasis were monitored through bioluminescence imaging (see chapter 3 for details). (**B**) Quantitation of the tumour size metastasis to lung. The intensities were quantified using live imaging (see chapter 4 for details). (**C**) Validating the expression of TIP60 in both cell lines and tumours. Proteins isolated from tumours were probed with indicated antibodies.

5.2   Depleting TIP60 promotes cell migration and invasion

Conversely, to test if depletion of TIP60 could increase cell migration, I reduced TIP60 levels in MCF10A cells using siRNA and performed wound-healing assays. I observed that when depleting TIP60, cells loose cell-cell adhesion, become more elongated and mesenchymal (**Figure 21**). Additionally, TIP60 depletion enhanced cell motility by >40%, resulting in a much faster closure of the wound as compared to siControl-treated cells (**Figure 22A, B**). Furthermore, similar results were also observed in MCF10A overexpressing wild-type TIP60 (**Figure 22C, D**). These data suggest that in epithelial cells, downregulation of TIP60 could trigger cell migration and invasion.
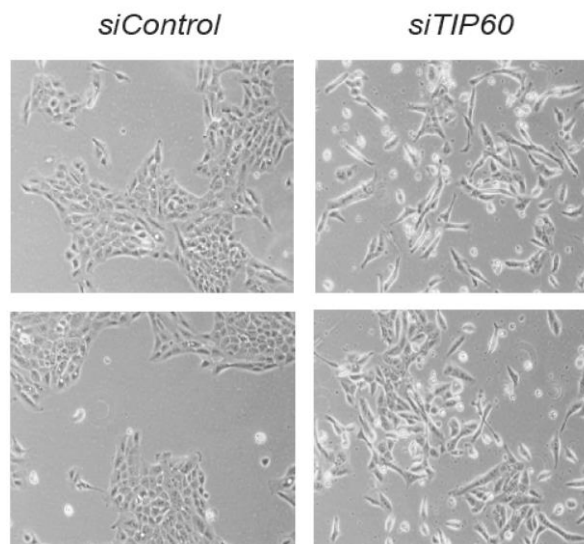
Figure 21. Morphology of MCF10A cells treated with *siControl* and *siTIP60*.
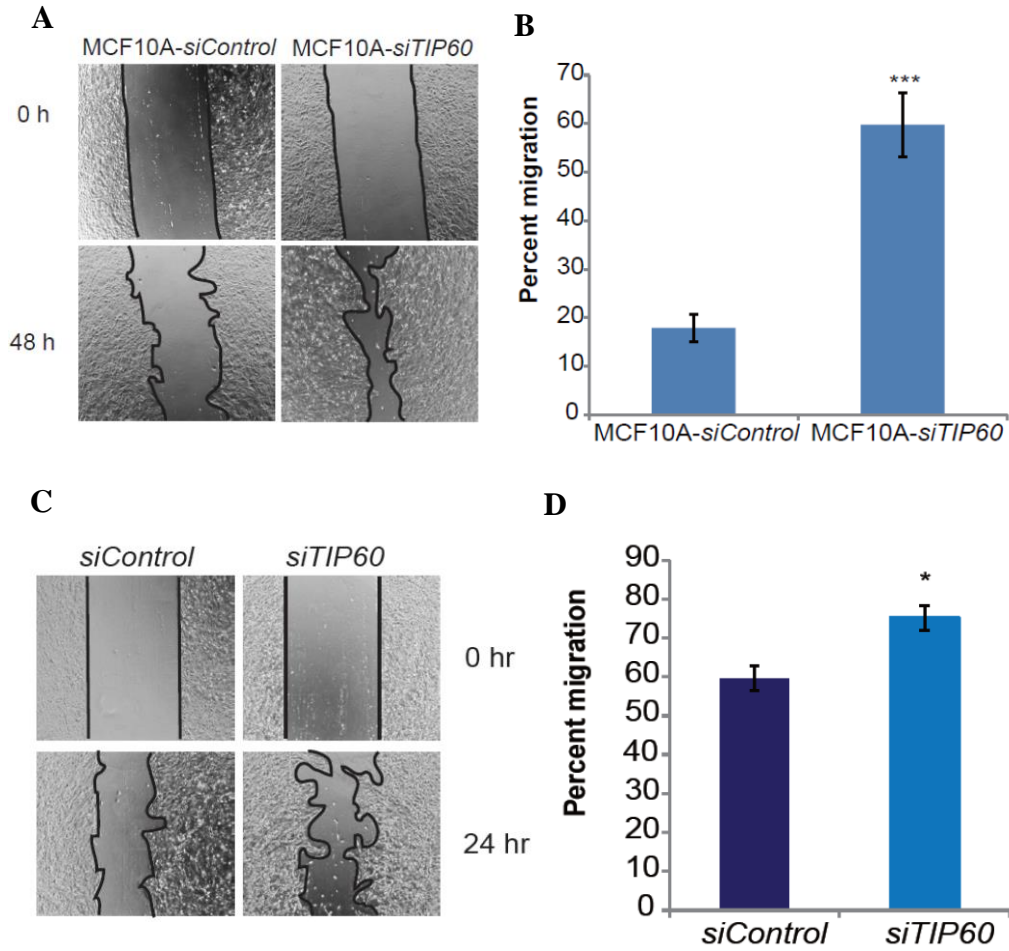
Figure 22. Depleting TIP60 promotes cell migration *in vitro*.

(**A-B**) Depletion of TIP60 increases cell migration. MCF10A cells were treated with indicated siRNAs. Representative images are shown in **A** and quantitation in **B**. ***, $p < 0.001$. (**C-D**) Stable TIP60-expressing MCF10A cells show a similar phenotype as the parental cells. Representative images of M10FT60WT cells treated with siControl and siTIP60 were shown in **C** and quantification in **D**. *, $p < 0.05$.

5.3 Depleting TIP60 alters the expression and localization of EMT markers

TIP60 mediated EMT phenotype was studied by screening the expression of EMT markers in TIP60-depleted cells. Interestingly, I found the transcript levels of two of the major mesenchymal markers SNAIL2 (*SNAI2*) and FIBRONECTIN (*FN1*) to be elevated by ~2 and ~10 fold, respectively. I also observed a 50% reduction in the expression of epithelial marker Epithelial Cell Adhesion Molecule (*EpCAM*) (**Figure 23A**); these findings were re-capitulated at the protein level (**Figure 23B**) and in another breast epithelial cell line, MCF7 (**Figure 23C**). SNAIL2 is one of the master regulators of EMT, as its expression in epithelial cells triggers the first and necessary phase of the EMT process; i.e., desmosomal disruption and cell spreading (Taube et al., 2010; Villarejo et al., 2014). This essentially occurs because of SNAIL2's functions as a transcriptional repressor of epithelial genes, such as *EpCAM*, and as an activator of the mesenchymal gene *FN1*. EpCAM is involved in cell-cell recognition and adhesion, whereas FIBRONECTIN is a key component of the extracellular matrix promoting cell migration (Park and Schwarzbauer, 2014; Stanisavljevic et al., 2011; Sun et al., 2014). I also found that the cells depleted of TIP60 undergo plasma membrane-to-cytoplasmic re-localization of E-CADHERIN (**Figure 24A**) and β-CATENIN (**Figure 24B**) compared to the control cells.
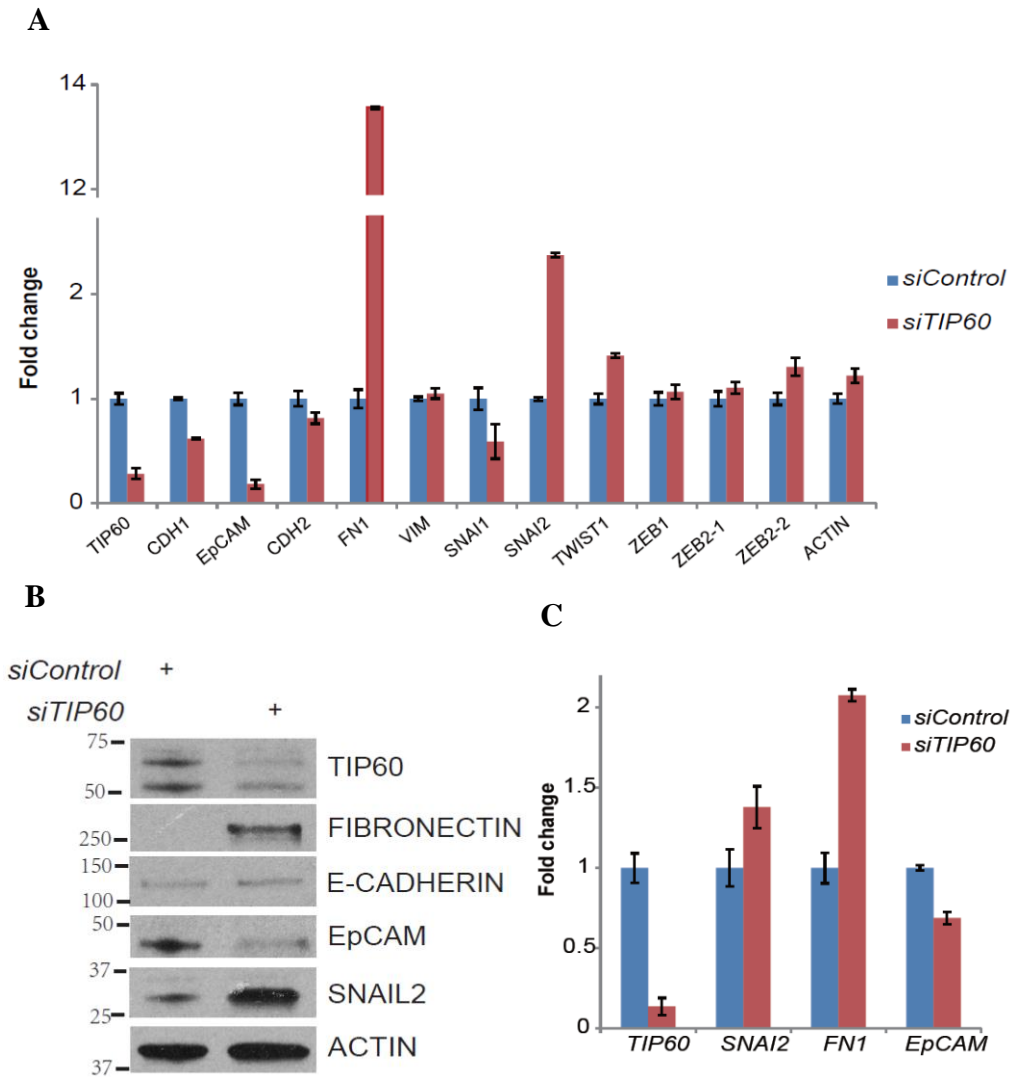
Figure 23. Overexpression of TIP60 alters the expression of EMT markers.

(**A**) Expression analysis of the genes involved in EMT after depletion of TIP60. Results were analysed as fold change against siControl-treated cells. (**B**) Western blot analysis of the proteins showing changes in expression after depletion of TIP60. (**C**) Depletion of TIP60 in MCF7 cells shows similar expression patterns of EMT markers as in MCF10A cells, as detailed in (**A**).

A

B
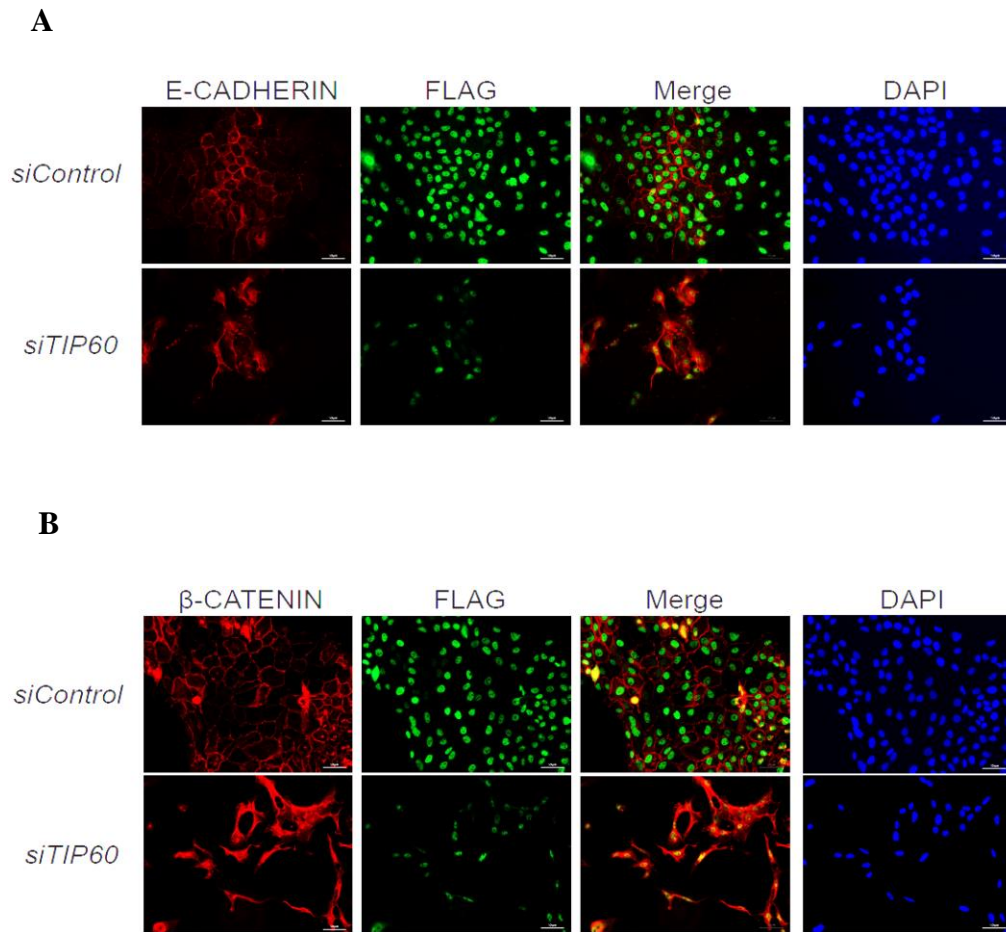
Figure 24. Depletion of TIP60 results in cell membrane-to-cytoplasmic re-localization of E-CADHERIN and β-CATENIN.

Depletion of TIP60 results in cell membrane-to-cytoplasmic re-localization of E-cadherin (**A**) and β-catenin (**B**). Flag-TIP60 was detected using Anti-Flag antibody. Decrease on the Flag signal indicates efficient depletion of TIP60.

5.4 Alteration of the expression of EMT markers is TIP60 specific and dependent on TIP60 catalytic activity

To rule out any off-target effects of the siRNA, three cell lines using MCF10A cells as the parental cell line were generated: MSCV vector control (M10MSCV), wild-type TIP60 (M10FT60WT) and a siRNA-resistant wild-type TIP60 (M10FT60*WT) (**Table 2**). The siRNA-resistant constructs were generated by synonymous mutations; i.e., the siRNA targeting site was mutated such that the nucleotide sequence was modified, but the protein sequence remained unchanged. To test if these cell lines behaved similar to the parental cell line, we depleted both the endogenous and exogenous TIP60 and performed wound-healing assays, mRNA quantitation, and protein expression assays. **Figure 25** confirms that the knockdown of both exogenous and endogenous TIP60 produced phenotypes similar to that of the parental MCF10A cell line.
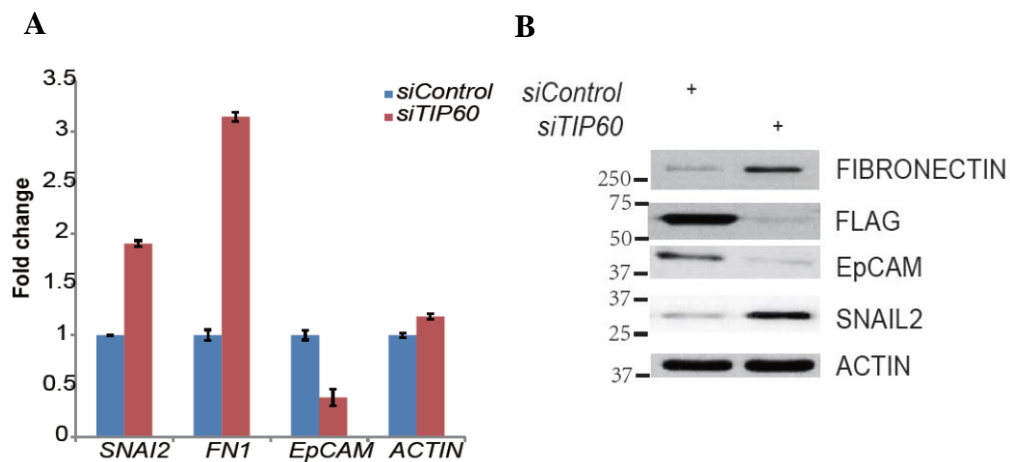
Figure 25. Stable TIP60-expressing MCF10A cells show a similar phenotype as the parental cells.

(**A**) Expression analysis for the EMT markers in M10FT60WT treated with siControl or siTIP60. (**B**) Western blot analysis of the proteins showing changes in expression, as shown in (**A**).

Figure 26 validates expression of TIP60 (wild-type, catalytic dead and siRNA resistant form) in the stable cell lines mentioned above. As shown in **Figure 26A**, treatment with *siTIP60*, only the endogenous, but not the siRNA resistant form of TIP60 was depleted, demonstrating a successful rescue of TIP60 level under these conditions.

Overexpression of TIP60 resulted in a 50% reduction in *FN1* expression and a 2-fold increase in *EpCAM* expression (**Figure 27A, B**). Importantly, the expression of siRNA-resistant TIP60 rescued the levels of *FN1* and *EpCAM* at both the RNA and protein levels, indicating this phenotype was TIP60-specific (**Figure 27**). However, *SNAI2* expression could only be rescued partially in such a scenario (**Figure 27C**). Since *FN1* has been reported to upregulate *SNAI2* to promote metastasis, it is possible that the reduction in TIP60 provides the initial trigger to up-regulate *SNAI2*, but that *FN1* maintains *SNAI2's* levels during metastasis (Knowles et al., 2013).

To gain a deeper insight into the molecular mechanism of TIP60's function, whether the lysine acetyltransferase activity of TIP60 is required for SNAIL2-mediated regulation of EMT. Thus a cell line expressing TIP60 that was catalytically inactive and siRNA-resistant (M10FT60*KD) was generated. Intriguingly, this form of TIP60 failed to rescue the expression level of *FN1* and *EpCAM* (**Figure 27**), indicating that the catalytic activity of TIP60 is required to regulate the expression of these genes, both at the mRNA and protein levels.

A

B
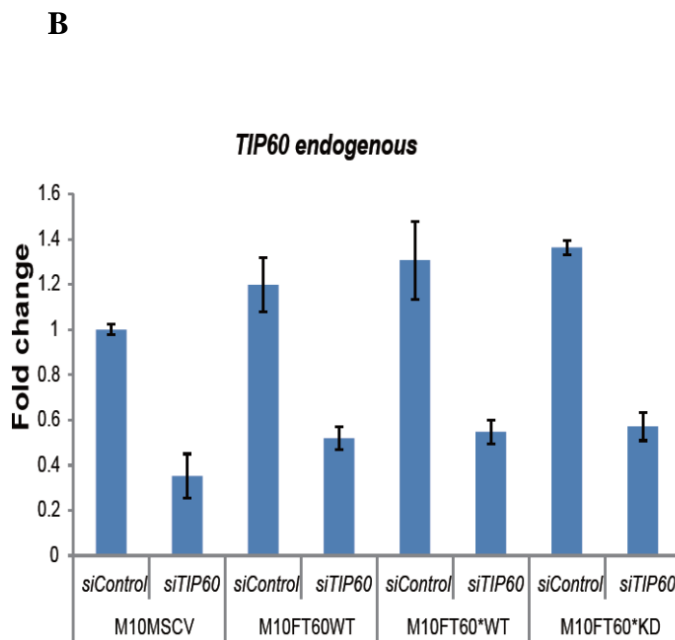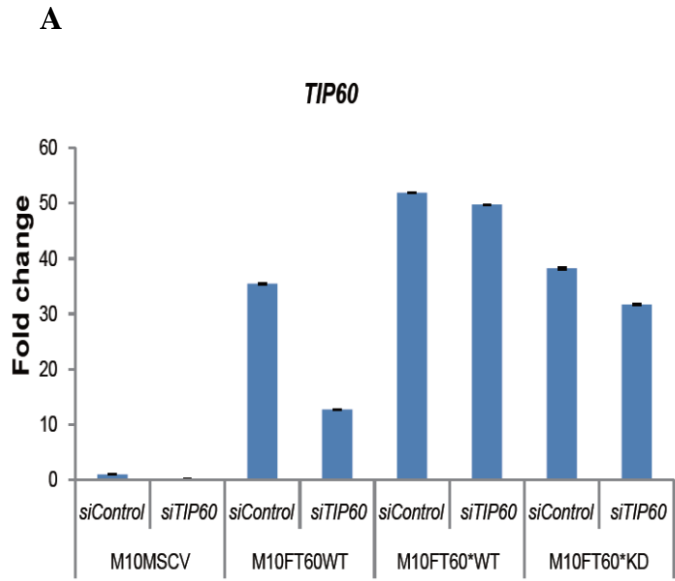
Figure 26. Expression of TIP60 in MCF10A stable cell lines.

Expression analysis of level of total TIP60 (**A**) and endogenous TIP60 (**B**) in different stable cell lines.

A

EpCAM

B

FN1

C

SNAI2

D
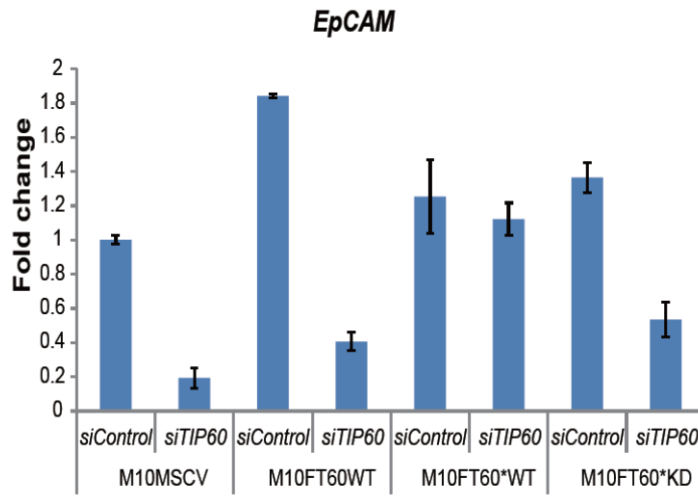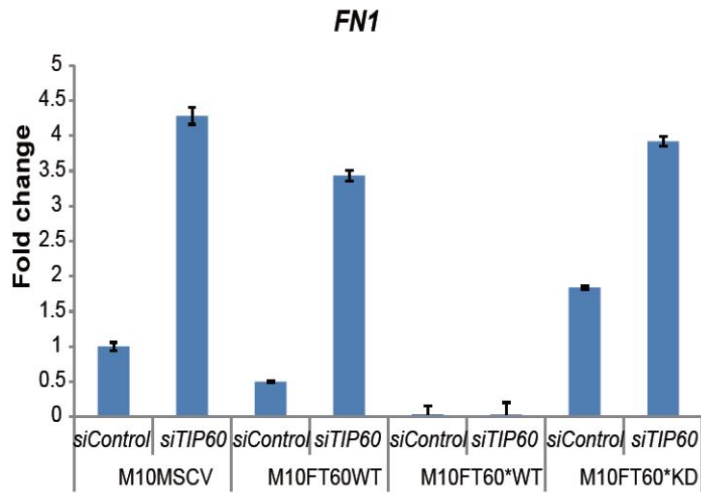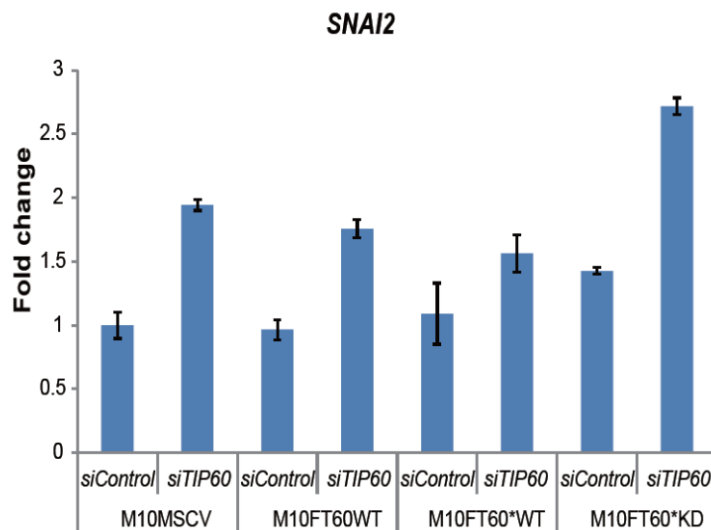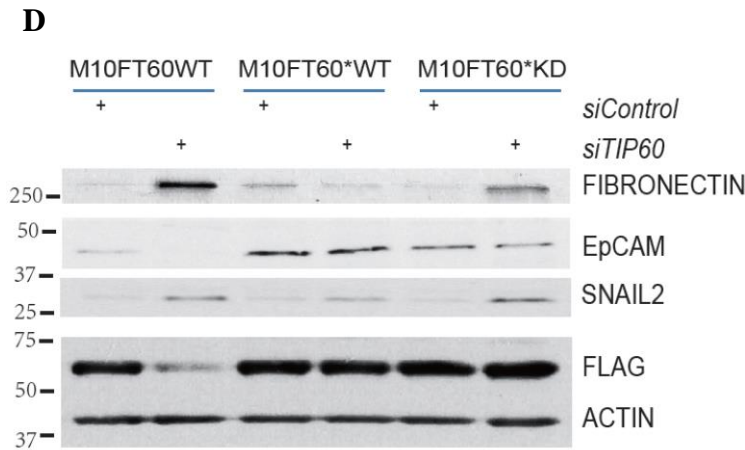
Figure 27. TIP60 mediated inhibition of Epithelial-mesenchymal transition is specific to TIP60 and depends on its catalytic activity.

(**A-C**) Expression analysis of genes identified to change when TIP60 is depleted using siTIP60 in parental (MCF10A), vector control (M10MSCV), stable cells expressing wild-type TIP60 (M10FT60WT), siRNA-resistant wild-type TIP60 (M10FT60*WT) and catalytically inactive and siRNA-resistant TIP60 (M10FT60*KD). (**D**) Western blots for the proteins with differential expression upon TIP60 depletion.

To further strengthen this observation is TIP60 specific and catalytic activity dependent, cell lysates from MDA-MB-231 cells with overexpression of either wild-type TIP60 or catalytic inactive form of TIP60 (MM-Luc-MSCV, MM-Luc-FT60WT, MM-Luc-FT60KD) were examined using western blot. EpCAM level increased by overexpressing wild-type TIP60 compared to control but not catalytic inactive form of TIP60 (**Figure 28**). This was in contrast to MCF10A, where the expression of EpCAM was inversely modulated upon depleting TIP60 (**Figure 23B**). FIBRONECTIN and SNAIL2 expression did not alter in MDA-MB-231 cells by overexpressing wild-type TIP60 or catalytic inactive form of TIP60 (data not shown). This could be due to the feedback regulation between FIBRONECTIN and SNAIL2 in highly metastatic cells, as discussed above. High levels of FIBRONECTIN and

SNAIL2 could upregulate each other and ensure maintenance of both of them at high level in more metastatic cells. However, restoration of EpCAM level is sufficient to inhibit cell migration and invasion (Tai et al., 2007), which explains the inhibitory function of TIP60 in MDA-MB-231 cell metastasis. This suggests that the regulation of EpCAM plays a predominant role in TIP60 mediated inhibition of breast cancer metastasis.
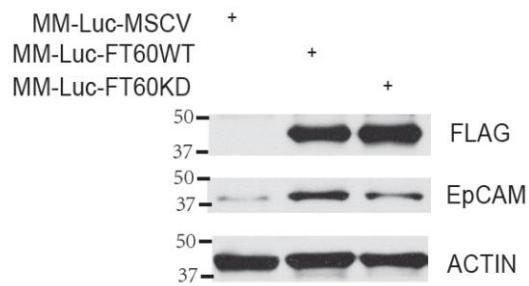
Figure 28. The expression of EpCAM in MDA-MB-231 cells overexpressing either wild-type TIP60 or catalytic inactive form of TIP60.

Chapter 6

TIP60 regulates expression of EpCAM and FIBRONECTIN through regulating the expression and function of SNAIL2

6.1 Regulation of cell migration by TIP60 is SNAIL2 dependent

SNAIL2 belongs to the family of zinc finger transcription factors, which regulates the expression of EMT-related genes by interacting with the E-boxes in their promoter regions (Huang et al., 2012; Thiery et al., 2009; Villarejo et al., 2014; Yang and Weinberg, 2008). To investigate the role of SNAIL2 in TIP60 mediated alteration of the expression of EMT markers, both TIP60 and SNAIL2 were depleted and I observed that, in comparison with the single depletion of TIP60, the co-depletion was able to rescue both *FN1* and *EpCAM* at the mRNA and protein levels (**Figure 29**). This suggests that TIP60 regulation on the expression of *FN1* and *EpCAM* was SNAIL2 dependent.

To further investigate the biological implication, wound-healing assay using MCF10A cells with depleted TIP60 alone or TIP60 and SNAIL2 together was performed. A 40% increase in cell migration was observed when TIP60 alone was depleted and this was further reduced nearly 30% when both TIP60 and SNAIL2 were depleted (**Figure 30**), suggesting that regulation of cell migration by TIP60 is SNAIL2 dependent.
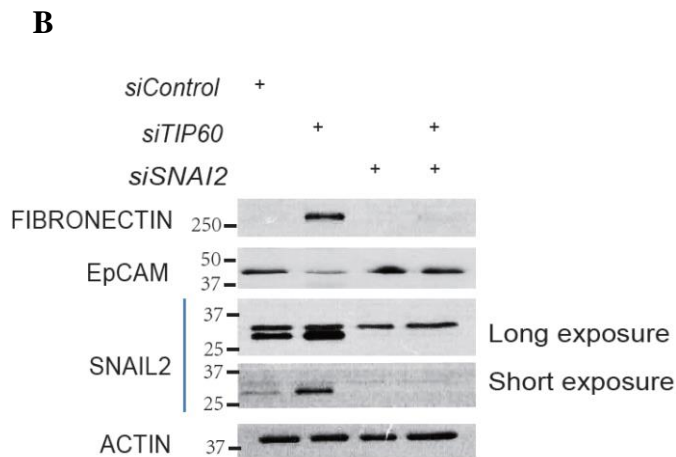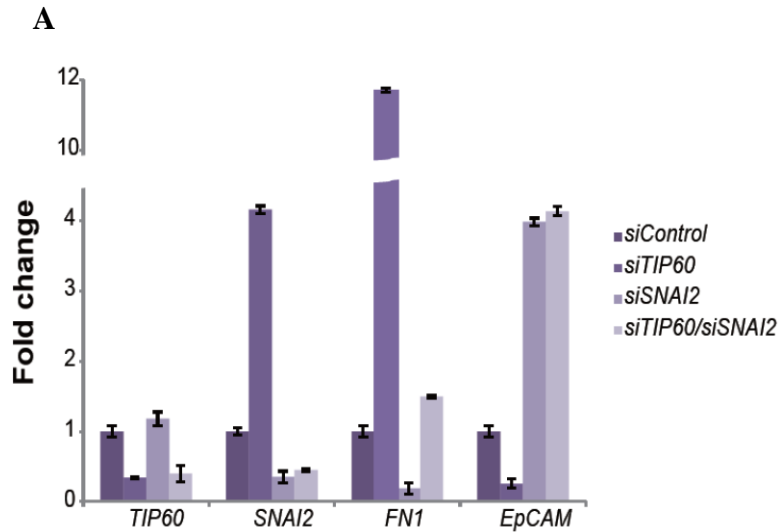
Figure 29. TIP60 regulates Epithelial-mesenchymal transition through regulating SNAIL2.

(**A**) Change in expression of the genes in TIP60-depleted condition is SNAIL2 dependent. mRNA levels of genes identified to be differentially expressed when TIP60 is depleted either alone or in combination with SNAIL2 in MCF10A cells. (**B**) Western blot analysis of the differentially expressed genes.

A
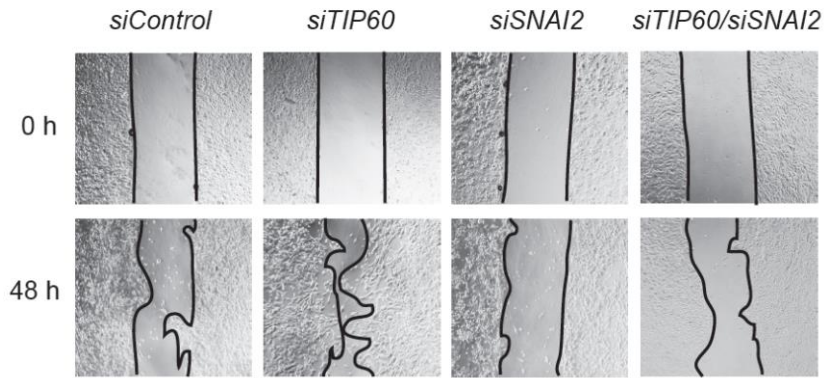
B
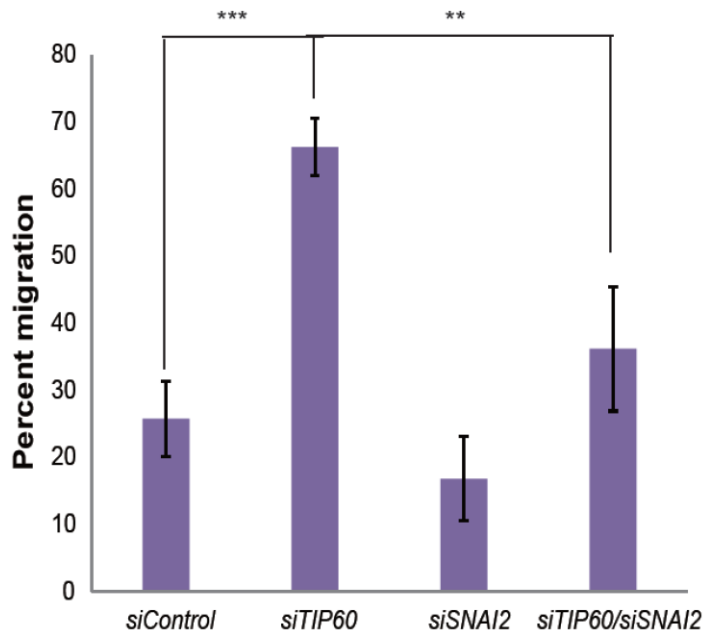
Figure 30 Regulation of the cell migration by TIP60 is SNAIL2 dependent.

Wound-healing assay was performed as described in chapter 3. The increased cell migration after depletion of TIP60 was restored by co-depleting TIP60 and SNAIL2. The representative pictures are shown in (**A**) and quantification in (**B**), **, $P<0.01$; ***, $P<0.001$.

6.2 TIP60 inhibits SNAIL2 enrichment on its target promoters

SNAIL2 has previously been implicated in the promoter-dependent transcriptional regulation of EMT genes. Thus, whether the TIP60-mediated transcriptional regulation of *EpCAM* and *FN1* also occurred through the promoter regions of these genes need to be ascertained. To this end, ChIP-qPCR (chromatin immunoprecipitation quantitative PCR) was performed using an anti-SNAIL2 antibody in presence or absence of TIP60. Primers were designed to amplify different regions of the promoters of *FN1* and *EpCAM* (**Figure 31A, B**). Among the primers tested, two were chosen for each promoter, one from the distal site, which lacked E-box motif (SNAIL2 binding site), and the other from the proximal site, which showed enrichment for SNAIL2 association (**Figure 31C, D and Table 3**). When the occupancy of SNAIL2 on these promoters was tested in wild-type (MCF10A) cells, I found a significant increase in SNAIL2 occupancy on the *FN1* and *EpCAM* promoters in the absence of TIP60 (**Figure 32A**). In order to test if these changes were TIP60 specific and if the catalytic activity of TIP60 was required to inhibit the binding of SNAIL2 to the promoters, SNAIL2's occupancy in the three stable cell lines was checked, M10FT60WT, M10FT60*WT, and M10FT60*KD (**Figure 32B-D**). Remarkably, I found that the enrichment of SNAIL2 on *FN1* and *EpCAM* promoter (**Figure 32B**) can be restored back to control level by overexpressing wild-type TIP60 (**Figure 32C**) but this was not observed when catalytically inactive form of TIP60 was overexpressed (**Figure 32D**), suggesting that the SNAIL2 promoter occupancy was regulated by TIP60 and was dependent on TIP60's catalytic activity. Validation of the knockdown is in **Figure 33**.
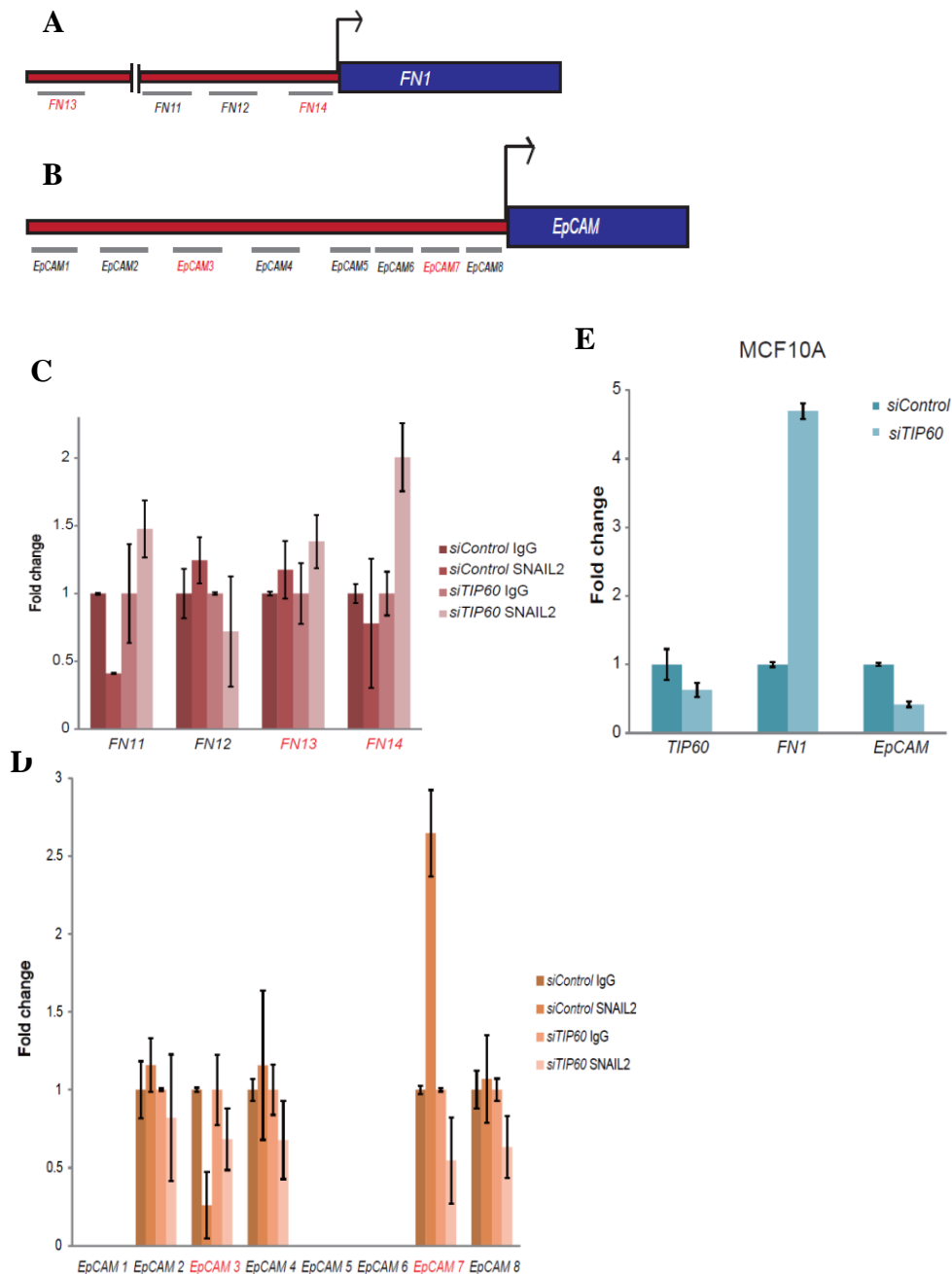
Figure 31. Screening the ChIP-qPCR primers for *FN1* and *EpCAM* promoters.

(**A, B**) Schematics of the promoter and 5' regions of the *FN1* and *EpCAM*. The qPCR primer sets for chromatin immunoprecipitation (ChIP) are shown in the schematics and detailed in **Table 3**. Promoters and 5'UTR regions: *FN1*, GenBank: AF550582.1; *EpCAM*, GenBank: AY148099.1. (**C, D**) ChIP-qPCR analysis of MCF10A cells transfected with TIP60 siRNA. The SNAIL2-bound DNA was immunoprecipitated using the anti-SNAIL2 antibody. Two primer sets from each promoter—one on the distal site and the other on the proximal—were chosen for further analysis: *FN13* and *FN14* for *FN1* promoter, and *EpCAM3* and *EpCAM7* for *EpCAM* promoter. Primer sets that were chosen are marked red in the figures. Results of qPCR are plotted as fold change against IgG control. (**E**) TIP60 knockdown efficiency of the ChIP samples in (**C**), and (**D**).
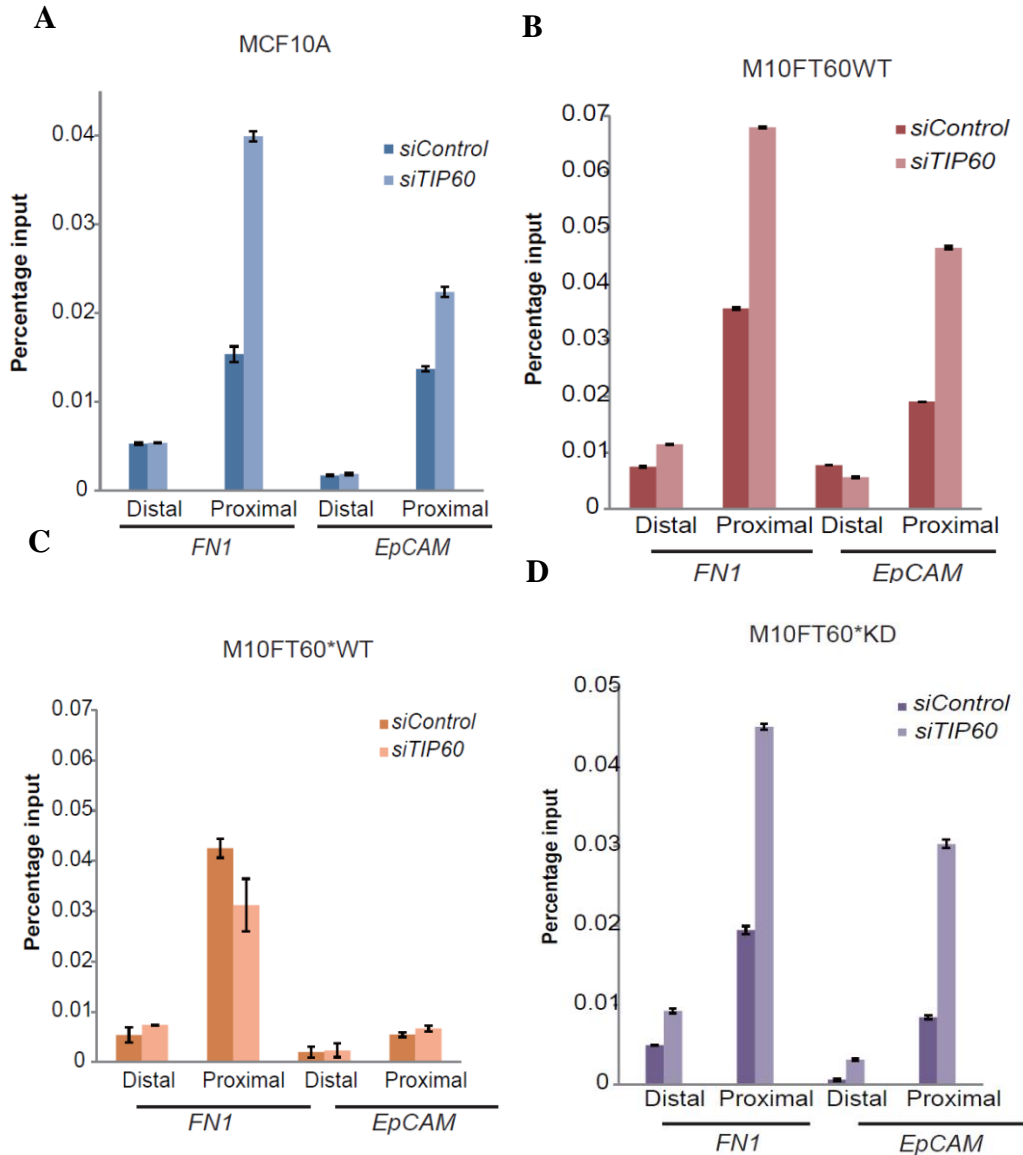
Figure 32. TIP60 regulates SNAIL2 enrichment on target promoters.

(**A**) Chromatin immunoprecipitation quantitative PCR (ChIP-qPCR) assays were performed to check the enrichment of SNAIL2 on target promoters in the presence or absence of TIP60. Results were analysed and are represented as percentage input. RNA isolates from the cells of the same experiment were used to check the expression levels by RT-qPCR (**Figure 32**). (**B-D**). SNAIL2 binding to its target promoter is regulated by TIP60 and depends on its catalytic activity. ChIP-qPCR analysis for SNAIL2 binding was performed in the presence (*siControl*) or absence (*siTIP60*) of TIP60 in MCF10A cells stably expressing wild-type TIP60 (M10FT60WT), siRNA-resistant, wild-type TIP60 (M10FT60*WT) or the catalytically inactive and siRNA-resistant TIP60 (M10FT60*KD). The *FN1* and *EpCAM* promoters were immunoprecipitated and analysed as in (**A**).
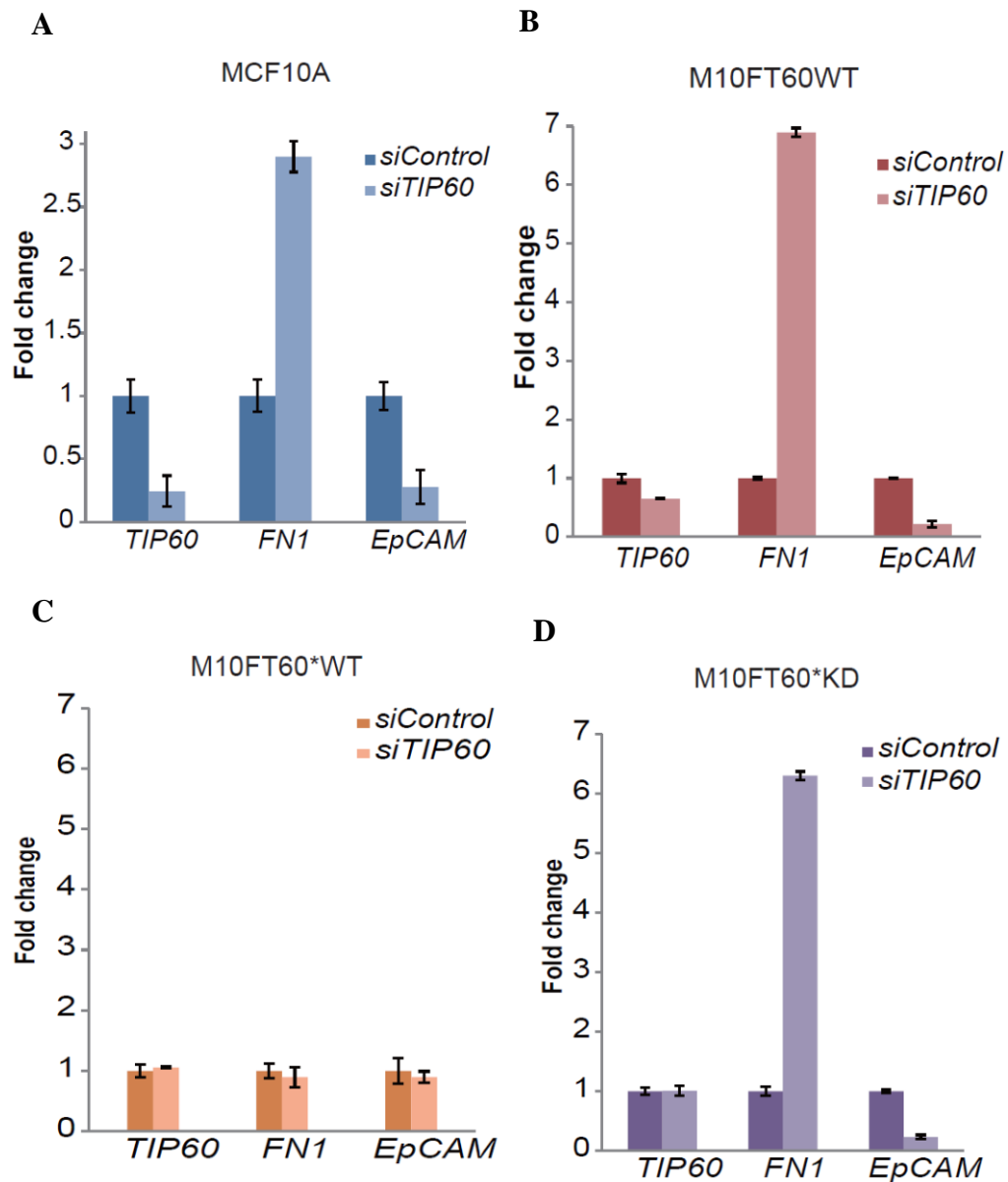
Figure 33. *TIP60* knockdown efficiency of the ChIP samples in **Figure 32**.

MCF10A (**A**), M10FT60WT (**B**), M10FT60*WT (**C**) and M10FT60*KD (**D**) were treated with *siControl* and *siTIP60* for 72 hours. Small aliquot were harvested for checking the knockdown efficiency. The rest of the cells were used for ChIP experiment in **Figure 32**.

Chapter 7

Cross talk between two epigenetic regulators, TIP60 and DNMT1 determines the metastasis potential of breast cancer

7.1 TIP60 regulates the expression of EMT markers through regulating the stability of DNMT1

DNMT1 is known to induce EMT by repressing expression of cell adhesion molecules (Fukagawa et al., 2015). Since DNMT1 is destabilized by TIP60 (Du et al., 2010b), whether SNAIL2 mediated repression of epithelial genes were DNMT1 dependent was tested. DNMT1 was depleted using siRNA either alone or in combination with TIP60. Depletion of TIP60 stabilized DNMT1 at protein level (**Figure 34A-C**), suggesting that TIP60 regulates the protein stability of DNMT1. When compared to TIP60 depletion, the co-depletion of TIP60 and DNMT1 rescued *FN1* and *EpCAM* both at the mRNA and protein levels (**Figure 34D, E**). Interestingly, SNAIL2 was also rescued both at mRNA and protein levels when TIP60 and DNMT1 were co-depleted (**Figure 34D, E**). Taken together, these data suggest that TIP60 regulates the expression of SNAIL2 as well as *FN1* and *EpCAM* through its ability to destabilize DNMT1.
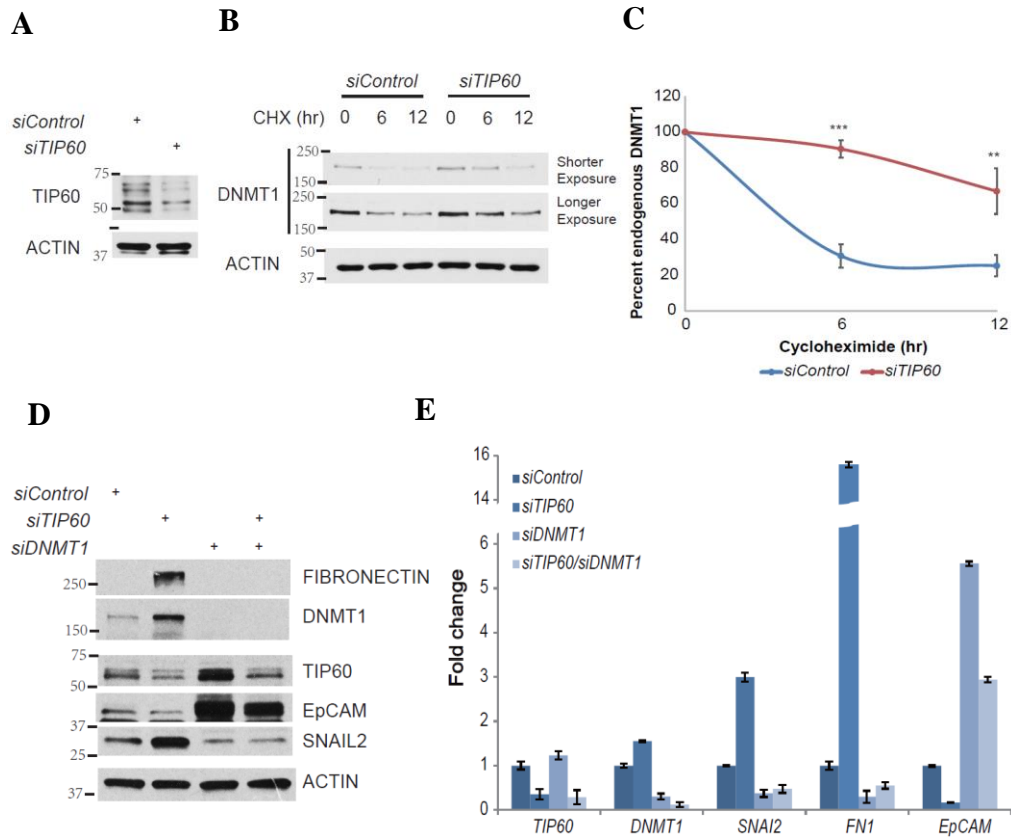
Figure 34. Epithelial-mesenchymal transition in absence of TIP60 is DNMT1 dependent.

(**A-C**) TIP60 regulates DNMT1 protein stability. MCF10A cells transfected with *siControl* or *siTIP60* were treated with 100 µg/ml cycloheximide for up to 12 hours. Cell lysates from indicating time points were examined by western blot (**B**) and quantified (**C**), **, $P<0.01$; ***, $P<0.001$. The knockdown efficiency of TIP60 was shown in (**A**). (**D**) Protein levels of genes identified to be differentially expressed when TIP60 is depleted either alone or in combination with DNMT1 in MCF10A cells. (**E**) mRNA expression analysis of the differentially expressed genes by qPCR

7.2   TIP60 and DNMT1 levels regulates the cell migration potential

To have a biological readout of DNMT1 mediated activation of the EMT program, DNMT1's effect on cell migration in TIP60 depleted condition was tested. For this, wound-healing assay was performed. I observed a 50% increase of cell migration when TIP60 alone was depleted and this was rescued to 20% when both TIP60 and DNMT1 were co-depleted (**Figure 35A, B**). These data suggests that decreased levels of TIP60 stabilizes DNMT1, which results in increased cell migration.
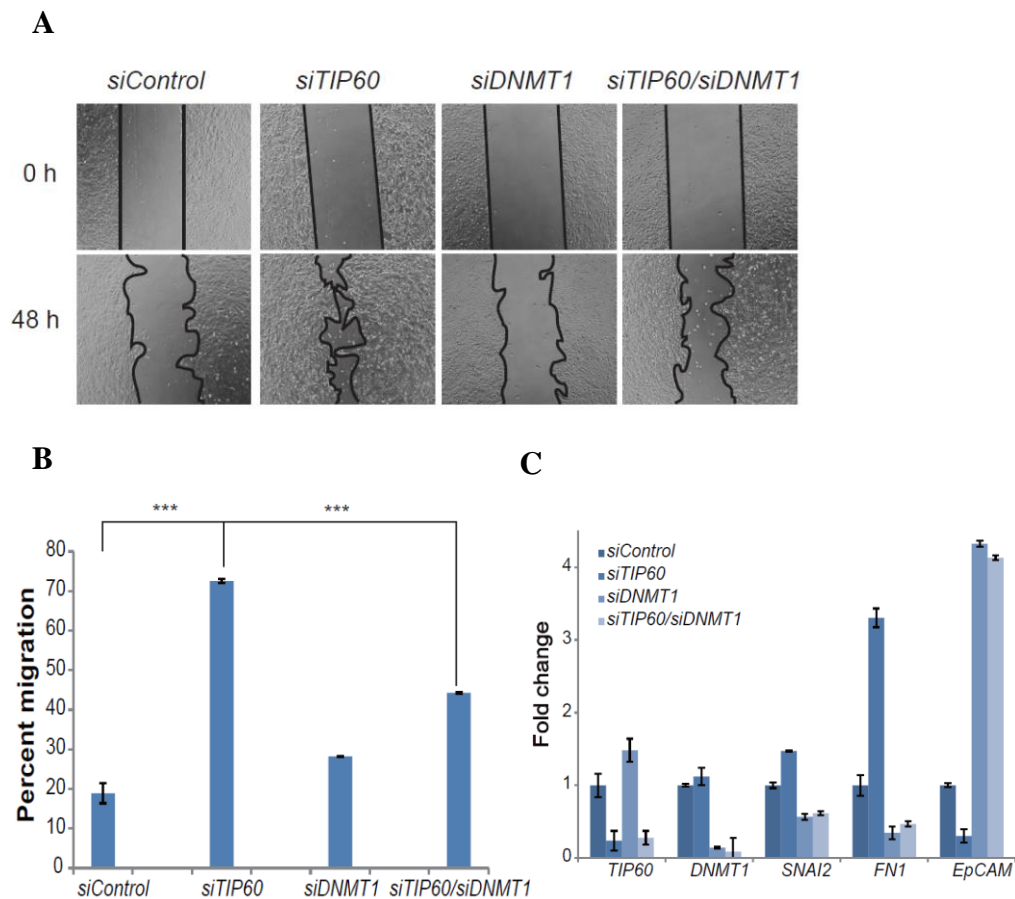
Figure 35. TIP60 regulates cell migration *in vitro* by ablating DNMT1.

(**A**) The representative pictures of wound healing assay. (**B**) Quantifications of wound healing assay from at least three independent experiments. ***, $p<0.001$. (**C**) TIP60 and DNMT1 knockdown efficiency of the samples used in **A** and **B**. Error bars represent standard deviation.

7.3 TIP60 regulates the DNA methylation statues on *EpCAM* promoter

In order to identify the molecular determinant of DNMT1-SNAIL2 driven EMT program, I sought to estimate DNA methylation on SNAIL2 regulated promoters. For this, MCF10A cells were treated with different siRNA combinations (*siControl*, *siTIP60*, *siDNMT1*, *siTIP60+siDNMT1*). Genomic DNA was isolated and the methylation specific sequencing was performed. A significant increase in DNA methylation on *EpCAM* promoter (-51 to -32) in TIP60 depleted cells was observed, and interestingly, this was rescued when TIP60 was co-depleted with DNMT1 (**Figure 36A, B**), suggesting that the increased methylation observed was dependent on DNMT1. However, depleting DNMT1 alone did not change the DNA methylation in this region, this may be because the basal level of DNA methylation in this region is due to other DNA methyltransferases such as DNMT3A or DNMT3B (**Figure 37**). The DNA methylation in this region (-51 to -32) was fully dependent on DNMT1 only in the absence of TIP60, as co-depleting TIP60 and DNMT1 reduced this increased DNA methylation level to nearly zero (**Figure 36A, B**). I also noted that depleting TIP60 did not change DNA methylation on *EpCAM* 1st intron region +542 to +601 (**Figure 36C**), suggesting that the intron region was not responsive to decreased levels of TIP60. However, depletion of DNMT1 alone showed a subtle decrease in DNA methylation on 1st intron region +542 to +601 (**Figure 36C**). In summary, these results suggest that DNMT1 methylate both regions on *EpCAM* promoter, but TIP60 only affects DNMT1 mediated DNA methylation on promoter region -51 to -32 which was next to SNAIL2 binding

site (E-Box binding site) and overlaps with the SNAIL2 enrichment region on *EpCAM* promoter (**Figure 32**).
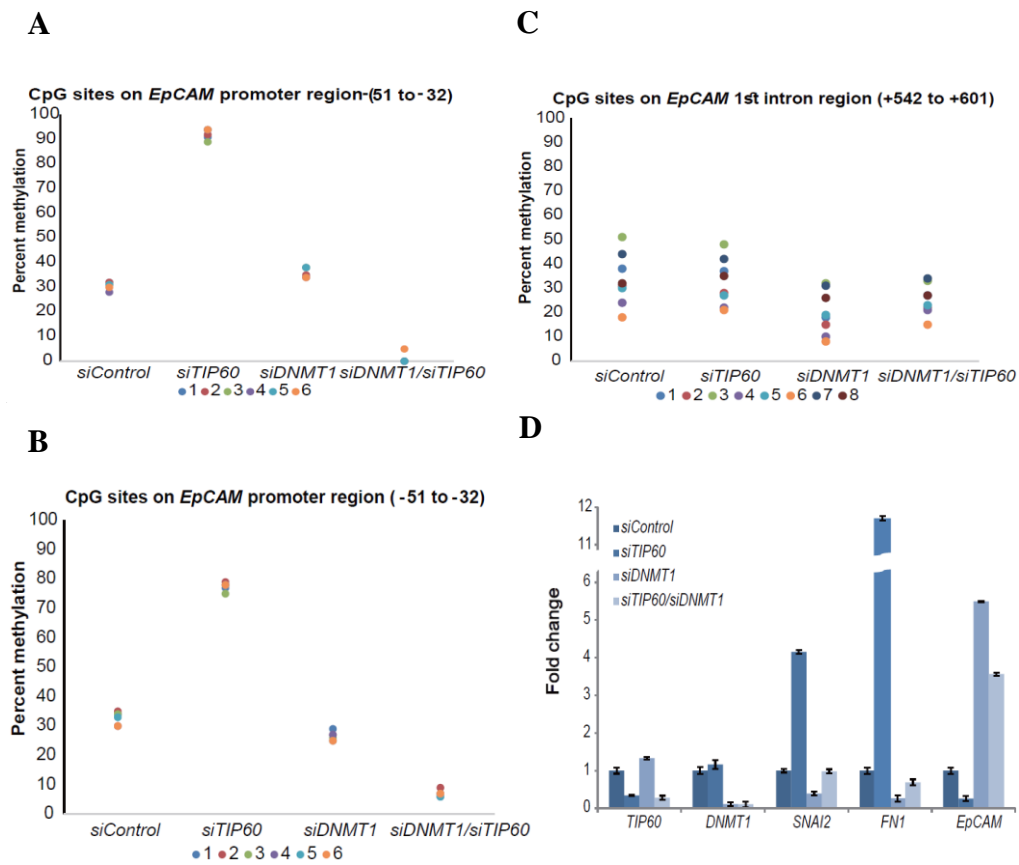
Figure 36. Recruitment of DNMT1 to *EpCAM* promoter results in its hypermethylation in the context of depleting TIP60.

(**A, B, C**) TIP60 only regulates DNMT1 mediated DNA methylation on *EpCAM* promoter region -51 to -32 (**A, B**) but not on region +542 to +601 (**C**). TIP60 and DNMT1 were depleted in MCF10A cells either alone or in combination. DNA from cells was isolated and bisulphite pyrosequencing was performed as detailed in Methods. (**D**) *TIP60* and *DNMT1* knockdown efficiency for the samples used for bisulphite pyrosequencing represented above.
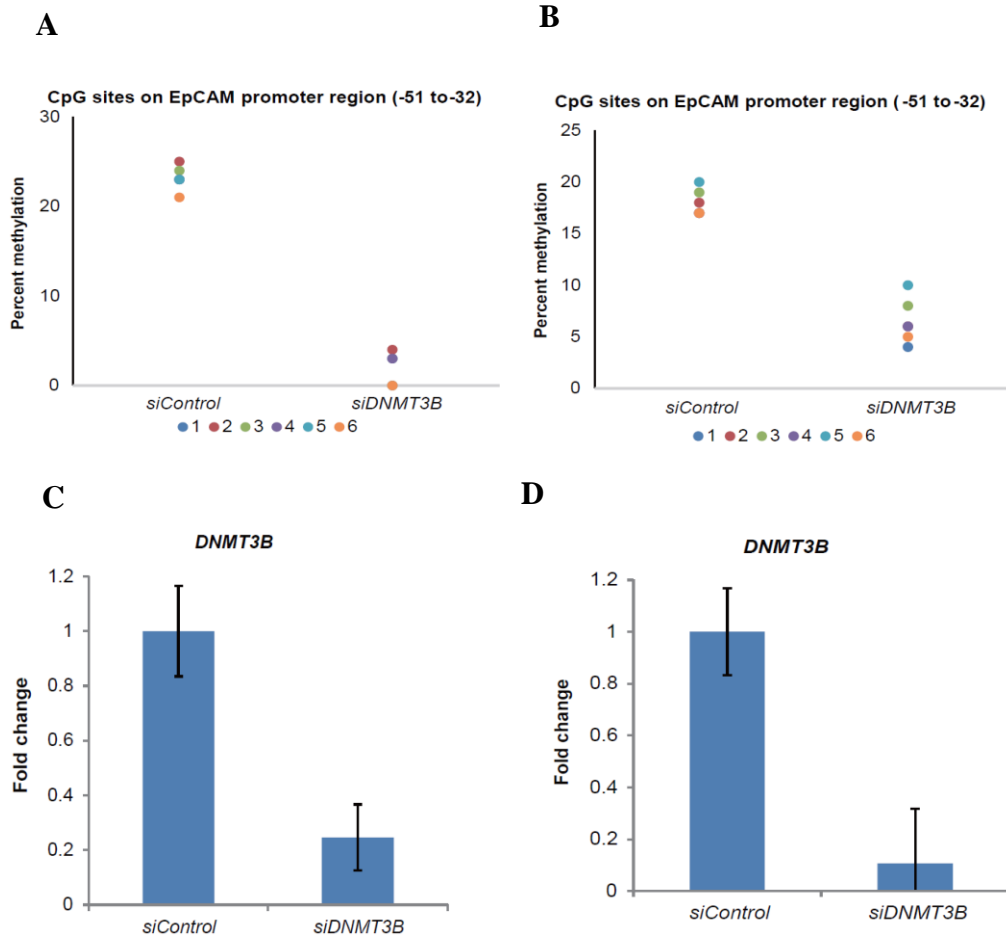
Figure 37. The basal level of DNA methylation on *EpCAM* promoter region (-51 to -32) presents in *siControl* cells is due to DNMT3B de novo methylation.

(**A, B**) Genomic DNA isolated from MCF10A cells transfected with *siControl* or *siDNMT3B* was used to perform bisulphite pyrosequencing. (**C, D**) The knockdown efficiency of DNMT3B in (**A, B**)

7.4 SNAIL2 recruits DNMT1 to *EpCAM* promoter in the absence of TIP60

Next, I sought to investigate the molecular mechanism of DNMT1 mediated repression of *EpCAM* expression. For this, I checked methylation status of *EpCAM* promoter on depleting SNAIL2 and TIP60. I observed that the increased DNA methylation on *EpCAM* promoter region -51 to -32 on depleting TIP60 was further decreased significantly on depleting both TIP60 and SNAIL2 (**Figure 38A, B**), suggesting that TIP60 regulates DNMT1-dependent DNA methylation on *EpCAM* promoter through SNAIL2. However, it did not show any changes on *EpCAM* 1st intron region +542 to +601 (**Figure 38C**). To further investigate the mechanism of SNAIL2 mediated regulation of DNA methylation on *EpCAM* promoter, I first depleted SNAIL2 and observed no change in DNMT1 level (both protein and mRNA) (**Figure 39A and data not shown**). Then a ChIP-qPCR experiment using antibody against DNMT1 was performed, interestingly I observed an increase in the enrichment of DNMT1 on *EpCAM* promoter region (-51 to -32) upon depleting TIP60 (**Figure 39B**). This increase of DNMT1 enrichment further reduced to control level upon co-depleting SNAIL2 and TIP60 (**Figure 39B**). However, the enrichment of DNMT1 on *EpCAM* 1st intron region (+542 to +601) did not change upon depleting SNAIL2. These suggest that SNAIL2 only regulates the recruitment of DNMT1 to *EpCAM* promoter region (-51 to -32), which contains SNAIL2 binding site. To further investigate the association between DNMT1 and SNAIL2, FLAG-DNMT1 and SNAIL2-MYC were co-expressed in 293T cell. FLAG-DNMT1 was immunoprecipitated and associated SNAIL2-MYC was observed by western

blot (**Figure 39C**). Taken together, these results suggest that DNMT1 catalyse the DNA methylation on both *EpCAM* promoter region -51 to -32 and region +542 to +601. SNAIL2recruits DNMT1 to *EpCAM* promoter region -51 to - 3 2 and this is inhibited by TIP60 (**Figure 39D**).
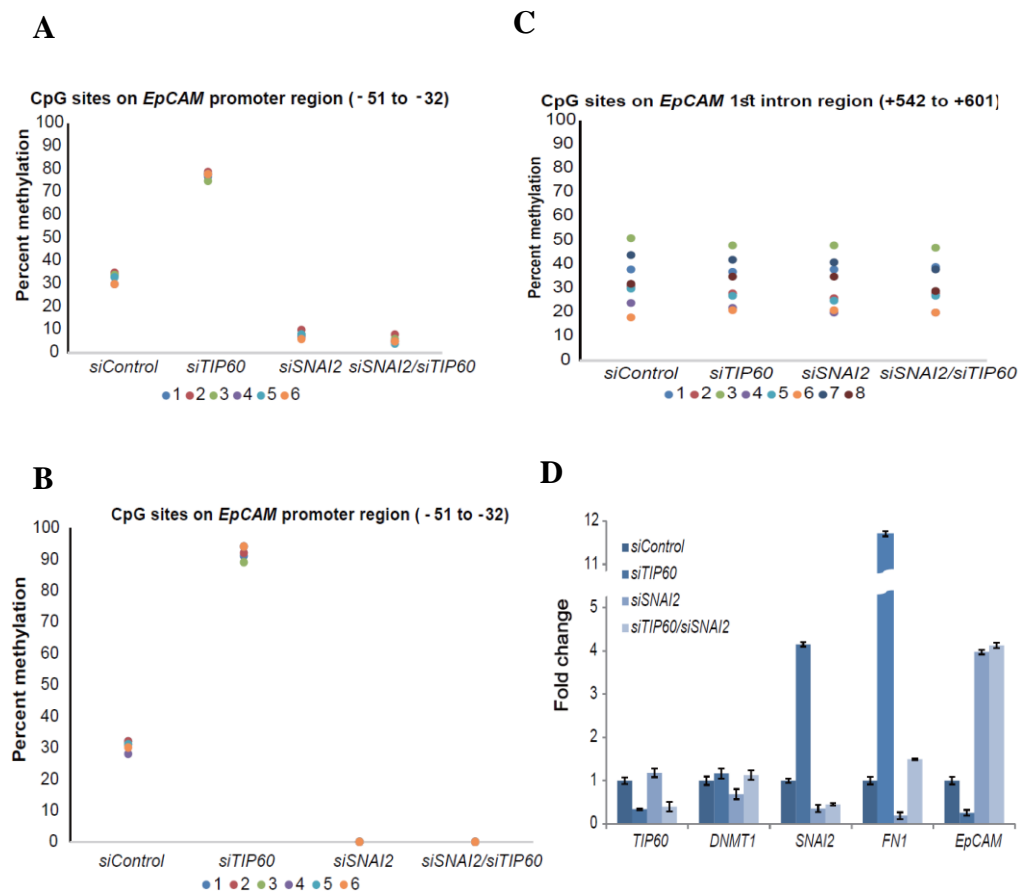
Figure 38. SNAIL2 dependent regulation of *EpCAM* promoter hypermethylation in the context of depleting TIP60.

SNAIL2 specifically regulates methylation on *EpCAM* promoter region -51 to -32 (**A, B**) but not on promoter region +542 to +601 (**C**) in the absence of TIP60. (**D**) TIP60 and SNAIL2 knockdown efficiency for the samples used for bisulphite pyrosequencing represented above.
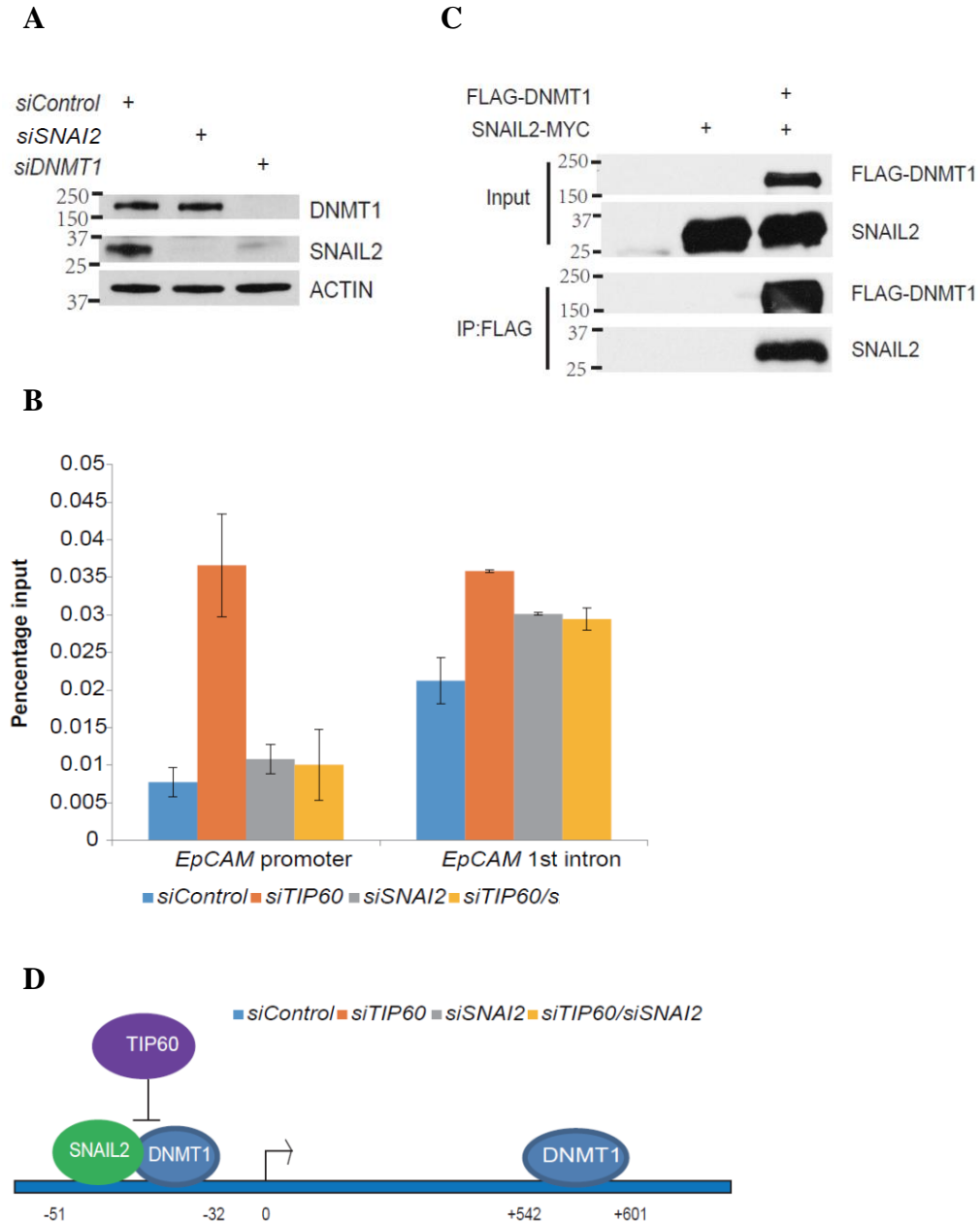
Figure 39. SNAIL2 recruits DNMT1 to target promoter.

(**A**) Depletion of SNAIL2 does not change the level of DNMT1. (**B**) DNMT1 was recruited to *EpCAM* promoter region (-51 to -32) by SNAIL2 in the absence of TIP60. ChIP-qPCR using the antibody against DNMT1 was performed. Two pairs of primers were designed to amplify the *EpCAM* promoter region (-51 to -32) and *EpCAM* 1st intron region (+542 to +601) respectively. The *EpCAM* promoter region amplified here overlaps with the region amplified by previous *EpCAM* proximal primers used in **Figure 31**, but more specific to CpG sites tested in this region. (**C**) DNMT1 associates with SNAIL2. FLAG-DNMT1 and SNAIL2-MYC were co-expressed in 293T. Co-immunoprecipitation was performed as detailed in chapter 3. FLAG-DNMT1 was immunoprecipitated and associated SNAIL2-MYC was probed using western blot. (**D**) Model of the mechanism of the regulation of *EpCAM* promoter hypermethylation involving TIP60, DNMT1 and SNAIL2.

Chapter 8

Discussion

Changes in chromatin landscape play an important role in the process of carcinogenesis. DNA methylation and post-translation modification on histone tails are among the most investigated epigenetic alterations, and have been implicated in tumourigenesis. TIP60, as a histone acetyltransferase, is a chromatin remodeler involved in multiple cellular physiological process and its decreased expression has been reported in several cancers (Chen et al., 2012; Gorrini et al., 2007; Gupta et al., 2013; Jha et al., 2010; Sakuraba et al., 2009). Viral oncoproteins were also reported to destabilize TIP60 in viral-induced cancers (Gupta et al., 2013; Jha et al., 2010), and restoring TIP60 level has been shown to inhibit tumour growth (Subbaiah et al., 2015) suggesting a tumour suppressive function. In HPV-induced cervical cancers, HPV E6 destabilizes TIP60 in an E6AP independent manner (Jha et al., 2010). However, the mechanism of E6 mediated TIP60 degradation was not identified. In this study, I demonstrated that EDD1 is utilized by E6 to destabilize TIP60 and depleting EDD1 results in the stabilisation of TIP60 and further inhibits tumour growth, pheno-copying the overexpression of TIP60 (**Figure 40**). Reactivation of TIP60 through the inhibition of EDD1 is a potential therapy to treat cervical cancer (**Figure 41**).

As a tumour suppressor, TIP60 activates downstream pathways to induce tumour suppression. Besides the upstream regulation mechanism of TIP60 by HPV E6, the downstream tumour suppression pathways were not explored. The main role of TIP60 identified to date is the maintenance of genomic stability, in addition to regulating apoptosis and transcription. However, recent

studies indicate that TIP60 might involve in more other downstream pathways, for example, TIP60 downregulation correlates with metastasis in several cancers (Chen et al., 2012; Kim et al., 2005; Sakuraba et al., 2009). This leaves an interesting gap about the mechanism of TIP60 mediated inhibition on cancer metastasis. In this study, I identified that TIP60 inhibits EMT through ablating DNMT1-SNAIL2 axis as evidenced by both *in vitro* and *in vivo* models (**Figure 42**). Mechanistically, depletion of TIP60 promotes EMT by stabilizing DNMT1, which results in increased expression of SNAIL2. The upregulated SNAIL2 would then recruit DNMT1 to *EpCAM* promoter region (-51 to -32), resulting in hypermethylation of *EpCAM* promoter and repression of *EpCAM* expression. This study has identified the mechanism of TIP60 mediated inhibition of EMT program and has discovered an important link between two epigenetic modulators – TIP60 and DNMT1. The data presented here imply four potential therapeutic strategies to treat SNAIL2 driven metastatic breast cancers: (i) Reactivation of TIP60; (ii) Restoration of TIP60 dependent acetylation on DNMT1; (iii) Inhibition of DNMT1 activity by inhibitors; (iv) Synergy between DNMT1 inhibitor and histone deacetylase (HDAC) inhibitor.

Taken together, I have identified TIP60 function as a tumour suppressor in two ways: inhibits both tumour growth and cancer metastasis. Additionally, I have also discovered the mechanism of E6 mediated destabilization of TIP60 in cervical cancer and identified the mechanism of TIP60 mediated inhibition on breast cancer metastasis. **Most importantly**, this study implies potential **therapeutic** ways to treat cancer: (i) reactivating TIP60 through inhibiting

EDD1 and (ii) synergy between demethylating agent (DNMT1 inhibitor) and HDAC inhibitor.
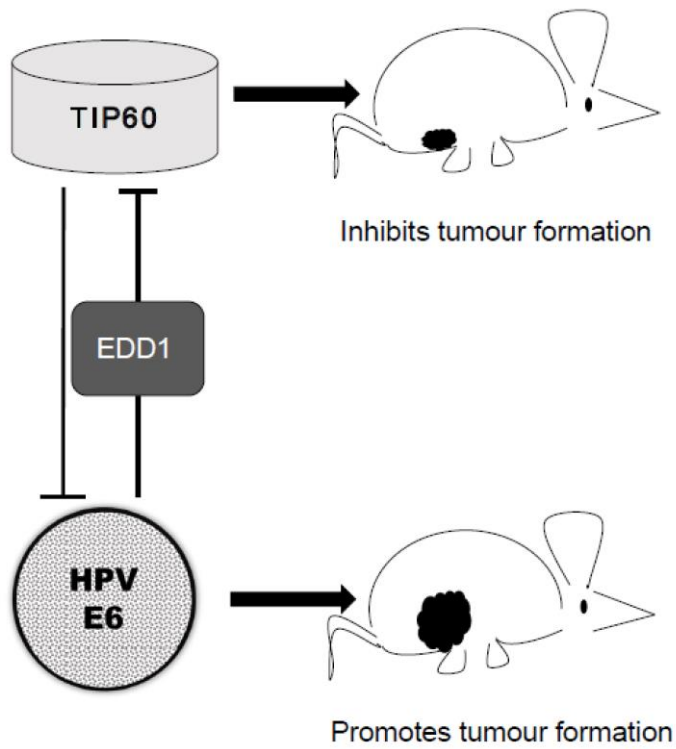
Figure 40 Model for HPV E6 mediated TIP60 degradation.

HPV E6 utilizes EDD1 to destabilize TIP60 and promotes tumour formation.
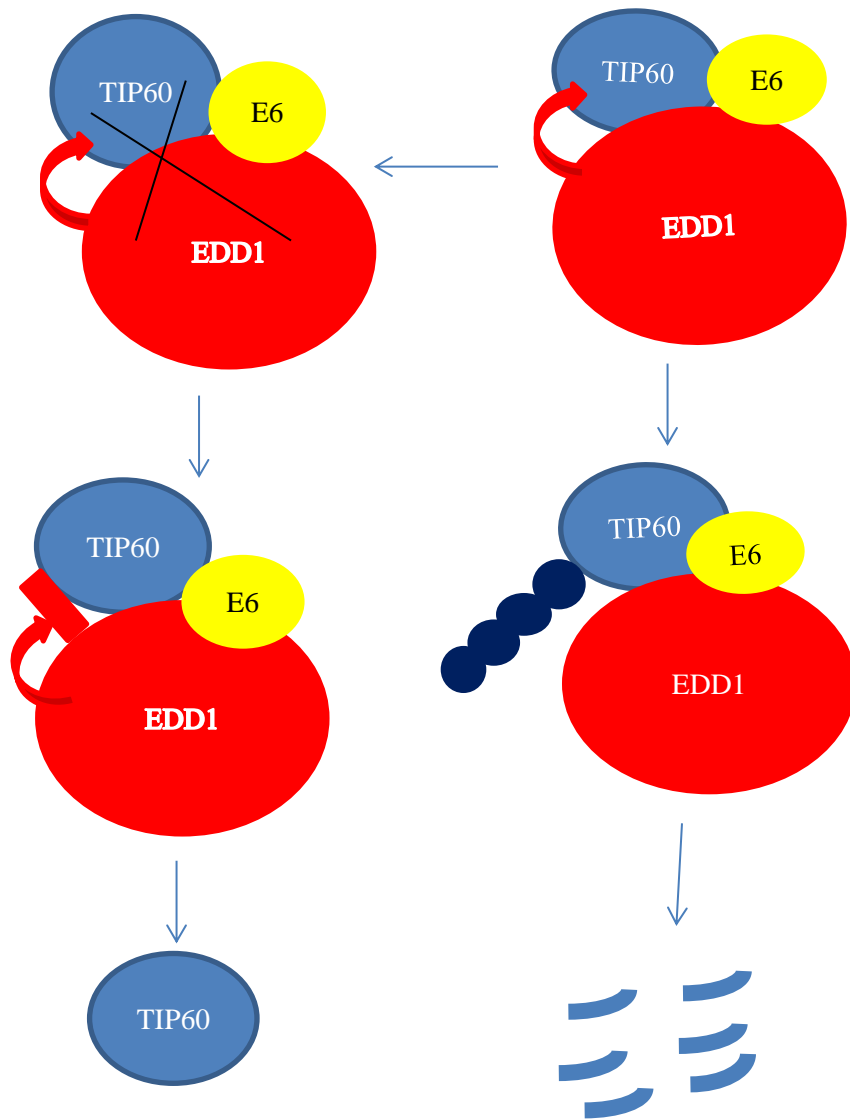
Figure 41. Model for the mechanism of HPV E6 mediated TIP60 degradation.

HPV E6 utilizes EDD1 to destabilize TIP60 through ubiquitin-dependent proteasome degradation. Restoration of TIP60 by inhibiting the interaction between EDD1 and TIP60 might be a therapeutic way to treat cancer.
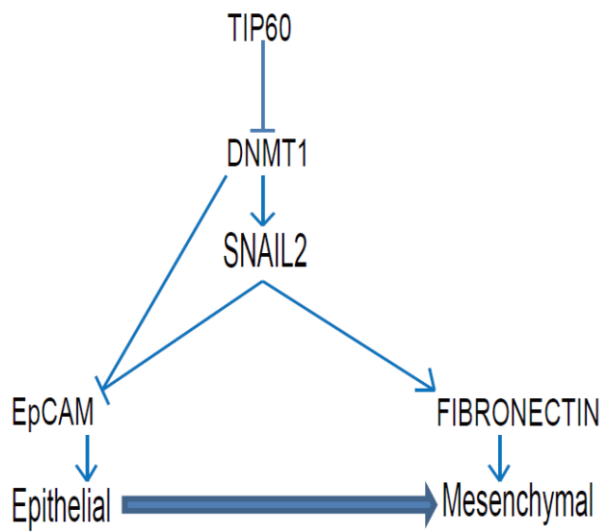
Figure 42. Model for TIP60-mediated inhibition of Epithelial- mesenchymal transition.

TIP60 destabilizes DNMT1 and inhibits SNAIL2 driven EMT program. Decreased level of TIP60 increases SNAIL2 level and DNA methylation level on the *EpCAM* promoter.

8.1 As a tumour suppressor, TIP60 inhibits tumour growth both *in vitro* and *in vivo*

TIP60 functions as a tumour suppressor in multiple ways. For example, TIP60 acetylation on p53 lysine 120 acts as a switch between p53 induced cell cycle arrest and apoptosis, pushing the cell towards apoptosis (Sykes et al., 2006; Tang et al., 2006). Additionally, during DNA Damage Response, TIP60 is known to be recruited to DNA damage site through histone H3 lysine 9 trimethylation, facilitating TIP60 acetylation on Ataxia Telangiectasia Mutated (ATM) which would activate ATM signalling and induce cell cycle arrest (Sun et al., 2005). Furthermore, TIP60 dependent acetylation on p21 (Cip1/WAF1) lysine 161 and 163 is required for the stabilization of p21 and facilitates p21 mediated cell cycle arrest during DNA damage response (Lee et al., 2013). Additionally, Gorrini et al. from Amati's group found that the immunohistochemical staining of TIP60 was decreased in mammary carcinomas and they further identified that TIP60 as a haplo-insufficient tumour suppressor in MYC-induced lymphomagenesis (Gorrini et al., 2007). However, most of these TIP60 mediated tumour suppressor pathways are dependent on p53.

In this study, I identified TIP60 as a tumour suppressor in HPV-induced cervical cancer. Overexpressing TIP60 inhibits colony formation of HeLa cells *in vitro* (**Figure 6**) and tumour growth *in vivo* (**Figure 7, 8**). HPV oncoprotein E6 is known to destabilize p53 through an E3 ubiquitin ligase, E6AP (Huibregtse et al., 1991; Scheffner et al., 1993), in HeLa cells. The fact that TIP60 could inhibit tumour growth in functionally p53 null cells, indicates that TIP60 might regulate a novel tumour suppressor pathway which is

independent of p53. A transcriptome analysis using RNA sequencing and a proteomic analysis using mass spectrometry could be done to identify the p53 independent tumour suppression pathway mediated by TIP60.

8.2 Reactivation of TIP60 by inhibiting EDD1 might be a potential cancer therapy

EDD1 (E3 identified by Differential Display), also known as UBR5 (Ubiquitin protein ligase E3 component n-recognin 5) is often mutated and/or overexpressed in cancer (**Figure 43**). As previously reported, in breast cancer, EDD1 overexpression correlates with gene copy number increase (Clancy et al., 2003). While in ovarian cancer, the overexpression of EDD1 associates with high risk of disease recurrence and death (O'Brien et al., 2008). Furthermore, ovarian cancer with high EDD1 expression resistant to cisplatin and the sensitivity to cisplatin can be restored when EDD1 was depleted, suggesting a new therapeutic target for chemo-resistant ovarian cancer (O'Brien et al., 2008).

This study revealed the mechanism of TIP60 degradation in cervical cancer. In cervical cancer, TIP60 is destabilized by EDD1 (**Figure 9, 10**) and HPV E6 utilizes this mechanism to degrade TIP60 (**Figure 11**). Additionally, I identified that inhibition of EDD1 restores TIP60 level and inhibits colony formation *in vitro* (**Figure 12**) and tumour growth *in vivo* (**Figure 13, 14**). These results indicate that TIP60 is a substrate of EDD1 ubiquitin ligase. Therefore, for future study, it would be very interesting to map the interaction domain between TIP60 and EDD1 through performing co-immunoprecipitation experiment by overexpressing different deletion constructs of TIP60. By mapping the interaction domain, small molecule

compound can be designed to ablate the interaction and restore TIP60 level in cervical cancers. This might possess huge therapeutic value. Furthermore, since EDD1 is a well-known oncogene overexpressed in multiple cancers, TIP60 might be destabilized in the same way by EDD1 in other cancers other than cervical cancers. Therefore, EDD1-TIP60 inhibitor might be a potential universal cancer treatment drug.
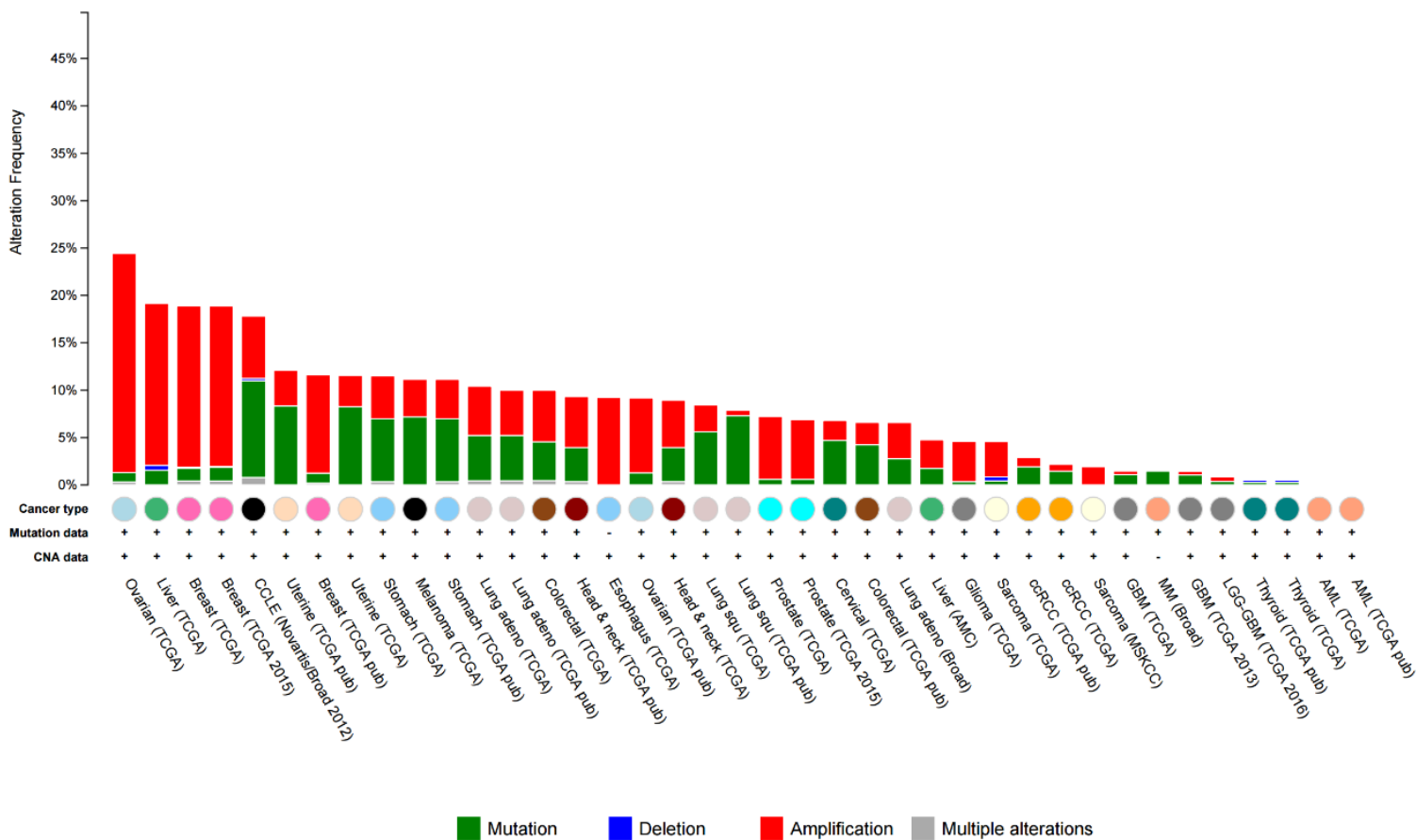
Figure 43. EDD1 is overexpressed and/or mutated in multiple cancers. Data obtained from cBioPortal.

8.3 Viral oncoproteins other than HPV E6 might also destabilize TIP60 through the ubiquitin pathway

Fifteen percent of human cancers worldwide maybe attributed to viruses (zur Hausen, 1991). Especially in cervical cancer and liver cancer, viruses are one of the major risk factors for cancer development. Both RNA and DNA viruses are shown to be capable of inducing cancer development. Human papilloma virus (HPV), Epstein-Barr virus (EBV), Hepatitis B virus (HBV), Human herpes virus 8 [(HHV-8) also known as Kaposi sarcoma-associated herpes virus (KSHV)] and Merkel cell polyomavirus (MCV) are the DNA viruses known to cause human cancers. Human T-lymphotrophic virus-1 (HTLV-1) and Hepatitis C virus (HCV) are the oncogenic RNA virus. Adenovirus is not known to contribute to human cancer, but it can transform human cells and can also contribute to tumour development in new-born rats (Gupta et al., 2013).

Till now, TIP60 has been reported to be destabilized by HPV and adenovirus. Adenovirus destabilizes TIP60 through its oncoproteins EIB55K and E4orf6, however the ligase involved in this mechanism has not been identified yet (Gupta et al., 2013). HPV oncoprotein E6 destabilizes TIP60 through an E6AP independent manner (Jha et al., 2010), and this study has identified EDD1 to be the ligase involved in targeting TIP60 to degradation.

These findings might suggest that other oncoviruses might also be capable of destabilizing TIP60. It is very interesting to investigate TIP60 stability in other oncovirus infected cells. Further, it would be interesting to see if the stability is dependent on the ubiquitin proteasome system. EDD1 might be the ligase utilized by other oncoviruses. If not, a ligase screen could be done to

identify all the ligases that regulate the stability of TIP60. Most importantly, if TIP60 is destabilized by all the oncoviruses, restoring TIP60 level by targeting the ubiquitin ligase involved might be a universal therapeutic way to treat all the virus induced cancers.

8.4 EpCAM participates in inhibition of tumour invasion and is regulated by promoter hypermethylation

EpCAM is one of the epithelial genes involved in inhibiting the EMT process. It is known that EpCAM level would increase in the initial stage of cancer development but decreases dramatically during malignant transformation and progression (Joo et al., 2005). Loss of *EpCAM* expression is associated with aggressive cancers and poor prognoses (Kim et al., 2003; Songun et al., 2005). Moreover, *EpCAM* expression level is lower in circulating and metastatic tumour cells than in their corresponding primary tumours (Rao et al., 2005; Takes et al., 2001). These imply that dynamic change of *EpCAM* expression level is a regulated event during the process of tumour invasion and metastasis (Jojovic et al., 1998).

Expression of *EpCAM* is regulated through epigenetic regulation including promoter methylation and histone modification. It was shown that methylation on H3K9 associates with the repression of *EpCAM* expression (Margueron et al., 2005). However, DNA hypermethylation of *EpCAM* promoter is the key determinant for repression of *EpCAM* expression (Tai et al., 2007). The methylation status of *EpCAM* promoter anti-correlates with *EpCAM* expression (Tai et al., 2007). Additionally, DNA methyltransferase inhibitor (5-aza-2'-deoxycytidine) treatment reactivated the *EpCAM* expression and inhibited cancer cell invasiveness (Alberti et al., 1994; Spizzo

et al., 2007), suggesting a role of DNA hypermethylation in regulating *EpCAM* expression. Interestingly, HDACi (Trichostatin A) treatment has a less significant effect on *EpCAM* expression compared to DNA methyltransferase inhibitor (5-aza-2'-deoxycytidine) treatment, suggesting a dominant role of DNA methylation in regulating *EpCAM* expression (Tai et al., 2007).

Although DNA methylation seems to have a dominant role, it is likely that histone modifications and DNA methylation would work together since DNA methyltransferase inhibitor (5-aza-2'-deoxycytidine) and HDACi (Trichostatin A) treatment together, synergistically resulted in a higher activation of *EpCAM* expression compared to each individual treatment. (Tai et al., 2007). This suggests a correlation between histone modifiers and DNA methyltransferase in regulating target gene expression.

This study has identified a mechanism of regulation of DNA hypermethylation on *EpCAM* promoter, which involves TIP60, DNMT1 and SNAIL2 (**Figure 17-39**). In clinical samples, expression of *EpCAM* might inhibit the metastatic property of tumours and therefore correlates with better prognoses of patients (Basak et al., 2000) and loss of *EpCAM* expression might be a potential marker for the malignancy of cancer (Takes et al., 1997). Since the *EpCAM* expression is repressed by promoter DNA hypermethylation this finding might suggest a new strategy to reactivate *EpCAM* expression in tumour for the treatment of cancer.

8.5 TIP60 antagonizes DNMT1 in regulating *EpCAM* expression

Aberrant DNA methylation is one of the key epigenetic mechanisms that contributes to the process of carcinogenesis (Robertson, 2001). DNA methylation catalysed by DNMTs primarily occurs on the CpG island of the promoter regions and results in gene repression (McCabe et al., 2009). DNMT1 is reported to methylate promoters of epithelial genes such as *EpCAM* and *CDH1*, and results in the repression of cell adhesion molecules and promotes EMT process (Alberti et al., 1994; Fukagawa et al., 2015; Melki et al., 1999; Spizzo et al., 2007; Tai et al., 2007).

This study has reported a novel function of TIP60 to regulate DNMT1 degradation and inhibit EMT process in a DNMT1 dependent manner (**Figure 34, 35**). Additionally, TIP60 inhibits DNMT1 recruitment on *EpCAM* promoter by inhibiting SNAIL2 function (**Figure 39**), which results in hypomethylation of *EpCAM* promoter and further promotion of expression (**Figure 36, 38**). Taken together, TIP60 regulates DNMT1 through both protein stability and chromatin enrichment. More importantly, this regulation of DNMT1 required TIP60's catalytic activity.

Moving forward, one lead from this study would be to investigate whether the same mechanism of TIP60-DNMT1 axis is also found in other cellular processes. If so, the drug inhibitor targeting this mechanism might has a more general therapeutic value.

8.6 SNAIL2 recruits DNMT1 to target promoter for repression

SNAIL family proteins are known to repress expression of cell adhesion molecule and promote expression of mesenchymal related molecule. Previous

studies have indicated that SNAIL1 recruits epigenetic repressor complex such as HDAC1/2, PRC2, LSD1 and G9a (Lin et al., 2014) to *CDH1* promoter for maintaining the repression. Whereas, recruitment of p65 subunit of NK-κB and PARP1 by SNAIL1 to *FN1* promoter activates its expression (Stanisavljevic et al., 2011).

However, little is known for mechanism of SNAIL2 mediated regulation. Previous studies investigating both SNAIL1 and SNAIL2 together, assumed that SNAIL2 behaves similar to SNAIL1, thus SNAIL2 was not studied in detail. As it has been recently reported that a non-equivalent role of SNAIL1 and SNAIL2 in repression of E-CADHERIN expression (Villarejo et al., 2014) (Ye et al., 2015), it would be interesting to identify the molecular mechanism of SNAIL2 mediated regulation.

Here, we showed that both *EpCAM* and *FN1* are direct targets of SNAIL2 (**Figure 31-33**). More interestingly, we showed that SNAIL2 recruits DNMT1 to *EpCAM* promoter region -51 to -32 for repression in the absence of TIP60 (**Figure 39**). SNAIL2 utilizes this mechanism to trigger DNA hypermethylation on *EpCAM* promoter and regulates *EpCAM* expression (**Figure 38**). As little is known about SNAIL2 mediated regulation, this study reveals a novel mechanism of SNAIL2 mediated gene expression. Whether SNAIL2 generally utilizes this mechanism in repressing other target genes needs further investigation.

8.7 DNMT1 is recruited by certain transcription factor to specific site

As a maintenance DNA methyltransferase, DNMT1 copies the pre-existing DNA methylation onto the new DNA strand during DNA replication (Sharif et al., 2007). Interaction with replication component, PCNA and URHF1, is crucial for DNMT1 function during replication (Qin et al., 2015; Schermelleh et al., 2007). Previous studies based on chromatin immunoprecipitation revealed that DNMT1-PCNA-URHF1 complex methylates DNA without site specific (Hervouet et al., 2010).

However, little is known about DNMT1 mediated site-specific DNA methylation. Previous reported that DNMT1 might interact with transcription factors such as SP1 and trigger site-specific methylation (Hervouet et al., 2010). More studies need to be done to reveal this mechanism as DNMT1 might also function as a site-specific DNA methyltransferase which would be crucial for gene expression.

This study revealed a novel transcription factor, SNAIL2, which interacts with DNMT1 (**Figure 39C**) and recruits DNMT1 to specific site of EpCAM promoter (**Figure 39B**). This finding suggests that DNMT1/transcription factors interaction might be a more common mechanism of DNMT1-regulated gene expression.

8.8 TIP60 inhibits SNAIL2-DNMT1 recruitment to target promoter and activates gene expression

Histone acetylation is normally correlated with gene activation. The acetylation usually happens on the lysine residue of histone tails resulting in

neutralization of positive charge and reduction of histone associating affinity for DNA (Hong et al., 1993). As a consequence, this will alter the nucleosome confirmation and increase the accessibility of transcription regulator to chromatin (Lee et al., 1993; Norton et al., 1989; Vettese-Dadey et al., 1996). On the other hand, DNA methylation which occurs on CpG island of gene promoter results in gene repression (McCabe et al., 2009).

DNA methylation has been found to be correlated with histone deacetylation (El-Osta and Wolffe, 2000). Acetylated histones are enriched in unmethylated DNA region but absent from methylated DNA region (Irvine et al., 2002). Additionally, reports showed that histone deacetylase complex is recruited by methylated DNA through methyl-CpG binding protein MeCP2 (Jones et al., 1998; Kaludov and Wolffe, 2000; Nan et al., 1998). Furthermore, a study showed that histone H3 and H4 acetylation negatively correlated with DNA methylation in the regulation of death-associated protein kinase (Satoh et al., 2002). These suggest that histone acetylation and DNA methylation might work inversely to regulate gene expression. However, the mechanism remains unknown. This study might indicate a novel mechanism of histone acetylation inhibits DNA methylation.

TIP60 is known to activate gene expression through facilitating histone acetylation (Frank et al., 2003; Kim et al., 2005). Additionally, this study showed that TIP60 induces *EpCAM* promoter hypomethylation through inhibiting SNAIL2-DNMT1 recruitment (**Figure 36-39**). Most importantly, the inhibition of SNAIL2 recruitment required TIP60 acetyltransferase activity (**Figure 31-33**). Taken together, TIP60 might inhibit SNAIL2-DNMT1 recruitment through mediating histone acetylation. Future, chromatin

103

immunoprecipitation of TIP60 mediated histone acetylation need to be done to confirm this hypothesis.

8.9   Synergy of DNMT1 inhibitor and histone deacetylase inhibitor might be a therapeutic way to treat cancers

Histone deacetylase (HDAC) and DNA methylation are two of the major epigenetic repression systems in cell. Additionally, both these regulatory mechanism are involved in cancer initiation, progression and maintenance.

For histone deacetylase, aberrant expression has been shown in multiple cancers (Ozdag et al., 2006), such as breast cancer (Krusche et al., 2005), lung cancer (Minamiya et al., 2011), liver cancer (Rikimaru et al., 2007), prostate cancer (Weichert et al., 2008b), gastric cancer (Weichert et al., 2008a) and colorectal cancer (Weichert et al., 2008c). Additionally, HDAC has been shown to involve in the silencing of tumour suppressor in cancers, such as p21 (Glozak and Seto, 2007) and BRCA1 (breast cancer 1) (Eot-Houllier et al., 2009). Therefore, histone deacetylase inhibitors have been used in cancer therapy, for example vorinostat and romidepsin for T cell lymphoma (Duvic et al., 2007; Piekarz et al., 2009).

For DNA methylation, its role in carcinogenesis has been discussed in previous section. Hypermethylation of tumour suppressor gene is often observed in cancers. Thus, azacitidine, a DNMT inhibitor is used to prevent hypermethylation and treatment of therapy (Constantinides et al., 1977).

As discussed in above section, the link between histone deacetylase and DNA methylation has been identified. Additionally, histone acetylation and DNA methylation has been shown to work inversely in regulating gene expression. Therefore, targeting DNMTs and HDACs by inhibitors might be an efficient regime for cancer treatment (Cameron et al., 1999; Fraczek et al.,

2012). Studies have already showed that 5-aza-2'deoxycytidine (DNMT inhibitor) and TSA (HDAC inhibitor) combination treatment re-expressed repressed gene much higher than TSA or 5-aza-2'deoxycytidine alone (Chiurazzi et al., 1999). Additionally, TSA and 5-aza-2'deoxycytidine combination treatment has showed to robust prolong effect on cancers (Cameron et al., 1999).

This study revealed a novel mechanism of TIP60 mediated ablation of SNAIL2-DNMT1 axis in an acetylation dependent manner and supports the notion that combination of HDAC inhibitor and DNMT1 inhibitor might have therapeutic value in treatment of SNAIL2 driven breast cancer.

8.10 Regulation of SNAIL2

SNAIL2 is one of the members of SNAIL family proteins. Among all the members, SNAIL1 is studied extensively, whereas less is known about SNAIL2. In most of the cases, SNAIL1/2 were considered to be involved in similar mechanistic pathways, however, in some cases they were demonstrated to have diverse functions (Ye et al., 2015). As far as SNAIL1 is concerned, it is regulated at different levels. For instance, at transcriptional level, *SNAI1* is regulated by signalling pathways such as TGF-β (Peinado et al., 2003), Notch (Sahlgren et al., 2008; Timmerman et al., 2004), WNT (Bachelder et al., 2005; Zhou et al., 2004; Zhou and Hung, 2005) and HIF1-α (Imai et al., 2003). At post-transcriptional level, SNAIL1 is known to be regulated by several microRNAs such as *miR-9* (Liu et al., 2012a), *miR-34* (Kim et al., 2011), *Let-7d* (Chang et al., 2011) and *miR-30a* (Kumarswamy et al., 2012). At protein level, SNAIL1's stability is known to be regulated by E3 ubiquitin ligases such as FBXL14 (Lander et al., 2011) and β-TRCP(Zhou et al., 2004) and

kinases such as GSK3β (Yook et al., 2006), LATS2 (Zhang et al., 2012), PKD1 (Du et al., 2010a) and PAK1 (Yang et al., 2005). Whereas *SNAI2* has been previously reported to be transcriptionally regulated by several transcription factors, such as ELF5 (Chakrabarti et al., 2012), FOXA1, KLF4 (Liu et al., 2012b), SOX3 (Acloque et al., 2011) and SIM2s (Laffin et al., 2008). At post-transcriptional level, SNAIL2 is regulated by several microRNAs such as *miR-1/200* (Liu et al., 2013) and *miR-203* (Zhang et al., 2011), and is known to be phosphorylated by kinases such as GSK3β (Wu et al., 2012) and FBXL14 (Vernon and LaBonne, 2006). Interestingly, these phosphorylation stabilizes SNAIL2 which is similar to the effect on SNAIL1.

In this study, we have identified expression of SNAIL2 to be regulated by DNMT1 (**Figure 34, 39**). However, I did not observe any change in DNA methylation on *SNAI2* promoter (data not shown), suggesting an indirect role of DNMT1 in regulating *SNAI2* transcription. Further studies investigating the molecular mechanism of DNMT1 dependent SNAIL2 regulation will be an exciting avenue to explore.

8.11 Cancer metastasis assays

Curing the primary tumour has high success rates, metastasis is always difficult to treat and is the main cause of cancer related death (McClatchey, 1999). During the metastasis, tumour cells must migrate and invade to the circulating system, travel to distant organ, invade and migrate out of the circulating system and finally adhesion and form a new tumour at distant place. Thus invasion, migration and adhesion are main cellular behaviours related to metastasis (McClatchey, 1999).

To further investigate metastasis process as well as to develop drug targeting this process, it is necessary to have experimentally model metastasis both *in vitro* and *in vivo*.

In vitro modelling systems focus on the cellular properties of metastasis: invasion and migration. Several models have been developed to assess the ability of cell migration and invasion. Wound-healing assay is commonly used to evaluate cell migration (Chen et al., 2012; Oxmann et al., 2008). Same as what has been used in this study, the ability of cells to migrate and the speed at which it closes the wound. *In vitro* invasion assay is usually performed using an invasion chamber with Matrigel coated (Korah et al., 2000) and is commercial available. These chamber with Matrigel mimic the situation of tumour cells passing through the barrier and invading into the circulating system. The invasion ability is evaluated by the number of cells invading to the opposite site of the chamber. Moreover, chemotactic invasion could also be measured by adding additional chemo-attractions into the bottom layer.

Confocal microscopy is also commonly used in *in vitro* models (Kim and Wirtz, 2011). This technique allows researchers to visualize cell migration and invasion more easily. With this technique, researchers are able to target one single cell or a group of cells, and monitor the process of cell migration and adhesion on a cultured plate or cell invading through a chamber. Fluorescence or bioluminescent molecules are often used to label the cells in order to efficient visualization of the migration and invasion process (Bos et al., 2010).

In vitro models are convenient and time saving, and can be used to define the function of potential metastasis regulators or targeting drugs with a short

turnaround time. However, metastasis is a complicated cascade with multiple steps and requires microenvironment. These models can only provide avenues to analyse limited events of metastasis cascade and its challenging to mimic microenvironment *in vitro* (Bos et al., 2010). Therefore, *in vivo* models could be more accurate systems to study metastasis.

There are several experimental models used to model metastasis *in vivo*. Immunodeficiency mice are used as animal model in these *in vivo* assays. The classic assay is to inject cancer cells into the tail vein of the immunodeficiency mice and test their ability to form tumour in lung. Additionally, intra-cardiac injection could also be performed and the ability of cancer cells to form tumour in distal organs, mostly lung, is evaluated same way as tail vein injection. Finally, intravenous injection via mesenteric vein is also used to evaluate liver metastasis (Li et al., 2010). Bioluminescent labelling of injected cells allows them to be tracked by microscopy without sacrificing the mice. The advantages of these assays are the successful measurement of late stage of metastasis. However, they fail to measure the earlier angiogenesis and invasion stages of the metastasis progress. Therefore, these assays might be an incomplete measurement of complete metastasis (Bos et al., 2010; McClatchey, 1999; Mendoza et al., 2010).

Another *in vivo* assay is to inject the cancer cells directly into the peritoneum and their ability to adhere to the surrounding mesothelium (McClatchey, 1999). The advantage of this assay is the successful measurement of the adhesion and survival of cancer cells under physiological relevant scenarios (McClatchey, 1999). However, this assay fails to evaluate

the entire migration and invasion process of metastasis and in my opinion is less rigorous than tail vein injection.

Investigating the regulating gene of metastasis as well as developing drug targeting metastasis requires better metastasis models. A truly physiological model should involves subcutaneous injection, formation of primary tumour, angiogenesis, spontaneous invasion, entering the circulating system, extravasation, seeding and forming new tumour in distant sites. Additionally, organ specific metastasis model is also needed to study certain organ metastasis, such as liver metastasis or lung metastasis, as different cancers usually metastasis to specific organs.

Recent studies have urged the community for a better physiological model for metastasis. However, this is not well-studied due to the incredible infrequent occurring of endogenously arising metastasis in mouse compared to human (McClatchey, 1999). Thus, the challenge of metastasis study in future is to develop better modelling system. These modelling systems would provide us more accurate strategies to develop rational treatment and screen potential drugs.

References

Acloque, H., Ocana, O.H., Matheu, A., Rizzoti, K., Wise, C., Lovell-Badge, R., and Nieto, M.A. (2011). Reciprocal repression between Sox3 and snail transcription factors defines embryonic territories at gastrulation. Dev Cell *21*, 546-558.

Alberti, S., Nutini, M., and Herzenberg, L.A. (1994). DNA methylation prevents the amplification of TROP1, a tumor-associated cell surface antigen gene. Proc Natl Acad Sci U S A *91*, 5833-5837.

Auger, A., Galarneau, L., Altaf, M., Nourani, A., Doyon, Y., Utley, R.T., Cronier, D., Allard, S., and Cote, J. (2008). Eaf1 is the platform for NuA4 molecular assembly that evolutionarily links chromatin acetylation to ATP-dependent exchange of histone H2A variants. Mol Cell Biol *28*, 2257-2270.

Ayoub, N., Jeyasekharan, A.D., Bernal, J.A., and Venkitaraman, A.R. (2008). HP1-beta mobilization promotes chromatin changes that initiate the DNA damage response. Nature *453*, 682-686.

Ayrapetov, M.K., Gursoy-Yuzugullu, O., Xu, C., Xu, Y., and Price, B.D. (2014). DNA double-strand breaks promote methylation of histone H3 on lysine 9 and transient formation of repressive chromatin. Proc Natl Acad Sci U S A *111*, 9169-9174.

Bachelder, R.E., Yoon, S.O., Franci, C., de Herreros, A.G., and Mercurio, A.M. (2005). Glycogen synthase kinase-3 is an endogenous inhibitor of Snail transcription: implications for the epithelial-mesenchymal transition. J Cell Biol *168*, 29-33.

Bararia, D., Trivedi, A.K., Zada, A.A., Greif, P.A., Mulaw, M.A., Christopeit, M., Hiddemann, W., Bohlander, S.K., and Behre, G. (2008). Proteomic identification of the MYST domain histone acetyltransferase TIP60 (HTATIP) as a co-activator of the myeloid transcription factor C/EBPalpha. Leukemia *22*, 800-807.

Barski, A., Cuddapah, S., Cui, K., Roh, T.Y., Schones, D.E., Wang, Z., Wei, G., Chepelev, I., and Zhao, K. (2007). High-resolution profiling of histone methylations in the human genome. Cell *129*, 823-837.

Basak, S., Eck, S., Gutzmer, R., Smith, A.J., Birebent, B., Purev, E., Staib, L., Somasundaram, R., Zaloudik, J., Li, W.*, et al.* (2000). Colorectal cancer vaccines: antiidiotypic antibody, recombinant protein, and viral vector. Ann N Y Acad Sci *910*, 237-252; discussion 252-233.

Bestor, T.H. (2000). The DNA methyltransferases of mammals. Hum Mol Genet *9*, 2395-2402.

Borrow, J., Stanton, V.P., Jr., Andresen, J.M., Becher, R., Behm, F.G., Chaganti, R.S., Civin, C.I., Disteche, C., Dube, I., Frischauf, A.M.*, et al.* (1996). The translocation t(8;16)(p11;p13) of acute myeloid leukaemia fuses a putative acetyltransferase to the CREB-binding protein. Nat Genet *14*, 33-41.

Bos, P.D., Nguyen, D.X., and Massague, J. (2010). Modeling metastasis in the mouse. Curr Opin Pharmacol *10*, 571-577.

Boyer, B., and Thiery, J.P. (1993). Epithelium-mesenchyme interconversion as example of epithelial plasticity. APMIS *101*, 257-268.

Cameron, E.E., Bachman, K.E., Myohanen, S., Herman, J.G., and Baylin, S.B. (1999). Synergy of demethylation and histone deacetylase inhibition in the re-expression of genes silenced in cancer. Nat Genet *21*, 103-107.

Chakrabarti, R., Hwang, J., Andres Blanco, M., Wei, Y., Lukacisin, M., Romano, R.A., Smalley, K., Liu, S., Yang, Q., Ibrahim, T.*, et al.* (2012). Elf5 inhibits the epithelial-mesenchymal transition in mammary gland development and breast cancer metastasis by transcriptionally repressing Snail2. Nat Cell Biol *14*, 1212-1222.

Chang, C.J., Hsu, C.C., Chang, C.H., Tsai, L.L., Chang, Y.C., Lu, S.W., Yu, C.H., Huang, H.S., Wang, J.J., Tsai, C.H.*, et al.* (2011). Let-7d functions as novel regulator of

epithelial-mesenchymal transition and chemoresistant property in oral cancer. Oncol Rep *26*, 1003-1010.

Charvet, C., Wissler, M., Brauns-Schubert, P., Wang, S.J., Tang, Y., Sigloch, F.C., Mellert, H., Brandenburg, M., Lindner, S.E., Breit, B.*, et al.* (2011). Phosphorylation of Tip60 by GSK-3 determines the induction of PUMA and apoptosis by p53. Mol Cell *42*, 584-596.

Chen, G., Cheng, Y., Tang, Y., Martinka, M., and Li, G. (2012). Role of Tip60 in human melanoma cell migration, metastasis, and patient survival. J Invest Dermatol *132*, 2632-2641.

Chen, P.B., Chen, H.V., Acharya, D., Rando, O.J., and Fazzio, T.G. (2015). R loops regulate promoter-proximal chromatin architecture and cellular differentiation. Nat Struct Mol Biol *22*, 999-1007.

Chiurazzi, P., Pomponi, M.G., Pietrobono, R., Bakker, C.E., Neri, G., and Oostra, B.A. (1999). Synergistic effect of histone hyperacetylation and DNA demethylation in the reactivation of the FMR1 gene. Hum Mol Genet *8*, 2317-2323.

Clancy, J.L., Henderson, M.J., Russell, A.J., Anderson, D.W., Bova, R.J., Campbell, I.G., Choong, D.Y., Macdonald, G.A., Mann, G.J., Nolan, T.*, et al.* (2003). EDD, the human orthologue of the hyperplastic discs tumour suppressor gene, is amplified and overexpressed in cancer. Oncogene *22*, 5070-5081.

Col, E., Caron, C., Chable-Bessia, C., Legube, G., Gazzeri, S., Komatsu, Y., Yoshida, M., Benkirane, M., Trouche, D., and Khochbin, S. (2005). HIV-1 Tat targets Tip60 to impair the apoptotic cell response to genotoxic stresses. EMBO J *24*, 2634-2645.

Constantinides, P.G., Jones, P.A., and Gevers, W. (1977). Functional striated muscle cells from non-myoblast precursors following 5-azacytidine treatment. Nature *267*, 364-366.

Cooper, B., Schneider, S., Bohl, J., Jiang, Y., Beaudet, A., and Vande Pol, S. (2003). Requirement of E6AP and the features of human papillomavirus E6 necessary to support degradation of p53. Virology *306*, 87-99.

Craft, N., Bruhn, K.W., Nguyen, B.D., Prins, R., Liau, L.M., Collisson, E.A., De, A., Kolodney, M.S., Gambhir, S.S., and Miller, J.F. (2005). Bioluminescent imaging of melanoma in live mice. J Invest Dermatol *125*, 159-165.

Doyon, Y., and Cote, J. (2004). The highly conserved and multifunctional NuA4 HAT complex. Curr Opin Genet Dev *14*, 147-154.

Du, C., Zhang, C., Hassan, S., Biswas, M.H., and Balaji, K.C. (2010a). Protein kinase D1 suppresses epithelial-to-mesenchymal transition through phosphorylation of snail. Cancer Res *70*, 7810-7819.

Du, Z., Song, J., Wang, Y., Zhao, Y., Guda, K., Yang, S., Kao, H.Y., Xu, Y., Willis, J., Markowitz, S.D.*, et al.* (2010b). DNMT1 stability is regulated by proteins coordinating deubiquitination and acetylation-driven ubiquitination. Sci Signal *3*, ra80.

Duvic, M., Talpur, R., Ni, X., Zhang, C., Hazarika, P., Kelly, C., Chiao, J.H., Reilly, J.F., Ricker, J.L., Richon, V.M.*, et al.* (2007). Phase 2 trial of oral vorinostat (suberoylanilide hydroxamic acid, SAHA) for refractory cutaneous T-cell lymphoma (CTCL). Blood *109*, 31-39.

Ehrenhofer-Murray, A.E., Rivier, D.H., and Rine, J. (1997). The role of Sas2, an acetyltransferase homologue of Saccharomyces cerevisiae, in silencing and ORC function. Genetics *145*, 923-934.

El-Osta, A., and Wolffe, A.P. (2000). DNA methylation and histone deacetylation in the control of gene expression: basic biochemistry to human development and disease. Gene Expr *9*, 63-75.

Eot-Houllier, G., Fulcrand, G., Magnaghi-Jaulin, L., and Jaulin, C. (2009). Histone deacetylase inhibitors and genomic instability. Cancer Lett *274*, 169-176.

Espada, J., Peinado, H., Lopez-Serra, L., Setien, F., Lopez-Serra, P., Portela, A., Renart, J., Carrasco, E., Calvo, M., Juarranz, A., *et al.* (2011). Regulation of SNAIL1 and E-cadherin function by DNMT1 in a DNA methylation-independent context. Nucleic Acids Res *39*, 9194-9205.

Fraczek, J.E., Vinken, M., Tourwe, D., Vanhaecke, T., and Rogiers, V. (2012). Synergetic effects of DNA demethylation and histone deacetylase inhibition in primary rat hepatocytes. Invest New Drugs *30*, 1715-1724.

Frank, S.R., Parisi, T., Taubert, S., Fernandez, P., Fuchs, M., Chan, H.M., Livingston, D.M., and Amati, B. (2003). MYC recruits the TIP60 histone acetyltransferase complex to chromatin. EMBO Rep *4*, 575-580.

Fukagawa, A., Ishii, H., Miyazawa, K., and Saitoh, M. (2015). deltaEF1 associates with DNMT1 and maintains DNA methylation of the E-cadherin promoter in breast cancer cells. Cancer Med *4*, 125-135.

Glozak, M.A., and Seto, E. (2007). Histone deacetylases and cancer. Oncogene *26*, 5420-5432.

Gorrini, C., Squatrito, M., Luise, C., Syed, N., Perna, D., Wark, L., Martinato, F., Sardella, D., Verrecchia, A., Bennett, S., *et al.* (2007). Tip60 is a haplo-insufficient tumour suppressor required for an oncogene-induced DNA damage response. Nature *448*, 1063-1067.

Gupta, A., Jha, S., Engel, D.A., Ornelles, D.A., and Dutta, A. (2013). Tip60 degradation by adenovirus relieves transcriptional repression of viral transcriptional activator EIA. Oncogene *32*, 5017-5025.

Hay, E.D. (1995). An overview of epithelio-mesenchymal transformation. Acta Anat (Basel) *154*, 8-20.

Hervouet, E., Vallette, F.M., and Cartron, P.F. (2010). Dnmt1/Transcription factor interactions: an alternative mechanism of DNA methylation inheritance. Genes Cancer *1*, 434-443.

Hilfiker, A., Hilfiker-Kleiner, D., Pannuti, A., and Lucchesi, J.C. (1997). mof, a putative acetyl transferase gene related to the Tip60 and MOZ human genes and to the SAS genes of yeast, is required for dosage compensation in Drosophila. EMBO J *16*, 2054-2060.

Hlubek, F., Lohberg, C., Meiler, J., Jung, A., Kirchner, T., and Brabletz, T. (2001). Tip60 is a cell-type-specific transcriptional regulator. J Biochem *129*, 635-641.

Hoek, K., Rimm, D.L., Williams, K.R., Zhao, H., Ariyan, S., Lin, A., Kluger, H.M., Berger, A.J., Cheng, E., Trombetta, E.S., *et al.* (2004). Expression profiling reveals novel pathways in the transformation of melanocytes to melanomas. Cancer Res *64*, 5270-5282.

Hong, L., Schroth, G.P., Matthews, H.R., Yau, P., and Bradbury, E.M. (1993). Studies of the DNA binding properties of histone H4 amino terminus. Thermal denaturation studies reveal that acetylation markedly reduces the binding constant of the H4 "tail" to DNA. J Biol Chem *268*, 305-314.

Howley, P.M., and Livingston, D.M. (2009). Small DNA tumor viruses: large contributors to biomedical sciences. Virology *384*, 256-259.

Huang, J., Stewart, A., Maity, B., Hagen, J., Fagan, R.L., Yang, J., Quelle, D.E., Brenner, C., and Fisher, R.A. (2014). RGS6 suppresses Ras-induced cellular transformation by facilitating Tip60-mediated Dnmt1 degradation and promoting apoptosis. Oncogene *33*, 3604-3611.

Huang, R.Y., Guilford, P., and Thiery, J.P. (2012). Early events in cell adhesion and polarity during epithelial-mesenchymal transition. J Cell Sci *125*, 4417-4422.

Huibregtse, J.M., Scheffner, M., and Howley, P.M. (1991). A cellular protein mediates association of p53 with the E6 oncoprotein of human papillomavirus types 16 or 18. EMBO J *10*, 4129-4135.

Huibregtse, J.M., Scheffner, M., and Howley, P.M. (1993). Localization of the E6-AP regions that direct human papillomavirus E6 binding, association with p53, and ubiquitination of associated proteins. Mol Cell Biol *13*, 4918-4927.

Husemann, Y., Geigl, J.B., Schubert, F., Musiani, P., Meyer, M., Burghart, E., Forni, G., Eils, R., Fehm, T., Riethmuller, G.*, et al.* (2008). Systemic spread is an early step in breast cancer. Cancer Cell *13*, 58-68.

Imai, T., Horiuchi, A., Wang, C., Oka, K., Ohira, S., Nikaido, T., and Konishi, I. (2003). Hypoxia attenuates the expression of E-cadherin via up-regulation of SNAIL in ovarian carcinoma cells. Am J Pathol *163*, 1437-1447.

Irvine, R.A., Lin, I.G., and Hsieh, C.L. (2002). DNA methylation has a local effect on transcription and histone acetylation. Mol Cell Biol *22*, 6689-6696.

Jacobs, S.A., and Khorasanizadeh, S. (2002). Structure of HP1 chromodomain bound to a lysine 9-methylated histone H3 tail. Science *295*, 2080-2083.

Jacquet, K., Fradet-Turcotte, A., Avvakumov, N., Lambert, J.P., Roques, C., Pandita, R.K., Paquet, E., Herst, P., Gingras, A.C., Pandita, T.K.*, et al.* (2016). The TIP60 Complex Regulates Bivalent Chromatin Recognition by 53BP1 through Direct H4K20me Binding and H2AK15 Acetylation. Mol Cell *62*, 409-421.

Jha, S., and Dutta, A. (2009). RVB1/RVB2: running rings around molecular biology. Mol Cell *34*, 521-533.

Jha, S., Vande Pol, S., Banerjee, N.S., Dutta, A.B., Chow, L.T., and Dutta, A. (2010). Destabilization of TIP60 by human papillomavirus E6 results in attenuation of TIP60-dependent transcriptional regulation and apoptotic pathway. Mol Cell *38*, 700-711.

Johnson, W.E., Li, C., and Rabinovic, A. (2007). Adjusting batch effects in microarray expression data using empirical Bayes methods. Biostatistics *8*, 118-127.

Jojovic, M., Adam, E., Zangemeister-Wittke, U., and Schumacher, U. (1998). Epithelial glycoprotein-2 expression is subject to regulatory processes in epithelial-mesenchymal transitions during metastases: an investigation of human cancers transplanted into severe combined immunodeficient mice. Histochem J *30*, 723-729.

Jones, P.A., and Baylin, S.B. (2007). The epigenomics of cancer. Cell *128*, 683-692.

Jones, P.L., Veenstra, G.J., Wade, P.A., Vermaak, D., Kass, S.U., Landsberger, N., Strouboulis, J., and Wolffe, A.P. (1998). Methylated DNA and MeCP2 recruit histone deacetylase to repress transcription. Nat Genet *19*, 187-191.

Joo, M., Kim, H., Kim, M.K., Yu, H.J., and Kim, J.P. (2005). Expression of Ep-CAM in intestinal metaplasia, gastric epithelial dysplasia and gastric adenocarcinoma. J Gastroen Hepatol *20*, 1039-1045.

Kaidi, A., and Jackson, S.P. (2013). KAT5 tyrosine phosphorylation couples chromatin sensing to ATM signalling. Nature *498*, 70-74.

Kaludov, N.K., and Wolffe, A.P. (2000). MeCP2 driven transcriptional repression *in vitro*: selectivity for methylated DNA, action at a distance and contacts with the basal transcription machinery. Nucleic Acids Res *28*, 1921-1928.

Kamine, J., Elangovan, B., Subramanian, T., Coleman, D., and Chinnadurai, G. (1996). Identification of a cellular protein that specifically interacts with the essential cysteine region of the HIV-1 Tat transactivator. Virology *216*, 357-366.

Karnani, N., Taylor, C., Malhotra, A., and Dutta, A. (2007). Pan-S replication patterns and chromosomal domains defined by genome-tiling arrays of ENCODE genomic areas. Genome Res *17*, 865-876.

Kim, D.H., and Wirtz, D. (2011). Recapitulating cancer cell invasion *in vitro*. Proc Natl Acad Sci U S A *108*, 6693-6694.

Kim, J.H., Herlyn, D., Wong, K.K., Park, D.C., Schorge, J.O., Lu, K.H., Skates, S.J., Cramer, D.W., Berkowitz, R.S., and Mok, S.C. (2003). Identification of epithelial cell adhesion molecule autoantibody in patients with ovarian cancer. Clin Cancer Res *9*, 4782-4791.

Kim, J.H., Kim, B., Cai, L., Choi, H.J., Ohgi, K.A., Tran, C., Chen, C., Chung, C.H., Huber, O., Rose, D.W*., et al.* (2005). Transcriptional regulation of a metastasis suppressor gene by Tip60 and beta-catenin complexes. Nature *434*, 921-926.

Kim, N.H., Kim, H.S., Li, X.Y., Lee, I., Choi, H.S., Kang, S.E., Cha, S.Y., Ryu, J.K., Yoon, D., Fearon, E.R*., et al.* (2011). A p53/miRNA-34 axis regulates Snail1-dependent cancer cell epithelial-mesenchymal transition. J Cell Biol *195*, 417-433.

Knowles, L.M., Gurski, L.A., Engel, C., Gnarra, J.R., Maranchie, J.K., and Pilch, J. (2013). Integrin alphavbeta3 and fibronectin upregulate Slug in cancer cells to promote clot invasion and metastasis. Cancer Res *73*, 6175-6184.

Korah, R.M., Sysounthone, V., Golowa, Y., and Wieder, R. (2000). Basic fibroblast growth factor confers a less malignant phenotype in MDA-MB-231 human breast cancer cells. Cancer Res *60*, 733-740.

Krusche, C.A., Wulfing, P., Kersting, C., Vloet, A., Bocker, W., Kiesel, L., Beier, H.M., and Alfer, J. (2005). Histone deacetylase-1 and -3 protein expression in human breast cancer: a tissue microarray analysis. Breast Cancer Res Treat *90*, 15-23.

Kumar, A.P., Loo, S.Y., Shin, S.W., Tan, T.Z., Eng, C.B., Singh, R., Putti, T.C., Ong, C.W., Salto-Tellez, M., Goh, B.C*., et al.* (2013). Manganese Superoxide Dismutase Is a Promising Target for Enhancing Chemosensitivity of Basal-like Breast Carcinoma. Antioxid Redox Signal.

Kumarswamy, R., Mudduluru, G., Ceppi, P., Muppala, S., Kozlowski, M., Niklinski, J., Papotti, M., and Allgayer, H. (2012). MicroRNA-30a inhibits epithelial-to-mesenchymal transition by targeting Snai1 and is downregulated in non-small cell lung cancer. Int J Cancer *130*, 2044-2053.

Laffin, B., Wellberg, E., Kwak, H.I., Burghardt, R.C., Metz, R.P., Gustafson, T., Schedin, P., and Porter, W.W. (2008). Loss of singleminded-2s in the mouse mammary gland induces an epithelial-mesenchymal transition associated with up-regulation of slug and matrix metalloprotease 2. Molecular and cellular biology *28*, 1936-1946.

Lander, R., Nordin, K., and LaBonne, C. (2011). The F-box protein Ppa is a common regulator of core EMT factors Twist, Snail, Slug, and Sip1. J Cell Biol *194*, 17-25.

Lee, D.Y., Hayes, J.J., Pruss, D., and Wolffe, A.P. (1993). A positive role for histone acetylation in transcription factor access to nucleosomal DNA. Cell *72*, 73-84.

Lee, M.S., Seo, J., Choi, D.Y., Lee, E.W., Ko, A., Ha, N.C., Yoon, J.B., Lee, H.W., Kim, K.P., and Song, J. (2013). Stabilization of p21 (Cip1/WAF1) following Tip60-dependent acetylation is required for p21-mediated DNA damage response. Cell Death Differ *20*, 620-629.

Legube, G., Linares, L.K., Lemercier, C., Scheffner, M., Khochbin, S., and Trouche, D. (2002). Tip60 is targeted to proteasome-mediated degradation by Mdm2 and accumulates after UV irradiation. EMBO J *21*, 1704-1712.

Legube, G., and Trouche, D. (2003). Identification of a larger form of the histone acetyl transferase Tip60. Gene *310*, 161-168.

Lemercier, C., Legube, G., Caron, C., Louwagie, M., Garin, J., Trouche, D., and Khochbin, S. (2003). Tip60 acetyltransferase activity is controlled by phosphorylation. J Biol Chem *278*, 4713-4718.

Li, Q., Wei, D., Wang, L., Wang, L., Jia, Z., Le, X., Gao, Y., Huang, S., and Xie, K. (2010). Modeling liver metastasis using a tumor cell line derived from an enhanced green fluorescent protein transgenic mouse. Clin Exp Metastasis *27*, 11-18.

Liang, Z., Yoon, Y., Votaw, J., Goodman, M.M., Williams, L., and Shim, H. (2005). Silencing of CXCR4 blocks breast cancer metastasis. Cancer Res *65*, 967-971.

Lin, S.Y., Li, T.Y., Liu, Q., Zhang, C., Li, X., Chen, Y., Zhang, S.M., Lian, G., Liu, Q., Ruan, K*., et al.* (2012). GSK3-TIP60-ULK1 signaling pathway links growth factor deprivation to autophagy. Science *336*, 477-481.

Lin, Y., Dong, C., and Zhou, B.P. (2014). Epigenetic regulation of EMT: the Snail story. Curr Pharm Des *20*, 1698-1705.

Liu, S., Kumar, S.M., Lu, H., Liu, A., Yang, R., Pushparajan, A., Guo, W., and Xu, X. (2012a). MicroRNA-9 up-regulates E-cadherin through inhibition of NF-kappaB1-Snail1 pathway in melanoma. J Pathol *226*, 61-72.

Liu, Y.N., Abou-Kheir, W., Yin, J.J., Fang, L., Hynes, P., Casey, O., Hu, D., Wan, Y., Seng, V., Sheppard-Tillman, H*., et al.* (2012b). Critical and reciprocal regulation of KLF4 and SLUG in transforming growth factor beta-initiated prostate cancer epithelial-mesenchymal transition. Molecular and cellular biology *32*, 941-953.

Liu, Y.N., Yin, J.J., Abou-Kheir, W., Hynes, P.G., Casey, O.M., Fang, L., Yi, M., Stephens, R.M., Seng, V., Sheppard-Tillman, H*., et al.* (2013). MiR-1 and miR-200 inhibit EMT via Slug-dependent and tumorigenesis via Slug-independent mechanisms. Oncogene *32*, 296-306.

Luijsterburg, M.S., Dinant, C., Lans, H., Stap, J., Wiernasz, E., Lagerwerf, S., Warmerdam, D.O., Lindh, M., Brink, M.C., Dobrucki, J.W*., et al.* (2009). Heterochromatin protein 1 is recruited to various types of DNA damage. J Cell Biol *185*, 577-586.

Margueron, R., Trojer, P., and Reinberg, D. (2005). The key to development: interpreting the histone code? Curr Opin Genet Dev *15*, 163-176.

McCabe, M.T., Brandes, J.C., and Vertino, P.M. (2009). Cancer DNA methylation: molecular mechanisms and clinical implications. Clin Cancer Res *15*, 3927-3937.

McClatchey, A.I. (1999). Modeling metastasis in the mouse. Oncogene *18*, 5334-5339.

ME, L.L., Vidal, F., Gallardo, D., Diaz-Fuertes, M., Rojo, F., Cuatrecasas, M., Lopez-Vicente, L., Kondoh, H., Blanco, C., Carnero, A*., et al.* (2006). New p53 related genes in human tumors: significant downregulation in colon and lung carcinomas. Oncol Rep *16*, 603-608.

Melki, J.R., Vincent, P.C., and Clark, S.J. (1999). Concurrent DNA hypermethylation of multiple genes in acute myeloid leukemia. Cancer Res *59*, 3730-3740.

Mendoza, A., Hong, S.H., Osborne, T., Khan, M.A., Campbell, K., Briggs, J., Eleswarapu, A., Buquo, L., Ren, L., Hewitt, S.M*., et al.* (2010). Modeling metastasis biology and therapy in real time in the mouse lung. J Clin Invest *120*, 2979-2988.

Mikeska, T., Felsberg, J., Hewitt, C.A., and Dobrovic, A. (2011). Analysing DNA methylation using bisulphite pyrosequencing. Methods Mol Biol *791*, 33-53.

Minamiya, Y., Ono, T., Saito, H., Takahashi, N., Ito, M., Mitsui, M., Motoyama, S., and Ogawa, J. (2011). Expression of histone deacetylase 1 correlates with a poor prognosis in patients with adenocarcinoma of the lung. Lung Cancer *74*, 300-304.

Miyamoto, N., Izumi, H., Noguchi, T., Nakajima, Y., Ohmiya, Y., Shiota, M., Kidani, A., Tawara, A., and Kohno, K. (2008). Tip60 is regulated by circadian transcription factor clock and is involved in cisplatin resistance. J Biol Chem *283*, 18218-18226.

Munger, K., and Howley, P.M. (2002). Human papillomavirus immortalization and transformation functions. Virus Res *89*, 213-228.

Nan, X., Ng, H.H., Johnson, C.A., Laherty, C.D., Turner, B.M., Eisenman, R.N., and Bird, A. (1998). Transcriptional repression by the methyl-CpG-binding protein MeCP2 involves a histone deacetylase complex. Nature *393*, 386-389.

Nielsen, P.R., Nietlispach, D., Mott, H.R., Callaghan, J., Bannister, A., Kouzarides, T., Murzin, A.G., Murzina, N.V., and Laue, E.D. (2002). Structure of the HP1 chromodomain bound to histone H3 methylated at lysine 9. Nature *416*, 103-107.

Norton, V.G., Imai, B.S., Yau, P., and Bradbury, E.M. (1989). Histone acetylation reduces nucleosome core particle linking number change. Cell *57*, 449-457.

O'Brien, P.M., Davies, M.J., Scurry, J.P., Smith, A.N., Barton, C.A., Henderson, M.J., Saunders, D.N., Gloss, B.S., Patterson, K.I., Clancy, J.L.*, et al.* (2008). The E3 ubiquitin ligase EDD is an adverse prognostic factor for serous epithelial ovarian cancer and modulates cisplatin resistance *in vitro*. Br J Cancer *98*, 1085-1093.

Oxmann, D., Held-Feindt, J., Stark, A.M., Hattermann, K., Yoneda, T., and Mentlein, R. (2008). Endoglin expression in metastatic breast cancer cells enhances their invasive phenotype. Oncogene *27*, 3567-3575.

Ozdag, H., Teschendorff, A.E., Ahmed, A.A., Hyland, S.J., Blenkiron, C., Bobrow, L., Veerakumarasivam, A., Burtt, G., Subkhankulova, T., Arends, M.J.*, et al.* (2006). Differential expression of selected histone modifier genes in human solid cancers. BMC Genomics *7*, 90.

Pandey, A.K., Zhang, Y., Zhang, S., Li, Y., Tucker-Kellogg, G., Yang, H., and Jha, S. (2015). TIP60-miR-22 axis as a prognostic marker of breast cancer progression. Oncotarget *6*, 41290-41306.

Park, J., and Schwarzbauer, J.E. (2014). Mammary epithelial cell interactions with fibronectin stimulate epithelial-mesenchymal transition. Oncogene *33*, 1649-1657.

Patel, J.H., Du, Y., Ard, P.G., Phillips, C., Carella, B., Chen, C.J., Rakowski, C., Chatterjee, C., Lieberman, P.M., Lane, W.S.*, et al.* (2004). The c-MYC oncoprotein is a substrate of the acetyltransferases hGCN5/PCAF and TIP60. Mol Cell Biol *24*, 10826-10834.

Peinado, H., Quintanilla, M., and Cano, A. (2003). Transforming growth factor beta-1 induces snail transcription factor in epithelial cell lines: mechanisms for epithelial mesenchymal transitions. The Journal of biological chemistry *278*, 21113-21123.

Piekarz, R.L., Frye, R., Turner, M., Wright, J.J., Allen, S.L., Kirschbaum, M.H., Zain, J., Prince, H.M., Leonard, J.P., Geskin, L.J.*, et al.* (2009). Phase II multi-institutional trial of the histone deacetylase inhibitor romidepsin as monotherapy for patients with cutaneous T-cell lymphoma. J Clin Oncol *27*, 5410-5417.

Prall, F. (2007). Tumour budding in colorectal carcinoma. Histopathology *50*, 151-162.

Prat, A., Parker, J.S., Karginova, O., Fan, C., Livasy, C., Herschkowitz, J.I., He, X., and Perou, C.M. (2010). Phenotypic and molecular characterization of the claudin-low intrinsic subtype of breast cancer. Breast Cancer Res *12*, R68.

Qin, W., Wolf, P., Liu, N., Link, S., Smets, M., La Mastra, F., Forne, I., Pichler, G., Horl, D., Fellinger, K.*, et al.* (2015). DNA methylation requires a DNMT1 ubiquitin interacting motif (UIM) and histone ubiquitination. Cell Res *25*, 911-929.

Ran, Q., and Pereira-Smith, O.M. (2000). Identification of an alternatively spliced form of the Tat interactive protein (Tip60), Tip60(beta). Gene *258*, 141-146.

Rao, C.G., Chianese, D., Doyle, G.V., Miller, M.C., Russell, T., Sanders, R.A., Jr., and Terstappen, L.W. (2005). Expression of epithelial cell adhesion molecule in carcinoma cells present in blood and primary and metastatic tumors. Int J Oncol *27*, 49-57.

Regha, K., Sloane, M.A., Huang, R., Pauler, F.M., Warczok, K.E., Melikant, B., Radolf, M., Martens, J.H., Schotta, G., Jenuwein, T.*, et al.* (2007). Active and repressive chromatin are interspersed without spreading in an imprinted gene cluster in the mammalian genome. Mol Cell *27*, 353-366.

Reifsnyder, C., Lowell, J., Clarke, A., and Pillus, L. (1996). Yeast SAS silencing genes and human genes associated with AML and HIV-1 Tat interactions are homologous with acetyltransferases. Nat Genet *14*, 42-49.

Rikimaru, T., Taketomi, A., Yamashita, Y., Shirabe, K., Hamatsu, T., Shimada, M., and Maehara, Y. (2007). Clinical significance of histone deacetylase 1 expression in patients with hepatocellular carcinoma. Oncology *72*, 69-74.

Robertson, K.D. (2001). DNA methylation, methyltransferases, and cancer. Oncogene *20*, 3139-3155.

Sahlgren, C., Gustafsson, M.V., Jin, S., Poellinger, L., and Lendahl, U. (2008). Notch signaling mediates hypoxia-induced tumor cell migration and invasion. Proc Natl Acad Sci U S A *105*, 6392-6397.

Sakuraba, K., Yasuda, T., Sakata, M., Kitamura, Y.H., Shirahata, A., Goto, T., Mizukami, H., Saito, M., Ishibashi, K., Kigawa, G.*, et al.* (2009). Down-regulation of Tip60 gene as a potential marker for the malignancy of colorectal cancer. Anticancer Res *29*, 3953-3955.

Sapountzi, V., Logan, I.R., and Robson, C.N. (2006). Cellular functions of TIP60. Int J Biochem Cell Biol *38*, 1496-1509.

Satoh, A., Toyota, M., Itoh, F., Kikuchi, T., Obata, T., Sasaki, Y., Suzuki, H., Yawata, A., Kusano, M., Fujita, M.*, et al.* (2002). DNA methylation and histone deacetylation associated with silencing DAP kinase gene expression in colorectal and gastric cancers. Br J Cancer *86*, 1817-1823.

Scheffner, M., Huibregtse, J.M., Vierstra, R.D., and Howley, P.M. (1993). The HPV-16 E6 and E6-AP complex functions as a ubiquitin-protein ligase in the ubiquitination of p53. Cell *75*, 495-505.

Schermelleh, L., Haemmer, A., Spada, F., Rosing, N., Meilinger, D., Rothbauer, U., Cardoso, M.C., and Leonhardt, H. (2007). Dynamics of Dnmt1 interaction with the replication machinery and its role in postreplicative maintenance of DNA methylation. Nucleic Acids Res *35*, 4301-4312.

Schmidt, W.M., Sedivy, R., Forstner, B., Steger, G.G., Zochbauer-Muller, S., and Mader, R.M. (2007). Progressive up-regulation of genes encoding DNA methyltransferases in the colorectal adenoma-carcinoma sequence. Mol Carcinog *46*, 766-772.

Sharif, J., Muto, M., Takebayashi, S., Suetake, I., Iwamatsu, A., Endo, T.A., Shinga, J., Mizutani-Koseki, Y., Toyoda, T., Okamura, K.*, et al.* (2007). The SRA protein Np95 mediates epigenetic inheritance by recruiting Dnmt1 to methylated DNA. Nature *450*, 908-912.

Shi, J., Wang, Y., Zeng, L., Wu, Y., Deng, J., Zhang, Q., Lin, Y., Li, J., Kang, T., Tao, M.*, et al.* (2014). Disrupting the interaction of BRD4 with diacetylated Twist suppresses tumorigenesis in basal-like breast cancer. Cancer Cell *25*, 210-225.

Songun, I., Litvinov, S.V., van de Velde, C.J., Pals, S.T., Hermans, J., and van Krieken, J.H. (2005). Loss of Ep-CAM (CO17-1A) expression predicts survival in patients with gastric cancer. Br J Cancer *92*, 1767-1772.

Spizzo, G., Gastl, G., Obrist, P., Fong, D., Haun, M., Grunewald, K., Parson, W., Eichmann, C., Millinger, S., Fiegl, H.*, et al.* (2007). Methylation status of the Ep-CAM promoter region in human breast cancer cell lines and breast cancer tissue. Cancer Lett *246*, 253-261.

Squatrito, M., Gorrini, C., and Amati, B. (2006). Tip60 in DNA damage response and growth control: many tricks in one HAT. Trends Cell Biol *16*, 433-442.

Stanisavljevic, J., Porta-de-la-Riva, M., Batlle, R., de Herreros, A.G., and Baulida, J. (2011). The p65 subunit of NF-kappaB and PARP1 assist Snail1 in activating fibronectin transcription. J Cell Sci *124*, 4161-4171.

Stucki, M., Clapperton, J.A., Mohammad, D., Yaffe, M.B., Smerdon, S.J., and Jackson, S.P. (2005). MDC1 directly binds phosphorylated histone H2AX to regulate cellular responses to DNA double-strand breaks. Cell *123*, 1213-1226.

Subbaiah, V.K., Zhang, Y., Rajagopalan, D., Abdullah, L.N., Yeo-Teh, N.S., Tomaic, V., Banks, L., Myers, M.P., Chow, E.K., and Jha, S. (2015). E3 ligase EDD1/UBR5 is utilized by the HPV E6 oncogene to destabilize tumor suppressor TIP60. Oncogene.

Sun, X., Fa, P., Cui, Z., Xia, Y., Sun, L., Li, Z., Tang, A., Gui, Y., and Cai, Z. (2014). The EDA-containing cellular fibronectin induces epithelial-mesenchymal transition in lung cancer cells through integrin alpha9beta1-mediated activation of PI3-K/AKT and Erk1/2. Carcinogenesis *35*, 184-191.

Sun, Y., Jiang, X., Chen, S., Fernandes, N., and Price, B.D. (2005). A role for the Tip60 histone acetyltransferase in the acetylation and activation of ATM. Proc Natl Acad Sci U S A *102*, 13182-13187.

Sun, Y., Jiang, X., and Price, B.D. (2010). Tip60: connecting chromatin to DNA damage signaling. Cell Cycle *9*, 930-936.

Sun, Y., Jiang, X., Xu, Y., Ayrapetov, M.K., Moreau, L.A., Whetstine, J.R., and Price, B.D. (2009). Histone H3 methylation links DNA damage detection to activation of the tumour suppressor Tip60. Nat Cell Biol *11*, 1376-1382.

Sun, Y., Xu, Y., Roy, K., and Price, B.D. (2007). DNA damage-induced acetylation of lysine 3016 of ATM activates ATM kinase activity. Mol Cell Biol *27*, 8502-8509.

Sykes, S.M., Mellert, H.S., Holbert, M.A., Li, K., Marmorstein, R., Lane, W.S., and McMahon, S.B. (2006). Acetylation of the p53 DNA-binding domain regulates apoptosis induction. Mol Cell *24*, 841-851.

Tai, K.Y., Shiah, S.G., Shieh, Y.S., Kao, Y.R., Chi, C.Y., Huang, E., Lee, H.S., Chang, L.C., Yang, P.C., and Wu, C.W. (2007). DNA methylation and histone modification regulate silencing of epithelial cell adhesion molecule for tumor invasion and progression. Oncogene *26*, 3989-3997.

Taipale, M., Rea, S., Richter, K., Vilar, A., Lichter, P., Imhof, A., and Akhtar, A. (2005). hMOF histone acetyltransferase is required for histone H4 lysine 16 acetylation in mammalian cells. Mol Cell Biol *25*, 6798-6810.

Takes, R.P., Baatenburg de Jong, R.J., Schuuring, E., Hermans, J., Vis, A.A., Litvinov, S.V., and van Krieken, J.H. (1997). Markers for assessment of nodal metastasis in laryngeal carcinoma. Arch Otolaryngol Head Neck Surg *123*, 412-419.

Takes, R.P., Baatenburg de Jong, R.J., Wijffels, K., Schuuring, E., Litvinov, S.V., Hermans, J., and van Krieken, J.H. (2001). Expression of genetic markers in lymph node metastases compared with their primary tumours in head and neck cancer. J Pathol *194*, 298-302.

Tan, T.Z., Miow, Q.H., Miki, Y., Noda, T., Mori, S., Huang, R.Y., and Thiery, J.P. (2014). Epithelial-mesenchymal transition spectrum quantification and its efficacy in deciphering survival and drug responses of cancer patients. EMBO Mol Med *6*, 1279-1293.

Tang, J., Cho, N.W., Cui, G., Manion, E.M., Shanbhag, N.M., Botuyan, M.V., Mer, G., and Greenberg, R.A. (2013). Acetylation limits 53BP1 association with damaged chromatin to promote homologous recombination. Nat Struct Mol Biol *20*, 317-325.

Tang, Y., Luo, J., Zhang, W., and Gu, W. (2006). Tip60-dependent acetylation of p53 modulates the decision between cell-cycle arrest and apoptosis. Mol Cell *24*, 827-839.

Taube, J.H., Herschkowitz, J.I., Komurov, K., Zhou, A.Y., Gupta, S., Yang, J., Hartwell, K., Onder, T.T., Gupta, P.B., Evans, K.W.*, et al.* (2010). Core epithelial-to-mesenchymal transition interactome gene-expression signature is associated with

claudin-low and metaplastic breast cancer subtypes. Proc Natl Acad Sci U S A *107*, 15449-15454.

Taubert, S., Gorrini, C., Frank, S.R., Parisi, T., Fuchs, M., Chan, H.M., Livingston, D.M., and Amati, B. (2004). E2F-dependent histone acetylation and recruitment of the Tip60 acetyltransferase complex to chromatin in late G1. Mol Cell Biol *24*, 4546-4556.

Thiery, J.P. (2002). Epithelial-mesenchymal transitions in tumour progression. Nat Rev Cancer *2*, 442-454.

Thiery, J.P., Acloque, H., Huang, R.Y., and Nieto, M.A. (2009). Epithelial-mesenchymal transitions in development and disease. Cell *139*, 871-890.

Timmerman, L.A., Grego-Bessa, J., Raya, A., Bertran, E., Perez-Pomares, J.M., Diez, J., Aranda, S., Palomo, S., McCormick, F., Izpisua-Belmonte, J.C.*, et al.* (2004). Notch promotes epithelial-mesenchymal transition during cardiac development and oncogenic transformation. Genes Dev *18*, 99-115.

Valsesia-Wittmann, S., Magdeleine, M., Dupasquier, S., Garin, E., Jallas, A.C., Combaret, V., Krause, A., Leissner, P., and Puisieux, A. (2004). Oncogenic cooperation between H-Twist and N-Myc overrides failsafe programs in cancer cells. Cancer Cell *6*, 625-630.

Verhaak, R.G., Hoadley, K.A., Purdom, E., Wang, V., Qi, Y., Wilkerson, M.D., Miller, C.R., Ding, L., Golub, T., Mesirov, J.P.*, et al.* (2010). Integrated genomic analysis identifies clinically relevant subtypes of glioblastoma characterized by abnormalities in PDGFRA, IDH1, EGFR, and NF1. Cancer Cell *17*, 98-110.

Vernon, A.E., and LaBonne, C. (2006). Slug stability is dynamically regulated during neural crest development by the F-box protein Ppa. Development *133*, 3359-3370.

Vettese-Dadey, M., Grant, P.A., Hebbes, T.R., Crane- Robinson, C., Allis, C.D., and Workman, J.L. (1996). Acetylation of histone H4 plays a primary role in enhancing transcription factor binding to nucleosomal DNA *in vitro*. EMBO J *15*, 2508-2518.

Villarejo, A., Cortes-Cabrera, A., Molina-Ortiz, P., Portillo, F., and Cano, A. (2014). Differential role of Snail1 and Snail2 zinc fingers in E-cadherin repression and epithelial to mesenchymal transition. The Journal of biological chemistry *289*, 930-941.

Wang, J., and Chen, J. (2010). SIRT1 regulates autoacetylation and histone acetyltransferase activity of TIP60. J Biol Chem *285*, 11458-11464.

Weichert, W., Roske, A., Gekeler, V., Beckers, T., Ebert, M.P., Pross, M., Dietel, M., Denkert, C., and Rocken, C. (2008a). Association of patterns of class I histone deacetylase expression with patient prognosis in gastric cancer: a retrospective analysis. Lancet Oncol *9*, 139-148.

Weichert, W., Roske, A., Gekeler, V., Beckers, T., Stephan, C., Jung, K., Fritzsche, F.R., Niesporek, S., Denkert, C., Dietel, M.*, et al.* (2008b). Histone deacetylases 1, 2 and 3 are highly expressed in prostate cancer and HDAC2 expression is associated with shorter PSA relapse time after radical prostatectomy. Br J Cancer *98*, 604-610.

Weichert, W., Roske, A., Niesporek, S., Noske, A., Buckendahl, A.C., Dietel, M., Gekeler, V., Boehm, M., Beckers, T., and Denkert, C. (2008c). Class I histone deacetylase expression has independent prognostic impact in human colorectal cancer: specific role of class I histone deacetylases *in vitro* and *in vivo*. Clin Cancer Res *14*, 1669-1677.

Wu, J.C., Sundaresan, G., Iyer, M., and Gambhir, S.S. (2001). Noninvasive optical imaging of firefly luciferase reporter gene expression in skeletal muscles of living mice. Mol Ther *4*, 297-306.

Wu, Z.Q., Li, X.Y., Hu, C.Y., Ford, M., Kleer, C.G., and Weiss, S.J. (2012). Canonical Wnt signaling regulates Slug activity and links epithelial-mesenchymal transition

with epigenetic Breast Cancer 1, Early Onset (BRCA1) repression. Proc Natl Acad Sci U S A *109*, 16654-16659.

Xiao, H., Chung, J., Kao, H.Y., and Yang, Y.C. (2003). Tip60 is a co-repressor for STAT3. J Biol Chem *278*, 11197-11204.

Xiao, Y., Nagai, Y., Deng, G., Ohtani, T., Zhu, Z., Zhou, Z., Zhang, H., Ji, M.Q., Lough, J.W., Samanta, A.*, et al.* (2014). Dynamic interactions between TIP60 and p300 regulate FOXP3 function through a structural switch defined by a single lysine on TIP60. Cell Rep *7*, 1471-1480.

Yamamoto, T., and Horikoshi, M. (1997). Novel substrate specificity of the histone acetyltransferase activity of HIV-1-Tat interactive protein Tip60. J Biol Chem *272*, 30595-30598.

Yang, C., Wu, J., and Zheng, Y.G. (2012a). Function of the active site lysine autoacetylation in Tip60 catalysis. PLoS One *7*, e32886.

Yang, J., and Weinberg, R.A. (2008). Epithelial-mesenchymal transition: at the crossroads of development and tumor metastasis. Dev Cell *14*, 818-829.

Yang, S., Zhang, J.J., and Huang, X.Y. (2012b). Mouse models for tumor metastasis. Methods Mol Biol *928*, 221-228.

Yang, Z., Rayala, S., Nguyen, D., Vadlamudi, R.K., Chen, S., and Kumar, R. (2005). Pak1 phosphorylation of snail, a master regulator of epithelial-to-mesenchyme transition, modulates snail's subcellular localization and functions. Cancer Res *65*, 3179-3184.

Ye, X., Tam, W.L., Shibue, T., Kaygusuz, Y., Reinhardt, F., Ng Eaton, E., and Weinberg, R.A. (2015). Distinct EMT programs control normal mammary stem cells and tumour-initiating cells. Nature *525*, 256-260.

Yook, J.I., Li, X.Y., Ota, I., Hu, C., Kim, H.S., Kim, N.H., Cha, S.Y., Ryu, J.K., Choi, Y.J., Kim, J.*, et al.* (2006). A Wnt-Axin2-GSK3beta cascade regulates Snail1 activity in breast cancer cells. Nat Cell Biol *8*, 1398-1406.

Zhang, K., Rodriguez-Aznar, E., Yabuta, N., Owen, R.J., Mingot, J.M., Nojima, H., Nieto, M.A., and Longmore, G.D. (2012). Lats2 kinase potentiates Snail1 activity by promoting nuclear retention upon phosphorylation. EMBO J *31*, 29-43.

Zhang, Z., Zhang, B., Li, W., Fu, L., Zhu, Z., and Dong, J.T. (2011). Epigenetic Silencing of miR-203 Upregulates SNAI2 and Contributes to the Invasiveness of Malignant Breast Cancer Cells. Genes Cancer *2*, 782-791.

Zhou, B.P., Deng, J., Xia, W., Xu, J., Li, Y.M., Gunduz, M., and Hung, M.C. (2004). Dual regulation of Snail by GSK-3beta-mediated phosphorylation in control of epithelial-mesenchymal transition. Nat Cell Biol *6*, 931-940.

Zhou, B.P., and Hung, M.C. (2005). Wnt, hedgehog and snail: sister pathways that control by GSK-3beta and beta-Trcp in the regulation of metastasis. Cell Cycle *4*, 772-776.

Ziv, Y., Bielopolski, D., Galanty, Y., Lukas, C., Taya, Y., Schultz, D.C., Lukas, J., Bekker-Jensen, S., Bartek, J., and Shiloh, Y. (2006). Chromatin relaxation in response to DNA double-strand breaks is modulated by a novel ATM- and KAP-1 dependent pathway. Nat Cell Biol *8*, 870-876.

zur Hausen, H. (1991). Viruses in human cancers. Science *254*, 1167-1173.

zur Hausen, H. (2002). Papillomaviruses and cancer: from basic studies to clinical application. Nat Rev Cancer *2*, 342-350.

Appendices:

Chapter 1

TIP60 levels in pathophysiological scenarios

1.1   Downregulation of TIP60 correlates with a higher grade of cancer and cancer metastasis in pathophysiological scenario

Having established that TIP60 abrogates SNAIL2 function and maintains cells in an epithelial state, the relevance of TIP60 in breast cancers was analyzed. *TIP60* expression levels in 3,992 breast cancer and 22 normal breast tissue samples was determined, and whether *TIP60* expression correlated with the breast cancer EMT score in these samples was investigated; the EMT score, ϵ [-1.0, +1.0], was used to estimate the EMT phenotype of each sample (Tan et al., 2014). In support of the findings, *TIP60* expression had a negative correlation with EMT score in patient samples (Spearman Correlation Coefficient, Rho = -0.191, p = 2.08E-34) (**Figure 44A**). The levels of *TIP60* in various grades and types of breast cancer samples was also checked and found *TIP60* to be significantly down-regulated in high-grade breast cancers (Mann–Whitney U-test, p = 2.56E-11) (**Figure 44B**). After further sub-classifying these tumours into the six breast cancer subtype signatures (Basal, Claudin-Low, Luminal-A, Luminal-B, ERBB2+, and Normal-like), a significantly high *TIP60* expression to be associated with the Luminal-A subtype was observed, which has a good prognosis (Mann–Whitney U-test, p = 7.56E-14), and significantly lower *TIP60* expression in the molecular subtypes with poorer prognosis, Basal, Claudin-Low, and

ERBB2+ was also observed (Mann–Whitney U-test, p = 3.69E-16, p = 0.0169, and p = 1.83E-7, respectively) (**Figure 44C**).
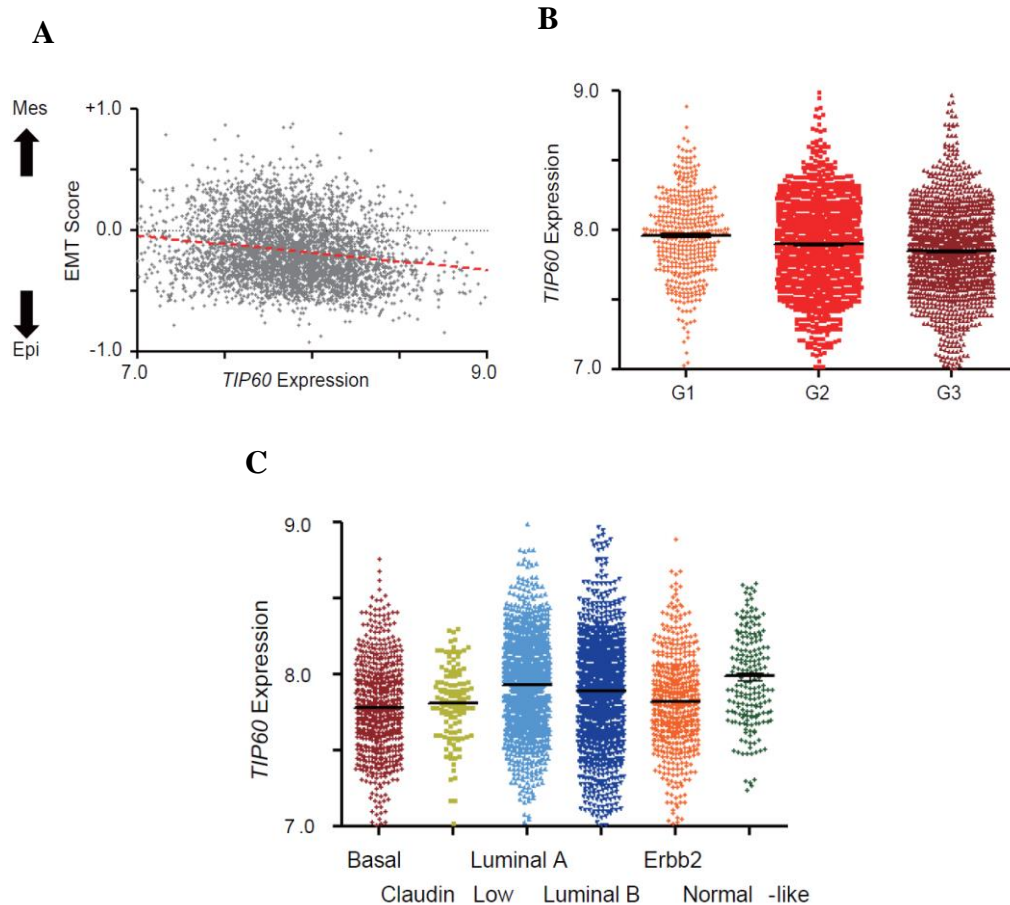
Figure 44. *TIP60* expression was negatively correlated with Epithelial-mesenchymal transition (EMT), and is a prognostic marker for higher grade of cancer and metastasis in breast cancer patients. TIP60 expression was analysed in 3,992 breast cancer tumours and 22 normal breast tissue samples.

(**A**) *TIP60* expression negatively correlated with EMT score (Spearman Correlation Coefficient, *Rho* = -0.191, *p* = 2.08E-34). (**B**) *TIP60* expression decreases as breast cancer progresses. Samples were classified as grade 1 (G1), G2 and G3, and the *p*-value was determined using the Mann–Whitney *U*-test (G1 vs G2, *p* = 9.73e-5; G1 vs G3, *p* = 2.56e-11; G2 vs G3, *p* = 1.28e-4). (**C**) *TIP60* is differentially expressed in breast cancer subtype signatures. Relative mRNA level of *TIP60* is shown for Basal, Claudin-Low, Luminal-A, Luminal-B, ERBB2+, and Normal-like breast cancer samples (Basal vs Rest, *p* = 3.69e-16; Claudin-Low vs Rest, *p* = 0.0169; Luminal-A vs Rest, *p* = 7.56e-14; Luminal-B vs Rest, *p* = 0.1477; ERBB2+ vs Rest, *p* = 1.83e-7; Normal-like vs Rest, *p* = 1.77e-5; analysis by Mann–Whitney *U*-test).

1.2 Downregulation of TIP60 correlates with low survival rate in pathophysiological scenarios

In terms of a correlation between patient Overall Survival (OS)/ Disease Free Survival (DFS) and *TIP60* expression, breast cancers with higher *TIP60* expression to show better prognoses for OS and DFS were observed (log-rank test, $p = 0.08$ and $p = 0.0017$, respectively) (**Figure 45A, B**). Comparing breast cancers with the 25% highest *TIP60* expression (fourth quartile; Q4) with those with the 25% lowest *TIP60* expression (first quartile; Q1), even more significant differences with respect to OS and DFS were found (log-rank test, $p = 0.0054$ and $p = 0.0004$, respectively) (**Figure 45C, D**). These data strengthen the findings that *TIP60* expression is reduced in more aggressive cancers, and that patients with a higher level of *TIP60* have a better prognosis in terms of OS and DFS.
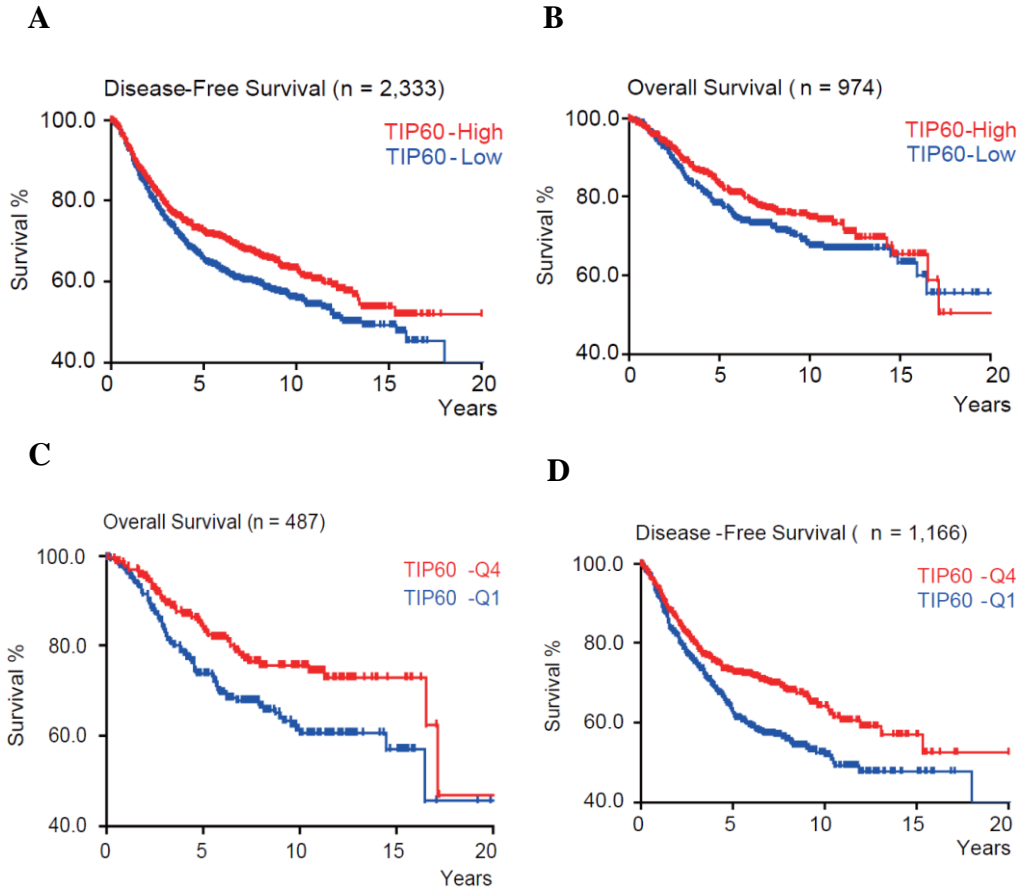
Figure 45. Patients with lower levels of *TIP60* have higher relapse and low survival.

(**A**) Survival curve of 2,333 patients with relapse. Log-rank p = 0.0017; median survival (month), TIP60<median = 13.62; TIP60≥median = undefined; hazard ratio = 1.249 (1.087 - 1.436). (**B**) Overall survival of 974 patients with a log-rank p = 0.0882; median survival (months), TIP60<median =undefined,TIP60≥median = undefined; hazard ratio = 1.241 (0.9682 - 1.590). (**C**) Survival curve of 487 patients categorized into quartile 4 (Q4=high TIP60), or quartile 1 (Q1=low TIP60) with a log-rank p = 0.0054; median survival (month), TIP60_Q1 = 16.47, TIP60_Q4 = 17.1; hazard ratio = 1.613 (1.152 - 2.258). (**D**) Disease-free survival curve of 1,166 patients from Q4 and Q1. Log-rank p = 0.0004; median survival (month), TIP60_Q1 = 10.47, TIP60_Q4 = undefined; hazard ratio = 1.429 (1.175–1.738).

Chapter 2

Publications

ORIGINAL ARTICLE

E3 ligase EDD1/UBR5 is utilized by the HPV E6 oncogene to destabilize tumor suppressor TIP60

VK Subbaiah[1,6], Y Zhang[1,6], D Rajagopalan[1,2], LN Abdullah[1], NSL Yeo-Teh[1,3], V Tomaić[4], L Banks[4], MP Myers[4], EK Chow[1,5] and S Jha[1,2]

Tat-interacting protein of 60 kDa (TIP60) is an essential lysine acetyltransferase implicated in transcription, DNA damage response and apoptosis. TIP60 protein expression is reduced in cancers. In cervical cancers, human papillomavirus (HPV) E6 oncogene targets cellular p53, Bak and some of the PDZ domain-containing proteins for proteasome-mediated degradation through E6AP ligase. Recently, E6 oncogene from high-risk and low-risk categories was also shown to target TIP60. However, the molecular mechanisms and whether destabilization of TIP60 contributes to HPV E6-mediated transformation remain unanswered. Our proteomic analyses revealed EDD1 (E3 identified by differential display), an E3 ligase generally overexpressed in cancers as a novel interacting partner of TIP60. By investigating protein turnover and ubiquitination assays, we show that EDD1 negatively regulates TIP60's stability through the proteasome pathway. Strikingly, HPV E6 uses this function of EDD1 to destabilize TIP60. Colony-formation assays and soft agar assays show that gain of function of TIP60 or depletion of EDD1 in HPV-positive cervical cancer cells significantly inhibits cell growth in vitro. This phenotype is strongly supported by the in-vivo studies where re-activation of TIP60 in cervical cancer cells dramatically reduces tumor formation. In summary, we have discovered a novel ligase through which E6 destabilizes TIP60. Currently, in the absence of an effective therapeutic vaccine for malignant cervical cancers, cervical cancer still remains to be a major disease burden. Hence, our studies implying a distinct tumor suppressor role for TIP60 in cervical cancers show that reactivation of TIP60 could be of therapeutic value.

INTRODUCTION

HIV-1 Tat-interacting protein of 60 kDa (TIP60) is one of the well-characterized members of the MYST family of lysine acetyltransferases (KAT).[1] Initially discovered as an HIV-1 Tat transactivator,[2] several groups have later reported its role as a chromatin-modifying enzyme in transcriptional regulation, DNA repair, apoptosis and maintenance of stem cell features.[3–7] TIP60 elicits these functions either transcriptionally by acetylation of histones when recruited to specific promoters[8–10] or non-transcriptionally by altering the activity of non-histone proteins.[11–14] Emphasizing its major role in gene expression regulation, the homozygous disruption of TIP60 causes embryonic lethality, implying its importance in mammalian development.[15] In addition, mice that are haploid for TIP60 are predisposed to tumors, making TIP60 a haploinsufficient tumor suppressor.[16]

Owing to TIP60's role in diverse functions as discussed above, the cellular levels, stability and activity of TIP60 are also tightly regulated. In the absence of any stimuli, TIP60 is an unstable protein with a half-life of 30–190 min, maintained at low levels by the proteasome pathway,[2,17,18] and its catalytic activity is regulated by posttranslational modifications such as phosphorylation.[19,20]

EDD1 (E3 identified by differential display) also known as UBR5 (ubiquitin protein ligase E3 component n-recognin 5) is an HECT (homologous to E6AP C-terminus) domain-containing ligase,

which was originally isolated as a progestin-induced gene.[21] Mutations in EDD1 lead to imaginal disc hyperplasia in Drosophila and suggest a critical role for EDD1 in cellular proliferation and differentiation.[22] It is linked to DNA-damage signaling pathway[23,24] and directly regulates progestin-mediated signaling pathway[21] and mitogen-activated protein kinase pathway.[25] A more direct role for EDD1 in carcinogenesis is suggested by its overexpression in several cancers, including ovarian and breast cancer,[26,27] whereas truncating mutations have been detected in gastric and colon cancers.[28]

Information regarding the functional role of TIP60 in viral-mediated cancers has been very limited. In addition, few available reports propose a contradictory role for TIP60 as a suppressor of EBV and HCMV viral infection,[29–31] whereas in contrast the human T-cell lymphotropic virus type-1 p30II enhances c-Myc-transforming activity by stabilizing c-Myc-TIP60-containing chromatin remodeling complexes,[32] suggesting TIP60 could promote carcinogenesis. In the context of human papillomavirus (HPV)-mediated cervical cancers, TIP60 functions as a cellular repressor of HPV E6 expression and E6 in turn destabilizes TIP60.[33] This destabilization was independent of the E6AP, an essential ligase known to mediate E6 functions or MDM2 E3 ligases,[33] and hence information regarding the mechanisms of E6-mediated TIP60 destabilization and whether this function of E6 contributes to its oncogenicity are currently unknown. In this study, we show that

[1]Cancer Science Institute of Singapore, National University of Singapore, Singapore; [2]Department of Biochemistry, National University of Singapore, Singapore; [3]NUS Graduate School for Integrative Sciences and Engineering, National University of Singapore, Singapore; [4]International Centre for Genetic Engineering and Biotechnology, Trieste, Italy and [5]Department of Pharmacology, Yong Loo Lin School of Medicine, National University of Singapore, Singapore. Correspondence: Professor S Jha, 14 Medical Drive, Center for Translational Medicine, MD6-13-02J, 117599, Singapore.
E-mail: csisjha@nus.edu.sg
[6]These authors are the co-first authors.
Received 2 December 2014; revised 4 May 2015; accepted 7 June 2015; published online 3 August 2015

E3 ligase EDD1 is a novel and functionally important interacting partner of TIP60. TIP60–EDD1 regulation is physiologically significant as HPV E6 destabilizes TIP60 through EDD1 in cervical cancers. Most importantly, TIP60 strongly inhibits tumor formation *in vivo*, demonstrating the biological importance of cross-talk between HPVE6, EDD1 and TIP60.
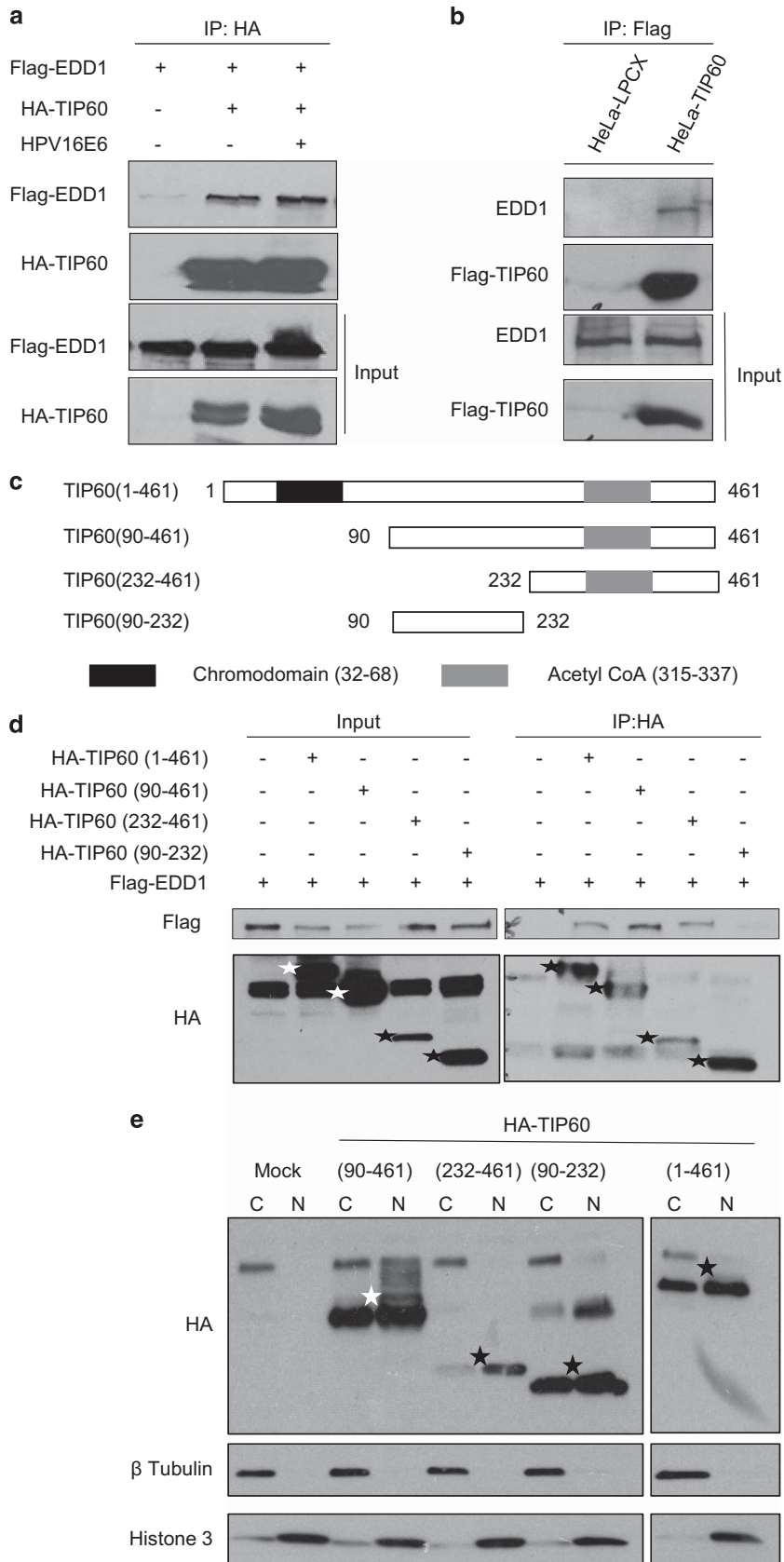
RESULTS

Proteomic analyses identifies EDD1/UBR5 as a novel interacting partner of TIP60

To investigate the molecular mechanisms of HPV E6-mediated TIP60 degradation, we performed a proteomic screen for TIP60-interacting partners. HEK-293 cells were transfected with HA-TIP60 expression plasmid in the presence and the absence of HPV 16 E6. After 24 h, the cells were treated with the proteasome inhibitor MG132 for 4 h, to prevent the degradation of TIP60. The cellular extracts were then immunoprecipitated with anti-hemagglutinin (HA)-conjugated agarose beads and the complexes were subjected to mass spectrometric analysis. The resulting protein profiles were compared with those obtained from mock-transfected cells to exclude nonspecific interactions. Several known interacting proteins such as histone H4 and histone H2A were identified in the screen, which are well-established substrates for TIP60.[34] Among the novel potential interacting partners identified, we decided to further investigate a 300-kDa protein called EDD1 or UBR5. EDD1 is the mammalian ortholog of the *Drosophila melanogaster* hyperplastic disc protein and is a member of the HECT domain family of E3 ubiquitin ligases.[21] More interestingly, HPV E6 degrades TIP60 in a proteasomal-dependent manner[33] and EDD1 is a ubiquitin ligase closely involved with the proteasomal pathway, which has been shown previously to interact with E6 and E6AP.[35] This raises the possibility that EDD1 could mediate the E6 function in this context. To confirm the cellular interaction between EDD1 and TIP60, 293T cells were transfected with HA-TIP60 expression plasmid along with Flag-EDD1 in the presence or the absence of HPV16 E6. After 24 h, the cells were treated with MG132 for 4 h and then the cellular extracts were immunoprecipitated using anti-HA-conjugated agarose beads. EDD1 bound to the agarose beads was detected by western blotting using anti-Flag antibody. EDD1 specifically co-immunoprecipitated with TIP60 (Figure 1a). However, this interaction seems to be HPV E6 independent, as TIP60 co-immunoprecipitated both in the presence or the absence of HPV16 E6. To confirm the interaction between TIP60 and EDD1 at endogenous levels, HeLa-LPCX and HeLa-TIP60 cells were seeded in 10-cm dishes. After 24 h, the cells were collected, proteins extracted using RIPA buffer, the lysates immunoprecipitated using anti-Flag agarose beads and the co-immunoprecipitating EDD1 detected using anti-EDD1 antibody (Figure 1b). To further map the binding region on TIP60, Flag-EDD1 was transfected either alone or in combination with a series of HA-tagged deletion mutants of TIP60 (Figure 1c). The cellular extracts were immunoprecipitated using anti-HA-conjugated agarose beads and the co-immunoprecipitating EDD1 was detected using anti-Flag antibody. EDD1 strongly co-immunoprecipitated with full-length wild-type (WT) TIP60 (aa 1–461) and the deletion mutant construct of TIP60 in which the chromodomain at the N-terminus was deleted (aa 90–461) (Figure 1d). However, this interaction was abolished on simultaneously deleting the chromodomain at the N-terminus and the functional acetyl CoA domain at the C-terminus of TIP60 (aa 90–232), and this was not due to mis-localization of the deletion mutants of TIP60 (Figure 1e). This indicates that EDD1 interacts with TIP60 specifically through the C-terminus containing the acetyl CoA domain. To confirm this, we generated a TIP60 deletion mutant construct comprising a C-terminus with the acetyl CoA domain (aa 232–461). The results in Figure 1d confirmed that

EDD1 recognizes and interacts with TIP60 through acetyl CoA domain. Taken together, these results demonstrate that EDD1 is a novel interacting partner of TIP60 in the presence and the absence of HPV E6, and it recognizes TIP60 through the acetyl CoA domain at the C-terminus.

Depletion of EDD1 increases TIP60 levels and regulates its turnover

To address the physiological relevance of this novel interaction, we tested whether modulating the endogenous cellular levels of EDD1 could affect the endogenous TIP60 levels. We therefore performed transient small interfering RNA (siRNA) knockdown experiments in HPV-positive CaSki and HeLa cells. Cells were transfected with siRNA against control, EDD1 or TIP60 for 72 h and cellular lysates were immunoblotted for endogenous TIP60 protein using anti-TIP60 antibody. The results show that ablation of endogenous EDD1 increases TIP60 protein levels and the specificity of the TIP60 band was confirmed, as siRNA against TIP60 decreased the levels of the respective band (Figures 2a and b). We next tested whether EDD1 regulates TIP60 stability in cervical cancer cell line lacking HPV E6 expression; for this, C33A cells were transfected with siRNA against control, EDD1 or TIP60 for 72 h, and cellular lysates were immunoblotted for endogenous TIP60 protein. The results show that ablation of endogenous EDD1 by siRNA does not result in increased TIP60 protein level (Figure 2c). In order to investigate the mechanism of EDD1-mediated decrease in TIP60 levels, we generated HeLa cells with stable knockdown of endogenous EDD1 and confirmed the increase in TIP60 protein levels in these cells (Figure 2d). As EDD1 negatively regulates TIP60 protein levels, we next sought to resolve whether this is due to EDD1 regulating TIP60 transcriptionally. For this, total RNA was isolated from HeLa cells stably expressing short hairpin RNA against control or EDD1 sequences and was subjected to real-time PCR analysis (Figure 2e). The TIP60 mRNA levels in the shEDD1-stable cells did not change significantly compared with the control cells. Hence, we hypothesized that EDD1 might directly increase TIP60 protein turnover. To investigate this, HeLa-shcontrol or HeLa-shEDD1 cells were treated with cycloheximide for various time points, to block protein synthesis. The residual levels of endogenous TIP60 were then determined using anti-TIP60 antibody. Under normal circumstances, TIP60 has a half-life of < 1 h, which is extended on depleting endogenous EDD1 (Figures 2f and g). Based on these results, we decided to ascertain the effects of HPV E6 on TIP60 protein levels in the absence of endogenous EDD1. For this, we generated 293T cells stably expressing short hairpin RNA against EDD1. Cells stably expressing shEDD1 were selected with puromycin antibiotic and depletion of EDD1 was ascertained by western blotting (Figure 2h). As shown earlier, HPV18 E6 destabilizes TIP60;[33] however, this function of E6 was impaired in EDD1-depleted cells (Figures 2i and j). To test whether this is due to decreased half-life of TIP60, Flag-TIP60 was transfected in the cells with decreased EDD1 levels (shEDD1) either alone or in combination with HPV18 E6 for 24 h, then treated with cycloheximide for indicated times and the total cellular lysates were analyzed by western blotting. The results and quantifications in Figures 2k and l demonstrate that ectopically expressed TIP60 has a half-life < 2 h, which is further decreased in the presence of HPV 18E6. More interestingly, this effect of E6 is abolished in shEDD1 cells, suggesting that E6 regulates TIP60 half-life through EDD1. In addition, the expression level of TIP60 is not significantly altered in shEDD1 cells compared with shcontrol. In summary, these results demonstrate the direct role for EDD1 in regulating TIP60 protein levels in HPV-positive cells.

a

IP: HA

Flag-EDD1	+	+	+
HA-TIP60	-	+	+
HPV16E6	-	-	+

Flag-EDD1

HA-TIP60

Flag-EDD1

HA-TIP60

Input

b

IP: Flag

HeLa-LPCX   HeLa-TIP60

EDD1

Flag-TIP60

EDD1

Flag-TIP60

Input

c

TIP60(1-461)   1 [————————] 461

TIP60(90-461)   90 [————————] 461

TIP60(232-461)   232 [————————] 461

TIP60(90-232)   90 [————] 232

■ Chromodomain (32-68)   ▇ Acetyl CoA (315-337)

d

	Input					IP:HA				
HA-TIP60 (1-461)	-	+	-	-	-	-	+	-	-	-
HA-TIP60 (90-461)	-	-	+	-	-	-	-	+	-	-
HA-TIP60 (232-461)	-	-	-	+	-	-	-	-	+	-
HA-TIP60 (90-232)	-	-	-	-	+	-	-	-	-	+
Flag-EDD1	+	+	+	+	+	+	+	+	+	+

Flag

HA

e

HA-TIP60

| Mock | (90-461) | (232-461) | (90-232) | (1-461) |

C N   C N   C N   C N   C N

HA

β Tubulin

Histone 3

EDD1 ubiquitinates and degrades TIP60 through proteasomal pathway

EDD1 is an E3 ubiquitin ligase and is involved in ubiquitination or ubiquitin binding.[36] We aimed to explore the mechanism of EDD1-mediated destabilization of TIP60. To do so, 293T cells were transfected with Flag-TIP60 expression plasmid, either alone or in combination with Flag-EDD1 expression plasmid. After 24 h, the cells were treated with dimethyl sulfoxide vehicle control or treated with 10 µg/ml of MG132 for 4 h. The total cellular lysates were subjected to western blotting and the remaining TIP60 levels were detected using anti-Flag antibody. The results in Figure 3a show that EDD1 induces a significant decrease in TIP60 protein levels and this is due to the enhanced proteasomal degradation of TIP60, as treatment with MG132 for 4 h abolished the effect of EDD1. TIP60 alone on treatment with MG132 is restored to similar levels. Plasmid expressing β-galactosidase was used to demonstrate the transfection efficiency and also served as a negative control. The key feature of the HECT class of E3 ligases is their ability to covalently bind ubiquitin through a conserved cysteine residue located in their HECT domain.[37] Furthermore, substitution of this conserved cysteine at position 2768 to alanine abolishes the ability to bind to the ubiquitin and degrade its substrates.[21,23] We were interested in comparing the effects of the ligase-dead mutant of EDD1 (referred to as EDD1-Mut (C2768A)) and the wild type EDD1-WT on TIP60 levels. To do so, 293T cells were transfected with Flag-TIP60 expression plasmid, either alone or in combination with increasing amounts of EDD1-WT or EDD1-Mut (C2768A). After 24 h, cellular extracts were prepared and both TIP60 and EDD1 were detected using anti-Flag antibody. Although both the proteins are Flag tagged, they could be distinguished on a western blot because of the marked differences in their molecular weights. The results in Figure 3b show that EDD1-WT decreases TIP60 protein levels in a dose-dependent manner and this effect is not observed in the presence of EDD1-Mut (C2768A), suggesting that destabilization of TIP60 by EDD1 requires the ligase activity of EDD1. We then extended our study to address the question whether EDD1 could also polyubiquitinate TIP60 in vivo. For this, 293T cells were transfected with Myc-TIP60 expression plasmid, either alone or co-transfected with the Flag-EDD1-WT or EDD1-Mut (C2768A) and HA-Ubiquitin expression plasmids in various combinations as shown in Figure 3c. After 24 h, the cellular extracts were immunoprecipitated using anti-HA-conjugated agarose beads and the HA-Ubiquitin-bound TIP60 was then detected by western blotting using anti-Myc antibody. The results from Figure 3c and quantification from four independent experiments in Figure 3d show that TIP60 co-immunoprecipitated with ubiquitin and this is clearly enhanced in the presence of EDD1-WT. Interestingly, TIP60 co-immunoprecipitated less efficiently when the EDD1-Mut (C2768A) was expressed, suggesting that destabilization of TIP60 by EDD1 is through ubiquitin-mediated proteasome degradation. In order to investigate whether EDD1 targets the functionally active form of TIP60, Flag-TIP60-WT or the HAT (histone acetyltransferase) mutant of TIP60 (TIP60-KD) was transfected

alone or in combination with the EDD1-WT and analyzed by western blotting. TIP60-WT protein levels were efficiently downregulated by EDD1, confirming the earlier results, whereas in sharp contrast the HAT mutant of TIP60 is resistant to degradation by EDD1 (Figure 3e). We next investigated whether EDD1 interacts with TIP60-KD. For this, EGFP-EDD1 was transfected alone or in combination with Flag-TIP60-WT or Flag-TIP60-KD and co-immunoprecipitation assay was performed. Intriguingly, EDD1 interacted with TIP60-KD mutant similar to TIP60-WT (Figure 3f), although EDD1 failed to degrade the TIP60-KD mutant.

## Overexpression of TIP60 inhibits cellular growth

TIP60 is a tumor suppressor and is a transcriptional repressor of E6 expression. Therefore, we reasoned that gain of function of TIP60 might also antagonize E6-mediated cellular growth, thereby inhibiting tumor cell growth in cervical cancer cells. To address this, we used retroviral system to generate HeLa cells (Figure 4a) and CaSki cells (Figure 4b) stably expressing Flag-TIP60. TIP60 regulation by EDD1 was confirmed by transfecting HeLa-TIP60 cells individually with siRNA against control, EDD1, 18E6/E7 or TIP60 for 72 h and cellular lysates were immunoblotted for TIP60 protein using anti-Flag antibody. The results in Figure 4c show that transient depletion of EDD1 in HeLa-TIP60 stable cells did not significantly change TIP60 mRNA levels compared with the control cells, despite efficient depletion of EDD1. In addition, depletion of endogenous EDD1 stabilizes TIP60 protein levels confirming our earlier results. Similarly, ablation of HPV 18E6/E7 also stabilized TIP60 levels as previously published[33] (Figure 4d). Ablation of HPV 18E6/E7 was confirmed by rescue in p53 levels. In addition, the specificity of the TIP60 band was also confirmed, as siRNA against TIP60 showed a significant decrease in TIP60 levels detected using the anti-Flag antibody. Similar results were obtained in CaSki cells and off-target effect was ruled out by using three independent siRNA targeting EDD1 (Figure 4e and Supplementary Figure S1). Finally, transient depletion of EDD1 combined with cycloheximide treatment shows that under normal circumstances ectopically expressed TIP60 has a half-life of < 1 h, which is extended on depleting endogenous EDD1 (Figures 4f and g). These results further confirm our previous results at the endogenous level.

We then characterized the growth ability of HeLa-TIP60 and CaSki-TIP60 stable cells in vitro by colony-forming assay. HeLa-LPCX vector control or HeLa-TIP60-expressing cells were seeded at very low density ($1 \times 10^3/9.5\,cm^2$) for colony-formation assays (CFAs) and maintained in antibiotic selection. After 3 weeks the colonies were fixed, stained and quantified. Representative images in Figures 5a (i) and (ii) and the quantifications in Figure 5b show that expression of TIP60 compared with control inhibited the ability of HeLa cells to form colonies by 90%. Interestingly, the morphology of HeLa-TIP60 cells were dramatically different and suggested that the cells undergo senescence under the reduced serum conditions in comparison with the control cells. Similar results were observed in CaSki cells (Figures 5c and d).

Figure 1. EDD1 interacts with TIP60. (**a**) TIP60 interacts with EDD1. 293T cells were transfected with plasmids as shown and treated with MG132 for 4 h before using the lysates for co-immunoprecipitation. TIP60 and EDD1 were detected using anti-HA and anti-Flag antibodies, respectively. (**b**) HeLa-LPCX or HeLa-TIP60 cells (1×10^6) were seeded in 10-cm dishes. After 24 h, total cellular lysates were subjected to Flag immunoprecipitation and western blotted for endogenous EDD1. (**c**) Schematic of the different TIP60 mutant constructs used in the experiment depicting the length of the fragments. The amino acid numbers corresponds to TIP60 isoform 3 (NP_874368). (**d**) EDD1 interacts with TIP60 WT through TIP60's C-terminal acetyl CoA domain. Co-immunoprecipitation assay performed on 293T lysates transfected with various plasmids as shown. EDD1 was detected using anti-Flag antibody. (**e**) TIP60 full length and deletion proteins are localized in the nucleus. 293T cells were transfected with plasmids expressing various TIP60 fragments. Nuclear and cytoplasmic fractionation was performed, and TIP60 fragments were probed by immunoblotting with anti-HA antibody. Histone H3 and β-tubulin serve as a marker for nuclear and cytoplasmic fraction, respectively.

Furthermore, TIP60 was also able to efficiently inhibit the ability of HeLa cells to form colonies in *in vitro* anchorage-independent CFA when compared with the control (Figures 5e and f). The cellular phenotype observed in Figure 5a (ii) suggests that stable expression of TIP60 in HeLa cells induces cell cycle arrest and this is due to the decreased levels of endogenous E6, as total
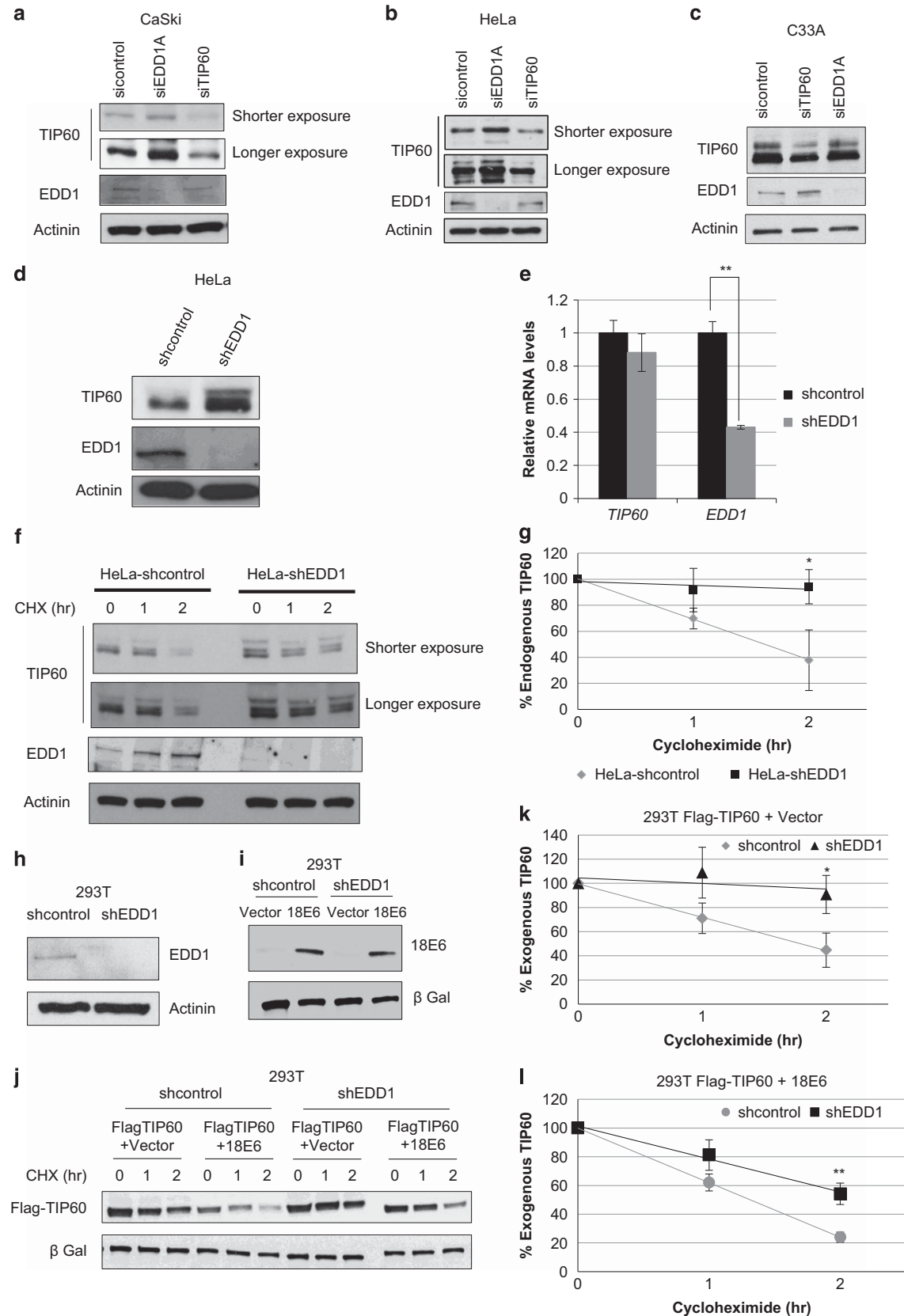
cellular extracts from HeLa-TIP60 cells showed a marked down-regulation of endogenous HPV 18 E6 levels compared with the control cells (Figure 5g) and this is consistent with mRNA data from previous studies.[33] We next asked the question whether the growth defects seen in HeLa-TIP60 cells could be rescued by overexpression of HPV 18 E6. For this, HeLa-LPCX and HeLa-TIP60 cells were transiently transfected with pcDNA vector alone or pcDNA 18 E6 expression plasmids. After 24 h, 2×10^3 number of cells were seeded for CFAs and were maintained in antibiotic selection. After 14 days, the colonies were fixed, stained and quantified. Representative images in Figure 5i and the quantifications in Figure 5j show that expression of HPV 18 E6 in HeLa-TIP60 cells could significantly rescue the growth compared with control and there was no change in growth of HeLa-LPCX cells expressing HPV 18 E6 compared with HeLa-LPCX. The expression of transfected HPV 18 E6 was verified by western blot analysis (Figure 5h).

Based on promising in vitro results, we wanted to confirm this strong phenotype of TIP60 on cellular growth in vivo. Six-week-old NOD/SCID mice were subcutaneously injected with 1×10^6 HeLa-LPCX or HeLa-TIP60 cells. The tumor size was measured at every 7-day interval for 7 weeks. The representative images and quantifications from Figures 6a (i–iii) and Supplementary Figures S2A and B show that the tumors induced by HeLa-LPCX cells were significantly reduced with TIP60 expression. We were then highly interested in verifying the TIP60 expression in these tumors. The total protein from the tumor tissue was extracted and western blotted for anti-Flag to detect TIP60. As shown in Figure 6a (iv), anti-Flag band corresponding to TIP60 was detected only from tumors induced by HeLa-TIP60 cells and not in the control.

Depletion of EDD1 affects cell growth

As EDD1 destabilizes TIP60, we wanted to investigate whether stable depletion of endogenous EDD1 could result in a similar phenotype as observed with HeLa-TIP60 stable cells. To do this, we tested the ability of HeLa-shcontrol and shEDD1 cells to form colonies in vitro in CFAs. The representative images and quantifications in Figures 6b and c show that loss of EDD1 (HeLa-shEDD1) significantly inhibits the colony-forming efficiency of HeLa cells similar to HeLa-TIP60 cells and this was TIP60 specific, as depletion of TIP60 rescued the growth inhibition (Figures 6b and c and Supplementary Figures S3A and B). We wanted to confirm the growth inhibition with reduced levels of EDD1 in vivo. To do so, 1×10^5 cells of either HeLa-shcontrol or HeLa-shEDD1 cells were injected subcutaneously into the mice. The tumor size was measured at 7-day intervals over a period of 5 weeks. The representative images and quantifications from Figures 6d (i–iii) and Supplementary Figures S4A and B show that the tumors induced by HeLa-shcontrol cells were significantly reduced on stable ablation of endogenous EDD1 expression, suggesting the biological importance of TIP60's regulation by EDD1. The knockdown of EDD1 expression and stabilization of TIP60 in the tumors were verified by western blot analysis (Figure 6d (iv)).

DISCUSSION

The deregulation in the expression of upstream transcriptional regulators, either at mRNA or protein levels, leading to an abnormal activation or repression of essential cellular targets is a prominent feature reported in various diseases and cancers. TIP60 is a transcriptional co-factor involved in several essential cellular physiological processes and its aberrant expression has been reported in several cancers.[2,33,38,39] TIP60's major role in maintaining genomic stability enables the suppression of potential transforming activities leading to cancer. These observations hence suggest the requirement for tight regulation of TIP60 expression and function. In HPV-driven cervical cancers, HPV E6 destabilizes TIP60; however, information about molecular mechanisms regulating E6-mediated TIP60 destabilization and its implications in HPV-driven cervical cancers is still lacking. Our findings demonstrate that the E3 ubiquitin ligase EDD1 is a potential cellular-interacting partner of TIP60 in both HPV-negative 293T cells and HPV-positive cells (HeLa) (Figures 1a and b), a negative regulator of TIP60 stability in HPV-positive cells (HeLa and CaSki) (Figures 2a and b). On the same lines, overexpression shows that TIP60 associates with EDD1 independent of HPV E6 (Figure 1a), suggesting that the EDD1 and TIP60 interaction is a general phenomenon not restricted to cells derived from cervical cancers, and factors that could increase TIP60–EDD1 interaction would regulate EDD1-mediated destabilization of TIP60. This finding is significant considering the inverse correlation in TIP60 and EDD1 expression reported in a variety of cancers (breast, gastric and colon) and also the common function shared by EDD1 and TIP60 in the maintenance of genomic stability during DNA damage. The HAT activity of TIP60 can have pleiotropic effects in regulating cellular physiology. Our protein expression analysis demonstrating that EDD1 cannot destabilize the HAT mutant TIP60 (Figure 3e) demonstrates this versatility of HAT function. However, EDD1 is able to interact with HAT mutant TIP60, as the TIP60-KD mutant construct was made by point mutation and hence still retains the C-terminus with acetyl CoA region, essential for its interaction. Whether EDD1 is also affecting the HAT activity of TIP60 needs further analysis. E6AP is critical in mediating HPV E6 function in degradation of its substrates such as the major

---

Figure 2. EDD1 regulates the expression and stability of endogenous TIP60 in HPV-positive cells. (**a–c**) TIP60 expression is stabilized in EDD1-depleted HPV-positive cells (CaSki and HeLa) but not in HPV-negative cells (C33A). Cells were transiently transfected with indicated siRNA and the whole-cell lysates prepared from cells 72 h after transfection were probed for indicated proteins. Endogenous EDD1 was detected using EDD1 antibody and endogenous TIP60 was detected using anti-TIP60 antibody. (**d**) Whole-cell lysates prepared from HeLa-shcontrol and shEDD1 stable cells were probed for indicated proteins. (**e**) Real-time PCR analysis showing no significant change in TIP60 mRNA levels in HeLa shEDD1 cells compared with the control. The level of a given mRNA was measured by quantitative reverse transcriptase–PCR relative to that of actin mRNA. (**f**) HeLa-shcontrol and HeLa-shEDD1 cells were treated with 100 μg/ml of cycloheximide in phosphate-buffered saline (PBS) for indicated times, to inhibit protein synthesis. The cellular lysates were probed with indicated antibodies. (**g**) Graph represents collated results from three independent half-life experiments performed in HeLa-shcontrol and HeLa-shEDD1 cells. The band intensities were quantified using Image J software. TIP60 levels were normalized to 100% at time zero and s.d. estimated. (**h**) Generation of 293T stable shEDD1 cell line. Western blot analysis showing the stable knockdown of endogenous EDD1 in 293T shEDD1 cells compared with the shcontrol cells. (**j–l**) HPV18 E6 destabilizes TIP60 through EDD1. 293T cells stably expressing short hairpin RNA (shRNA) against control or EDD1 were transfected with Flag-TIP60 along with indicated plasmids. After 24 h, the cell lysates were analyzed by western blotting and probed for indicated proteins. (**k** and **l**) 293T shcontrol and 293T shEDD1 cells were transfected with 2.5 μg of Flag-TIP60 along with 5 μg of either pcDNA vector or pcDNA HPV 18 E6 expression plasmids. After 24 h, cells treated with 100 μg/ml of cycloheximide in PBS for indicates times and the cellular lysates were probed with indicated antibodies. (**k** and **l**) Graph representing collated results from three independent half-life experiments performed in 293T shcontrol and 293T shEDD1 stable cells. The band intensities were quantified using Image J software. TIP60 levels were normalized to 100% at time zero and s.d. estimated. Significance is represented as $*P < 0.05$ and $**P < 0.01$.
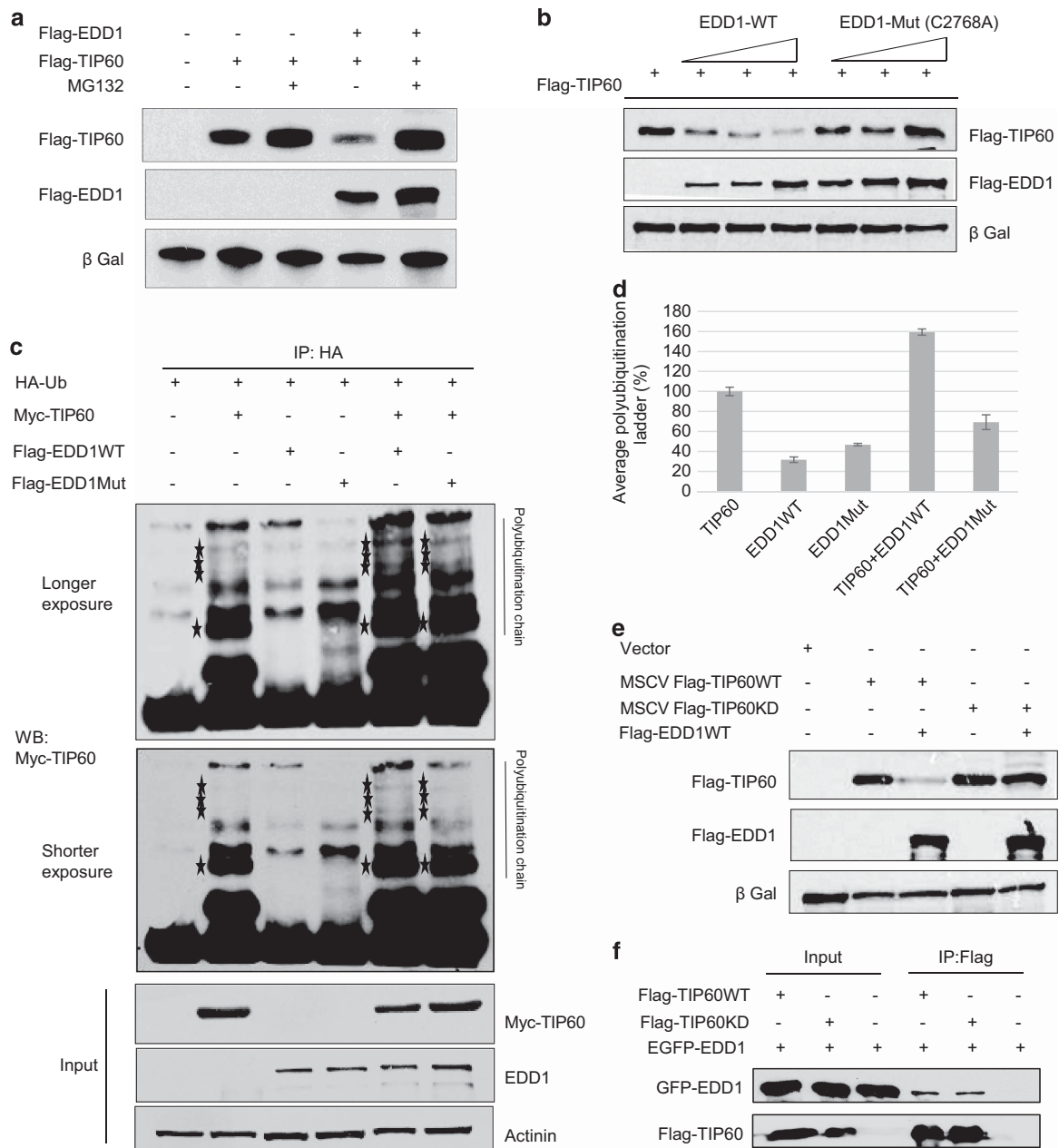
Figure 3. EDD1 destabilizes TIP60 through ubiquitin/proteasome pathway. (**a**) EDD1 destabilizes TIP60 through proteasome pathway. 293T cells were transfected with the plasmids shown and treated with 10 μg/ml MG132 for 4 h before harvesting. The total cellular lysates were probed with indicated antibodies. (**b**) EDD1 requires its ligase function to destabilize TIP60. 293T cells were transfected with different concentrations of WT EDD1 or ligase-dead mutant (C2768A). Cellular lysates were probed with anti-Flag to detect both TIP60 and EDD1. (**c**) EDD1 polyubiquitinates TIP60 *in vivo*. 293T cells were transfected with the various plasmids as shown. After 24 h, the lysates were immunoprecipitated with anti-HA-conjugated agarose beads and analyzed by western blot with indicated antibodies. (**d**) Quantitation of polyubiquitinated TIP60 from four independent experiments. (**e**) EDD1 regulates catalytically active form of TIP60. 293T cells were transfected with MSCV-TIP60 WT or MSCV-TIP60 HAT mutant along with EDD1. After 24 h, total cell lysates were probed with indicated antibodies. (**f**) EDD1 interacts with catalytically inactive form of TIP60. 293T cells were transfected with MSCV-TIP60 WT or MSCV-TIP60 HAT mutant along with EGFP-EDD1. After 24 h, total cell lysates were co-immunoprecipitated using anti-Flag beads and western blotted for EDD1 using anti-GFP antibody.

tumor suppressor p53 and apoptosis-inducing Bak protein.[40,41] However, the mutant form of HPV16 E6 was unable to bind to E6AP, showing that E6AP is dispensable for E6-mediated TIP60 destabilization.[33] Likewise MDM2, a ligase known to regulate TIP60 turnover, was also dispensable. We provide three lines of evidence to show that EDD1 mediates E6 function in this context: (i) depletion of endogenous EDD1 in HeLa and CaSki cells

upregulates TIP60 protein levels (both endogenous and exogenous (Figures 2 and 4)) but not the RNA (Figures 2e and 4c). (ii) Ablation of EDD1 in HeLa cells extends the half-life of TIP60 (both endogenous and exogenous (Figures 2 and 4)) from < 1 to > 2 h, demonstrating that EDD1 directly regulates TIP60 protein stability. (iii) Finally, we show that 18 E6 regulates TIP60 protein stability and this function is impaired in the absence of endogenous EDD1
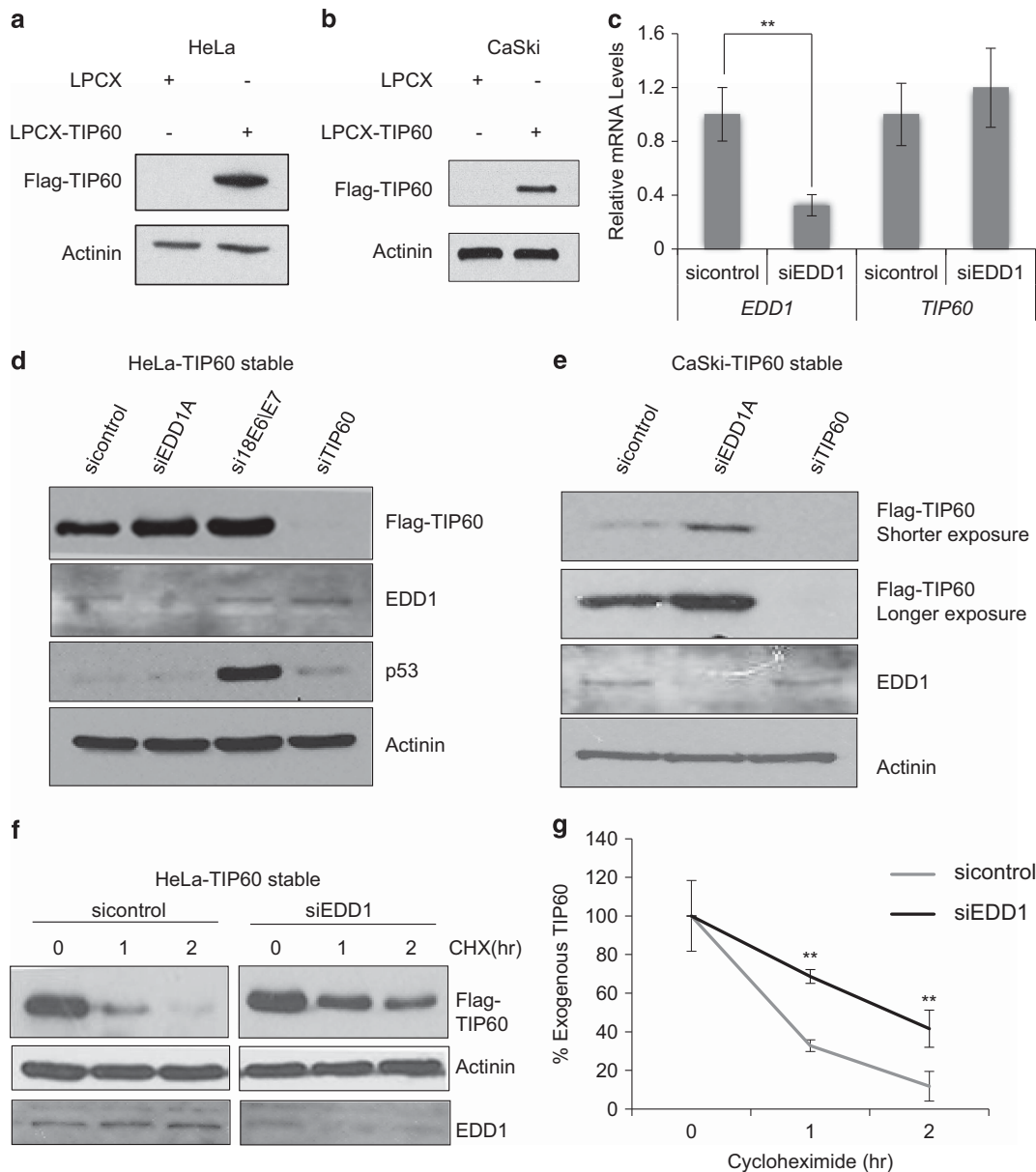
Figure 4. EDD1 regulates TIP60 turnover in HeLa-TIP60 stable cells. Western blot analysis confirming retroviral-induced TIP60 expression in HeLa-TIP60 (**a**) and in CaSki-TIP60 stable cell line (**b**). TIP60 was detected using anti-Flag antibody. (**c**) Endogenous EDD1 mRNA levels are decreased after transfecting HeLa-TIP60 stable cells with siRNA against EDD1, when compared with the control. Under the same conditions, there is no significant change in TIP60 mRNA levels. The level of a given mRNA was measured by quantitative reverse transcriptase–PCR relative to that of actin mRNA. (**d**) TIP60 expression is stabilized in EDD1-depleted HeLa-TIP60 cells. HeLa-TIP60 cells were transiently transfected with indicated siRNA and lysates prepared from cells 72 h after transfection were probed for indicated proteins. Endogenous EDD1 was detected using EDD1 antibody and TIP60 was detected using anti-Flag antibody. (**e**) TIP60 expression is stabilized in EDD1-depleted CaSki-TIP60 cells. Rest as in **d**. (**f**) HeLa-TIP60 cells were transfected with siRNA against control or EDD1. After 72 h, cells were treated with 50 µg/ml cycloheximide in phosphate-buffered saline (PBS) at indicated times, to inhibit protein synthesis. The cellular lysates were probed with indicated antibodies. (**g**) Graph represents the collated results obtained from three independent half-life experiments performed in HeLa-TIP60 cells to measure residual TIP60. The band intensities were quantified using Image J software. TIP60 levels were normalized to 100% at time zero and s.d. estimated. Significance is represented as **$P < 0.01$.

(Figures 2i–l). This mechanism is intriguing, as E6 interacts with EDD1, which negatively regulates E6 expression and its function in conjunction with E6AP.[35] The current study highlights another function of the E6–EDD1 interaction, independent of E6AP, which is favorable to E6 in the context of TIP60. These observations also suggest that EDD1 has a dual role in HPV-driven cervical cancers, where it could function as a tumor suppressor by negatively regulating E6 function, but in contrast also functions as a tumor promoter by mediating TIP60 destabilization. This is reminiscent of

EDD1's role in colon cancer where it functions as a tumor suppressor by stabilization of adenomatous polyposis coli and hence upregulates its function to inhibit β-catenin;[42] in contrast, EDD1 also ubiquitinates and upregulates Wnt-signaling-mediated β-catenin, thus promoting cancer development.[43] In addition to high-risk HPV16 and 18 E6, E6 from low-risk HPV11 and 8 also destabilizes TIP60,[33] but whether EDD1 mediates E6 function of these viruses also will be an interesting avenue to explore. HPV11 interacts with EDD1, although less efficiently when compared with

HPV 18.[35] Based on this, we speculate that EDD1 could mediate HPV 11 E6-mediated destabilization of TIP60.

Ubiquitylation mostly targets proteins to the 26 S proteasome for degradation, but it can also result in lysosomal targeting, alteration in subcellular localization, regulation of transcription and DNA repair.[44] By elucidating further the molecular mechanism through which EDD1 destabilizes TIP60, we provide evidence to show that EDD1 uses its ligase function to polyubiquitinate TIP60 and further subjects it to proteasome-mediated degradation (Figures 3a and c).
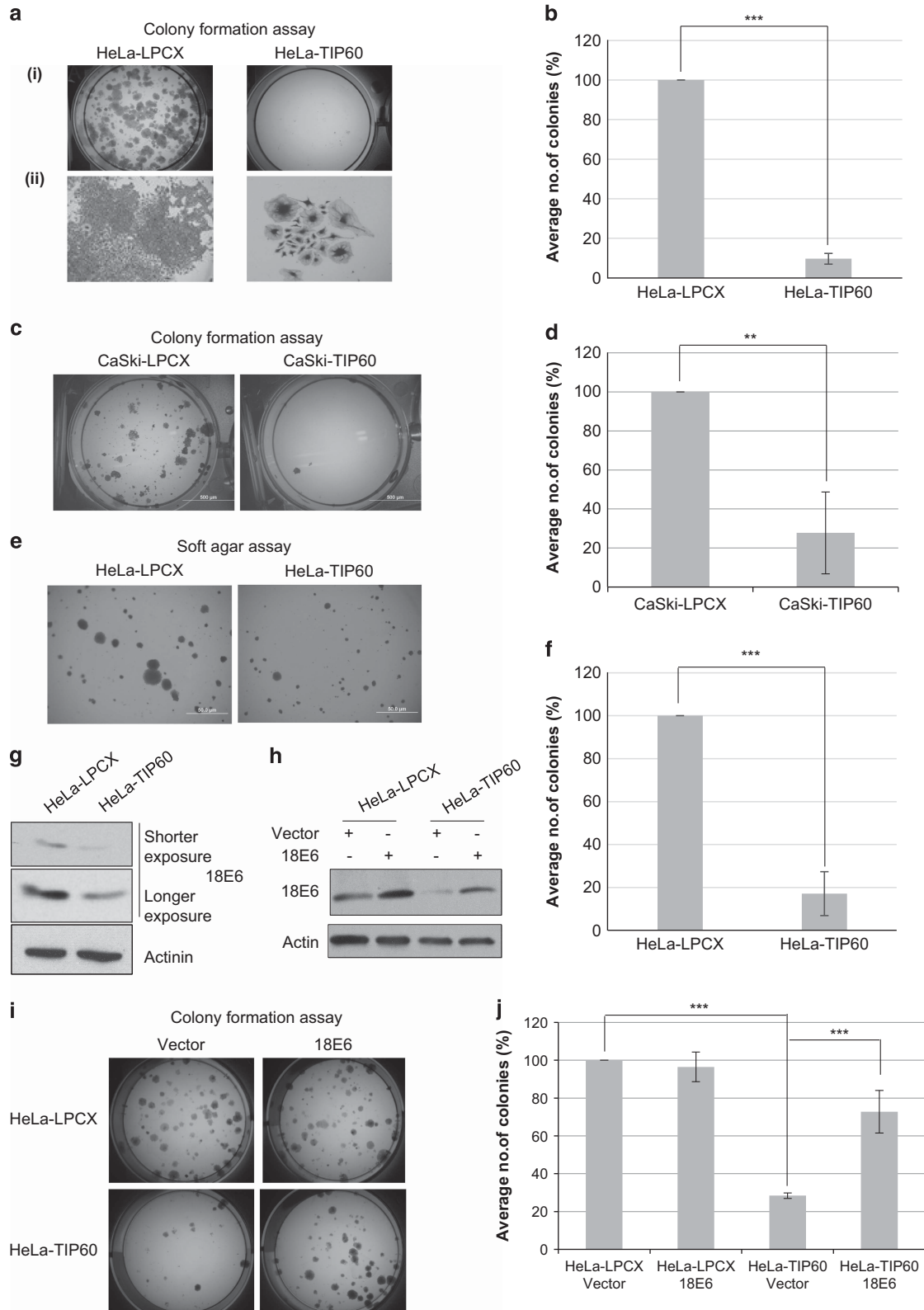
In the case of cervical cancer, HPV E6 destabilizes TIP60 and TIP60 suppresses the early major promoter of E6. We now show that gain of function of TIP60 in cervical cancers inhibits the ability of HPV-positive cells to form colonies *in vitro* (Figures 5a–f) and this strongly corresponds to inhibition of tumor growth *in vivo* (Figure 6a). The molecular mechanisms governing this strong phenotype of TIP60 needs further study. However, the CFA (Figures 5i and j) suggests that suppression of E6 expression—one of the major oncogenes regulating the transforming ability of papilloma viruses and possibly its downstream effector pathways—could mediate TIP60 function. This implies that in cervical cancers, one of the essential mechanisms through which HPV E6 oncogene promotes tumorigenesisis is by downregulating TIP60 protein level. We further provide evidence showing that regulation of TIP60 by EDD1 also contributes to TIP60-mediated phenotype both *in vitro* and *in vivo*. This is supported by similar *in-vitro* phenotype observed in HeLa-shEDD1 (Figures 6b and c) cells and HeLa-TIP60 stable cells (Figure 5a), and *in-vivo* phenotype (Figures 6a and d). Based on our studies, we propose a model (Figure 7) where in HPV-driven cervical cancers, HPV E6 destabilizes TIP60 through EDD1 to promote tumorgenesis and this activity is counteracted by TIP60, which suppresses E6 expression leading to tumor suppression. In summary, we propose that re-activation of TIP60 possibly through the inhibition of EDD1 could be of therapeutic value in treating HPV-driven malignant cervical cancers.

MATERIALS AND METHODS

Cells and transfection
All the cell lines used were cultured in Dulbecco's modified Eagle's medium with 10% fetal bovine serum. CaSki (American Type Culture Collection catalog number CRL-1550) was grown in RPMI medium with 10% fetal bovine serum. HeLa (American Type Culture Collection catalog number CLL-2) and HEK 293T (American Type Culture Collection catalog number CRL-3216) cells were transfected using calcium phosphate precipitation method. For siRNA transfection in HeLa, CaSki and C33A (American Type Culture Collection catalog number HTB-31) cells, transfection was carried out using 35 nM of annealed siRNA duplex (AIT) with Lipofectamine RNAiMAX (Invitrogen, Carlsbad, CA, USA) reagent following the manufacturer's instruction.

Plasmids and siRNAs
All the TIP60 constructs are described elsewhere.[33] pRcCMV-His-EDD1, pCDNA-β-Gal, short hairpin RNA constructs against control and EDD1 were kindly provided by Professor Lawrence Banks (ICGEB, Trieste, Italy). pCMV-Tag2B EDD1 (37188), pCMV-Tag2B EDD1 C2768A (37189) and EGFP-EDD1 (37190) were purchased from Addgene (Cambridge, MA, USA) and we thank the principal investigator Henderson MJ who deposited this plasmid in Addgene. MSCV-Flag-TIP60WT was generated by subcloning full-length TIP60 from pEF1α-TIP60-WT construct as described elsewhere[8] and MSCV-Flag-TIP60HAT mutant was generated by introducing point mutations[4] in

TIP60-WT. siRNA sequences for sicontrol, siTIP60 and si18E6/E7 are as described elsewhere.[33] siEDD1A: forward: 5′-CAACUUAGAUCUCCU GAAAdTdT-3′, reverse: 5′-UUUCAGGAGAUCUAAGUUGdTdT-3′; siEDD1B: forward: 5′-GAACAGCCCUUACAUGCAAdTdT-3′, reverse: 5′-UUGCAUGUAAGG GCUGUUCdTdT-3′; and siEDD1C was purchased from Life Technologies (Carlsbad, CA, USA; siRNA ID: s60863).

Western blotting and antibodies
Western blotting was performed as described elsewhere.[45] TIP60 antibody was generated in the lab as described previously.[46] Commercial available antibodies used are follows: Anti-HA (11583816001) Roche Life Science, Germany, anti-β-Gal (Z37880) (Promega, Madison, WI, USA), anti-penta-His (34660) (Roche, Germany), Anti-HA (E6779) beads, and anti-FlagM2 (A2220) beads (SIGMA, St Louis, MO, USA) all the other antibodies were purchased from SantaCruz (Santa Cruz, CA, USA), anti-Flag (sc-807), anti-Myc (sc-40), anti-EDD1 (H-300) (sc-367559), anti-p53 (sc-126), anti-GFP (GFP-B2) (sc9996) and anti-actinin (B-12) (sc-166524).

Mass spectrometry analysis and co-immunoprecipitation assays
Mass spectrometry analysis and co-immunoprecipitation assays was performed as described elsewhere.[45]

In vivo ubiquitination and half-life experiments
In vivo ubiquitination and half-life experiments was performed as described elsewhere.[45]

Real-time PCR analysis
Real-time PCR analysis was performed as described elsewhere.[33] Primers for real-time PCR were as follows: TIP60 forward primer: 5′-AATG TGGCCTGCATCCTAAC-3′ and reverse primer: 5′-TGTTTTCCCTTCCACTTTGG-3′; EDD1 forward primer: 5′-GAAGAGGTTGAGGTGGTGGA-3′ and reverse primer: 5′-CAGCTCCATATCACTCCCGT-3′; and Actin forward primer: 5′-CCAGAT CATGTTTGAGACCTTCAAC-3′ and reverse primer: 5′-CCAGAGGCGTACA GGGATAGC-3′.

Stable cell line generation
Stable cell line generation was performed as described elsewhere.[38]

CFA and soft agar assays
Cells (1×10^3) either in 5% serum or 2× Dulbecco's modified Eagle's medium supplemented with 20% fetal calf serum and 0.4% agar were used for CFA and soft agar assay, respectively. After 3 weeks, the colonies were stained with Giemsa stain and quantified using Image J software (http://imagej.nih.gov/ij/).

Cell fractionation assays
HEK293 cells in 10-cm dishes were transfected with 5 μg of plasmids expressing HA-tagged deletion mutants of TIP60. Twenty-four hours post transfection, the cells were collected and subjected to cytoplasmic and

Figure 5. TIP60 inhibits the growth of HPV-positive cells *in vitro*. (**a**) (i) Representative images from the CFA performed in HeLa stable cells (top panel) and the magnified images (ii) from the same assay (lower panel). The assay was performed as mentioned in 'Materials and Methods'. The cells were fixed and stained with crystal violet after 21 days. (**b**) Bar graph represents the collated results obtained from quantifications of two independent experiments (as shown in **a**) each in triplicates. Quantifications were performed using Image J software; s.d. is also shown. (**c**) Representative images from the CFA performed in CaSki stable cells. (**d**) Bar graph represents the collated results obtained from quantifications of two independent experiments (as shown in **c**), each in triplicates. Quantifications were performed using Image J software; s.d. is also shown. (**e**) Representative images from the soft agar assay performed in HeLa stable cells. The assay was performed as mentioned in the 'Materials and Methods'. The colonies were fixed and stained with crystal violet after 21 days. (**f**) Bar graph representing the collated results obtained from quantifications of two independent experiments, each in triplicates; s.d. is also shown. Quantifications were done using Image J software assigning a threshold value to define a colony. (**g**) TIP60 inhibits the ability of HeLa cells to form colonies by downregulating HPV 18 E6 protein levels. Total cellular extracts from HeLa-LPCX and HeLa-TIP60 were probed with indicated antibodies. (**h**–**j**) HPV 18 E6 rescues the growth defect in HeLa-TIP60 cells. HeLa-LPCX or HeLa-TIP60 cells were transiently transfected with indicated plasmids and western blotted for indicated antibodies. (**i**) Representative images from the CFA performed in HeLa stable cells indicated in **h**. The assay was performed as mentioned in 'Materials and Methods'. The cells were fixed and stained with crystal violet after 14 days. (**j**) Bar graph represents the collated results obtained from quantifications of four independent experiments. Quantifications were performed using Image J software; s.d. is also shown. Significance is represented as **$P < 0.01$ and ***$P < 0.001$.
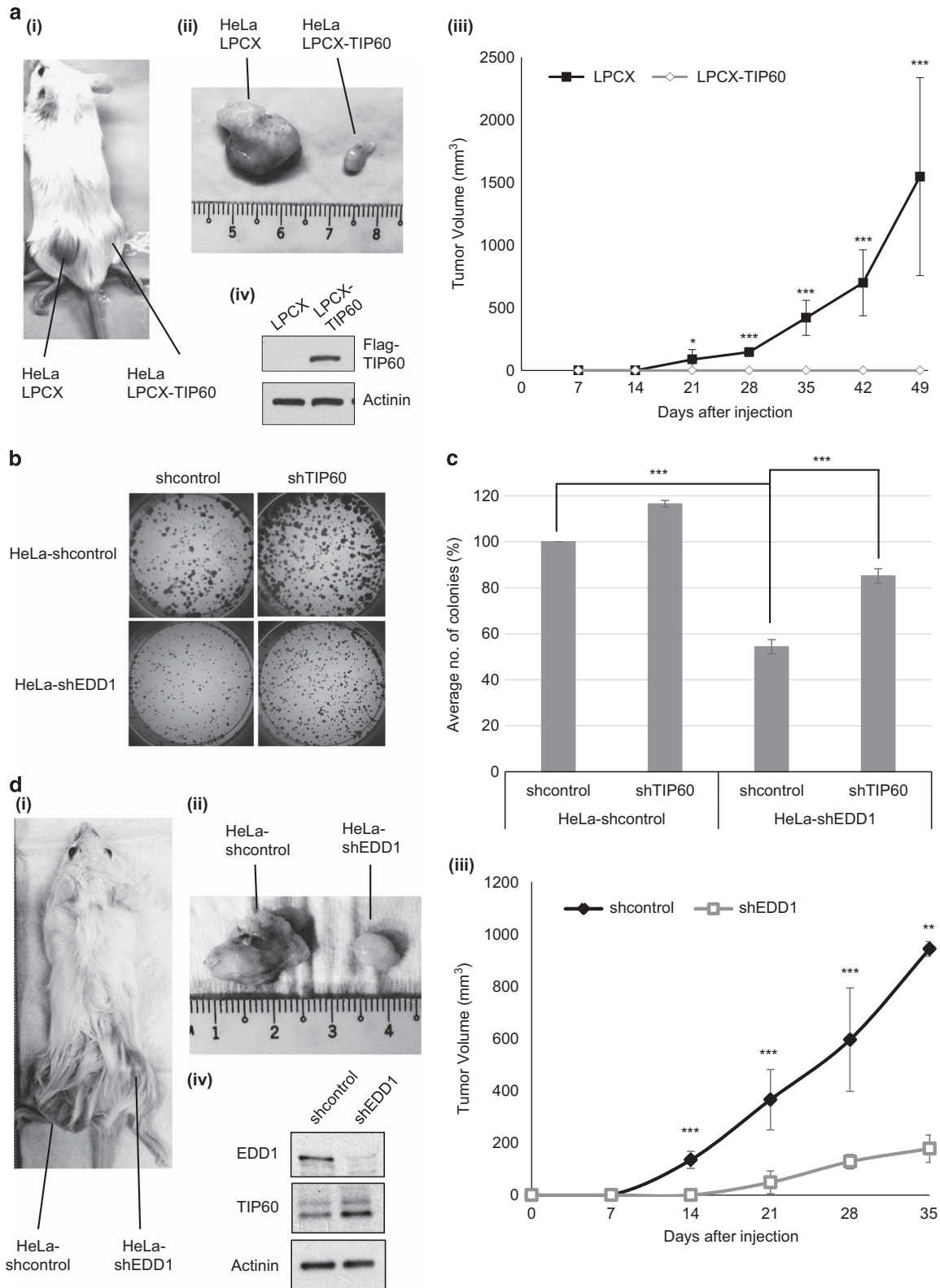
nuclear fractionation using NE-PER Cytoplasmic and Nuclear Extraction reagents (Life Technologies, catalog number 78833) following the manufacturer's instructions. The different fractions were run on SDS–polyacrylamide gel electrophoresis and the localization of the TIP60 deletion mutants was observed. β-Tubulin for cytoplasmic fraction and Histone H3 for nuclear fraction were used to validate the extraction procedure.

In-vivo mice experiment

Six-week-old NOD/SCID mice obtained from Invivos (Singapore) were randomly distributed and HeLa stable cell lines (HeLa-LPCX, HeLa-TIP60, HeLa-shcontrol or HeLa-shEDD1) resuspended in 100 μl of serum-free Dulbecco's modified Eagle's medium at a concentration of 1×10^7 cells/ml (for HeLa-LPCX or HeLa-TIP60 cells) and 1×10^6 cells/ml (for HeLa-shcontrol

Figure 7. Graphical model. HPV E6 and TIP60 negatively regulate each other's expression to either promote or inhibit tumor formation, respectively.

or HeLa-shEDD1) supplemented with BD Matrigel matrix (BD Biosciences, Bedford, MA, USA; 354234) and were injected subcutaneously into the right or the left flank of the mice. Tumors were examined at indicated times and total tumor volume recorded. Tumor volume (mm^3) was calculated using the formula: Volume $(V) = $ Width $(W)(2) \times$ Length $(L)/2$. The National University of Singapore Institutional Animal Care and Use Committee has approved the work done in this study, under protocol 102/12 in accordance with the National Advisory Committee for Laboratory Animal Research Guidelines (Guidelines on the Care and Use of Animals for Scientific Purposes) in facilities licensed by the Agri-Food and Veterinary Authority of Singapore, the regulatory body of the Singapore Animals and Birds Act.

Statistical analysis

For indicated experiments, an unpaired two-tailed Student's *t*-test was performed. Error bars indicate the s.d. of data collected from mentioned experimental repeats. Significance is represented as *$P < 0.05$, **$P < 0.01$ and ***$P < 0.001$.

CONFLICT OF INTEREST

The authors declare no conflict of interest.

REFERENCES

1 Utley RT, Cote J. The MYST family of histone acetyltransferases. *Curr Topics Microbiol Immunol* 2003; **274**: 203–236.

2 Col E, Caron C, Chable-Bessia C, Legube G, Gazzeri S, Komatsu Y et al. HIV-1 Tat targets Tip60 to impair the apoptotic cell response to genotoxic stresses. *EMBO J* 2005; **24**: 2634–2645.

3 Fazzio TG, Huff JT, Panning B. An RNAi screen of chromatin proteins identifies Tip60-p400 as a regulator of embryonic stem cell identity. *Cell* 2008; **134**: 162–174.

4 Ikura T, Ogryzko VV, Grigoriev M, Groisman R, Wang J, Horikoshi M et al. Involvement of the TIP60 histone acetylase complex in DNA repair and apoptosis. *Cell* 2000; **102**: 463–473.

5 Sapountzi V, Logan IR, Robson CN. Cellular functions of TIP60. *Int J Biochem Cell Biol* 2006; **38**: 1496–1509.

6 Squatrito M, Gorrini C, Amati B. Tip60 in DNA damage response and growth control: many tricks in one HAT. *Trends Cell Biol* 2006; **16**: 433–442.

7 Sterner DE, Berger SL. Acetylation of histones and transcription-related factors. *Microbiol Mol Biol Rev* 2000; **64**: 435–459.

8 Jha S, Shibata E, Dutta A. Human Rvb1/Tip49 is required for the histone acetyl-transferase activity of Tip60/NuA4 and for the downregulation of phosphorylation on H2AX after DNA damage. *Mol Cell Biol* 2008; **28**: 2690–2700.

9 Jha S, Dutta A. RVB1/RVB2: running rings around molecular biology. *Mol Cell* 2009; **34**: 521–533.

10 Kusch T, Florens L, Macdonald WH, Swanson SK, Glaser RL, Yates JR 3rd et al. Acetylation by Tip60 is required for selective histone variant exchange at DNA lesions. *Science* 2004; **306**: 2084–2087.

11 Lee MT, Leung YK, Chung I, Tarapore P, Ho SM. Estrogen receptor beta (ERbeta1) transactivation is differentially modulated by the transcriptional coregulator Tip60 in a cis-acting element-dependent manner. *J Biol Chem* 2013; **288**: 25038–25052.

12 Mahajan MA, Stanley FM. Insulin-activated Elk-1 recruits the TIP60/NuA4 complex to increase prolactin gene transcription. *Mol Cell Endocrinol* 2014; **382**: 159–169.

13 Sun Y, Xu Y, Roy K, Price BD. DNA damage-induced acetylation of lysine 3016 of ATM activates ATM kinase activity. *Mol Cell Biol* 2007; **27**: 8502–8509.

14 Tang Y, Luo J, Zhang W, Gu W. Tip60-dependent acetylation of p53 modulates the decision between cell-cycle arrest and apoptosis. *Mol Cell* 2006; **24**: 827–839.

15 Hu Y, Fisher JB, Koprowski S, McAllister D, Kim MS, Lough J. Homozygous disruption of the Tip60 gene causes early embryonic lethality. *Dev Dyn* 2009; **238**: 2912–2921.

16 Gorrini C, Squatrito M, Luise C, Syed N, Perna D, Wark L et al. Tip60 is a haplo-insufficient tumour suppressor required for an oncogene-induced DNA damage response. Nature 2007; 448: 1063–1067.

17 Legube G, Linares LK, Lemercier C, Scheffner M, Khochbin S, Trouche D. Tip60 is targeted to proteasome-mediated degradation by Mdm2 and accumulates after UV irradiation. EMBO J 2002; 21: 1704–1712.

18 Sho T, Tsukiyama T, Sato T, Kondo T, Cheng J, Saku T et al. TRIM29 negatively regulates p53 via inhibition of Tip60. Biochim Biophys Acta 2011; 1813: 1245–1253.

19 Kaidi A, Jackson SP. KAT5 tyrosine phosphorylation couples chromatin sensing to ATM signalling. Nature 2013; 498: 70–74.

20 Zheng H, Seit-Nebi A, Han X, Aslanian A, Tat J, Liao R et al. A posttranslational modification cascade involving p38, Tip60, and PRAK mediates oncogene-induced senescence. Mol Cell 2013; 50: 699–710.

21 Callaghan MJ, Russell AJ, Woollatt E, Sutherland GR, Sutherland RL, Watts CK. Identification of a human HECT family protein with homology to the Drosophila tumor suppressor gene hyperplastic discs. Oncogene 1998; 17: 3479–3491.

22 Mansfield E, Hersperger E, Biggs J, Shearn A. Genetic and molecular analysis of hyperplastic discs, a gene whose product is required for regulation of cell proliferation in Drosophila melanogaster imaginal discs and germ cells. Dev Biol 1994; 165: 507–526.

23 Henderson MJ, Russell AJ, Hird S, Munoz M, Clancy JL, Lehrbach GM et al. EDD, the human hyperplastic discs protein, has a role in progesterone receptor coactivation and potential involvement in DNA damage response. J Biol Chem 2002; 277: 26468–26478.

24 Henderson MJ, Munoz MA, Saunders DN, Clancy JL, Russell AJ, Williams B et al. EDD mediates DNA damage-induced activation of CHK2. J Biol Chem 2006; 281: 39990–40000.

25 Eblen ST, Kumar NV, Shah K, Henderson MJ, Watts CK, Shokat KM et al. Identification of novel ERK2 substrates through use of an engineered kinase and ATP analogs. J Biol Chem 2003; 278: 14926–14935.

26 Alpsoy A, Yasa S, Gunduz U.. Etoposide resistance in MCF-7 breast cancer cell line is marked by multiple mechanisms. Biomed Pharmacother 2014; 68: 351–355.

27 Bradley A, Zheng H, Ziebarth A, Sakati W, Branham-O'Connor M, Blumer JB et al. EDD enhances cell survival and cisplatin resistance and is a therapeutic target for epithelial ovarian cancer. Carcinogenesis 2014; 35: 1100–1109.

28 Mori Y, Sato F, Selaru FM, Olaru A, Perry K, Kimos MC et al. Instabilotyping reveals unique mutational spectra in microsatellite-unstable gastric cancers. Cancer Res 2002; 62: 3641–3645.

29 Chou S. Diverse cytomegalovirus UL27 mutations adapt to loss of viral UL97 kinase activity under maribavir. Antimicrob Agents Chemother 2009; 53: 81–85.

30 Li R, Zhu J, Xie Z, Liao G, Liu J, Chen MR et al. Conserved herpesvirus kinases target the DNA damage response pathway and TIP60 histone acetyltransferase to promote virus replication. Cell Host Microbe 2011; 10: 390–400.

31 Reitsma JM, Savaryn JP, Faust K, Sato H, Halligan BD, Terhune SS. Antiviral inhibition targeting the HCMV kinase pUL97 requires pUL27-dependent degradation of Tip60 acetyltransferase and cell-cycle arrest. Cell Host Microbe 2011; 9: 103–114.

32 Awasthi S, Sharma A, Wong K, Zhang J, Matlock EF, Rogers L et al. A human T-cell lymphotropic virus type 1 enhancer of Myc transforming potential stabilizes Myc-TIP60 transcriptional interactions. Mol Cell Biol 2005; 25: 6178–6198.

33 Jha S, Vande Pol S, Banerjee NS, Dutta AB, Chow LT, Dutta A. Destabilization of TIP60 by human papillomavirus E6 results in attenuation of TIP60-dependent transcriptional regulation and apoptotic pathway. Mol Cell 2010; 38: 700–711.

34 Kimura A, Horikoshi M.. Tip60 acetylates six lysines of a specific class in core histones in vitro. Genes Cells 1998; 3: 789–800.

35 Tomaic V, Pim D, Thomas M, Massimi P, Myers MP, Banks L. Regulation of the human papillomavirus type 18 E6/E6AP ubiquitin ligase complex by the HECT domain-containing protein EDD. J Virol 2011; 85: 3120–3127.

36 Honda Y, Tojo M, Matsuzaki K, Anan T, Matsumoto M, Ando M et al. Cooperation of HECT-domain ubiquitin ligase hHYD and DNA topoisomerase II-binding protein for DNA damage response. J Biol Chem 2002; 277: 3599–3605.

37 Huibregtse JM, Scheffner M, Beaudenon S, Howley PM. A family of proteins structurally and functionally related to the E6-AP ubiquitin-protein ligase. Proc Natl Acad Sci USA 1995; 92: 5249.

38 Gupta A, Jha S, Engel DA, Ornelles DA, Dutta A. Tip60 degradation by adenovirus relieves transcriptional repression of viral transcriptional activator EIA. Oncogene 2013; 32: 5017–5025.

39 Sun Y, Jiang X, Price BD. Tip60: connecting chromatin to DNA damage signaling. Cell Cycle 2010; 9: 930–936.

40 Huibregtse JM, Scheffner M, Howley PM. Cloning and expression of the cDNA for E6-AP, a protein that mediates the interaction of the human papillomavirus E6 oncoprotein with p53. Mol Cell Biol 1993; 13: 775–784.

41 Thomas M, Banks L. Inhibition of Bak-induced apoptosis by HPV-18 E6. Oncogene 1998; 17: 2943–2954.

42 Ohshima R, Ohta T, Wu W, Koike A, Iwatani T, Henderson M et al. Putative tumor suppressor EDD interacts with and up-regulates APC. Genes Cells 2007; 12: 1339–1345.

43 Hay-Koren A, Caspi M, Zilberberg A, Rosin-Arbesfeld R. The EDD E3 ubiquitin ligase ubiquitinates and up-regulates beta-catenin. Mol Biol Cell 2011; 22: 399–411.

44 Metzger MB, Hristova VA, Weissman AM. HECT and RING finger families of E3 ubiquitin ligases at a glance. J Cell Sci 2012; 125: 531–537.

45 Krishna Subbaiah V, Massimi P, Boon SS, Myers MP, Sharek L, Garcia-Mata R et al. The invasive capacity of HPV transformed cells requires the hDlg-dependent enhancement of SGEF/RhoG activity. PLoS Pathog 2012; 8: e1002543.

46 Frank SR, Parisi T, Taubert S, Fernandez P, Fuchs M, Chan HM et al. MYC recruits the TIP60 histone acetyltransferase complex to chromatin. EMBO Rep 2003; 4: 575–580.

Supplementary Information accompanies this paper on the Oncogene website (http://www.nature.com/onc)

TIP60-miR-22 axis as a prognostic marker of breast cancer progression

Amit Kumar Pandey[1], Yanzhou Zhang[1], Siting Zhang[3], Ying Li[1], Greg Tucker-Kellogg[3], Henry Yang[1], Sudhakar Jha[1,2]

[1]Cancer Science Institute of Singapore, Yong Loo Lin School of Medicine, National University of Singapore, Singapore

[2]Department of Biochemistry, Yong Loo Lin School of Medicine, National University of Singapore, Singapore

[3]Department of Biological Sciences, Faculty of Science, National University of Singapore, Singapore

Correspondence to:
Sudhakar Jha, **e-mail:** csisjha@nus.edu.sg

ABSTRACT

MicroRNAs (miRNAs) are 22- to 24-nucleotide, small, non-coding RNAs that bind to the 3'UTR of target genes to control gene expression. Consequently, their dysregulation contributes to many diseases, including diabetes and cancer. miR-22 is up-regulated in numerous metastatic cancers and recent studies have suggested a role for miR-22 in promoting stemness and metastasis. TIP60 is a lysine acetyl-transferase reported to be down-regulated in cancer but the molecular mechanism of this reduction is still unclear. In this study, we identify TIP60 as a target of miR-22. We show a negative correlation in the expression of TIP60 and miR-22 in breast cancer patients, and show that low levels of TIP60 and high levels of miR-22 are associated with poor overall survival. Furthermore, pathway analysis using high miR-22/low TIP60 and low miR-22/high TIP60 breast cancer patient datasets suggests association of TIP60/miR-22 with epithelial-mesenchymal transition (EMT), a key alteration in progression of cancer cells. We show that blocking endogenous miR-22 can restore TIP60 levels, which in turn decreases the migration and invasion capacity of metastatic breast cancer cell line. These results provide mechanistic insight into TIP60 regulation and evidence for the utility of the combination of TIP60 and miR-22 as prognostic indicator of breast cancer progression.

INTRODUCTION

Breast cancer is one of the most common and significant malignant diseases in women worldwide [1]. Although improvements in detection and treatment have decreased breast cancer mortality in recent years, the stage of detection and ability of cancer cells to metastasize to distant organs have been the major challenges in the successful prevention of and therapy, for this deadly disease. Cancer metastasis is a complex, multi-step process and is driven, promoted, and modulated by aberrantly deregulated cellular signals.

MicroRNAs (miRNAs) are a family of small non-protein-coding RNA molecules of approximately 22–24 nucleotides (nt) that function as key regulators of gene expression at the post-transcriptional level [2]. Since their initial discovery in *Caenorhabditis elegans* [3], thousands of microRNAs have been annotated and currently 2588, 765 and 1915 mature miRNA sequences in human, rat and mouse, respectively, have been catalogued in the microRNA registry (http://www.mirbase.org, V 21 June, 2014). miRNA dysregulation has been shown to contribute to the etiology of multiple diseases, including cancer, where miRNAs can act as either oncogenes or tumor suppressors [4–8]. Indeed, emerging evidence demonstrates that aberrant miRNA expression is linked to breast cancer progression [9, 10].

TIP60 (lysine acetyl-transferase) is part of a conserved multisubunit complex, NuA4, which is recruited by many transcription factors to their target promoters, where it acetylates histones and is involved in transcriptional regulation. TIP60 has been shown to play an important role in many processes such as cellular signaling, DNA damage repair and apoptosis

[11, 12], as well as cell cycle and checkpoint control [13]. Involvement of TIP60 in these various processes implies that its expression, stability and localization are regulated in the cell by various mechanisms.

In the current study, we show the first evidence of a non-coding RNA as regulator of TIP60 expression. We find the expression of miR-22 and TIP60 to be negatively correlated in invasive breast cancer tissues and breast cancer cell lines. Furthermore, we identified TIP60 as a miR-22 target and show that, by targeting TIP60, miR-22 stimulates the expression of epithelial-mesenchymal transition (EMT) genes. Using various cell culture models, we find miR-22 expression results in increased cell migration and invasion. Our data suggest that TIP60 and miR-22 could act as prognostic markers in breast cancer disease progression and that targeting the TIP60–miR-22 axis could lead to an effective therapeutic strategy for metastatic breast cancer.

RESULTS

TIP60 is a direct target of miR-22

TIP60 is known to be down-regulated in multiple cancers [14, 15]. Whereas we and others have identified TIP60 to be destabilized by viral oncogenes [16–19], other potential mechanisms of its downregulation are unknown. In order to investigate whether TIP60 expression could be regulated by miRNAs, we performed an *in silico* analysis using the Targetscan database (http://www.targetscan.org/) to identify putative miRNA seed-matching sequences in TIP60. We found one putative target binding site for miR-22 at the position 249–255 nt in the 3′UTR of TIP60 (Figure 1A). This identified seed sequence was also conserved among different species of TIP60, indicating the likely functional importance of this motif (Figure 1B). To further validate TIP60 as a target of miR-22, we cloned the 3′UTR of TIP60 into the pmirGLO dual-luciferase vector, and transiently co-transfected pmirGLO-TIP60 WT 3′UTR into MCF7 cells along with a miRNA mimic negative control (that does not target any known mRNA within the human transcriptome) or a miR-22 mimic either alone or in combination with miR inhibitor negative control. A miR-22 hairpin inhibitor was also transfected and used to show specificity of miR-22 for TIP60. After 48 h of transfection, cells were lysed and the protein was analyzed for luciferase activity. We measured a 40% reduction in the luciferase activity of pmirGLO-TIP60 WT 3′UTR with miR-22 mimic overexpression (Figure 1C), and this reduction could be rescued upon the co-transfection with the miR-22 hairpin inhibitor, suggesting specificity of this regulation (Figure 1C). In addition, we did not observe any difference in luciferase activity when pmirGLO-TIP60 WT 3′UTR was transfected with either miR mimic negative control or with miR inhibitor negative control alone, suggesting target specificity. To further demonstrate

that the decrease in luciferase activity is due to miR-22 binding to the seed sequence in the 3′ UTR of TIP60, we generated two 3′UTR mutant constructs: the first comprised point mutations in the miR-22 binding sites of TIP60 (pmirGLO-TIP60 Mut 3′UTR); in the second, we deleted the miR-22 seed sequence at the TIP60 3′UTR using site-directed mutagenesis (pmirGLO-TIP60 Del 3′UTR). Clones were confirmed by sequencing (Figure 1D). These mutants were then co-transfected along with the miR mimic negative control or miR-22 mimic. We observed no repression in luciferase activity after mutating or deleting the binding site (Figure 1E), suggesting that miR-22 directly interacts with the TIP60 3′UTR and targets TIP60.

miR-22 and TIP60 expression is negatively co-related

Having identified a miR-22 binding site in the 3′UTR of TIP60, we next sought to understand the physiological relevance of this regulation. We decided to focus on breast cancer, as a recent study by Song et al. [20] implicated the role of miR-22 in breast cancer. To this end, we analyzed the expression of TIP60 and miR-22 in a breast cancer dataset from The Cancer Genome Atlas (TCGA) database and found a small but significant negative correlation between TIP60 and miR-22 expression (Figure 2A). To investigate the potential biological significance of this negative correlation, we sought to identify a cell culture model that also showed a negative correlation between TIP60 and miR-22. For this, we analyzed the expression of miR-22 and TIP60 (mRNA and protein) in 12 breast cancer cell lines on the basis of their EMT score as described by Tan et.al. [21]. Interestingly, mesenchymal cell lines such as MDA-MB-231, Hs578T and MDA-MB-468 and epithelial cell line such as MCF-7 and T47D showed a negative correlation between miR-22 and TIP60 mRNA expression (Figure 2B and 2C), with high miR-22 and low TIP60 expression in the highly metastatic MDA-MB-231 cell line and Hs578T cell line, but high TIP60 and low miR-22 expression in the MCF7, T47D mild metastatic cells and MDA-MB-468 basal, triple-negative cells. A similar expression profile of TIP60 was also observed at the protein level (Figure 2D).

To further investigate whether miR-22 affects endogenous TIP60 expression, we focused on 2 of the 12 breast cancer cell lines: MCF7, an epithelial cell line that is mildly metastatic and has low miR-22 and high TIP60 expression and MDA-MB-231 which is a mesenchymal cell line, highly metastatic and has high miR-22 and low TIP60 expression. We then transfected the miR-22 mimic or miR mimic negative control and compared the level of TIP60 protein in MCF7 cells under these two conditions. Similarly, the MDA-MB-231 cell line was transfected with the miR-22 inhibitor or with a miR inhibitor negative control to examine endogenous changes

A Position 249-255 of TIP60 3' UTR

5' ... GACCAGAGGGAGCCAGGCAGCUG...
          | | | | | | |
hsa-miR-22   3'   UGUCAAGAAGUUGACCGUCGAA

B

Human	CAGGGACCAGAGGGAGCCA**GGCAGCU**GUGUACAGUGAGAA
Chimpanzee	CAGGGACCAGAGGGAGCCA**GGCAGCU**GUGUACAGUGAGAA
Mouse	CGUGGACCAAAGGGAUCCA**GGCAGCU**GUGUACAUUAAGAU
Rat	CAGGGACCAGGGGGACCCA**GGCAGCU**GUGUACACUAAGGC
Guinea pig	CAGGGACCAGAGGGAGCUG**GGCAGCU**GUGUACAGUGAGAU

C

3'UTR	+	+	+	+	+
miR-22 mimic	-	+	+	-	-
miR-22 inhibitor	-	-	+	-	-
miR mimic negative control	+	-	-	-	+
miR inhibitor negative control	+	+	-	+	-

D

TIP60 3'UTR Mut   CAGAGGGAGCCA**GAA**A**TT**TGTGTACAGTGAG
TIP60 3'UTR WT   CAGAGGGAGCCAGGCAGCTGTGTACAGTGAG
TIP60 3'UTR Del   CAGAGGGAGCCA------------TGTGTACAGTGAG

E

miR-22 mimic	-	+	-	+	-	+
miR mimic negative control	+	-	+	-	+	-

3'UTR WT   3'UTR MUT   3'UTR DEL

Figure 1: miR-22 binding site at the TIP60 3′UTR. A. Putative target binding site for miR-22 at the 3′UTR of the TIP60 gene, as predicted by Targetscan (http://www.targetscan.org/). **B.** The target site is highly conserved across the various indicated species. Highlighted nucleotides (in bold) indicate the putative miR-22 binding site. **C.** The miR-22 binding site on TIP60 3′UTR was confirmed by luciferase activity in MCF7 cells after co-transfection of pmirGLO-TIP60 3′-UTR plasmid with the indicated miRs (50 nM). **D.** Mutation of the miR-22 binding site in the 3′UTR of TIP60. **E.** MCF7 cells were co-transfected with a wild-type pmirGLO-TIP60 3′-UTR luciferase construct, or a construct containing a mutation in the predicted miR-22 binding site or construct having binding site deleted with either the miR-22 mimic or the negative control mimic. Luciferase expression was normalized to Renilla luciferase and the data is depicted as the mean ± SEM. The figure summarizes data from three independent experiments performed in triplicate. Analysis was performed using an unpaired two-tailed student's t-test. Significance is represented as ***$P < 0.001$; **$P < 0.01$.
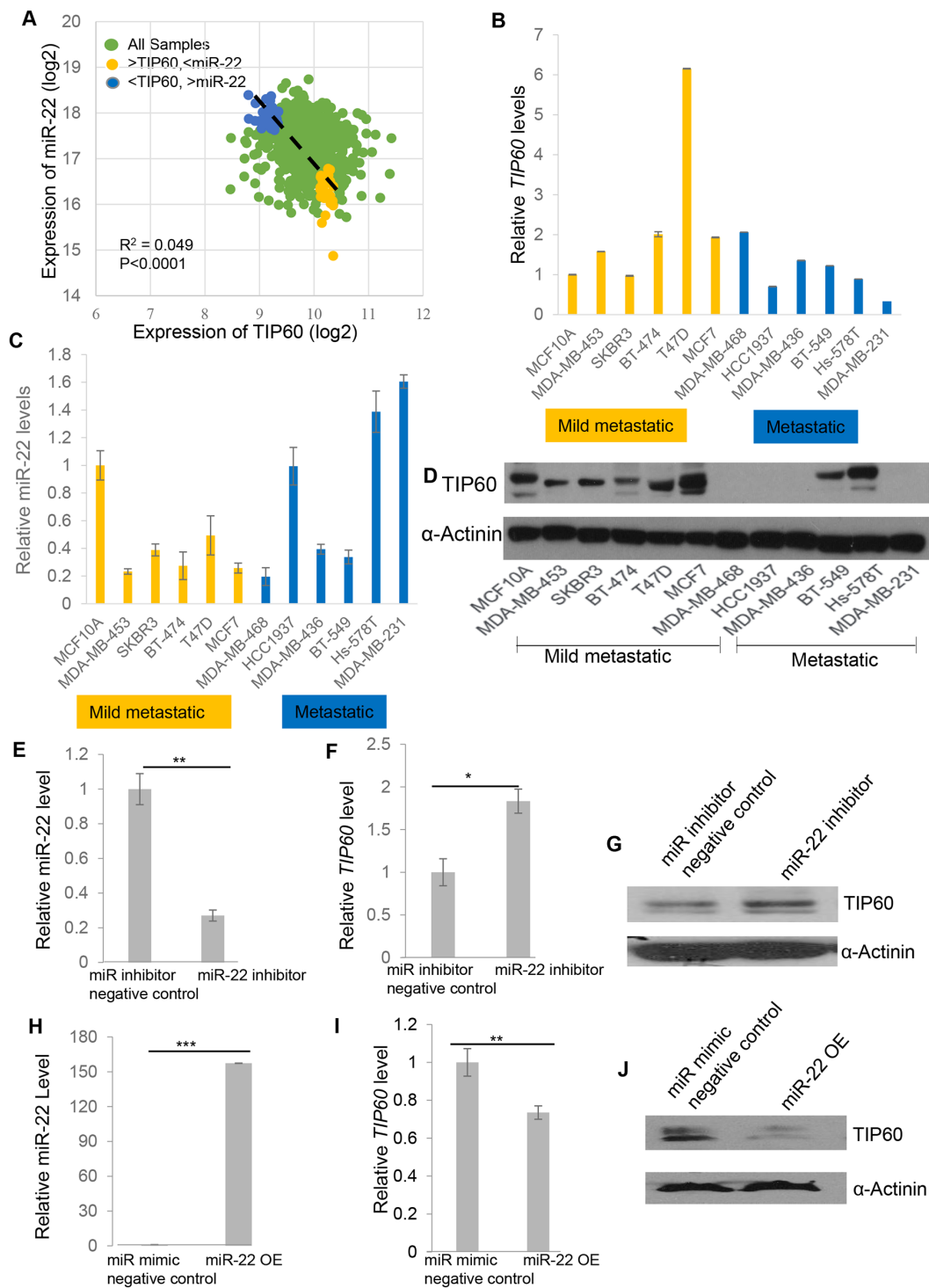
Figure 2: Negative correlation of TIP60 and miR-22 mRNA and protein levels in breast cancer patients and cell lines.
A. Negative correlation between miR-22 and TIP60 mRNA levels for each individual sample from the TCGA dataset. **B, C.** The expression of *TIP60* mRNA and miR-22 mRNA was detected by QRT-PCR in a panel of 12 breast cancer cell lines. Mild metastatic and metastatic cell lines are shown in yellow and blue colors, respectively. **D.** Western blot showing the expression of TIP60 in a panel of 12 breast cancer cell lines **E.** mRNA levels of miR-22 were decreased on miR-22 inhibition in MDA-MB-231 cells when transfected with miR-22 inhibitor for 48 h (50 nM). **F–G.** mRNA and protein levels of TIP60 were increased following inhibition of miR-22 in MDA-MB-231 cells when transfected with miR-22 inhibitor for 48 h (50 nM). **H.** Relative miR-22 levels were determined by QRT-PCR on miR-22 mimic overexpression (miR-22OE, 50 nM) in MCF7 cells. **I–J.** mRNA and protein levels of TIP60 were decreased following miR-22 mimic overexpression (50 nM) in MCF7 cells. The figure illustrates data from three independent experiments performed in triplicate. Significance is represented as *$P < 0.05$; **$P < 0.01$; ***$P < 0.001$.

in TIP60. We found that TIP60 expression was increased in MDA-MB-231 cells (Figure 2F–2G) and reduced in MCF7 cells (Figure 2I–2J) after inhibition (Figure 2E) or overexpression of miR-22 mimic (Figure 2H), respectively both at mRNA and protein level. These data indicate that miR-22 down-regulates endogenous TIP60 expression.

miR-22 regulates EMT genes by repressing TIP60

To determine the downstream effects of TIP60 regulation by miR-22, we performed Gene-Set Enrichment Analysis (GSEA) using msigdb.v4 (http://www.broad.mit.edu/gsea/) and compared 28 TCGA samples with high TIP60/low miR-22 expression with 28 samples with low TIP60/high miR-22 expression. Our GSEA analysis revealed enrichment of the epithelial-mesenchymal transition (EMT) pathway (Figure 3A). Since EMT is related to cellular migration and invasion, we sought to determine the effect of miR-22 on various EMT markers. We ablated miR-22 activity by transfecting MDA-MB-231 cells with the miR-22 inhibitor or overexpressed the miR-22 mimic in MCF7 cells. Aside from increased TIP60 levels (Figure 3B), we found that miR-22 inhibition in MDA-MB-231 cells resulted in increased *E-cadherin* levels, an epithelial marker that is lost upon execution of the EMT program (Figure 3C). Similar increase in *E-cadherin* was also found in MDA-MB-231-LPCX-TIP60 stable cell line. In comparison, MCF7 cells showed decreased TIP60 (Figure 3D) and *E-cadherin* levels (Figure 3E) and increased *N-cadherin* (mesenchymal marker) levels in the presence of miR-22 mimic (Figure 3E) and this effect was rescued on overexpressing TIP60 in MCF7 cell line. Further, we did not observe any changes in other EMT markers. These data suggest that miR-22 induces EMT like phenotype and this is associated with a change in the expression of TIP60. The phenotypic alterations induced by miR-22 mimic overexpression in MCF7 cells is observed by immuno-fluorescence staining of the E-cadherin. MCF7 cells treated with miR mimic negative control showed expression of E-cadherin (Figure 4A, mimic negative control) and this was reduced in miR-22 mimic overexpressed MCF7 cells (Figure 4A, miR-22 OE). We further examined the status of F-actin in the cells by phalloidin staining, since actin reorganization occurs during the EMT process [22]. In contrast to miR mimic negative control treated cells (Figure 4B, mimic negative control), overexpression of miR-22 mimic significantly induced actin fiber formation, typical of EMT (Figure 4B, miR-22 OE). These results indicated that the epithelial property of the cells might be lost when miR-22 mimic is overexpressed. We next examined whether miR-22 inhibition in MDA-MB-231 cell line shows the opposite effect. Indeed, inhibition of miR-22 activity in MDA-MB-231 cells showed increased E-cadherin expression (Figure 4C, miR-22 inhibitor) and decreased

Vimentin expression (Figure 4D, miR-22 inhibitor), which suggested the reversal of the EMT process and this effect was also observed in TIP60-overexpression MDA-MB-231 cell line (Figure 4C, 4D).

miR-22 inhibition suppresses cell migration and invasion by regulating TIP60 levels

Two key features of EMT are the ability of cells to migrate and invade. In order to investigate the role of miR-22 in these processes, we performed wound-healing and cell invasion assays. For this, MDA-MB-231 cells were transfected with miR-22 hairpin inhibitor or control hairpin inhibitor for 48 h and cells were serum starved for the next 12 h. We found that inhibiting miR-22 caused a significant decrease in the rate of wound closure in the MDA-MB-231 cell cultures at 12 h and 24 h as compared to that of control cells (Figure 5A). To further demonstrate that miR-22 increased cell migration through TIP60, we performed the wound-healing assay in MDA-MB-231 cell line stably overexpressing TIP60 without miR-22 target sequence. Interestingly, overexpression of TIP60 decreased cell migration and we did not observe any effect on migration in the presence of miR-22 inhibitor (Figure 5B). On the other hand, when miR-22 mimic was overexpressed in MCF7 cells, we observed a significant increase in cell migration as compared to the control cells (transfected with miR mimic negative control; Figure 5C). These findings suggest that repression of TIP60 by miR-22 increases cell migration and this can be reverted by ablating activity of miR-22 or through the overexpression of a TIP60 that lacks miR-22 binding site. Thus, miR-22 stimulates cell migration by targeting TIP60.

To assess invasion, we transfected MDA-MB-231 cells with or without the miR-22 inhibitor for 48 h. Cells were suspended in serum-free medium and loaded onto matrigel invasion chamber inserts. We observed that miR-22 inhibition reduces the invasive capacity of these cells (Figure 6A). To further confirm that this effect is mediated through TIP60, we transfected the stable TIP60-overexpressing MDA-MB-231 cells (lacking miR-22 binding site) with the miR-22 inhibitor, using vector-expressing cells as a control. To confirm the expression of the miR-22 and TIP60 after inhibition or overexpression of the miRNA, we quantitated the expression of miR-22 and TIP60 in the MDA-MB-231 cells transfected with or without miR-22 inhibitor and miR-22 mimic by Q-PCR (Supplementary Figure S1). We found a decrease in cell invasion in TIP60-overexpressing cells, which further confirms that the effect on cell invasion is mediated through TIP60 (Figure 6B). We also noted that, upon transfection with the miR-22 inhibitor, TIP60-overexpressing cells showed a further reduction in invasion. This may be due to an increase in endogenous TIP60 levels in these cell lines or miR-22 may target an additional factor involved in regulating invasion.
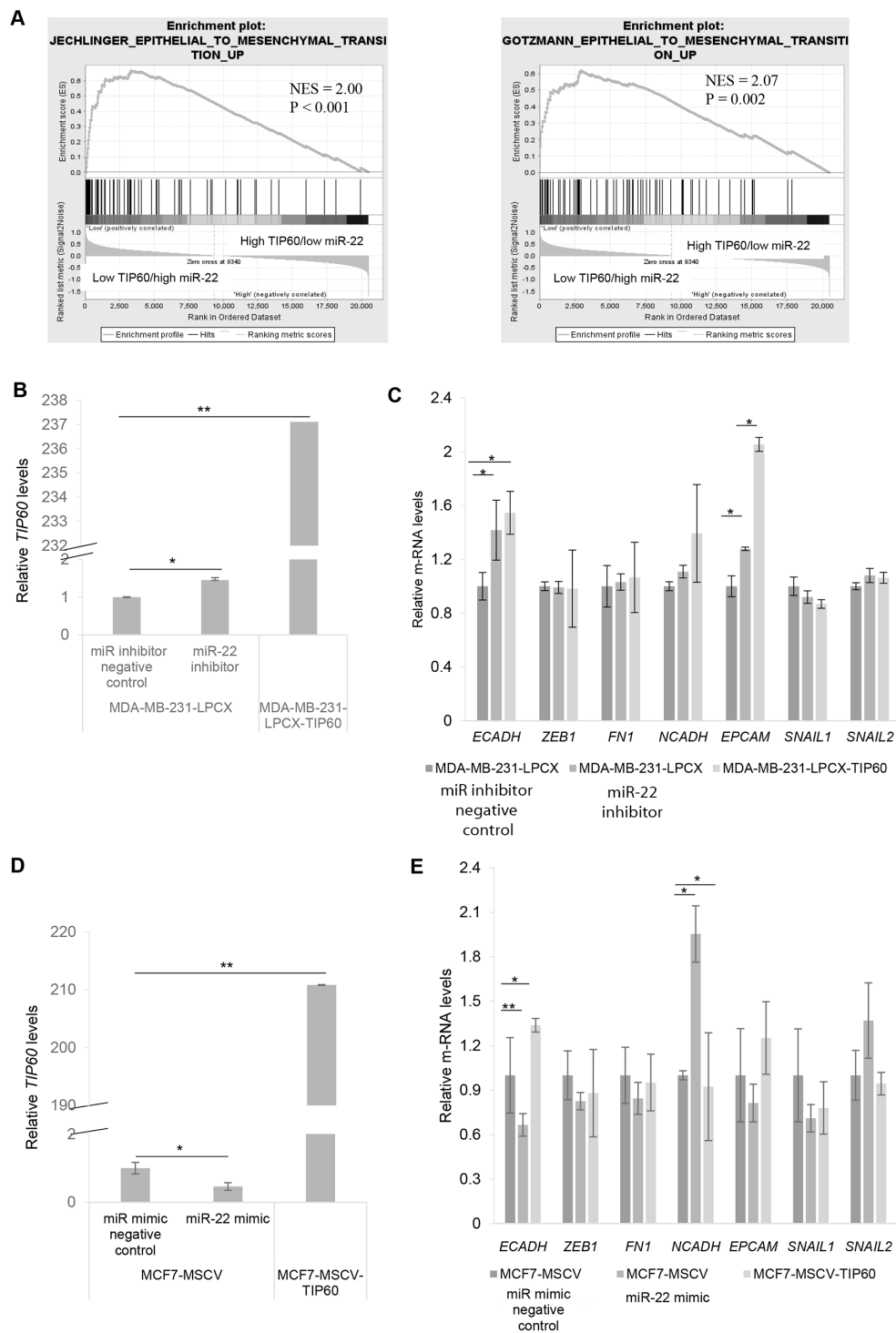
Figure 3: Expression levels of TIP60 and miR-22 suggest an epithelial-mesenchymal transition (EMT). A. Gene-Set Enrichment Analysis (GSEA) shows enrichment of factors linked to EMT in the samples with high miR-22 and low TIP60. **B.** The expression of TIP60 mRNA was detected by QRT-PCR in cells transfected with either miR inhibitor negative control or miR-22 inhibitor and also MDA-MB-231-LPCX-TIP60 stable cell line. **C.** QRT-PCR showing mRNA expression of EMT markers in cells transfected with either miR inhibitor negative control or miR-22 inhibitor and also MDA-MB-231-LPCX-TIP60 stable cell line. **D.** The expression of TIP60 mRNA was detected by QRT-PCR in cells transfected with either miR mimic negative control or miR-22 mimic overexpression and also MCF7-MSCV-TIP60 stable cell line. **E.** QRT-PCR showing mRNA expression of EMT markers in cells transfected with either miR mimic negative control or miR-22 mimic overexpression and also MCF7-MSCV-TIP60 stable cell line. The figure represents data from three independent experiments performed in triplicate. Significance is represented as *$P < 0.05$; **$P < 0.01$.
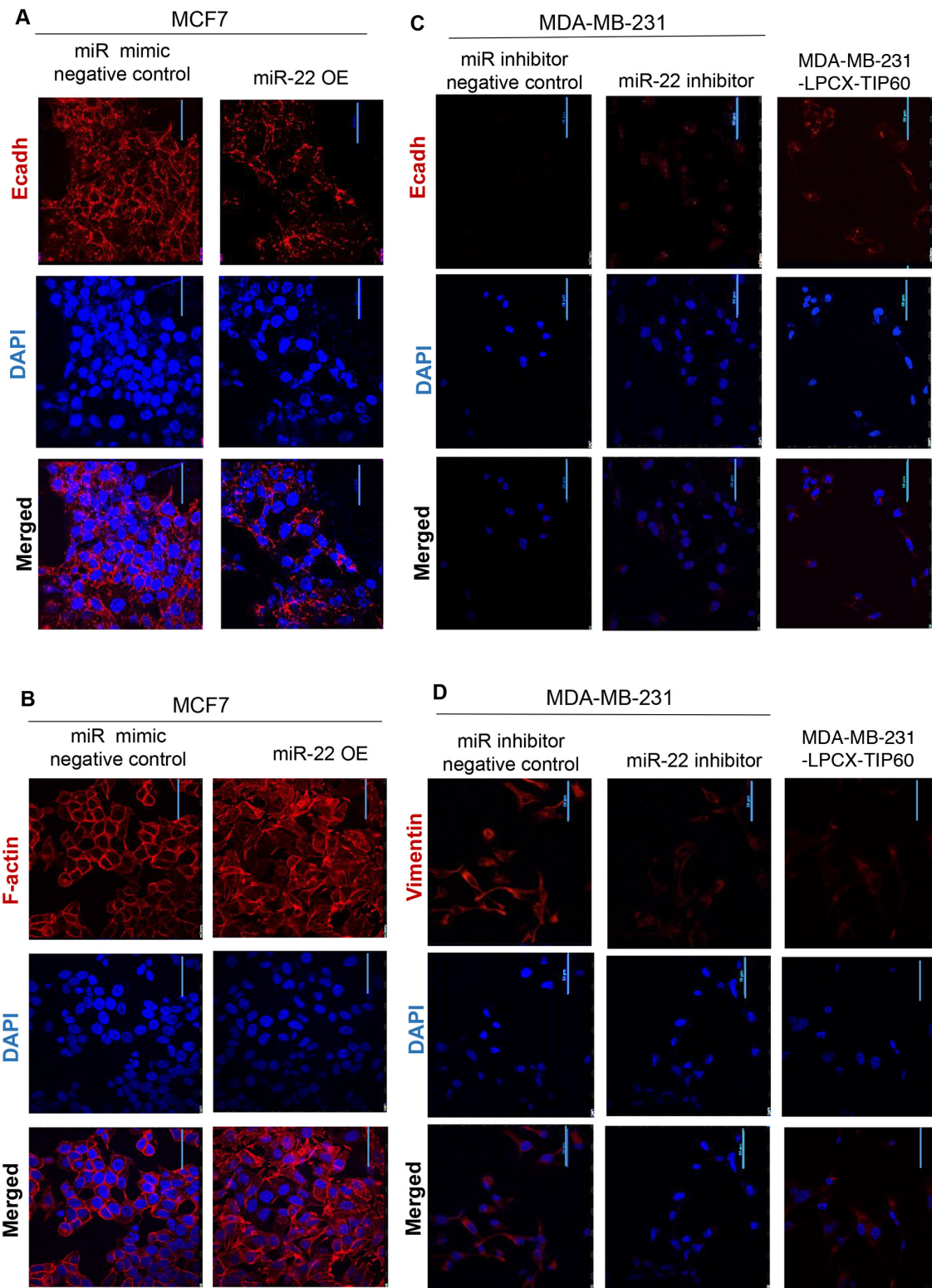
Figure 4: Immuno-fluorescence showing phenotypic alterations. A–B. Representative immuno-fluorescence images of E-cadherin and F-actin (red) are shown for MCF7 cells transfected with either miR mimic negative control or miR-22 mimic. Nuclei are stained with DAPI (blue). **C–D.** Representative immuno-fluorescence images of E-cadherin and Vimentin (red) are shown for MDA-MB-231 cells transfected with either miR-22 inhibitor negative control or miR-22 inhibitor or MDA-MB-231-LPCX-TIP60 stable cell line. Nuclei are stained with DAPI (blue). Immuno-fluorescence images were taken at 60X magnification with a nikon confocal microscope.
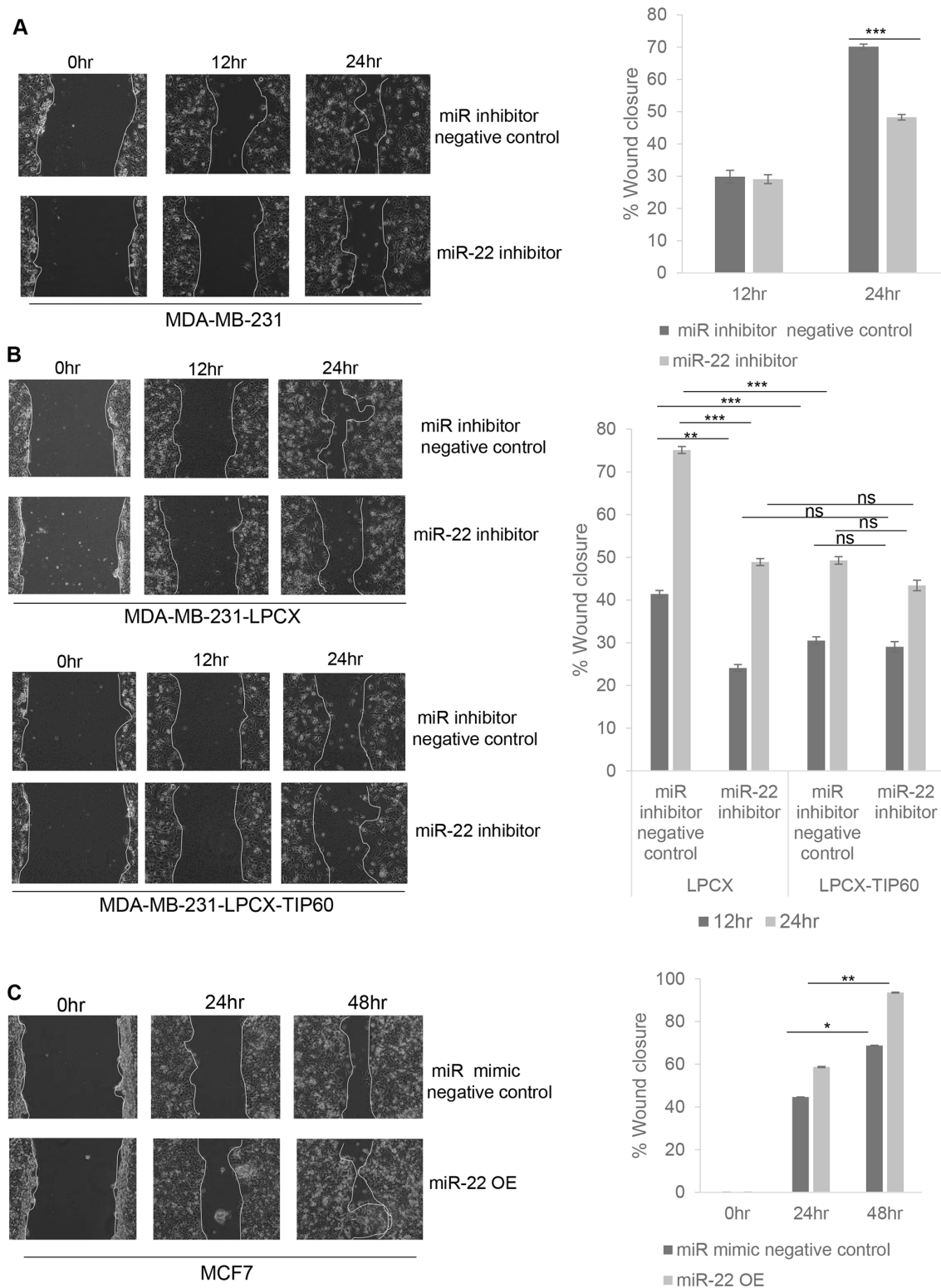
Figure 5: miR-22 increases cell migration by targeting expression of TIP60. MDA-MB-231 cells **A.** and MDA-MB-231-LPCX and MDA-MB-231-LPCX-TIP60 cells **B.** were treated with or without the miR-22 inhibitor for 24 h and analyzed by wound-healing assays 48 h after transfection using live-cell imaging (Nikon). The solid white line highlights the wound edge at 0 h and 24 h. **C.** MCF7 cells were transfected with miR-22 mimic and wound closure was analyzed as for (A) and (B) Data compiled from three independent experiments in triplicate, and images from one representative experiment are shown. Decreases in the gap area between the migrating cells from the opposite wound edge were quantified by measuring the distance (by scale) at three random points in the image. This quantification is represented in the figure. Data are the mean ± SEM with significance measured using unpaired two-tailed student's *t*-test. Significance is represented as *$P < 0.05$; ** $P < 0.01$; ***$P < 0.001$.
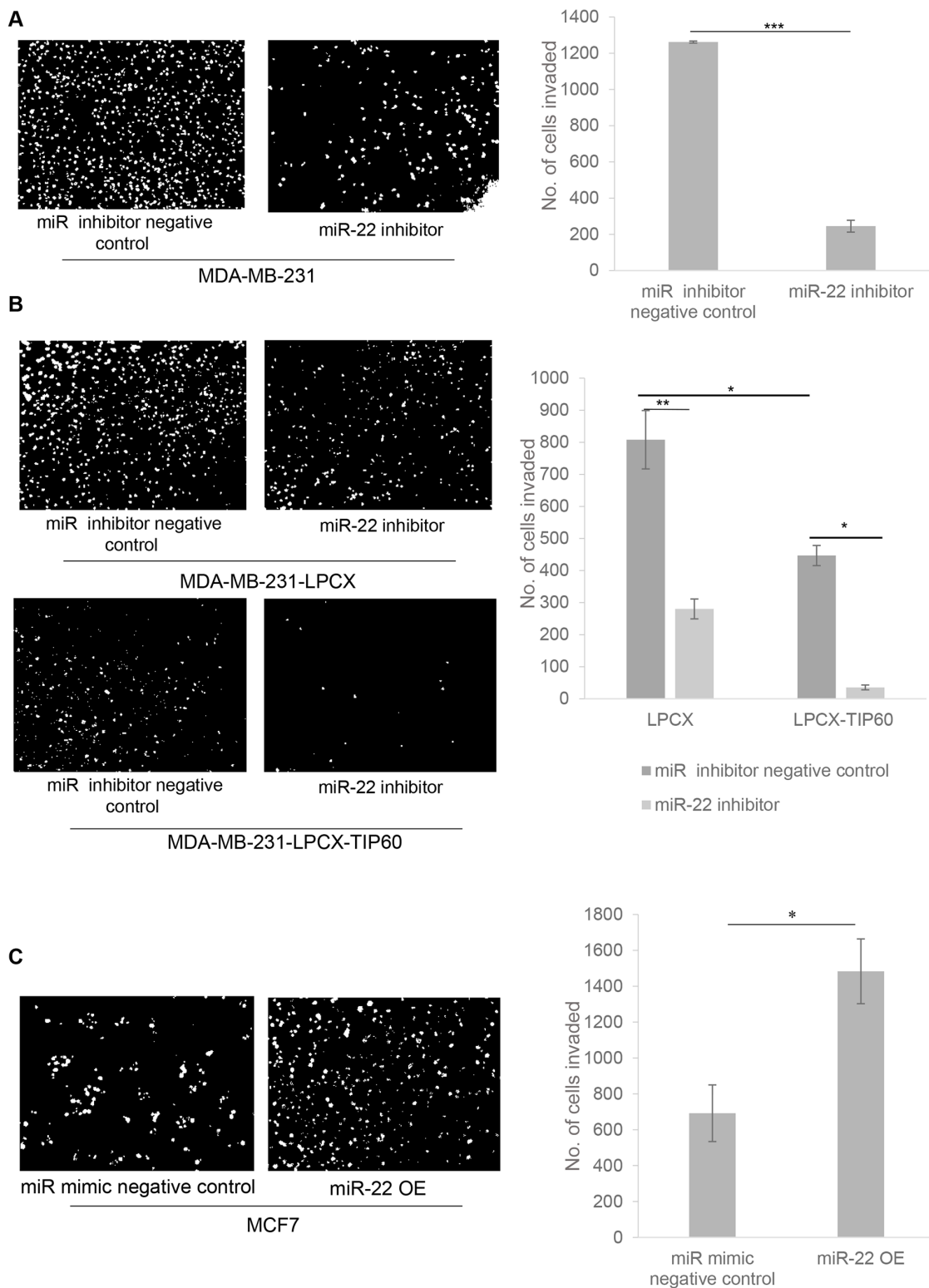
Figure 6: miR-22 inhibition results in decreased cell invasion. A. MDA-MB-231 cells were treated with or without miR-22 inhibitor and analyzed for their ability to invade into Matrigel transwell 48 h after transfection. **B.** MDA-MB-231-LPCX and MDA-MB-231-LPCX-TIP60 cells were treated with or without miR-22 inhibitor and analyzed using an invasion assay 48 h after transfection. miR-22 decreased MDA-MB-231-LPCX and MDA-MB-231-LPCX-TIP60 cell invasion, with a similar effect also seen in the TIP60 stable cell lines, as compared with vector alone. **C.** MCF7 cells were transfected with miR-22 mimic and wound closure was analyzed 48 h after transfection. miR-22 mimic overexpression increases cell invasion. Data compiled from three independent experiments in triplicate, and images from one representative experiment are shown. Data are the mean ± SEM and significance was determined using an unpaired two-tailed student's *t*-test. Significance is represented as *$P < 0.05$; **$P < 0.01$; ***$P < 0.001$.

Since miR-22 inhibition decreased cell invasion capacity, we next overexpressed miR-22 mimic in MCF7 cells for 48 h (Supplementary Figure S1). Cells were suspended in serum-free medium and loaded onto matrigel invasion chamber inserts. We found that miR-22 mimic overexpression increased the invasiveness of the cells (Figure 6C). These results suggest that miR-22 targets TIP60 leading to an increase in cell migration and invasion of breast cancer cells thereby promoting metastasis.

Levels of TIP60 and miR-22 as a predictor of disease progression in breast cancer

Having identified this interesting regulatory link between miR-22 and TIP60 in cell culture models and patient datasets, we sought to investigate its significance in a pathophysiological scenario. For this, we used available gene expression and survival data from the TCGA dataset and the GSE19783 from gene expression omnibus (GEO) database to compare overall survival between patient cohorts that exhibited high versus low TIP60 expression levels. We found that patients with high TIP60 and low miR-22 expression were associated with good survival prognoses ($P = 0.015$; Figure 7A, 7C) whereas patients with low TIP60 and high miR-22 levels showed poorer prognoses for survival ($P = 0.029$; Figure 7B, 7D). Breast cancer is classified into molecular subtypes; we investigated the expression of miR-22 and TIP60 in TCGA dataset for breast cancer and found no significant differences between different subtypes (Supplementary Figure S2). To rule out the possibility of other factors such as age, stage, ER status, PR status, and Her2 status determining the relationship between miR-22 and TIP60, multivariate analysis was performed. As summarized in Table 3, multivariate analysis linear regression elucidates variables significantly affecting expression level of TIP60 in breast cancer survival. Among factors such as age, stage, ER, PR and Her2 status, the strongest component that determines expression level of TIP60 in patient samples was miR-22 as illustrated by high eigenvalue (data not shown). Similarly, TIP60 was found to be the strongest factor in determining miR-22 expression level in breast cancer patient samples. Therefore, the model remained essentially unchanged when other components (age, stage, ER, PR and Her2 status) were dropped. Besides, patients with high expression of miR-22 are likely to have low expression of TIP60 and vice versa due to the negative regression coefficient of miR-22 and TIP60.

DISCUSSION

Metastasis—a cessation of neoplastic progression—is one of the main causes of death in patients with breast cancer. Epithelial–mesenchymal transition (EMT) is thought to be one of the key processes that causes benign tumor cells to transition into invasive and metastatic cells [23]. In this study, we showed that miR-22 expression potently activates the migration and invasive capacity of basal breast cancer cells. In addition, we show evidence to suggest that miR-22 has an oncogenic function in these cells. These findings are in line with the upregulation of miR-22 in more advanced stages of breast cancer and with previous reports which have also implicated miR-22 as an oncogene in breast cancer [24, 25]. Recently, Song et al. [20] showed that miR-22 antagonizes another miRNA, miR-200, through directly targeting of the methyl cytosine dioxygenase TET (ten-11 translocation) family members and, hence, chromatin remodeling toward miR-200 transcriptional silencing. Further, Lee et al. demonstrate a central role of miR-22 in the physiological regulation of MDC1-dependent DDR, a molecular mechanism of Akt1 activation and senescence leading to increased genomic instability, which fosters an environment that promotes tumorigenesis [26]. Although these studies implicate miR-22 as an oncogene, other studies have suggested a tumor suppressor function of miR-22. miR-22 was identified as a tumor suppressor gene in human colon cancers, influencing p53-dependent cellular fate through the formation of the p53–miR-22–p21 axis [27]. Another study showed miR-22 acts as tumor suppressor by targeting the Sp1 gene and inhibiting gastric cancer cell migration and invasion [28]. Additionally, miR-22 was also implicated in activating the cellular senescence program in cancer cells and acts as a tumor suppressor [29]. A recent study also shows miR-22 acts as a tumor suppressor by targeting GLUT1 and is directly correlated with the TNM stage, local relapse, distant metastasis, and survival of breast cancer patients [30]. Further investigations along these lines will be needed to ascertain whether miR-22 is an oncogene or a tumor suppressor.

The acetyl-transferase TIP60 is a *bona fide* tumor suppressor in cancer and its expression is down-regulated in colon carcinomas [15] and lung cancers [31]. Interestingly, in colon carcinoma, the ratio between TIP60 and p400 mRNAs is important for cancer progression [32]. However, the molecular determinant and underlying mechanism is yet to be discovered. Interestingly, downregulation of TIP60 in colorectal cancer is correlated with larger tumor size, distant metastasis, and a higher stage of tumor node metastasis classification; yet, the molecular mechanism of TIP60's downregulation is not known. Our study identifies a non-coding RNA that can regulate the expression of TIP60 in breast cancer. It would be interesting to investigate whether this regulation exists in colon cancer as well.

Pathways governed by TIP60 *via* its tumor suppressor function have yet to be identified. Gorrini et al. [33] showed that TIP60 is a haplo-insufficient tumor suppressor in Eμ-myc transgenic mice, and suggested that it is required for an oncogene-induced DNA damage response.
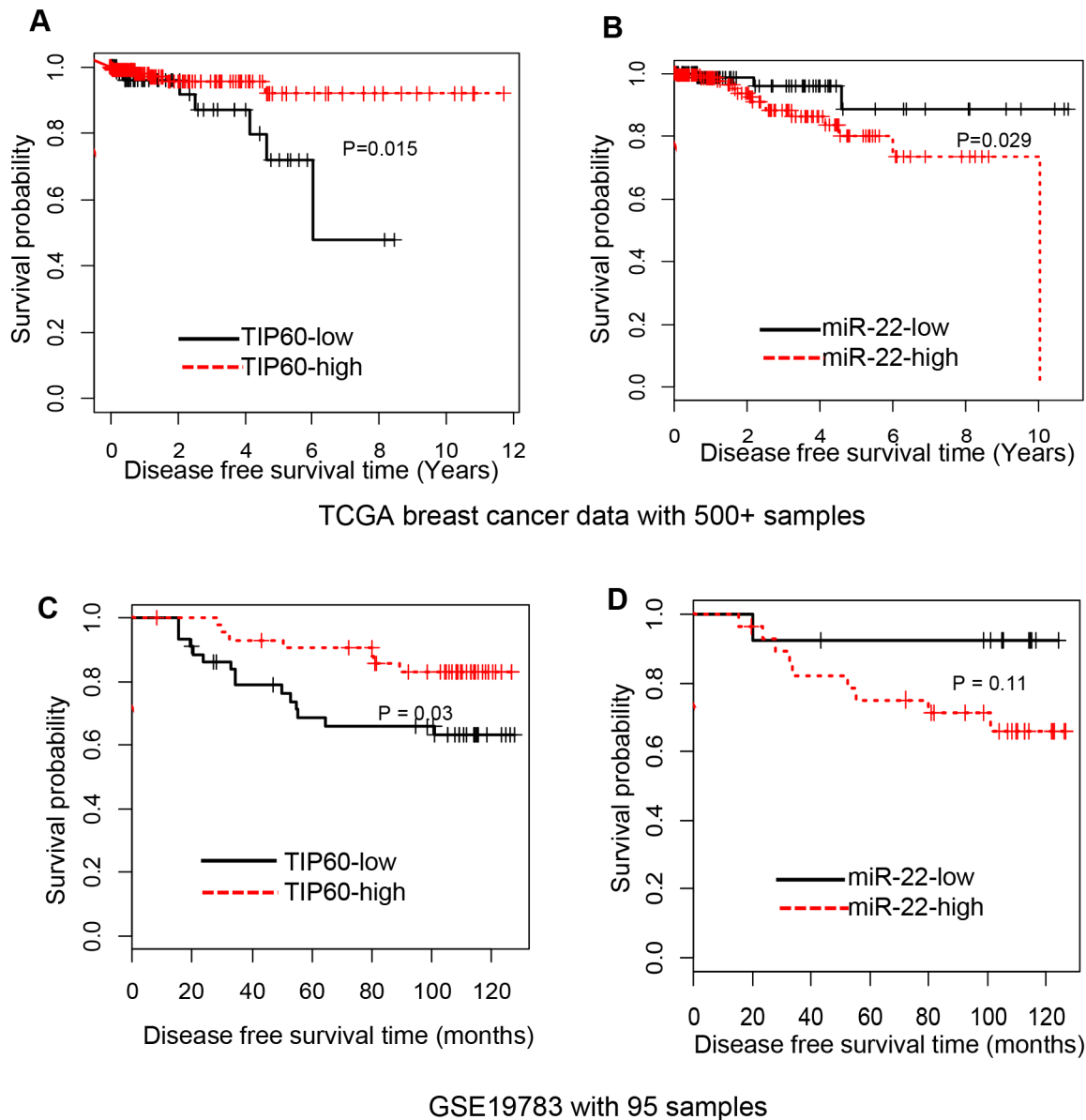
Figure 7: TIP60 and miR-22 expression in breast cancer tumors correlated with high and low survival, respectively.
A–B. Kaplan-Meier plot, based on breast cancer data from The Cancer Genome Atlas (TCGA), illustrates the survival probability for patients with low or high TIP60 and miR-22 expression levels in breast cancers. High expression of TIP60 leads to higher survival probability, whereas high expression of miR-22 leads to lower survival probability. $P < 0.015$ and $P < 0.029$, respectively. **C–D.** Kaplan-Meier plot, based on Gene express omnibus expression dataset (GSE19783), illustrates the survival probability for patients with low or high TIP60 and miR-22 expression levels in breast cancers. $P < 0.03$ and $P < 0.11$, respectively.

Collectively, these findings indicated that decreased TIP60 expression correlates with tumor development; but the molecular mechanism of TIP60's downregulation was still not clarified. We show, for the first time, that TIP60 is a direct target of miR-22 and its downregulation by miR-22 subsequently results in the activation of an EMT program. EMT is characterized by a loss of cell adhesion and the suppression of epithelial genes, such as *E-cadherin* concomitant with an acquisition of mesenchymal markers (including *N-cadherin, Vimentin*, and *Fibronectin*) and

increased cell motility and invasiveness. Numerous miRNAs have been linked to EMT pathways. For example, miR-9 can directly regulate *E-cadherin* by targeting its 3′UTR in human mammary epithelial cells, thereby promoting mesenchymal-like characteristics of the cells with increased motility and invasiveness [34]. miR-661 is shown to regulate *Nectin-1* and *StarD10* in the disassembly of epithelial cell junctions in SNAI1-expressing breast cancer cells [35]. Recently, the expression of miR-197 was found to induce EMT along with the downregulation of

p120-catenin in pancreatic cancer cells [36]. In contrast, in hepatic cancer cells, miR-194 overexpression results in reduced cell invasion, migration and metastasis by targeting *N-cadherin* [37]. Thus, we also investigated the regulatory effect of miR-22 on *E-cadherin* and *N-cadherin in vitro*. MCF7 is an estrogen alpha positive (ER+) and also an epithelial cell line. It is known that miR-22 regulates ER and miR-22 levels are reduced in ER+ cell lines [38, 39]. We showed that MCF7 cell line has reduced miR-22 levels and high TIP60 (tumor suppressor gene) levels. Overexpression of miR-22 in these cells reduced TIP60 levels and promotes invasion and migration. MDA-MB-231 being triple negative cell line (ER-, PR-, and Her2-) and a mesenchymal cell line has elevated level of miR-22 and reduce level of TIP60. We have shown that miR-22 is required to maintain the metastasis levels of the MDA-MB-231 cell line by targeting TIP60. Inhibition of miR-22 by the miR-22 inhibitor in highly metastatic MDA-MB-231 cells leads to a reduction of metastatic phenotypes, as well as an elevation of the expression of TIP60. Our data also showed that overexpression of miR-22 in MCF7 cells caused a decrease in *E-cadherin* levels and an increase in *N-cadherin* levels, thus promoting EMT. Alternatively, inhibition of miR-22 expression in MDA-MB-231 cells resulted in increased *E-cadherin* levels and suppressed EMT. Thus, miR-22 may promote EMT by inhibiting TIP60. During the initial stages of metastasis, epithelial cells undergo EMT, causing a loss of cell-cell contacts, increased motility and cell invasion. Further, in our gain- and loss-of-function experiments, we have demonstrated that miR-22 inhibition in the MDA-MB-231 metastatic cell line causes a decrease in cell migration as well as invasion, whereas its overexpression in MCF7 cells resulted in increased cell migration and invasion.

In conclusion, we have identified a novel link between miR-22 and TIP60 in breast cancer metastasis. miR-22 is upregulated in metastatic breast cancer cell lines as well as in patients with breast cancer, and causes the downregulation of TIP60 and modulation of the EMT pathway. Our study suggests that miR-22 and TIP60 levels could be used as a prognostic marker for breast cancer.

MATERIALS AND METHODS

Cell culture and reagents

Human breast epithelial and cancer cell lines, MCF10A (CRL-10317™), MCF-7, MDA-MB-231, were obtained from ATCC (Manassas, VA, USA). SkBR3, BT474, BT549, T47D, HS578T cells were generously provided by Prof. H. Phillip Koeffler (Cancer Science Institute, Singapore). MCF10A cells were cultured in DMEM/F12 medium supplemented with 5% horse serum and the medium was further supplemented with 20 ng/ml epithelial growth factor (EGF), 0.5 mg/ml hydrocortisone,

100 ng/ml cholera toxin, 10 μg/ml insulin. MCF-7 and MDA-MB-231 were maintained in DMEM; SkBR3 in DMEM supplemented with L-glutamine; HS578T in DMEM supplemented with insulin; and T47D and BT474 in RPMI-40 medium. All media were supplemented with 10% FBS and 100 U of penicillin and streptomycin and grown at 37°C with 5% CO_2. All tissue culture reagents were purchased from Invitrogen (Carlsbad, CA, USA) and Sigma-Aldrich (St. Louis, MO, USA).

Oligonucleotides, plasmids, and transfection

Lipofectamine RNAiMAX (Invitrogen) was used to transfect MCF7 and MDA-MB-231 cells. miR-22 mimic, miR mimic negative control, miR-22 inhibitor, and miR-22 negative control miRNA inhibitor were purchased from Dharmacon Research Inc. (Lafayette, CO, USA). The pmirGLO Dual-Luciferase vector was obtained from Promega (E1330; Fitchburg, WI, USA). To overexpress TIP60, the open reading frame was cloned into LPCX vector.

Quantitative reverse transcription PCR

Total RNA from cell lines was extracted using TRIzol Reagent (Invitrogen) as per manufacturer's instructions. RNA (2 μg) was reverse transcribed in a 20-μl reaction using iScript Supermix master mix (Bio-Rad, Hercules, CA, USA). For miRNA, cDNA was synthesized using a stem-loop specific primer for miR-22, and then subjected to real time PCR using 2 μl of a 1:5 dilution of the reverse-transcribed cDNA and SYBR green in an ABI Fast Q-PCR machine (Applied Biosystems, Foster City, CA, USA). The cycling conditions were as follows: 50°C for 2 min, 95°C for 5 min, and 40 cycles of 95°C for 15 sec followed by 60°C for 1 min (annealing and extension). Primer sequences are listed in Table 1. Each reaction was performed in triplicate. The data were normalized to GAPDH and U6 expression for mRNA and miRNA, respectively. The relative expression of each gene was quantified by the ΔΔCT method.

Luciferase assays

A dual-luciferase reporter vector was used to generate the luciferase constructs. The TIP60 3′UTR, containing the predicted binding site for miR-22, was amplified from genomic DNA by PCR. The PCR product was digested by *Pme*I and *Not*I enzymes and the digested fragment was cloned into pmirGLO luciferase plasmid to obtain a wild-type luciferase construct pmirGLO-TIP60 3′-UTR. To generate point mutant and deletion constructs, the putative miR-22 binding site in TIP60 3′-UTR was mutated or deleted using Quick-change Site-Direct Mutagenesis Kit (200522–5; Stratagene,

La Jolla, CA, USA) as per manufacturer's instructions. Cloning was confirmed by sequencing. Primers used for PCR and sequencing are listed in Table 2. For luciferase assays, MCF7 cells were plated in 12-well plates and 24 h later co-transfected with 50 nM miR-22 or miR mimic negative control and 50 nM miR-22 inhibitor, 100 ng pmirGLO or pmirGLO containing wild-type TIP60 3′-UTR or the corresponding mutant or deleted constructs. Forty-eight hours later, luciferase activity was measured using Dual-Luciferase Reporter Assay Kit (E1960; Promega) on a GLOmax microplate luminometer (Promega). Firefly luciferase signals were normalized using Renilla luciferase signals. All experiments were performed in triplicate.

Western blotting

Cells were lysed using RIPA lysis buffer [50 mM Tris (pH 7.5), 150 mM NaCl, 1% NP40, 0.25% sodium deoxycholate, 1 mM EDTA, 1 mM DTT and protease inhibitor cocktail]. Protein concentration was determined using the Bradford Protein Assay kit (500–0001; Bio-Rad). Equal amounts of protein were separated on SDS polyacrylamide gels and transferred to nitrocellulose membranes (162–0115; Bio-Rad) using the Bio-Rad semi-dry transfer apparatus. Membranes were blocked for

1 h with 5% skim milk in Tris-buffered saline containing 0.1% Tween-20, and then incubated overnight with primary antibody. Blots were then washed and incubated with secondary antibody, washed again, and visualized by chemiluminescence. β-actin (sc-81178) and α-actinin (sc-166524) were used as loading controls. The TIP60 serum antibody was generated in the lab. E-cadherin (BD-Bioscience), Vimentin (Cell Signaling), Alexa 594 secondary antibody and Alexa 594 phalloidin staining was bought from Life Technologies and mounting medium containing DAPI was purchased from Santa Cruz Biotechnology Inc.

Immuno-fluorescence

MDA-MB-231 cells were transfected with either miR mimic negative control or miR-22 mimic. Cells were cultured on cover slips for 48 h and then immuno-fluorescence assay was performed by fixing the cells for 15 min at room temp in 3.7% paraformaldehyde. Cells were washed 3 times with PBS and permeabilized by 0.5% Triton-X-100 for 5 min. Cells were then washed 2 times with PBS and 1 time with 0.1 M glycine in PBS. Cells were incubated in E-cadherin (1:400) and Vimentin (1:100) antibodies overnight in 0.5% Triton-X-100 in PBS. Next day cells were washed 3 times with PBS and then

Table 1: List of Q-PCR Primers

Serial No.	Name of the Gene	Forward primer Sequences	Reverse primer Sequences
1	TIP60	AATGTGGCCTGCATCCTAAC	TGTTTTCCCTTCCACTTTGG
2	miR-22	ACACTCCAGCTGGGAAGCTGCCAGTTGAAG	GGTGTCGTGGAGTCGGCAA
3	U6	CTCGCTTCGGCAGCACATATACT	ACGCTTCACGAATTTGCGTGTC
4	18S	GTAACCCGTTGAACCCCATT	CCATCCAATCGGTAGTAGCG
5	E-cadherin	TTACTGCCCCCAGAGGATGA	TGCAACGTCGTTACGAGTCA
6	Epcam	GCTGGCCGTAAACTGCTTTG	ACATTTGGCAGCCAGCTTTG
7	N-cadherin	CCGGTTTCATTTGAGGGCAC	TCCCTCAGGAACTGTCCCAT
8	Fibronectin	AACCCTTCCACACCCCAATC	ACTGGGTTGCTGACCAGAAG
9	Snail1	TCTTTCCTCGTCAGGAAGCC	GATCTCCGGAGGTGGGATGG
10	Snail2	CTCCTCATCTTTGGGGCGAG	CTTCAATGGCATGGGGGTCT
11	Zeb1	AGGATGACCTGCCAACAGAC	CTTCAGGCCCCAGGATTTCTT
12	miR-22 stem loop primer for c-DNA	CTCAACTGGTGTCGTGGAGTCGG CAATTCAGTTGAGACAGTTCT	

Table 2: List of Cloning 3′UTR Primers

Serial No.	Name of the primers (Q-PCR)	Sequences
1	TIP60–3′UTR- Forward primer	ATATGCGGCCGCGTGACCAGACACTGCCCACT
2	TIP60–3′UTR- Reverse primer	GCGCATCGATTGCATGGCTCTGGCATATAG

Table 3: Multivariant analysis

Variable		Sample number	R with miR-22	*P* value
ER-alpha_status	positive	320	0.037	0.45
	negative	101		
PR_status	positive	289	0.094	0.054
	negative	132		
Her2_status	positive	83	0.036	0.46
	negative	338		
Age	< = 50	141	0.006	0.90
	> 50	280		
Stage	I–II	321	0.030	0.54
	III–X	100		
TIP60		421	0.193	< 0.0001

incubated at 37°C for 30 min with secondary antibodies or with the F-actin dye. Cells were then washed 3 times with ultrapure water to remove the salts and were mounted on the slides using antifade reagent, and examined with confocal microscope (Nikon) at 60 X magnification. Similarly, MCF7 cells were transfected with either miR mimic negative control or miR-22 mimic for 48 h and immunofluorescence was performed similarly as described above.

Wound-healing assay

MDA-MB-231, MDA-MB-231-LPCX, MDA-MB-231-LPCX-TIP60 and MCF7 cells were seeded in 12-well plates and grown to 90% confluence. Cells were transfected with or without miR-22 inhibitor or miR-22 mimic. After 36 h of transfection, cells were serum starved overnight and a linear wound was created using a pipette tip. Wound closure was monitored using live cell imaging microscopy (Nikon, Tokyo, Japan) at an interval of 30 min for 24–48 h. Wound size was then measured randomly at three sites perpendicular to the wound.

Invasion assay

For the invasion assay, Corning BioCoat Matrigel Invasion Chambers with 8.0-μm PET Membrane were used (354480; Corning, Corning, NY, USA). As per the protocol, inserts were rehydrated for 2 h at 37°C and then MDA-MB-231, MDA-MB-231-LPCX, MDA-MB-231-LPCX-TIP60 cells transfected with or without miR-22 inhibitor and MCF7 cells transfected with or without miR-22 mimic were suspended in serum-free medium and loaded onto the chamber inserts. The inserts were placed into the wells of a 24-well plate that contained media supplemented with 10% FBS. Cells were incubated at 37°C and allowed to migrate and invade through the Matrigel and membrane pores. The upper Matrigel layer and cells were removed after 24 h (for MDA-MB-231 cells) or 72 h (for MCF7 cells) by scrubbing. The cells on the surface of the lower side of the membrane were fixed with 100% methanol and stained with Hoechst stain (33342; Life Technologies). Cells that migrated onto the lower surface were counted from representative areas using ImageJ software (NIH, Bethesda, MD).

Stable cell lines

Virus was generated by transfecting 5×10^6 293T cells with the plasmids [MSCV construct: i.e., MSCV vector alone (MSCV) and TIP60 overexpressing vector (MSCV TIP60) and LPCX construct: i.e., LPCX vector alone (LPCX) and TIP60 overexpressing vector (LPCX TIP60)], using Lipofectamine 2000, as per manufacturer's protocol. Viruses were harvested after 72 h of transfection and were used to infect 1×10^6 MCF7 or 2×10^6 MDA-MB-231-luc-D3H2LN cells together with polybrene (107689, Sigma-Aldrich) reagent (0.4 mg/ml). After 6 h, media containing the virus was replaced by growth media. After 24 h, puromycin was added into the growth media for selection. Media with antibiotics was changed every 48 h until the mock-transfected cells died. The cells were continuously selected for 2 weeks for the generation of stable cell lines.

Bioinformatics analysis

For survival data analysis, raw gene expression data were downloaded from The Cancer Genome Atlas (TCGA) breast cancer database (https://tcga-data.nci.nih.gov/tcga/) and from GEO databases, respectively. The downloaded TCGA breast cancer data were the RNA-seq dataset of level 3 and normalization of the data was performed based on the total mapable reads.

For microarray data (GSE19783), the Cross-Correlation method was used for data normalization [40]. In the survival analysis, the median intensity cross all samples was first used to classify the samples into the respective expression high and low groups. In order to minimize the false positives in classification of high and low expression groups, the samples with middle expression within the 15% range from the median expression value were removed. The analysis of the survival data was based on the Kaplan-Meier method. Gene-Set Enrichment Analysis (GSEA) was performed using msigdb.v4 (http://www.broad.mit.edu/gsea/), comparing 28 TCGA samples with high TIP60/low miR-22 expression versus 28 samples with low TIP60/high miR-22 expression.

A correlation of TIP60 with miR-22 was obtained based on the normalized data cross all samples in the cohort. In order to ensure that this correlation is not independent of subtypes, the multivariate analysis was performed. Using 400+ TCGA breast cancer samples available with all these factors, we performed principal component analysis (PCA) to identify the contributing fraction of each principal component (PC), and found that the first PC is dominant and contributes 98.2% among all PCs. Multiple linear regression with miR-22 as the dependent variable was performed, and the exploratory variables for the multiple regression included not only TIP60 expression but also the age, stage, ER status, PR status, and Her2 status.

ACKNOWLEDGMENTS AND FUNDING

CONFLICTS OF INTEREST

The authors declare no conflicts of interest.

Author contributions

AKP and SJ designed the experiments and wrote the manuscript. AKP performed all the experiments. YZ generated the MDA-MB-231-LPCX and MDA-MB-231-LPCX-TIP60 cell lines. HY and YL performed the bioinformatics analysis. SZ and GT-K were involved in multivariate analysis. SJ proposed and supervised the project.

REFERENCES

1. Wang Q, Zhao ZB, Wang G, Hui Z, Wang MH, Pan JF, Zheng H. High expression of KIF26B in breast cancer associates with poor prognosis. PloS one. 2013; 8:e61640.

2. Bartel DP. MicroRNAs: genomics, biogenesis, mechanism, and function. Cell. 2004; 116:281–297.

3. Lee RC, Feinbaum RL, Ambros V. The C. elegans heterochronic gene lin-4 encodes small RNAs with antisense complementarity to lin-14. Cell. 1993; 75:843–854.

4. Calin GA, Liu CG, Sevignani C, Ferracin M, Felli N, Dumitru CD, Shimizu M, Cimmino A, Zupo S, Dono M, Dell'Aquila ML, Alder H, Rassenti L, Kipps TJ, Bullrich F, Negrini M, et al. MicroRNA profiling reveals distinct signatures in B cell chronic lymphocytic leukemias. Proceedings of the National Academy of Sciences of the United States of America. 2004; 101:11755–11760.

5. Iorio MV, Ferracin M, Liu CG, Veronese A, Spizzo R, Sabbioni S, Magri E, Pedriali M, Fabbri M, Campiglio M, Menard S, Palazzo JP, Rosenberg A, Musiani P, Volinia S, Nenci I, et al. MicroRNA gene expression deregulation in human breast cancer. Cancer research. 2005; 65:7065–7070.

6. Lu J, Getz G, Miska EA, Alvarez-Saavedra E, Lamb J, Peck D, Sweet-Cordero A, Ebert BL, Mak RH, Ferrando AA, Downing JR, Jacks T, Horvitz HR, Golub TR. MicroRNA expression profiles classify human cancers. Nature. 2005; 435:834–838.

7. Michael MZ, SM OC, van Holst Pellekaan NG, Young GP, James RJ. Reduced accumulation of specific microRNAs in colorectal neoplasia. Molecular cancer research: MCR. 2003; 1:882–891.

8. Volinia S, Calin GA, Liu CG, Ambs S, Cimmino A, Petrocca F, Visone R, Iorio M, Roldo C, Ferracin M, Prueitt RL, Yanaihara N, Lanza G, Scarpa A, Vecchione A, Negrini M, et al. A microRNA expression signature of human solid tumors defines cancer gene targets. Proceedings of the National Academy of Sciences of the United States of America. 2006; 103:2257–2261.

9. Cui J, Bi M, Overstreet AM, Yang Y, Li H, Leng Y, Qian K, Huang Q, Zhang C, Lu Z, Chen J, Sun T, Wu R, Sun Y, Song H, Wei X, et al. MiR-873 regulates ERalpha transcriptional activity and tamoxifen resistance via targeting CDK3 in breast cancer cells. Oncogene. 2015; 34:3895–3907.

10. Ujihira T, Ikeda K, Suzuki T, Yamaga R, Sato W, Horie-Inoue K, Shigekawa T, Osaki A, Saeki T, Okamoto K, Takeda S, Inoue S. MicroRNA-574–3p, identified by microRNA library-based functional screening, modulates tamoxifen response in breast cancer. Scientific reports. 2015; 5:7641.

11. Ikura T, Ogryzko VV, Grigoriev M, Groisman R, Wang J, Horikoshi M, Scully R, Qin J, Nakatani Y. Involvement of the TIP60 histone acetylase complex in DNA repair and apoptosis. Cell. 2000; 102:463–473.

12. Kamine J, Elangovan B, Subramanian T, Coleman D, Chinnadurai G. Identification of a cellular protein that specifically interacts with the essential cysteine region of the HIV-1 Tat transactivator. Virology. 1996; 216:357–366.

13. Berns K, Hijmans EM, Mullenders J, Brummelkamp TR, Velds A, Heimerikx M, Kerkhoven RM, Madiredjo M, Nijkamp W, Weigelt B, Agami R, Ge W, Cavet G, Linsley PS, Beijersbergen RL, Bernards R. A large-scale RNAi screen in human cells identifies new components of the p53 pathway. Nature. 2004; 428:431–437.

14. Chen G, Cheng Y, Tang Y, Martinka M, Li G. Role of Tip60 in human melanoma cell migration, metastasis, and patient survival. J Invest Dermatol. 2012; 132:2632–2641.

15. Sakuraba K, Yasuda T, Sakata M, Kitamura YH, Shirahata A, Goto T, Mizukami H, Saito M, Ishibashi K, Kigawa G, Nemoto H, Sanada Y, Hibi K. Down-regulation of Tip60 gene as a potential marker for the malignancy of colorectal cancer. Anticancer research. 2009; 29:3953–3955.

16. Gupta A, Jha S, Engel DA, Ornelles DA, Dutta A. Tip60 degradation by adenovirus relieves transcriptional repression of viral transcriptional activator EIA. Oncogene. 2013; 32:5017–5025.

17. Jha S, Vande Pol S, Banerjee NS, Dutta AB, Chow LT, Dutta A. Destabilization of TIP60 by human papillomavirus E6 results in attenuation of TIP60-dependent transcriptional regulation and apoptotic pathway. Molecular cell. 2010; 38:700–711.

18. Reitsma JM, Savaryn JP, Faust K, Sato H, Halligan BD, Terhune SS. Antiviral inhibition targeting the HCMV kinase pUL97 requires pUL27-dependent degradation of Tip60 acetyltransferase and cell-cycle arrest. Cell host & microbe. 2011; 9:103–114.

19. Subbaiah VK, Zhang Y, Rajagopalan D, Abdullah LN, Yeo-Teh NS, Tomaic V, Banks L, Myers MP, Chow EK, Jha S. E3 ligase EDD1/UBR5 is utilized by the HPV E6 oncogene to destabilize tumor suppressor TIP60. Oncogene. 2015. doi: 10.1038/onc.2015.268. [Epub ahead of print].

20. Song SJ, Poliseno L, Song MS, Ala U, Webster K, Ng C, Beringer G, Brikbak NJ, Yuan X, Cantley LC, Richardson AL, Pandolfi PP. MicroRNA-antagonism regulates breast cancer stemness and metastasis via TET-family-dependent chromatin remodeling. Cell. 2013; 154:311–324.

21. Tan TZ, Miow QH, Miki Y, Noda T, Mori S, Huang RY, Thiery JP. Epithelial-mesenchymal transition spectrum quantification and its efficacy in deciphering survival and drug responses of cancer patients. EMBO molecular medicine. 2014; 6:1279–1293.

22. Kalluri R, Weinberg RA. The basics of epithelial-mesenchymal transition. J Clin Invest. 2009; 119:1420–1428.

23. Wang L, Wang J. MicroRNA-mediated breast cancer metastasis: from primary site to distant organs. Oncogene. 2012; 31:2499–2511.

24. Song SJ, Ito K, Ala U, Kats L, Webster K, Sun SM, Jongen-Lavrencic M, Manova-Todorova K, Teruya-Feldstein J, Avigan DE, Delwel R, Pandolfi PP. The oncogenic microRNA miR-22 targets the TET2 tumor suppressor to promote hematopoietic stem cell self-renewal and transformation. Cell stem cell. 2013; 13:87–101.

25. Wang X, Wang HK, Li Y, Hafner M, Banerjee NS, Tang S, Briskin D, Meyers C, Chow LT, Xie X, Tuschl T, Zheng ZM. microRNAs are biomarkers of oncogenic human papillomavirus infections. Proceedings of the National Academy of Sciences of the United States of America. 2014; 111:4262–4267.

26. Lee JH, Park SJ, Jeong SY, Kim MJ, Jun S, Lee HS, Chang IY, Lim SC, Yoon SP, Yong J, You HJ. MicroRNA-22 Suppresses DNA Repair and Promotes Genomic Instability through Targeting of MDC1. Cancer research. 2015; 75:1298–1310.

27. Tsuchiya N, Izumiya M, Ogata-Kawata H, Okamoto K, Fujiwara Y, Nakai M, Okabe A, Schetter AJ, Bowman ED, Midorikawa Y, Sugiyama Y, Aburatani H, Harris CC, Nakagama H. Tumor suppressor miR-22 determines p53-dependent cellular fate through post-transcriptional regulation of p21. Cancer research. 2011; 71:4628–4639.

28. Guo MM, Hu LH, Wang YQ, Chen P, Huang JG, Lu N, He JH, Liao CG. miR-22 is down-regulated in gastric cancer, and its overexpression inhibits cell migration and invasion via targeting transcription factor Sp1. Medical oncology. 2013; 30:542.

29. Xu D, Takeshita F, Hino Y, Fukunaga S, Kudo Y, Tamaki A, Matsunaga J, Takahashi RU, Takata T, Shimamoto A, Ochiya T, Tahara H. miR-22 represses cancer progression by inducing cellular senescence. J Cell Biol. 2011; 193:409–424.

30. Chen B, Tang H, Liu X, Liu P, Yang L, Xie X, Ye F, Song C, Xie X, Wei W. miR-22 as a prognostic factor targets glucose transporter protein type 1 in breast cancer. Cancer Lett. 2015; 356:410–417.

31. Lleonart M, Vidal F, Gallardo D, Diaz-Fuertes M, Rojo F, Cuatrecasas M, Lopez-Vicente L, Kondoh H, Blanco C, Carnero A, Ramon y Cajal S. New p53 related genes in human tumors: significant downregulation in colon and lung carcinomas. Oncology reports. 2006; 16:603–608.

32. Mattera L, Escaffit F, Pillaire MJ, Selves J, Tyteca S, Hoffmann JS, Gourraud PA, Chevillard-Briet M, Cazaux C, Trouche D. The p400/Tip60 ratio is critical for colorectal cancer cell proliferation through DNA damage response pathways. Oncogene. 2009; 28:1506–1517.

33. Gorrini C, Squatrito M, Luise C, Syed N, Perna D, Wark L, Martinato F, Sardella D, Verrecchia A, Bennett S, Confalonieri S, Cesaroni M, Marchesi F, Gasco M, Scanziani E, Capra M, et al. Tip60 is a haplo-insufficient tumour suppressor required for an oncogene-induced DNA damage response. Nature. 2007; 448:1063–1067.

34. Ma L, Young J, Prabhala H, Pan E, Mestdagh P, Muth D, Teruya-Feldstein J, Reinhardt F, Onder TT, Valastyan S, Westermann F, Speleman F, Vandesompele J, Weinberg RA. miR-9, a MYC/MYCN-activated microRNA, regulates E-cadherin and cancer metastasis. Nature cell biology. 2010; 12:247–256.

35. Vetter G, Saumet A, Moes M, Vallar L, Le Bechec A, Laurini C, Sabbah M, Arar K, Theillet C, Lecellier CH, Friederich E. miR-661 expression in SNAI1-induced epithelial to mesenchymal transition contributes to breast cancer cell invasion by targeting Nectin-1 and StarD10 messengers. Oncogene. 2010; 29:4436–4448.

36. Hamada S, Satoh K, Miura S, Hirota M, Kanno A, Masamune A, Kikuta K, Kume K, Unno J, Egawa S, Motoi F, Unno M, Shimosegawa T. miR-197 induces epithelial-mesenchymal transition in pancreatic cancer cells by targeting p120 catenin. Journal of cellular physiology. 2013; 228:1255–1263.

37. Meng Z, Fu X, Chen X, Zeng S, Tian Y, Jove R, Xu R, Huang W. miR-194 is a marker of hepatic epithelial cells and suppresses metastasis of liver cancer cells in mice. Hepatology. 2010; 52:2148–2157.

38. Xiong J, Yu D, Wei N, Fu H, Cai T, Huang Y, Wu C, Zheng X, Du Q, Lin D, Liang Z. An estrogen receptor alpha suppressor, microRNA-22, is downregulated in estrogen receptor alpha-positive human breast cancer cell lines and clinical samples. FEBS J. 2010; 277:1684–1694.

39. Pandey DP, Picard D. miR-22 inhibits estrogen signaling by directly targeting the estrogen receptor alpha mRNA. Molecular and cellular biology. 2009; 29:3783–3790.

40. Chua SW, Vijayakumar P, Nissom PM, Yam CY, Wong VV, Yang H. A novel normalization method for effective removal of systematic variation in microarray data. Nucleic acids research. 2006; 34:e38.

Article

TIP60 inhibits metastasis by ablating DNMT1−SNAIL2-driven epithelial-mesenchymal transition program

Yanzhou Zhang[1], Vanitha Krishna Subbaiah[1], Deepa Rajagopalan[1,2], Cheng Yong Tham[1,2], Lissa Nurrul Abdullah[1], Tan Boon Toh[1], Min Gong[3], Tuan Zea Tan[1], Shweta Pradip Jadhav[1], Amit Kumar Pandey[1], Neerja Karnani[2,3], Edward Kai-Hua Chow[1,4], Jean Paul Thiery[1,2,5], and Sudhakar Jha[1,2,*]

[1] Cancer Science Institute of Singapore, National University of Singapore, Singapore
[2] Department of Biochemistry, Yong Loo Lin School of Medicine, National University of Singapore, Singapore
[3] Singapore Institute for Clinical Sciences, A* STAR, National University of Singapore, Singapore
[4] Department of Pharmacology, Yong Loo Lin School of Medicine, National University of Singapore, Singapore
[5] Institute of Molecular and Cell Biology, A*STAR, Singapore
* Correspondence to: Sudhakar Jha, E-mail: csisjha@nus.edu.sg

HIV-Tat-interacting protein of 60 kDa (TIP60) is a lysine acetyltransferase and known to be downregulated in multiple cancers. Among various signalling pathways, TIP60 is implicated in regulating epithelial-mesenchymal transition (EMT). Here, we show that TIP60 expression abrogates cell migration and metastatic potential of breast cancer cells using *in vitro* and *in vivo* models. Mechanistically, we show that this is through its ability to destabilize DNMT1 and inhibit SNAIL2 function (SNAIL2-mediated EMT/cell migration). Depletion of TIP60 stabilizes DNMT1 and increases SNAIL2 levels, resulting in EMT. Recruitment of DNMT1 to the SNAIL2 targets in the absence of TIP60 increases DNA methylation on their promoter region and further represses the expression of epithelial markers. In pathophysiological scenario, we find TIP60 to be significantly downregulated in breast cancer patients with poor overall survival and disease-free survival prognoses. These data suggest that levels of TIP60 can be a prognostic marker of breast cancer progression and stabilization of TIP60 could be a promising strategy to treat cancers.

Introduction

Epigenetic regulators play an important role in maintaining chromatin state. One group of the key regulators of chromatin organization are enzymes that are involved in modification of histones. Among them, HIV-Tat-interacting protein 60 kDa (TIP60) is a lysine acetyltransferase implicated in multiple cellular pathways, including transcription, DNA damage-induced checkpoint activation, and apoptosis (Sun et al., 2005, 2007; Sapountzi et al., 2006; Squatrito et al., 2006; Sykes et al., 2006; Tang et al., 2006; Jha et al., 2008). This is achieved through its ability to acetylate both histones and non-histone proteins (Sun et al., 2005, 2007; Sykes et al., 2006; Tang et al., 2006). TIP60 also functions as a haploinsufficient tumour suppressor (Gorrini et al., 2007) and is downregulated in multiple types of cancer, including those induced by viruses (Jha et al., 2010; Gupta et al., 2013; Subbaiah et al., 2016).

Epithelial-mesenchymal transition (EMT) is considered as an important step in cancer metastasis and describes the process whereby polarized, immotile epithelial cells transform to motile, invasive mesenchymal-like cells capable of dissemination to multiple organs (Yang and Weinberg, 2008; Polyak and Weinberg, 2009; Thiery et al., 2009; Huang et al., 2012; De Craene and Berx, 2013; Tam and Weinberg, 2013). The transcription factors SNAIL1, SNAIL2, TWIST, ZEB1, and ZEB2 are among the most potent inducers of EMT in various physiological and pathological contexts.

Aberrant DNA methylation is one of the key epigenetic mechanisms that contributes to the process of carcinogenesis (Robertson, 2001). There are three classes of DNA methyltransferase (DNMTs): DNMT1, DNMT2, and DNMT3 (DNMT3A and DNMT3B) (Bestor, 2000). *De novo* DNA methylation is catalysed by DNMT3A and DNMT3B, whereas maintenance of DNA

methylation during cell proliferation is by DNMT1 (Jones and Baylin, 2007). Among all the DNMTs, DNMT1 is most abundantly expressed (Espada et al., 2011). DNA methylation catalysed by DNMTs primarily occurs on the CpG island of the promoter regions and results in gene repression (McCabe et al., 2009). DNMT1 is reported to methylate the promoter of epithelial genes such as the epithelial cell adhesion molecule (*EpCAM*) and *CDH1*, resulting in the repression of cell adhesion molecules and promotion of EMT process (Alberti et al., 1994; Melki et al., 1999; Spizzo et al., 2007; Tai et al., 2007; Fukagawa et al., 2015).

Recent studies have shown that TIP60 downregulation correlates with node positivity, metastasis, and poor survival rates (Kim et al., 2005; Sakuraba et al., 2009; Chen et al., 2012). In addition, TIP60 acetylation on DNMT1 promotes its degradation through an acetylation-driven ubiquitination mechanism (Du et al., 2010b). In this study, we show that TIP60 is an inhibitor of EMT. By using *in vitro* and *in vivo* models, we identify that TIP60 regulates SNAIL2 expression and function to promote expression of epithelial genes. Interestingly, this is through TIP60-mediated destabilization of DNMT1 and the ability of SNAIL2 to recruit DNMT1 to the promoter. In summary, we have identified the molecular mechanism of TIP60 inhibiting DNMT1 —SNAIL2-driven EMT program and suggest that targeting this axis might be of therapeutic importance.

Results

TIP60 inhibits cell migration and invasion both *in vitro* and *in vivo*

To identify the role of TIP60 as an inhibitor of EMT, we overexpressed TIP60 in a highly metastatic triple negative breast cancer cell line (MDA-MB-231), and depleted TIP60 in normal breast epithelial cells (MCF10A). Wound-healing and Boyden chamber assays were used to score for migration and invasion potential in each of these two scenarios. For all the experiments related to the metastatic breast cancer cell line, we used a derivative of MDA-MB-231 cells that stably express the luciferase gene (MDA-MB-231-Luc-D3H2LN); this enabled us not only to monitor cell migration, early tumour growth, and metastasis *in vivo*, but also to quantify tumour burden in an animal model. To test the ability of TIP60 to inhibit metastasis, we modified this cell line to stably overexpress either wild-type TIP60 (MM-Luc-FT60WT) or its catalytically inactive form (MM-Luc-FT60KD) (Supplementary Table S1). Cells stably expressing the vector (MM-Luc-MSCV) were used as the negative control. Overexpression of wild-type TIP60 inhibited cell migration and cell invasion *in vitro* by 50% (Figure 1A, B and Supplementary Figure S1A–E). Interestingly, this inhibition was dependent on the catalytic activity of TIP60, as overexpression of its catalytically inactive form failed to inhibit cell migration (Figure 1A and B). To confirm if the same phenotype could be observed in other metastatic breast cancer cell lines, wild-type TIP60 and catalytic inactive form of TIP60 were overexpressed in two other cell lines: HCC1937 (HCC1937-MSCV, HCC1937-TIP60WT, HCC1937-TIP60KD) and MDA-MB-468 (MM468-MSCV, MM468-TIP60WT, MM468-TIP60KD) (Supplementary Table S1). Similar to the

observation in MDA-MB-231 cells, overexpression of wild-type TIP60 inhibited the migration of both HCC1937 and MDA-MB-468 cells, while catalytic inactive form of TIP60 was unable to do so (Supplementary Figure S1G–L). Conversely, to test whether depletion of TIP60 could increase cell migration, we reduced TIP60 levels in MCF10A cells using siRNA and performed wound-healing assays. TIP60 depletion enhanced cell motility by >40%, resulting in a much faster closure of the wound as compared to *siControl*-treated cells (Figure 1C, D and Supplementary Figure S2A and B).

To extend these studies into an animal model system, we studied the metastasis of MDA-MB-231 cells in 6-week-old NOD/SCID mice, comparing the metastatic potential of TIP60 wild-type and control cells. In this *in vivo* study, MDA-MB-231 cells expressing the luciferase reporter gene (i.e. MM-Luc-MSCV, MM-Luc-FT60WT, and MM-Luc-FT60KD) were injected into mice through the tail vein, and fluorescence-based non-invasive imaging was used to monitor the metastasis of cells (Figure 1E). The results show that TIP60 overexpression led to a dramatic reduction in the extravasation potential of these cells scored by reduced lung metastasis as compared with the control cells, which is dependent on the catalytic activity of TIP60 (Figure 1E–G). These data suggest that TIP60 levels regulate the late process of metastasis *in vivo* and cell migration *in vitro*.

Depletion of TIP60 decreases the expression of epithelial genes and increases the expression of mesenchymal genes

TIP60-mediated EMT phenotype was verified by screening the expression of EMT markers in TIP60-depleted cells. Interestingly, we found that the transcript levels of two major mesenchymal markers *SNAI2* (SNAIL2) and *FN1* (FIBRONECTIN) were elevated by ~2 and ~10 folds, respectively. We also observed a 50% reduction in the expression of epithelial marker *EpCAM* (Figure 2A, Supplementary Figure S2C and Table S2). These findings were re-capitulated at the protein level (Figure 2B and Supplementary Figure S2D) and in another epithelial cell line MCF7 (Supplementary Figure S2E). SNAIL2 is one of the master regulators of EMT, as its expression in epithelial cells triggers the first and necessary phase of the EMT process, i.e. desmosomal disruption and cell spreading (Taube et al., 2010; Villarejo et al., 2014). This essentially occurs because SNAIL2 functions as a transcriptional repressor of epithelial genes, such as *EpCAM*, and as an activator of the mesenchymal gene *FN1*. EpCAM is involved in cell–cell recognition and adhesion, whereas FIBRONECTIN is a key component of the extracellular matrix promoting cell migration (Stanisavljevic et al., 2011; Park and Schwarzbauer, 2014; Sun et al., 2014). We also found that the cells depleted of TIP60 lose cell–cell adhesion, become more elongated and mesenchymal-like (Figure 2C and Supplementary Figure S1F) along with plasma membrane-to-cytoplasmic re-localization of E-CADHERIN and β-CATENIN (Figure 2D and E) compared to the control cells.

To rule out any off-target effects of the siRNA, we generated three cell lines using MCF10A cells as the parental cell line: MSCV vector control (M10MSCV), wild-type TIP60 (M10FT60WT),
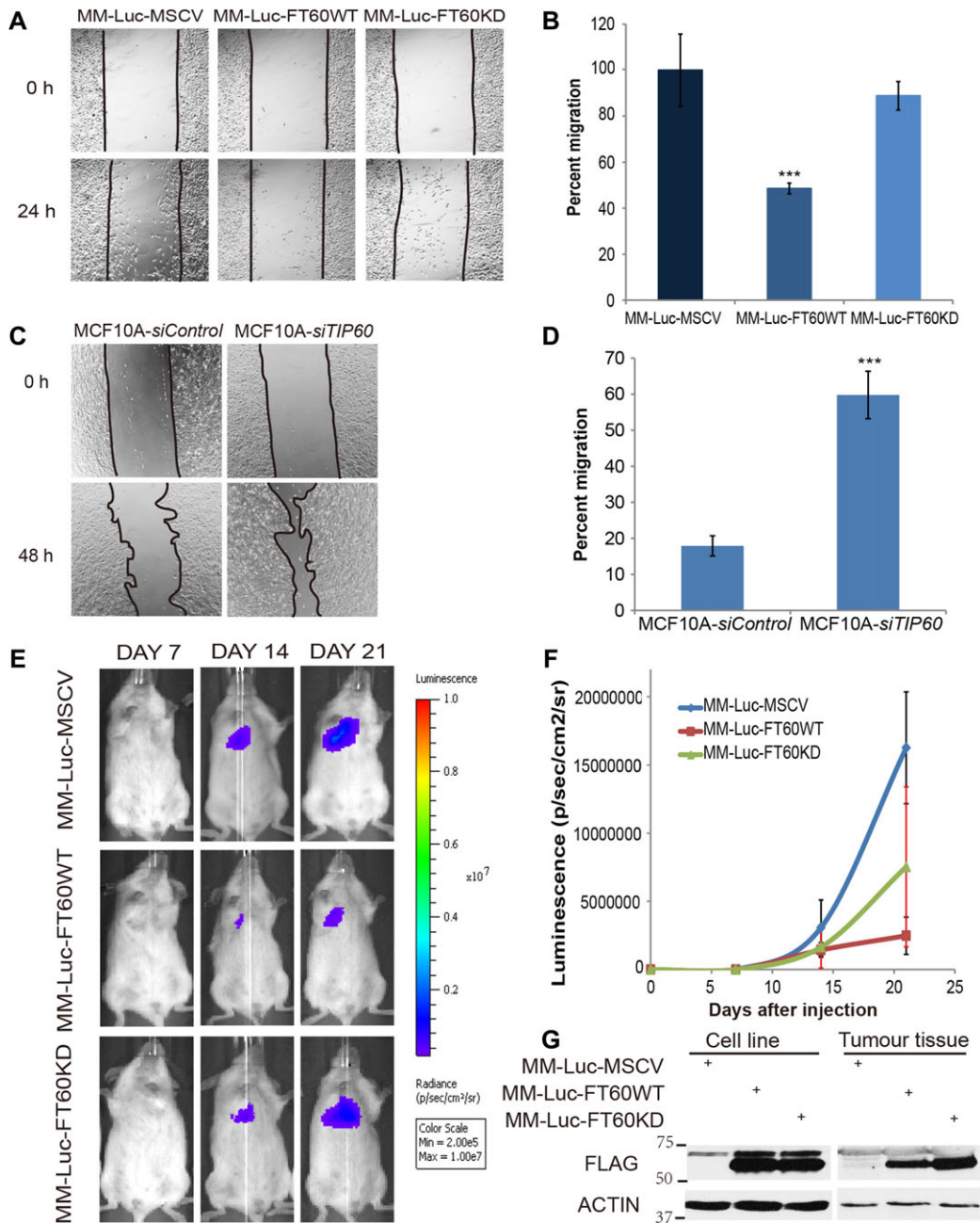
Figure 1 TIP60 inhibits EMT. (**A** and **B**) Overexpression of TIP60 inhibits cell migration. Wound-healing assays were performed using MDA-MB-231-Luc-D3H2LN cells expressing vector (MM-Luc-MSCV), wild-type TIP60 (MM-Luc-FT60WT), or the catalytically inactive form of TIP60 (MM-Luc-FT60KD) (see Materials and methods). Cell migration images are shown in **A** and the quantitation in **B**; ***$P < 0.001$. (**C** and **D**) Depletion of TIP60 increases cell migration. MCF10A cells were treated with indicated siRNAs. Representative images are shown in **C** and quantitation in **D**; ***$P < 0.001$. (**E**–**G**) TIP60 inhibits metastasis in an animal model. MDA-MB-231-Luc-D3H2LN cells (5×10^5) expressing different proteins as indicated were injected through the tail vein and tumour growth and metastasis were monitored through bioluminescence imaging (see Materials and methods). Representative images are shown in **E**, quantitation in **F**, and expression of TIP60 in **G**.

and a siRNA-resistant wild-type TIP60 (M10FT60*WT) (Supplementary Table S1). The siRNA-resistant constructs were generated by synonymous mutations, i.e. the siRNA-targeting site was mutated such that the protein sequence would not change. To test whether these cell lines behaved similar to the parental cell line, we depleted both the endogenous and

exogenous TIP60 and performed wound-healing assays, mRNA quantitation, and protein expression assays. Figure 3A–D confirms that the knockdown of both exogenous and endogenous TIP60 produced phenotypes similar to that of the parental MCF10A cell line. Overexpression of TIP60 resulted in a 50% reduction in *FN1* expression and a 2-fold increase in *EpCAM*
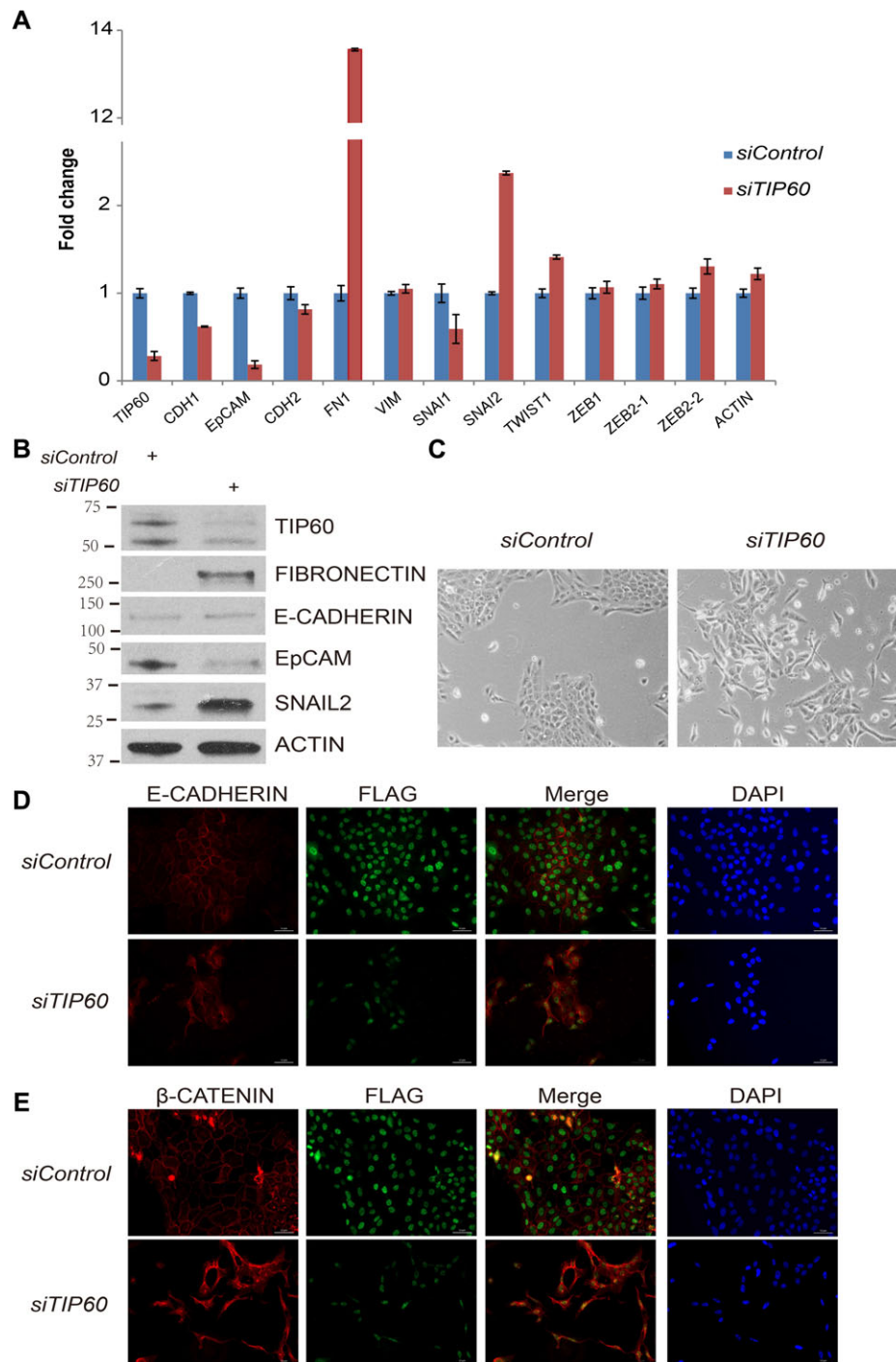
Figure 2 Reduced expression of TIP60 promotes EMT. (**A**) Expression analysis of the genes involved in EMT after depletion of TIP60. Results were analysed as fold change against *siControl*-treated cells. (**B**) Western blot analysis of the proteins showing changes in expression after depletion of TIP60. Total cell lysates were resolved on SDS-PAGE and probed with the indicated antibodies. ACTIN serves as a loading control for western blotting. (**C**) Morphology of MCF10A cells treated with *siControl* and *siTIP60*. (**D** and **E**) Depletion of TIP60 results in cell membrane-to-cytoplasmic re-localization of E-CADHERIN (**D**) and β-CATENIN (**E**).

expression (Figure 3C and D). Importantly, the expression of *siTIP60*-resistant TIP60 rescued the levels of *FN1* and *EpCAM* at both RNA and protein levels, indicating that this phenotype was TIP60 specific (Figure 3A–D and F). However, *SNAI2* expression

could only be rescued partially in such a scenario (Figure 3E). Because FIBRONECTIN has been previously shown to upregulate SNAIL2 to promote metastasis, it is plausible that the reduction in TIP60 provides the initial trigger to upregulate SNAIL2, then
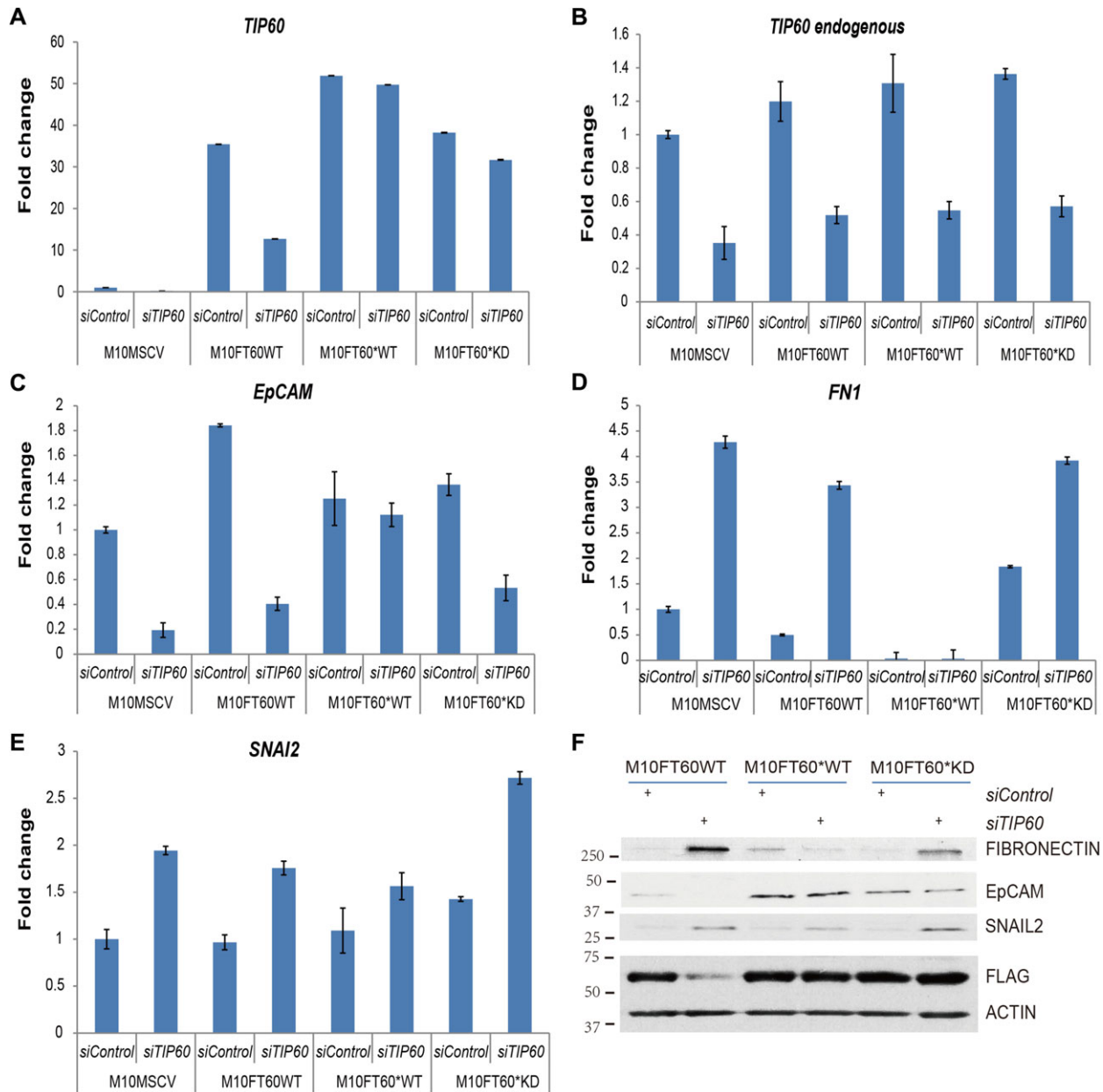
Figure 3 TIP60-mediated inhibition of EMT is specific to TIP60 and depends on its catalytic activity. (**A–E**) Expression analysis of genes identified to change when TIP60 is depleted using *siTIP60* in parental (MCF10A), vector control (M10MSCV), or stable cells expressing wild-type TIP60 (M10FT60WT), siRNA-resistant wild-type TIP60 (M10FT60*WT), and catalytically inactive and siRNA-resistant TIP60 (M10FT60*KD). Results are represented as fold change against *siControl*-treated MCF10A cells. (**F**) Western blots for the proteins with differential expression upon TIP60 depletion. Lysates were prepared from the indicated cell lines, and proteins were resolved on SDS-PAGE and blotted for the indicated antibodies. ACTIN served as a loading control.

FIBRONECTIN maintains SNAIL2 levels during metastasis (Knowles et al., 2013).

To gain a deeper insight into the molecular mechanism of TIP60 function, we next sought to determine whether the lysine acetyltransferase activity of TIP60 is required for SNAIL2-mediated regulation of EMT. We thus generated a cell line expressing TIP60 that was catalytically inactive and siRNA-resistant (M10FT60*KD). Intriguingly, this form of TIP60 failed to

rescue the expression level of *FN1* and *EpCAM* (Figure 3A–F), indicating that the catalytic activity of TIP60 is required to regulate the expression of these genes, at both mRNA and protein levels.

To further strengthen that this observation is TIP60 specific and catalytic activity dependent, cell lysates from MDA-MB-231 cells with overexpression of either wild-type TIP60 or catalytic inactive form of TIP60 (MM-Luc-MSCV, MM-Luc-FT60WT, MM-

Luc-FT60KD) were examined by western blotting. EpCAM level increased by overexpressing wild-type TIP60 compared to control but not catalytic inactive form of TIP60 (Supplementary Figure S2F). This was in contrast to MCF10A, where the expression of EpCAM was inversely modulated upon depleting TIP60 (Figure 2B). *FN1* and *SNAI2* expression was not altered in MDA-MB-231 cells by overexpressing wild-type TIP60 or catalytic inactive form of TIP60 (data not shown). This could be due to the feedback regulation between *FN1* and *SNAI2* in highly metastatic cells, as discussed earlier. High levels of *FN1* and *SNAI2* could upregulate each other and ensure the maintainance of both genes at high level in more metastatic cells. However, restoration of EpCAM level is sufficient to inhibit cell migration and invasion (Tai et al., 2007), which explains the inhibitory function of TIP60 in MDA-MB-231 cell metastasis. This suggests that the regulation of EpCAM plays a predominant role in TIP60-mediated inhibiton of breast cancer metastasis.

Alteration of expression of EMT-related genes in the absence of TIP60 is SNAIL2 dependent

SNAIL2 belongs to the family of zinc finger transcription factors, which regulates the expression of EMT-related genes by interacting with the E-boxes in their promoter regions (Yang and Weinberg, 2008; Thiery et al., 2009; Huang et al., 2012; Villarejo et al., 2014). To test the role of SNAIL2 in TIP60-mediated alteration of the expression of EMT markers, we depleted both TIP60 and SNAIL2 and found that compared with the depletion of TIP60 alone, the co-depletion could rescue both *FN1* and *EpCAM* at both mRNA and protein levels (Figure 4A and B), suggesting that TIP60 regulation of the expression of *FN1* and *EpCAM* is SNAIL2 dependent. To further investigate the biological implication, wound-healing assay using MCF10A cells depleting either TIP60 alone or TIP60 and SNAIL2 together was performed. A 40% increase in cell migration by depleting TIP60 was observed and this was further reduced by nearly 30% upon
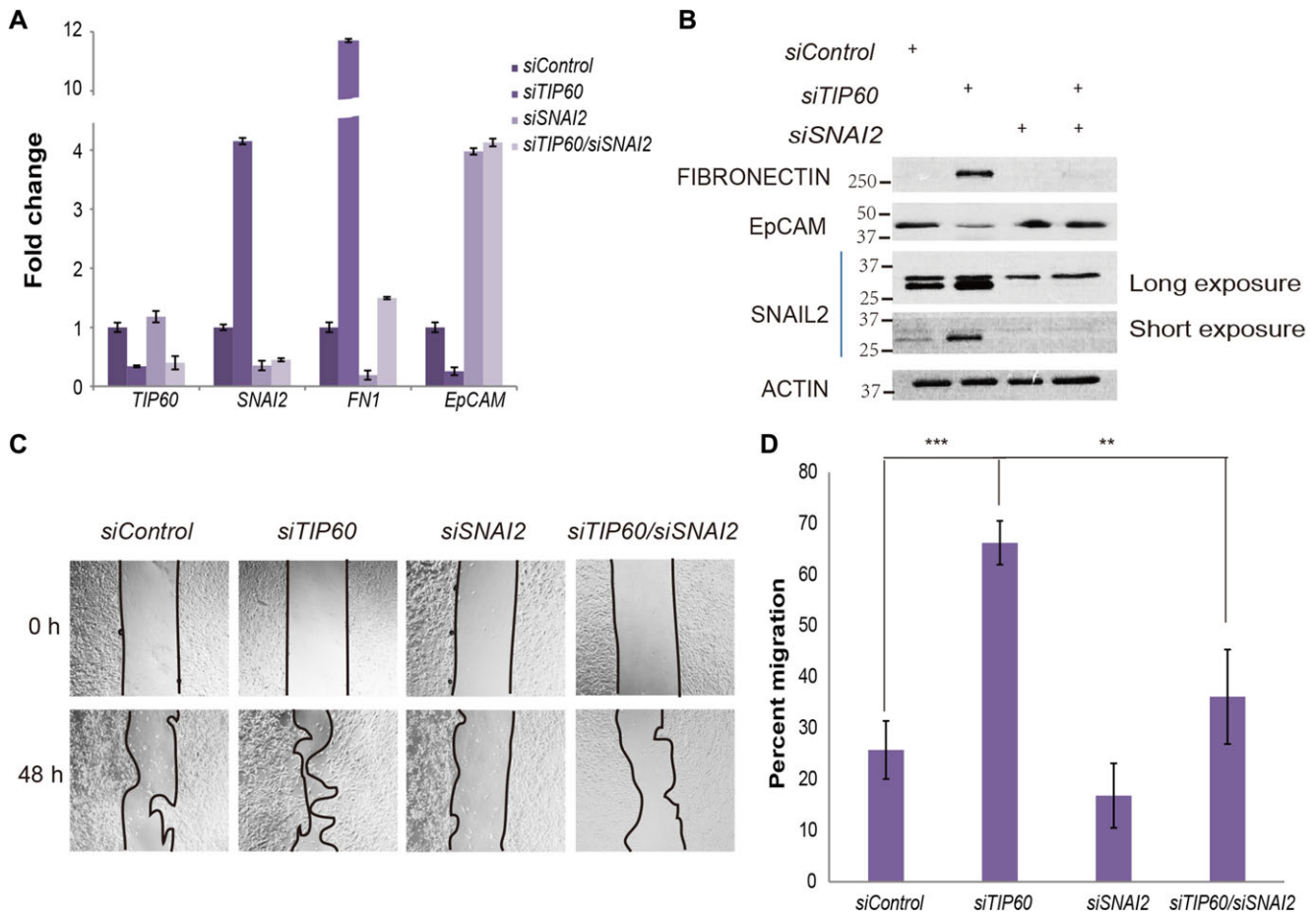
Figure 4 TIP60 regulates EMT through regulating SNAIL2. (**A**) The change in gene expression under TIP60-depleted condition is SNAIL2 dependent. mRNA levels of genes identified to be differentially expressed when TIP60 is depleted either alone or in combination with SNAIL2 in MCF10A cells. Results were analysed and are represented as fold change against *siControl*-treated cells. (**B**) Western blot analysis of the differentially expressed genes. Lysates were prepared from MCF10A cells treated with indicated siRNAs and resolved on SDS-PAGE. The levels of proteins were checked by probing with indicated antibodies. ACTIN served as a loading control. (**C** and **D**) The increased cell migration after depletion of TIP60 was restored by co-depleting TIP60 and SNAIL2. Wound-healing assay was performed as described in Materials and methods. The representative pictures are shown in **C** and quantification in **D**. **$P < 0.01$; ***$P < 0.001$.

co-depleting TIP60 and SNAIL2 (Figure 4C and D), suggesting that regulation of cell migration by TIP60 is SNAIL2 dependent.

TIP60 affects SNAIL2 localizing on its target promoters

SNAIL2 has previously been implicated in the promoter-dependent transcriptional regulation of EMT genes. Thus, we next sought to ascertain whether the TIP60-mediated transcriptional regulation of *EpCAM* and *FN1* also occurred through the promoter regions of these genes. To this end, chromatin immunoprecipitation quantitative polymerase chain reaction (ChIP-qPCR) was performed using an anti-SNAIL2 antibody in the presence or absence of TIP60. Primers were designed to amplify different regions of the promoters of *FN1* and *EpCAM* (Supplementary Figure S3A and C). Among the primers tested,

two were chosen for each promoter, one from the distal site, which lacked SNAIL2 binding, and the other from the proximal site, which showed enrichment for SNAIL2 occupancy (Supplementary Figure S3B, D, and E). When the occupancy of SNAIL2 on these promoters was tested in wild-type (MCF10A) cells, we found a significant increase in SNAIL2 binding on the *FN1* and *EpCAM* promoters in the absence of TIP60 (Figure 5A). In order to test whether these changes were TIP60 specific and whether the catalytic activity of TIP60 was required to inhibit the binding of SNAIL2 to the promoters, we checked SNAIL2 occupancy in the three stable cell lines M10FT60WT, M10FT60*WT, and M10FT60*KD (Figure 5B–D). Remarkably, we found that the enrichment of SNAIL2 on *FN1* and *EpCAM* promoters (Figure 5B) can be restored back to control level by
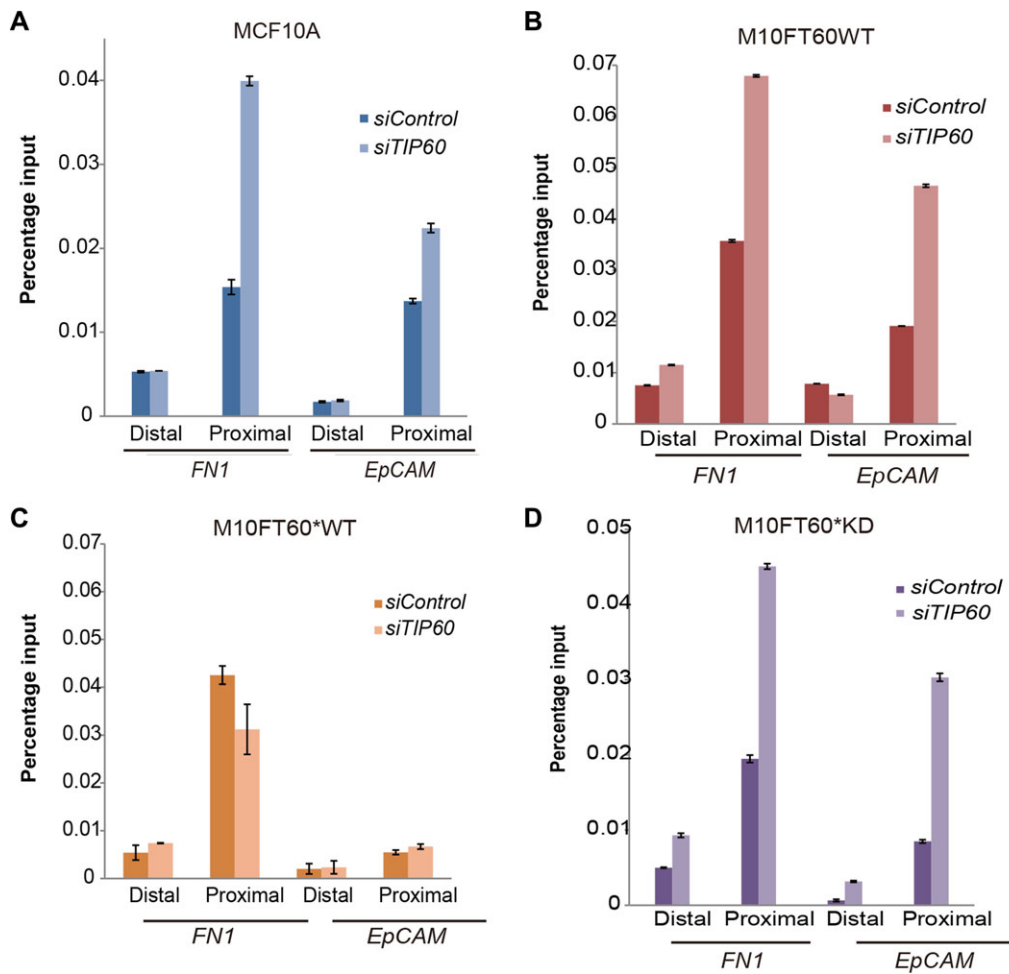

Figure 5 TIP60 affects SNAIL2 occupancy on target promoters. (**A**) ChIP-qPCR assays were performed to check the occupancy of SNAIL2 in the presence or absence of TIP60. MCF10A cells were transfected with *siControl* or *siTIP60*. Binding of SNAIL2 to the *FN1* and *EpCAM* promoters were investigated using anti-SNAIL2 antibody by qPCR analysis. Results were analysed and are represented as percent input. Aliquots of the cells from the same experiment were used to isolate RNA to check the expression levels by RT-qPCR. The TIP60 knockdown efficiency and levels of indicated genes are shown in Supplementary Figure S4. (**B–D**) SNAIL2 binding to its target promoter is regulated by TIP60 and depends on its catalytic activity. ChIP-qPCR analysis for SNAIL2 binding was performed in the presence (*siControl*) or absence of TIP60 (*siTIP60*) in MCF10A cells stably expressing wild-type TIP60 (M10FT60WT), siRNA-resistant wild-type TIP60 (M10FT60*WT), or the catalytically inactive siRNA-resistant form of TIP60 (M10FT60*KD). The *FN1* and *EpCAM* promoters were immunoprecipitated and analysed as in **A**.

overexpressing wild-type TIP60 (Figure 5C), but this was not observed when catalytically dead form of TIP60 was overexpressed (Figure 5D), suggesting that the SNAIL2 promoter occupancy was regulated by TIP60 and was dependent on the catalytic activity of TIP60. The TIP60 knockdown and the effect on *EpCAM* and *FN1* expression were confirmed by qPCR (Supplementary Figure S4).

The regulation of SNAIL2 by TIP60 is DNMT1 dependent

DNMT1 is a known EMT inducer by repressing expression of cell adhesion molecules (Fukagawa et al., 2015). Since DNMT1 is destabilized by TIP60 (Du et al., 2010b), we tested whether SNAIL2-mediated repression of epithelial genes is DNMT1 dependent. We depleted DNMT1 using siRNA either alone or in combination with TIP60. Depletion of TIP60 stabilized DNMT1 at protein level (Figure 6A–C), suggesting that TIP60 regulates the protein stability of DNMT1. When compared to TIP60 depletion alone, the co-depletion of TIP60 and DNMT1 rescued *FN1* and *EpCAM* at both mRNA and protein levels (Figure 6D and E). Interestingly, *SNAI2* was also rescued at both mRNA and protein levels when TIP60 and DNMT1 were co-depleted (Figure 6D and E). These data suggest that TIP60 regulates the expression of *SNAI2* as well as *FN1* and *EpCAM* through its ability to destabilize DNMT1. To test the biological significance of DNMT1-mediated activation of EMT program, we tested the effect of DNMT1 on cell migration under TIP60-depleted condition. We observed a 50% increase of cell migration when TIP60 was depleted alone and this was rescued to 20% when TIP60 and DNMT1 were co-depleted (Figure 6F, G and Supplementary Figure S5A). These data suggest that decreased levels of TIP60 stabilize DNMT1, which results in increased cell migration.

SNAIL2 recruits DNMT1 to repress EpCAM expression in the context of TIP60

In order to identify the molecular determinant of DNMT1−SNAIL2-driven EMT program, we sought to estimate DNA methylation on SNAIL2-regulated promoters. For this, MCF10A cells were treated with different siRNA combinations (*siControl*, *siTIP60*, *siDNMT1*, *siTIP60+siDNMT1*). Genomic DNA was isolated and the methylation-specific sequencing was performed. We observed a significant increase in DNA methylation on *EpCAM* promoter (−51 to −32) in TIP60-depleted cells. Interestingly, this was rescued when TIP60 was co-depleted with DNMT1 (Figure 7A, Supplementary Figures S6A and S5B), suggesting that the increased methylation observed was dependent on DNMT1. However, depleting DNMT1 alone did not change DNA methylation in this region. This may be because the basel level of DNA methylation in this region is due to other DNA methyltransferases (Supplementary Figure S6C–F). The DNA methylation in this region (−51 to −32) was fully dependent on DNMT1 only in the absence of TIP60, as co-depleting TIP60 and DNMT1 reduced the increased DNA methylation level to nearly zero (Figure 7A and Supplementary Figure S6A). We also noted that depleting TIP60 did not change DNA methylation on *EpCAM* 1st intron region (+542 to +601) (Figure 7B and

Supplementary Figure S5B), suggesting that this region is not responsive to decreased levels of TIP60. However, depletion of DNMT1 alone showed decrease in DNA methylation on 1st intron region (+542 to +601) (Figure 7B). In summary, these results suggest that DNMT1 methylates both regions on *EpCAM* promoter, but TIP60 only affects DNMT1-mediated DNA methylation on promoter region (−51 to −32), which has SNAIL2-binding sites and overlaps with the SNAIL2 enrichment region on *EpCAM* promoter tested earlier (Figure 5).

Next, we sought to investigate the molecular mechanism of DNMT1-mediated repression of *EpCAM* expression. For this, we checked methylation status of *EpCAM* promoter upon depleting SNAIL2 and TIP60. We observed that DNA methylation on *EpCAM* promoter region (−51 to −32) was significantly increased by depleting TIP60 but further decreased by depleting both TIP60 and SNAIL2 (Figure 7C, Supplementary Figures S6B and S5C), suggesting that TIP60 regulates DNMT1-dependent DNA methylation on *EpCAM* promoter through SNAIL2. However, this was not observed on *EpCAM* 1st intron region (+542 to +601) (Figure 7D and Supplementary Figure S5C). To further investigate the mechanism of SNAIL2-regulated DNA methylation on *EpCAM* promoter, we depleted SNAIL2 but did not observe any change in DNMT1 level (both protein and mRNA) (Figure 7E and data not shown). Following this, ChIP-qPCR experiment using antibody against DNMT1 was performed. Interestingly, we observed an increase in the enrichment of DNMT1 on *EpCAM* promoter region (−51 to −32) upon depleting TIP60, but the DNMT1 enrichment was similar to control level upon co-depleting SNAIL2 and TIP60 (Figure 7F). However, the enrichment of DNMT1 on *EpCAM* 1st intron region (+542 to +601) did not change upon depleting SNAIL2. These data suggests that SNAIL2 regulates the recruitment of DNMT1 to *EpCAM* promoter region (−51 to −32), which contains SNAIL2-binding site in the absence of TIP60. To further investigate the association between DNMT1 and SNAIL2, FLAG-DNMT1 and SNAIL2-MYC were co-expressed in 293T cells. FLAG-DNMT1 was immunoprecipitated and association with SNAIL2-MYC was observed by western blotting (Figure 7G). Taken together, these results suggest that DNMT1 catalyses DNA methylation on both *EpCAM* promoter region (−51 to −32) and 1st intron region (+542 to +601) and TIP60 inhibits SNAIL2−DNMT1-dependent methylation on *EpCAM* promoter region (−51 to −32) (Figure 7H).

Lower levels of TIP60 is a poor prognosis for overall survival and disease-free survival of breast cancer patients

Having established that TIP60 abrogates SNAIL2 function and maintains cells in an epithelial state, we then analysed the relevance of TIP60 in breast cancers. We determined *TIP60* expression levels in 3992 breast cancer and 22 normal breast tissue samples, and sought to investigate whether *TIP60* expression correlated with the breast cancer EMT score in these samples. The EMT score, ε [−1.0, +1.0], was used to estimate the EMT phenotype of each sample (Tan et al., 2014). In support of our findings, *TIP60* expression had a negative correlation with the
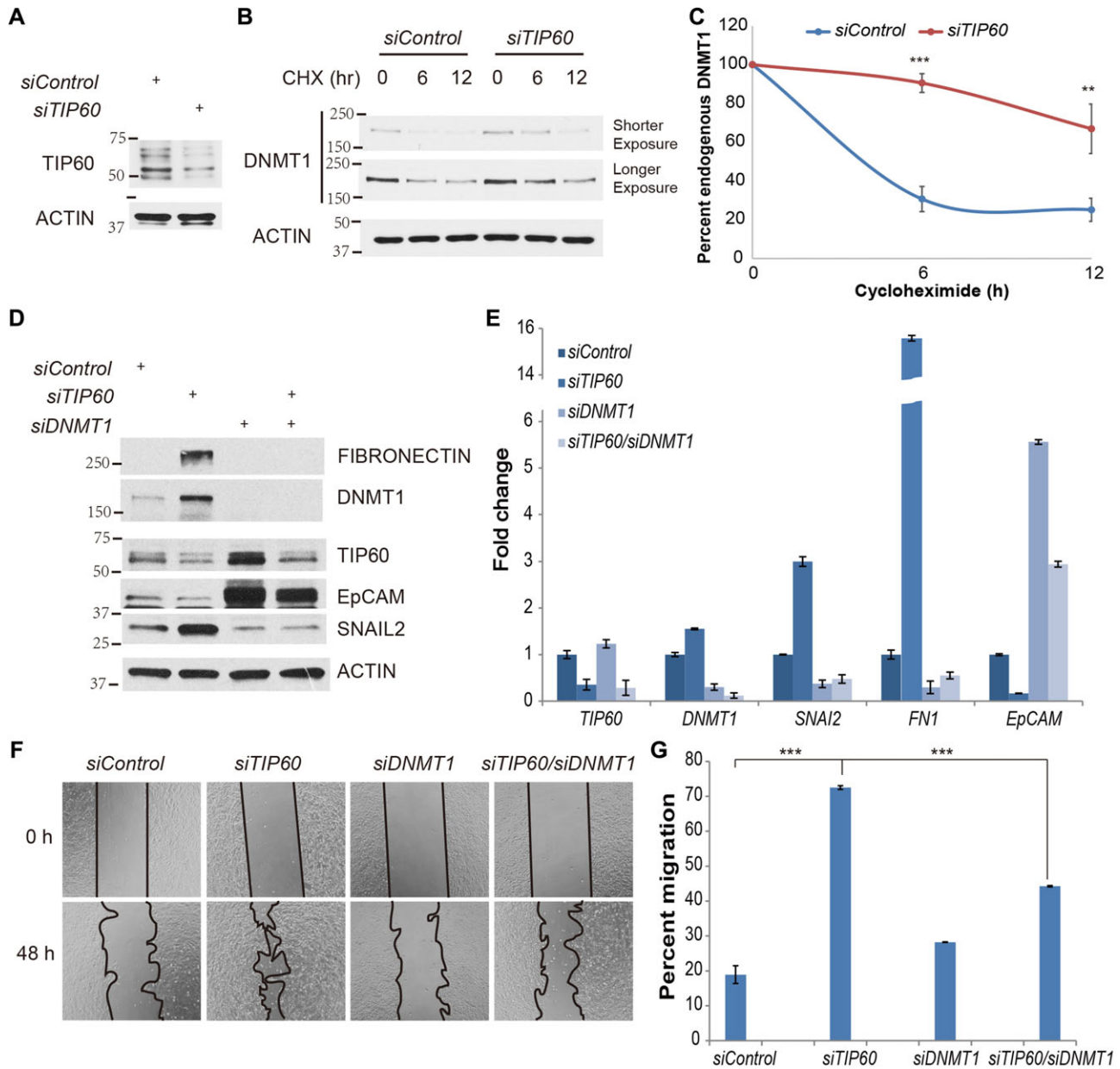
Figure 6 EMT in the absence of TIP60 is DNMT1 dependent. (**A–C**) TIP60 regulates DNMT1 protein stability. MCF10A cells transfected with *siControl* or *siTIP60* were treated with 100 μg/ml cycloheximide for up to 12 h. Cell lysates from indicating time points were examined by western blotting (**B**) and quantified (**C**). *******P* < 0.01; ***P < 0.001. The TIP60 knockdown efficiency is shown in **A**. (**D**) Protein levels of genes identified to be differentially expressed when TIP60 is depleted either alone or in combination with DNMT1 in MCF10A cells. Cells were harvested after 72 h and lysates were resolved on SDS-PAGE and membrane was probed with indicated antibodies. ACTIN served as a loading control. (**E**) mRNA expression analysis of the differentially expressed genes. Results were analysed and are represented as fold change against *siControl*-treated cells. (**F** and **G**) The increased cell migration after depletion of TIP60 was restored by co-depleting TIP60 and DNMT1. Wound-healing assay was performed as described in Materials and methods. The representative pictures are shown in **F** and quantification in **G**. ***P < 0.001.

EMT score in patient samples (Spearman Correlation Coefficient, *Rho* = −0.191, *P* = 2.08E−34) (Figure 8A). We also checked the levels of *TIP60* in various grades and types of breast cancer samples and found that *TIP60* was significantly downregulated in high-grade breast cancers (Mann–Whitney *U*-test, *P* = 2.56E−11) (Figure 8B). After further sub-classifying these tumours

into the six breast cancer subtype signatures (Basal, Claudin-Low, Luminal-A, Luminal-B, ERBB2+, and Normal-like), we observed a significantly high *TIP60* expression associated with the Luminal-A subtype, which has a good prognosis (Mann–Whitney *U*-test, *P* = 7.56E−14), and significantly lower *TIP60* expression in the poorer-prognosed molecular subtypes,
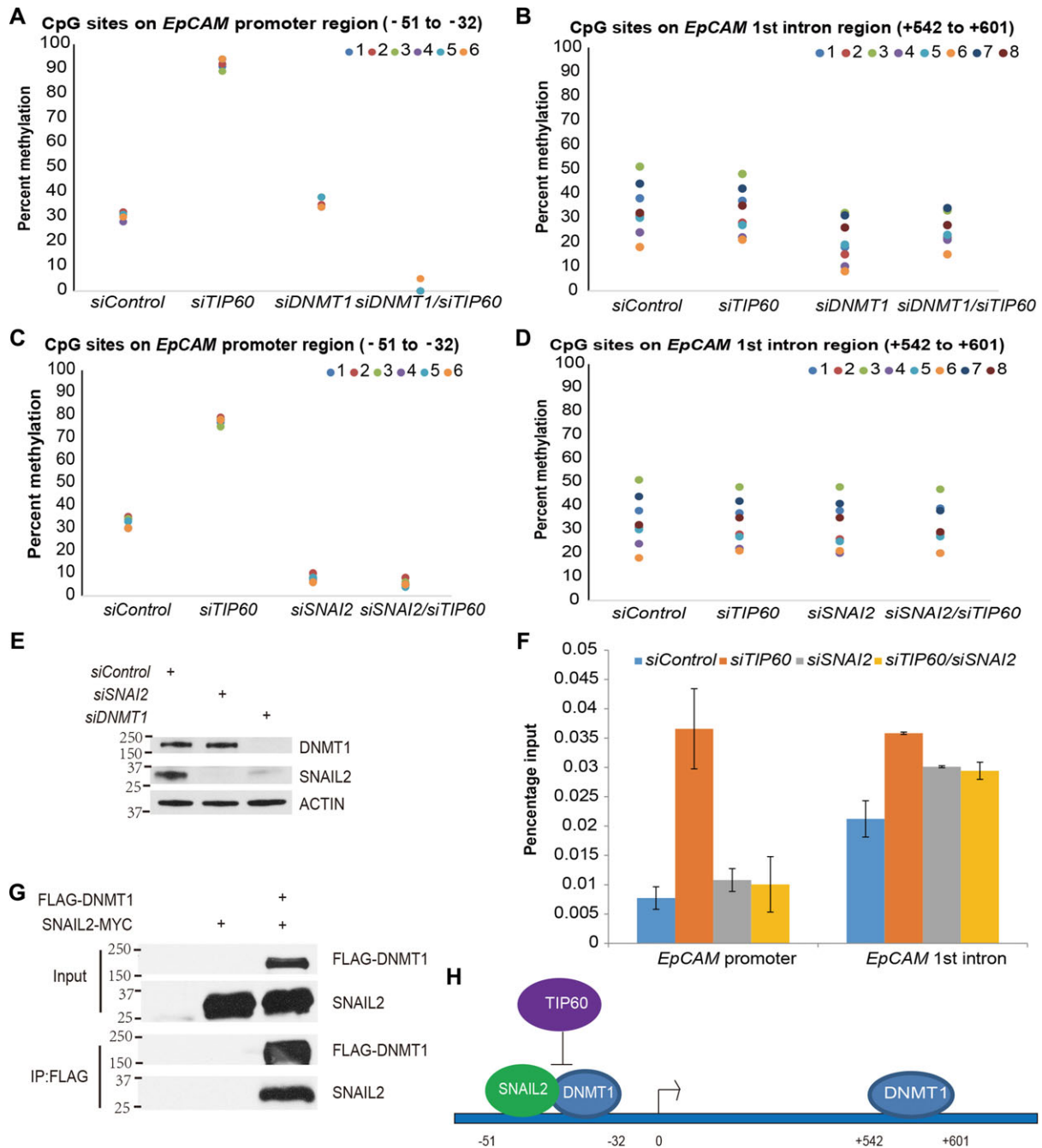
Figure 7 SNAIL2-dependent recruitment of DNMT1 to *EpCAM* promoter results in its hypermethylation in the context of depleting TIP60. (**A** and **B**) TIP60 only regulates DNMT1-mediated DNA methylation on *EpCAM* promoter region (−51 to −32) (**A**) but not on region (+542 to +601) (**B**). TIP60 and DNMT1 were depleted in MCF10A cells either alone or together. DNA from cells was isolated and bisulphite pyrosequencing was performed as mentioned in Materials and methods. (**C** and **D**) SNAIL2 recruits DNMT1 to *EpCAM* promoter region (−51 to −32) (**C**) but not to region (+542 to +601) (**D**), which is required for TIP60-mediated regulation of *EpCAM* promoter hypermethylation. (**E**) Depletion of SNAIL2 does not change the level of DNMT1. (**F**) DNMT1 was recruited to *EpCAM* promoter region (−51 to −32) by SNAIL2 in the absence of TIP60. ChIP-qPCR using the antibody against DNMT1 was performed. Two pairs of primers were designed to amplify the *EpCAM* promoter region (−51 to −32) and *EpCAM* 1st intron region (+542 to +601), respectively. The *EpCAM* promoter region amplified here overlaps with the region amplified by the *EpCAM* proximal primers used in Figure 5, but more specific to CpG sites tested in this region. (**G**) DNMT1 associates with SNAIL2. FLAG-DNMT1 and SNAIL2-MYC were co-expressed in 293T. Co-immunoprecipitation was performed as indicated in Materials and methods. FLAG-DNMT1 was immunoprecipitated and associated SNAIL2-MYC was probed by western blotting. (**H**) A model of the mechanism of the regulation of *EpCAM* promoter hypermethylation, which involves TIP60, DNMT1, and SNAIL2.
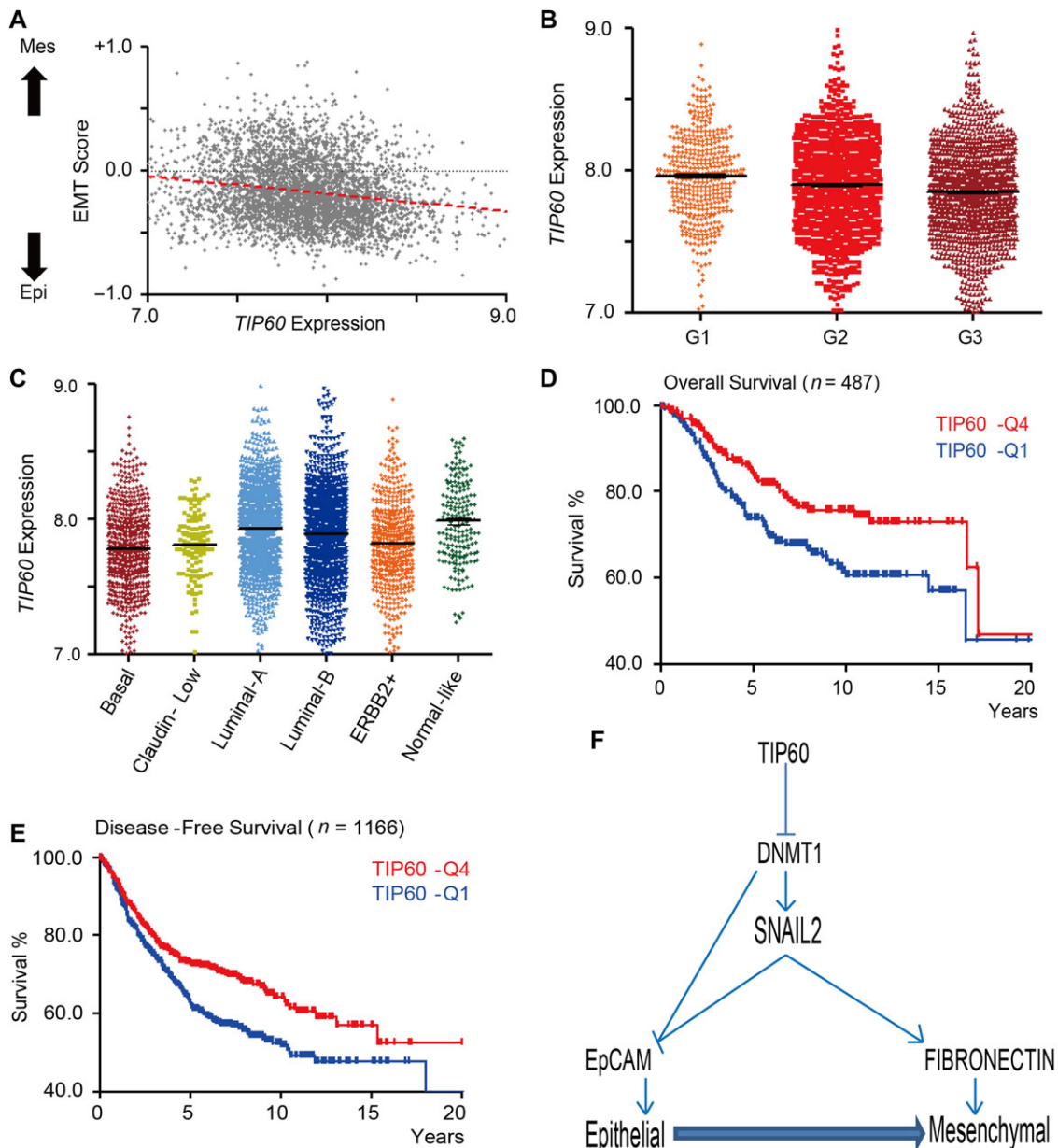
Figure 8 *TIP60* expression was negatively correlated with EMT, and is a prognostic marker for OS and DFS in breast cancer patients. *TIP60* expression was analysed in 3992 breast cancer tumours and 22 normal breast tissue samples (see Materials and methods). (**A**) *TIP60* expression negatively correlated with EMT score (Spearman Correlation Coefficient, *Rho* = −0.191, *P* = 2.08E−34). (**B**) *TIP60* expression decreases as breast cancer progresses. Samples were classified as grade 1 (G1), G2, and G3, and the *P*-value was determined using the Mann–Whitney *U*-test (G1 vs. G2, *P* = 9.73e−5; G1 vs. G3, *P* = 2.56e−11; G2 vs. G3, *P* = 1.28e−4). (**C**) *TIP60* is differentially expressed in breast cancer subtype signatures. Relative mRNA level of *TIP60* is shown for Basal, Claudin-Low, Luminal-A, Luminal-B, ERBB2+, and Normal-like breast cancer samples (Basal vs. Rest, *P* = 3.69e−16; Claudin-Low vs. Rest, *P* = 0.0169; Luminal-A vs. Rest, *P* = 7.56e−14; Luminal-B vs. Rest, *P* = 0.1477; ERBB2+ vs. Rest, *P* = 1.83e−7; Normal-like vs. Rest, *P* = 1.77e−5; Mann–Whitney *U*-test). (**D** and **E**) Higher *TIP60* expression associated with better prognosis in OS and DFS. (**D**) Survival curve of 487 patients categorized into quartile 4 (Q4 = high TIP60) or quartile 1 (Q1 = low TIP60) with a log-rank *P* = 0.0054; median survival (month), TIP60_Q1 = 16.47, TIP60_Q4 = 17.1; hazard ratio = 1.613 (1.152–2.258). (**E**) DFS curve of 1166 patients from Q4 and Q1. Log-rank *P* = 0.0004; median survival (month), TIP60_Q1 = 10.47, TIP60_Q4 = undefined; hazard ratio = 1.429 (1.175–1.738). (**F**) A model for TIP60-mediated inhibition of EMT. TIP60 destabilizes DNMT1 and inhibits SNAIL2-driven EMT program. Decreased level of *TIP60* increases SNAIL2 level and DNA methylation level on *EpCAM* promoter.

including Basal, Claudin-Low, and ERBB2+ (Mann–Whitney *U*-test, *P* = 3.69E−16, *P* = 0.0169, and *P* = 1.83E−7, respectively) (Figure 8C). In terms of a correlation between patient overall survival (OS)/disease-free survival (DFS) and *TIP60* expression, we found breast cancers with higher *TIP60* expression to show better prognoses for OS and DFS (log-rank test, *P* = 0.08 and *P* = 0.0017, respectively) (Supplementary Figure S7). Comparing breast cancers with the 25% highest *TIP60* expression (fourth quartile; Q4) with those with the 25% lowest *TIP60* expression (first quartile; Q1), we found even more significant differences in terms of OS and DFS (log-rank test, *P* = 0.0054 and *P* = 0.0004, respectively) (Figure 8D and E). These data strengthen our findings that *TIP60* expression is reduced in more aggressive cancers and patients with a higher level of *TIP60* have a better prognosis in terms of OS and DFS.

Discussion

Changes in chromatin landscape play an important role in the process of carcinogenesis. DNA methylation and post-translation modification on histone tails are among the most investigated epigenetic alterations and have been implicated in tumorigenesis. TIP60 is a chromatin remodeler involved in multiple cellular physiological process and its decreased expression has been reported in several cancers (Gorrini et al., 2007; Sakuraba et al., 2009; Jha et al., 2010; Chen et al., 2012; Gupta et al., 2013). Viral oncoproteins were also reported to destabilize TIP60 in virus-induced cancers (Jha et al., 2010; Gupta et al., 2013), and restoring its level inhibits tumour growth (Subbaiah et al., 2016), suggesting a tumour suppressor function.

In this study, we propose TIP60 as a potential inhibitor of breast cancer metastasis (Figure 8F). Our data suggest that TIP60 inhibits metastasis by inhibiting DNMT1 and SNAIL2—key regulators of EMT program. We provide four lines of evidence to support this mechanism: (i) TIP60 inhibits cell migration in both *in vitro* models and *in vivo* cancer metastasis model (Figure 1). (ii) TIP60 alters the expression of several EMT markers (*SNAI2*, *EpCAM*, and *FN1*), which depends on its catalytic activity (Figures 2 and 3). (iii) The alteration of expression of *EpCAM* and *FN1* by TIP60 is SNAIL2 dependent (Figures 4 and 5). (iv) TIP60 inhibits EMT process through both destabilizing DNMT1 (Figure 6) and inhibiting SNAIL2-dependent recruitment of DNMT1 to *EpCAM* promoter, resulting in promoter hypomethylation (Figure 7).

TIP60 is known to form a complex with DNMT1 through UHRF1, resulting in TIP60-mediated acetylation on DNMT1 and promoting DNMT1 ubiquitination-dependent degradation (Du et al., 2010b). This regulation of DNMT1 maintains the DNMT1 level at different stages of cell cycle, which would promote DNMT1 degradation at the end of S phase or the beginning of G2 phase (Du et al., 2010b). Previous studies also reported that TIP60-mediated DNMT1 degradation can be facilitated by regulator of G-protein signalling 6 (RGS6) to suppress Ras-induced cellular transformation (Huang et al., 2014), suggesting a tumour suppressor function of TIP60 by targeting DNMT1 for degradation. In this study, we have reported a novel function of

TIP60 to regulate DNMT1 degradation and inhibit EMT process. Whether TIP60–DNMT1 axis is also involved in other cellular processes needs further investigation.

SNAIL2 is one of the members of SNAIL family proteins. Among all the members, SNAIL1 is studied extensively, while less is known about SNAIL2. In most of the cases, SNAIL1/2 were considered to be involved in similar pathways; however, in some cases they were demonstrated to be diverse (Ye et al., 2015). As far as SNAIL1 is concerned, it is regulated at different levels. For instance, at transcriptional level, *SNAI1* is regulated by signalling pathways such as TGF-β (Peinado et al., 2003), NOTCH (Timmerman et al., 2004; Sahlgren et al., 2008), WNT (Zhou et al., 2004; Bachelder et al., 2005; Zhou and Hung, 2005), and HIF1-α (Imai et al., 2003). At post-transcriptional level, SNAIL1 is known to be regulated by several microRNAs such as *miR-9* (Liu et al., 2012a), *miR-34* (Kim et al., 2011), *Let-7d* (Chang et al., 2011), and *miR-30a* (Kumarswamy et al., 2012). At the protein level, SNAIL1 stability is known to be regulated by E3 ubiquitin ligases such as FBXL14 (Lander et al., 2011) and β-TRCP (Zhou et al., 2004) and kinases such as GSK3β (Yook et al., 2006), LATS2 (Zhang et al., 2012), PKD1 (Du et al., 2010a), and PAK1 (Yang et al., 2005). *SNAI2* has been previously reported to be transcriptionally regulated by several transcription factors, such as ELF5 (Chakrabarti et al., 2012), FOXA1, KLF4 (Liu et al., 2012b), SOX3 (Acloque et al., 2011), and SIM2s (Laffin et al., 2008). At post-transcriptional level, SNAIL2 is regulated by several microRNAs such as *miR-1/200* (Liu et al., 2013) and *miR-203* (Zhang et al., 2011), and is known to be phosphorylated by kinases such as GSK3β (Wu et al., 2012) and FBXL14 (Vernon and LaBonne, 2006). Interestingly, these phosphorylations stabilize SNAIL2, which is similar to SNAIL1. In this study, we have identified that the expression of *SNAI2* is regulated by DNMT1 (Figure 6D and E). However, we did not observe any change in DNA methylation on *SNAI2* promoter (data not shown), suggesting an indirect role of DNMT1 in regulating *SNAI2* transcription. Further studies investigating the molecular mechanism of DNMT1-dependent *SNAI2* regulation will be an exciting avenue to explore.

SNAIL family proteins are known to repress expression of cell adhesion molecule and promote expression of mesenchymal related molecules. Previous studies have indicated that SNAIL1 recruits epigenetic repressor complex such as HDAC1/2, PRC2, LSD1, and G9a (Lin et al., 2014) to *CDH1* promoter for maintaining the repression. On the other hand, recruitment of p65 subunit of NK-kB and PARP1 by SNAIL1 to *FN1* promoter activate its expression (Stanisavljevic et al., 2011). However, not much is known about the mechanism of SNAIL2-mediated regulation. Previous studies investigating both SNAIL1 and SNAIL2 together assumed that SNAIL2 behaves similar to SNAIL1, thus SNAIL2 was not studied in detail. A non-equivalent role of SNAIL1 and SNAIL2 in repression of *CDH1* expression has been recently reported (Villarejo et al., 2014; Ye et al., 2015) and it would be interesting to identify the molecular determinants involved in regulating the mechanism of SNAIL2-mediated regulation. Here,

we show that both *EpCAM* and *FN1* are direct targets of SNAIL2 and SNAIL2 enrichment on target promoters was regulated by TIP60 (Figure 5). Additionally, we show that SNAIL2 recruits DNMT1 to *EpCAM* promoter region (−51 to −32), which overlaps with SNAIL2 enrichment site, and maintains repression of *EpCAM* expression through promoter hypermethylation in the absence of TIP60 (Figure 7A–D).

EpCAM is one of the epithelial genes involved in inhibiting EMT process. It is known that *EpCAM* level would decrease dramatically during malignant transformation and progression (Joo et al., 2005). Mechanistically, it was shown that hypermethylation of *EpCAM* promoter was the key determinant for repression of *EpCAM* expression (Tai et al., 2007). Interestingly, DNA methyltransferase inhibitor (5-aza-2′-deoxycytidine) and HDACi (Trichostatin A) treatment reactivated the *EpCAM* expression and inhibited cancer cell invasiveness (Alberti et al., 1994; Spizzo et al., 2007). Our findings indicated an upstream mechanism of regulation of DNA hypermethylation on *EpCAM* promoter, which involved TIP60, DNMT1, and SNAIL2.

In summary, we show that TIP60 acts as an inhibitor of EMT in breast cancer cells. Mechanistically, depletion of TIP60 promotes EMT by stabilizing DNMT1, which results in increased expression of SNAIL2. The excess SNAIL2 would then recruit DNMT1 to *EpCAM* promoter region (−51 to −32), resulting in hypermethylation of *EpCAM* promoter and repression of *EpCAM* expression. This study has identified the mechanism of TIP60-mediated inhibition of EMT program and has discovered an important link between two epigenetic modulators—TIP60 and DNMT1. The data presented in this study also imply that the reactivation of TIP60 or the restoration of TIP60-dependent acetylation on DNMT1 might be a potential therapeutic strategy to treat SNAIL2-driven metastatic breast cancers.

Materials and methods
In vitro invasion assay
In vitro invasion assay was performed as described previously (Korah et al., 2000) using the BD Matrigel™ Invasion chamber and 24-well plate 8.0 Micron insert (BD Biocoat™, Cat. No. 354480). Briefly, 50000 MM-Luc-MSCV, MM-Luc-FT60WT, or MM-Luc-FT60KD cells were seeded onto the top layer of the chamber and mixed with serum-free media. The bottom layer was filled with 750 μl growth media comprising 2% foetal bovine serum. After 8 h, cells that had invaded into the bottom layer were stained and quantitated using ImageJsoftware (http://imagej.nih.gov/ij/).

Wound-healing assay
Wound-healing assays were performed as described previously (Oxmann et al., 2008; Chen et al., 2012). Briefly, siRNA-transfected (*siControl*, *siTIP60*, *siDNMT1*, *siTIP60/siDNMT1*, *siSNAI2*, *siTIP60/siSNAI2*, and *siDNMT3B*) MCF10A cells or the stable metastatic breast cancer cells were seeded into the wells of 24-well plates at 100% confluence. Cells were maintained in complete media for 12 h for adhesion. Cells were then subjected to serum-starved conditions for next 24 h. A wound was created

using a fine pipette tip and the detached cells were removed by gently washing the wells with phosphate-buffered saline. The closure of wound was monitored every 24 h. For MCF10A, HCC1937, and MDA-MB-468 cells, the area of the wound was measured at 0 h and the percentage of movement was calculated by using the following formula: (area of wound at 0 h − area of wound at *n* h)/area of wound at 0 h × 100, where *n* is a specific time. For MDA-MB-231-luc-D3H2LN, the number of cells migrated during gap healing were counted. Each experimental group was repeated three times.

Chromatin immunoprecipitation quantitative PCR (ChIP-qPCR)
ChIP was performed as described earlier (Karnani et al., 2007; Jha et al., 2010). Briefly, 5×10^6 cells were transfected with *siControl* or *siTIP60* in a 15-cm plate. After 72 h of siRNA treatment, cells were cross-linked with 1% formaldehyde (SantaCruz Biotechnology, Cat. No. sc-203049A) for 10 min at room temperature, and then washed twice with ice-cold phosphate-buffered saline. For DNMT1 ChIP, cells were treated with 0.005 μM 5-aza-2′-deoxycytidine for 10 h before harvesting, in order to enrich chromatin bound DNMT1 (Lu et al., 2006; Patel et al., 2010). Cells were harvested by scraping and centrifuged at 1750 *g* for 15 min to collect the cell pellet. Cells were then resuspended in SDS lysis buffer (1% SDS, 0.01 M EDTA, and 0.05 M Tris-HCl, pH 8.0) and sonicated (ON: 15 sec and OFF: 45 sec at 30% amplitude for 15 cycles) to obtain DNA fragments ranging from 100 to 500 bp. Chromatin was isolated by centrifuging at 15300 *g* for 15 min at 4°C and the supernatant was collected for immunoprecipitation.

Immunoprecipitation was performed with anti-SNAIL2 antibody (Cell Signaling Technology, Cat. No. 9585) or anti-DNMT1 antibody (Abcam, Cat. No. ab87656) overnight at 4°C, followed by incubation with protein A/G PLUS agarose beads (SantaCruz Biotechnology, Cat. No. sc-2003) for 3 h. Beads were then washed with (i) low-salt immune complex buffer (0.1% SDS, 1% Triton X-100, 0.002 M EDTA, 0.02 M Tris-HCl, pH 8.0, and 0.15 M NaCl), (ii) high-salt immune complex buffer (0.1% SDS, 1% Triton X-100, 0.002 M EDTA, 0.02 M Tris-HCl, pH 8.0, and 0.5 M NaCl), (iii) LiCl buffer (0.25 M lithium chloride, 1% NP40, 0.001 M EDTA, 0.01 M Tris-HCl, pH 8.0, and 1% deoxycholate), and (iv) TE buffer (0.001 M EDTA and 0.01 M Tris-HCl, pH 8.0). Beads were eluted in 100 μl elution buffer (1% SDS and 0.0084% NaHCO₃) three times with agitation for 15 min each. Chromatin was reversedly cross-linked by adding 0.2 M NaCl and was heated at 65°C for 4 h. The proteins bound to DNA were digested by adding 20 μg proteinase K (AppliChem, Cat. No. 39450-01-6) and incubated at 45°C for 1 h. DNA was purified using a PCR purification kit (QIAGEN, Cat. No. 28106) and used as template for qPCR. The results were analysed and are represented as percent input. Supplementary Table S3 shows the sequence information for the primers used for qPCR.

DNA methylation analysis using bisulphite pyrosequencing
DNA methylation analyses were performed as described previously (Mikeska et al., 2011). Briefly, DNA was bisulphite

converted using EpiTect Fast DNA bisulfite kit (Qiagen) according to the manufacturer's protocol. Prior to pyrosequencing, PCR reactions were carried out using PyroMark PCR kit (Qiagen) in a 50 µl reaction volume (PCR primers used: promoter region: forward: GAAGGTTTTTTGTTTGTGTTTGTAT; reverse: [Btn] ACCCTCTCCACAAATATAAACC. 1st intron region: forward: GGGTATAATAGGGAGGGGATTAAG; reverse: [Btn] CCAAAACCATTTCCCTACCAA. Btn, biotin). An initial polymerase activation step of 15 min at 95°C was followed by 40 cycles of 30 sec at 94°C, 30 sec at 56°C, and 30 sec at 72°C, and a final step of 5 min at 72°C. The biotinylated PCR products were extracted with streptavidin sepharose beads (GE Healthcare) according to the manufacturer's instructions and released into a PSQ 96 Low Plate (Biotage) containing 40 µl pyrosequencing primer (promoter region: GAGACGAAGTATTTGGGG; 1st intron region: GGGAGGGGATTAAGA), which has been diluted with annealing buffer to a final concentration of 0.4 µM. The plate was incubated at 80°C for 2 min, cooled to room temperature, and run on a PyroMark ID machine (Biotage) using PyroMark Gold reagents (Qiagen) as specified by the manufacture. Results were analysed with PyroMark software for DNA methylation quantification.

Bioluminescence assay in mice

Tail-vein injection was performed as described previously (Liang et al., 2005; Yang et al., 2012). Briefly, 6-week-old NOD/SCID mice (Invivos) were divided into three groups with four mice per group. Each mouse received a tail-vein injection of 5×10^5 MM-Luc-MSCV, MM-Luc-FT60WT, or MM-Luc-FT60KD cells, and images were taken every 7 days after injection using IVIS 200 Pre-clinical *in vivo* Imaging System. All protocols for animal studies were reviewed and approved by the Institutional Animal Care and Use Committee at the National University of Singapore. Analyses of the images were performed as described previously (Wu et al., 2001; Craft et al., 2005) using Living Image software (IVIS imaging system).

Data preprocessing of Affymetrix microarray gene expression

Data processing of microarray gene expression of breast cancer samples is described elsewhere (Kumar et al., 2014). Briefly, 26 breast cancer cohorts on Affymetrix U133A or U133Plus2 were downloaded from Gene Expression Omnibus (GEO) and Array Express. Robust Multichip Average (RMA) normalisation was performed on each cohort, and the normalised data were standardised using ComBat (Johnson et al., 2007) to remove batch effects. The standardised data yielded a dataset of 3992 breast cancer tumours and 22 normal breast tissue samples.

Identification of breast cancer subtypes

Breast cancer subtype signature was obtained from the study by Prat et al. (2010). Subsequently, single sample Gene Set Enrichment Analysis (ssGSEA) (Verhaak et al., 2010) was performed to estimate enrichment scores for the six breast cancer subtype signatures (Basal, Claudin-Low, Luminal-A, Luminal-B, ERBB2+, and Normal-like) expressed in each sample. Each sample was then assigned a subtype depending on the ssGSEA enrichment score.

Statistical analysis

Statistical significance evaluations were computed by Mann–Whitney test, Spearman Correlation Coefficient, log-rank test of Graphpad Prism® version 5.04 and two sample two tailed student *t*-test. Error bars represent the standard deviation from at least three times of experiments.

Details for antibodies, siRNA sequences, generation of stable cell lines, siRNA transfection, immunofluorescences, co-immunoprecipitation, and primers for mutagenesis are in Supplementary Materials and methods.

Supplementary material

Supplementary material is available at *Journal of Molecular Cell Biology* online.

References

Acloque, H., Ocana, O.H., Matheu, A., et al. (2011). Reciprocal repression between Sox3 and snail transcription factors defines embryonic territories at gastrulation. Dev. Cell *21*, 546–558.

Alberti, S., Nutini, M. and Herzenberg, L.A. (1994). DNA methylation prevents the amplification of TROP1, a tumor-associated cell surface antigen gene. Proc. Natl Acad. Sci. USA *91*, 5833–5837.

Bachelder, R.E., Yoon, S.O., Franci, C., et al. (2005). Glycogen synthase kinase-3 is an endogenous inhibitor of Snail transcription: implications for the epithelial-mesenchymal transition. J. Cell Biol. *168*, 29–33.

Bestor, T.H. (2000). The DNA methyltransferases of mammals. Hum. Mol. Genet. *9*, 2395–2402.

Chakrabarti, R., Hwang, J., Andres Blanco, M., et al. (2012). Elf5 inhibits the epithelial-mesenchymal transition in mammary gland development and breast cancer metastasis by transcriptionally repressing Snail2. Nat. Cell Biol. 14, 1212–1222.

Chang, C.J., Hsu, C.C., Chang, C.H., et al. (2011). Let-7d functions as novel regulator of epithelial-mesenchymal transition and chemoresistant property in oral cancer. Oncol. Rep. 26, 1003–1010.

Chen, G., Cheng, Y., Tang, Y., et al. (2012). Role of Tip60 in human melanoma cell migration, metastasis, and patient survival. J. Invest. Dermatol. 132, 2632–2641.

Craft, N., Bruhn, K.W., Nguyen, B.D., et al. (2005). Bioluminescent imaging of melanoma in live mice. J. Invest. Dermatol. 125, 159–165.

De Craene, B. and Berx, G. (2013). Regulatory networks defining EMT during cancer initiation and progression. Nat. Rev. Cancer 13, 97–110.

Du, C., Zhang, C., Hassan, S., et al. (2010a). Protein kinase D1 suppresses epithelial-to-mesenchymal transition through phosphorylation of snail. Cancer Res. 70, 7810–7819.

Du, Z., Song, J., Wang, Y., et al. (2010b). DNMT1 stability is regulated by proteins coordinating deubiquitination and acetylation-driven ubiquitination. Sci. Signal. 3, ra80.

Espada, J., Peinado, H., Lopez-Serra, L., et al. (2011). Regulation of SNAIL1 and E-cadherin function by DNMT1 in a DNA methylation-independent context. Nucleic Acids Res. 39, 9194–9205.

Fukagawa, A., Ishii, H., Miyazawa, K., et al. (2015). deltaEF1 associates with DNMT1 and maintains DNA methylation of the E-cadherin promoter in breast cancer cells. Cancer Med. 4, 125–135.

Gorrini, C., Squatrito, M., Luise, C., et al. (2007). Tip60 is a haplo-insufficient tumour suppressor required for an oncogene-induced DNA damage response. Nature 448, 1063–1067.

Gupta, A., Jha, S., Engel, D.A., et al. (2013). Tip60 degradation by adenovirus relieves transcriptional repression of viral transcriptional activator EIA. Oncogene 32, 5017–5025.

Huang, J., Stewart, A., Maity, B., et al. (2014). RGS6 suppresses Ras-induced cellular transformation by facilitating Tip60-mediated Dnmt1 degradation and promoting apoptosis. Oncogene 33, 3604–3611.

Huang, R.Y., Guilford, P. and Thiery, J.P. (2012). Early events in cell adhesion and polarity during epithelial-mesenchymal transition. J. Cell Sci. 125, 4417–4422.

Imai, T., Horiuchi, A., Wang, C., et al. (2003). Hypoxia attenuates the expression of E-cadherin via up-regulation of SNAIL in ovarian carcinoma cells. Am. J. Pathol. 163, 1437–1447.

Jha, S., Shibata, E. and Dutta, A. (2008). Human Rvb1/Tip49 is required for the histone acetyltransferase activity of Tip60/NuA4 and for the downregulation of phosphorylation on H2AX after DNA damage. Mol. Cell. Biol. 28, 2690–2700.

Jha, S., Vande Pol, S., Banerjee, N.S., et al. (2010). Destabilization of TIP60 by human papillomavirus E6 results in attenuation of TIP60-dependent transcriptional regulation and apoptotic pathway. Mol. Cell 38, 700–711.

Johnson, W.E., Li, C. and Rabinovic, A. (2007). Adjusting batch effects in microarray expression data using empirical Bayes methods. Biostatistics 8, 118–127.

Jones, P.A. and Baylin, S.B. (2007). The epigenomics of cancer. Cell 128, 683–692.

Joo, M., Kim, H., Kim, M.K., et al. (2005). Expression of Ep-CAM in intestinal metaplasia, gastric epithelial dysplasia and gastric adenocarcinoma. J. Gastroen. Hepatol. 20, 1039–1045.

Karnani, N., Taylor, C., Malhotra, A., et al. (2007). Pan-S replication patterns and chromosomal domains defined by genome-tiling arrays of ENCODE genomic areas. Genome Res. 17, 865–876.

Kim, J.H., Kim, B., Cai, L., et al. (2005). Transcriptional regulation of a metastasis suppressor gene by Tip60 and β-catenin complexes. Nature 434, 921–926.

Kim, N.H., Kim, H.S., Li, X.Y., et al. (2011). A p53/miRNA-34 axis regulates Snail1-dependent cancer cell epithelial-mesenchymal transition. J. Cell Biol. 195, 417–433.

Knowles, L.M., Gurski, L.A., Engel, C., et al. (2013). Integrin αvβ3 and fibronectin upregulate Slug in cancer cells to promote clot invasion and metastasis. Cancer Res. 73, 6175–6184.

Korah, R.M., Sysounthone, V., Golowa, Y., et al. (2000). Basic fibroblast growth factor confers a less malignant phenotype in MDA-MB-231 human breast cancer cells. Cancer Res. 60, 733–740.

Kumar, A.P., Loo, S.Y., Shin, S.W., et al. (2014). Manganese superoxide dismutase is a promising target for enhancing chemosensitivity of basal-like breast carcinoma. Antioxid. Redox Signal. 20, 2326–2346.

Kumarswamy, R., Mudduluru, G., Ceppi, P., et al. (2012). MicroRNA-30a inhibits epithelial-to-mesenchymal transition by targeting Snai1 and is down-regulated in non-small cell lung cancer. Int. J. Cancer 130, 2044–2053.

Laffin, B., Wellberg, E., Kwak, H.I., et al. (2008). Loss of singleminded-2s in the mouse mammary gland induces an epithelial-mesenchymal transition associated with up-regulation of slug and matrix metalloprotease 2. Mol. Cell. Biol. 28, 1936–1946.

Lander, R., Nordin, K. and LaBonne, C. (2011). The F-box protein Ppa is a common regulator of core EMT factors Twist, Snail, Slug, and Sip1. J. Cell Biol. 194, 17–25.

Liang, Z., Yoon, Y., Votaw, J., et al. (2005). Silencing of CXCR4 blocks breast cancer metastasis. Cancer Res. 65, 967–971.

Lin, Y., Dong, C. and Zhou, B.P. (2014). Epigenetic regulation of EMT: the Snail story. Curr. Pharm. Des. 20, 1698–1705.

Liu, S., Kumar, S.M., Lu, H., et al. (2012a). MicroRNA-9 up-regulates E-cadherin through inhibition of NF-κB1-Snail1 pathway in melanoma. J. Pathol. 226, 61–72.

Liu, Y.N., Abou-Kheir, W., Yin, J.J., et al. (2012b). Critical and reciprocal regulation of KLF4 and SLUG in transforming growth factor β-initiated prostate cancer epithelial-mesenchymal transition. Mol. Cell. Biol. 32, 941–953.

Liu, Y.N., Yin, J.J., Abou-Kheir, W., et al. (2013). MiR-1 and miR-200 inhibit EMT via Slug-dependent and tumorigenesis via Slug-independent mechanisms. Oncogene 32, 296–306.

Lu, Y.C., Song, J., Cho, H.Y., et al. (2006). Cyclophilin a protects Peg3 from hypermethylation and inactive histone modification. J. Biol. Chem. 281, 39081–39087.

McCabe, M.T., Brandes, J.C. and Vertino, P.M. (2009). Cancer DNA methylation: molecular mechanisms and clinical implications. Clin. Cancer Res. 15, 3927–3937.

Melki, J.R., Vincent, P.C. and Clark, S.J. (1999). Concurrent DNA hypermethylation of multiple genes in acute myeloid leukemia. Cancer Res. 59, 3730–3740.

Mikeska, T., Felsberg, J., Hewitt, C.A., et al. (2011). Analysing DNA methylation using bisulphite pyrosequencing. Methods Mol. Biol. 791, 33–53.

Oxmann, D., Held-Feindt, J., Stark, A.M., et al. (2008). Endoglin expression in metastatic breast cancer cells enhances their invasive phenotype. Oncogene 27, 3567–3575.

Park, J. and Schwarzbauer, J.E. (2014). Mammary epithelial cell interactions with fibronectin stimulate epithelial-mesenchymal transition. Oncogene 33, 1649–1657.

Patel, K., Dickson, J., Din, S., et al (2010). Targeting of 5-aza-2'-deoxycytidine residues by chromatin-associated DNMT1 induces proteasomal degradation of the free enzyme. Nucleic Acids Res. 38, 4313–4324.

Peinado, H., Quintanilla, M. and Cano, A. (2003). Transforming growth factor β-1 induces snail transcription factor in epithelial cell lines: mechanisms for epithelial mesenchymal transitions. J. Biol. Chem. 278, 21113–21123.

Polyak, K. and Weinberg, R.A. (2009). Transitions between epithelial and mesenchymal states: acquisition of malignant and stem cell traits. Nat. Rev. Cancer 9, 265–273.

Prat, A., Parker, J.S., Karginova, O., et al. (2010). Phenotypic and molecular characterization of the claudin-low intrinsic subtype of breast cancer. Breast Cancer Res. 12, R68.

Robertson, K.D. (2001). DNA methylation, methyltransferases, and cancer. Oncogene 20, 3139–3155.

Sahlgren, C., Gustafsson, M.V., Jin, S., et al. (2008). Notch signaling mediates hypoxia-induced tumor cell migration and invasion. Proc. Natl Acad. Sci. USA 105, 6392–6397.

Sakuraba, K., Yasuda, T., Sakata, M., et al. (2009). Down-regulation of Tip60 gene as a potential marker for the malignancy of colorectal cancer. Anticancer Res. *29*, 3953–3955.

Sapountzi, V., Logan, I.R. and Robson, C.N. (2006). Cellular functions of TIP60. Int. J. Biochem. Cell Biol. *38*, 1496–1509.

Spizzo, G., Gastl, G., Obrist, P., et al. (2007). Methylation status of the Ep-CAM promoter region in human breast cancer cell lines and breast cancer tissue. Cancer Lett. *246*, 253–261.

Squatrito, M., Gorrini, C. and Amati, B. (2006). Tip60 in DNA damage response and growth control: many tricks in one HAT. Trends Cell Biol. *16*, 433–442.

Stanisavljevic, J., Porta-de-la-Riva, M., Batlle, R., et al. (2011). The p65 sub-unit of NF-κB and PARP1 assist Snail1 in activating fibronectin transcription. J. Cell Sci. *124*, 4161–4171.

Subbaiah, V.K., Zhang, Y., Rajagopalan, D., et al. (2016). E3 ligase EDD1/UBR5 is utilized by the HPV E6 oncogene to destabilize tumor suppressor TIP60. Oncogene *35*, 2062–2074.

Sun, X., Fa, P., Cui, Z., et al. (2014). The EDA-containing cellular fibronectin induces epithelial-mesenchymal transition in lung cancer cells through integrin α9β1-mediated activation of PI3-K/AKT and Erk1/2. Carcinogenesis *35*, 184–191.

Sun, Y., Jiang, X., Chen, S., et al. (2005). A role for the Tip60 histone acetyl-transferase in the acetylation and activation of ATM. Proc. Natl Acad. Sci. USA *102*, 13182–13187.

Sun, Y., Xu, Y., Roy, K., et al. (2007). DNA damage-induced acetylation of lysine 3016 of ATM activates ATM kinase activity. Mol. Cell. Biol. *27*, 8502–8509.

Sykes, S.M., Mellert, H.S., Holbert, M.A., et al. (2006). Acetylation of the p53 DNA-binding domain regulates apoptosis induction. Mol. Cell *24*, 841–851.

Tai, K.Y., Shiah, S.G., Shieh, Y.S., et al. (2007). DNA methylation and histone modification regulate silencing of epithelial cell adhesion molecule for tumor invasion and progression. Oncogene *26*, 3989–3997.

Tam, W.L. and Weinberg, R.A. (2013). The epigenetics of epithelial-mesenchymal plasticity in cancer. Nat. Med. *19*, 1438–1449.

Tan, T.Z., Miow, Q.H., Miki, Y., et al. (2014). Epithelial-mesenchymal transi-tion spectrum quantification and its efficacy in deciphering survival and drug responses of cancer patients. EMBO Mol. Med. *6*, 1279–1293.

Tang, Y., Luo, J., Zhang, W., et al. (2006). Tip60-dependent acetylation of p53 modulates the decision between cell-cycle arrest and apoptosis. Mol. Cell *24*, 827–839.

Taube, J.H., Herschkowitz, J.I., Komurov, K., et al. (2010). Core epithelial-to-mesenchymal transition interactome gene-expression signature is asso-ciated with claudin-low and metaplastic breast cancer subtypes. Proc. Natl Acad. Sci. USA *107*, 15449–15454.

Thiery, J.P., Acloque, H., Huang, R.Y., et al. (2009). Epithelial-mesenchymal transitions in development and disease. Cell *139*, 871–890.

Timmerman, L.A., Grego-Bessa, J., Raya, A., et al. (2004). Notch promotes epithelial-mesenchymal transition during cardiac development and onco-genic transformation. Genes Dev. *18*, 99–115.

Verhaak, R.G., Hoadley, K.A., Purdom, E., et al. (2010). Integrated genomic analysis identifies clinically relevant subtypes of glioblastoma character-ized by abnormalities in PDGFRA, IDH1, EGFR, and NF1. Cancer Cell *17*, 98–110.

Vernon, A.E. and LaBonne, C. (2006). Slug stability is dynamically regulated during neural crest development by the F-box protein Ppa. Development *133*, 3359–3370.

Villarejo, A., Cortes-Cabrera, A., Molina-Ortiz, P., et al. (2014). Differential role of Snail1 and Snail2 zinc fingers in E-cadherin repression and epithe-lial to mesenchymal transition. J. Biol. Chem. *289*, 930–941.

Wu, J.C., Sundaresan, G., Iyer, M., et al. (2001). Noninvasive optical imaging of firefly luciferase reporter gene expression in skeletal muscles of living mice. Mol. Ther. *4*, 297–306.

Wu, Z.Q., Li, X.Y., Hu, C.Y., et al. (2012). Canonical Wnt signaling regulates Slug activity and links epithelial-mesenchymal transition with epigenetic Breast Cancer 1, Early Onset (BRCA1) repression. Proc. Natl Acad. Sci. USA *109*, 16654–16659.

Yang, J. and Weinberg, R.A. (2008). Epithelial-mesenchymal transition: at the crossroads of development and tumor metastasis. Dev. Cell *14*, 818–829.

Yang, S., Zhang, J.J. and Huang, X.Y. (2012). Mouse models for tumor metas-tasis. Methods Mol. Biol. *928*, 221–228.

Yang, Z., Rayala, S., Nguyen, D., et al. (2005). Pak1 phosphorylation of snail, a master regulator of epithelial-to-mesenchyme transition, modu-lates snail's subcellular localization and functions. Cancer Res. *65*, 3179–3184.

Ye, X., Tam, W.L., Shibue, T., et al. (2015). Distinct EMT programs control normal mammary stem cells and tumour-initiating cells. Nature *525*, 256–260.

Yook, J.I., Li, X.Y., Ota, I., et al. (2006). A Wnt-Axin2-GSK3β cascade regulates Snail1 activity in breast cancer cells. Nat. Cell Biol. *8*, 1398–1406.

Zhang, K., Rodriguez-Aznar, E., Yabuta, N., et al. (2012). Lats2 kinase potenti-ates Snail1 activity by promoting nuclear retention upon phosphorylation. EMBO J. *31*, 29–43.

Zhang, Z., Zhang, B., Li, W., et al. (2011). Epigenetic silencing of miR-203 upregulates SNAI2 and contributes to the invasiveness of malignant breast cancer cells. Genes Cancer *2*, 782–791.

Zhou, B.P., Deng, J., Xia, W., et al. (2004). Dual regulation of Snail by GSK-3β-mediated phosphorylation in control of epithelial-mesenchymal transi-tion. Nat. Cell Biol. *6*, 931–940.

Zhou, B.P. and Hung, M.C. (2005). Wnt, hedgehog and snail: sister pathways that control by GSK-3β and β-Trcp in the regulation of metastasis. Cell Cycle *4*, 772–776.